Modelling the Effects of Inclination and Pipe Enlargement on Outflow Following Pipeline Rupture

A thesis submitted to the University of London for the degree of Doctor of Philosophy

SAYEH VAHEDI

Department of Chemical Engineering
University College London
Torrington Place London WC1E 7JE
September 2003

ProQuest Number: U642587

All rights reserved

INFORMATION TO ALL USERS
The quality of this reproduction is dependent upon the quality of the copy submitted.

In the unlikely event that the author did not send a complete manuscript
and there are missing pages, these will be noted. Also, if material had to be removed,
a note will indicate the deletion.

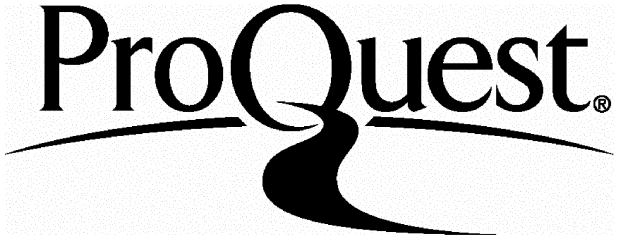

ProQuest U642587

Published by ProQuest LLC(2015). Copyright of the Dissertation is held by the Author.

All rights reserved.
This work is protected against unauthorized copying under Title 17, United States Code.
Microform Edition © ProQuest LLC.

ProQuest LLC
789 East Eisenhower Parkway
P.O. Box 1346
Ann Arbor, MI 48106-1346

Abstract

This thesis describes the development and testing of a numerical simulation based on the Method of Characteristics for predicting release rates following full bore rupture (FBR) of inclined or enlarged pipelines containing pressurised two-phase hydrocarbons. Two types of failure scenarios involving FBR of inclined pipelines are simulated. These include top end (low pressure) and bottom end (high pressure) rupture. It is found that in the case of top end rupture of the inclined pipeline, the resulting pressure wave propagation and consequently the discharge rate is decelerated compared to a horizontal pipeline. The converse is observed in the case of bottom end rupture. In the case of condensable gases undergoing a phase change during depressurisation, the effect of inclination is not linear, resulting in a dramatic decrease in the discharge rate as the angle of inclination exceeds 20^{o}. However, when the fluid remains in the gaseous state, the effect of inclination is negligible and the gravity term in the formulation of the conservation equations may be effectively ignored.

The results of application of the model to the hypothetical rupture of an enlarged pipeline undergoing a rapid change in its diameter reveal that "bottlenecking" results in a significant reduction in the release and hence the depressurisation rates following rupture. Once again, this effect is much more dramatic in the case of two-phase or liquid inventories as compared to those remaining in the gaseous state. This finding highlights the potential of using bottlenecking as an effective means of reducing the failure hazard associated with the accidental rupture of pressurised pipelines.

The effects of key parameters such as linear or curved characteristics, the size of the numerical discretisation time step and friction factor on the model's prediction are also examined. It has been observed that the simulation results obtained by applying linear characteristics are in better agreement with published experimental data compared to those based on curved characteristics. In addition, the computational run time for linear characteristics is significantly lower than that for curved characteristics.

Investigations relating to the effect of friction factor reveal that during highly transients flows (Re > 7000) such as those encountered during FBR, outflow is relatively independent of the friction factor correlation employed.

In the memory of my late father, Dr. J. Vahedi, who could not stay with us until the end of this work

ACKNOWLEDGEMENTS

Special thanks to God, the Source of all fulfilment, with whose help we can reach the rich and poor, humble and proud, wise and foolish. I have to thank god for all his blessing in my entire life and specially during studying for my PhD.

This thesis could not have been completed without the support of a great many people. I wish to take this opportunity to express my appreciation to the following people.

Professor Haroun Mahgerefteh, my supervisor for guiding me through this thesis and demanding my best work.

My dedicated parents, my father up there and my mother down here, for sacrificing the best moments of their lives to give me best of life.

My adored husband, Ali, for his priceless support and continuous encouragement. Thank you for having faith in me and giving me the strength to overcome any obstacle.

Mr Adeyemi Oke, my faithful friend and colleague for his constructive consultation in every single matter particularly during writing up my thesis.

Sepand and Arvand for accepting me as a part time mother while I was studying.

Behrad for all laughs and cries, "sweets and bitters", which we shared together.

My old colleagues Dr. Gerazounis and Dr. Falope for making our office such a pleasant atmosphere to work in.

Mr Henry Tillotson at UCL information Systems division for always being helpful and responding to my requests quickly and precisely.

Members of the office staff of the department of Chemical Engineering, UCL especially Pat Markey and Anna Harington.

All members of Computing & Electronic Systems of department of Chemical Engineering, UCL.

As a final word I have to say:

God bless everyone who made this work achievable.

LIST OF CONTENTS

Nomenclature

A	Pipe cross section area
a	Speed of sound
B	The horizontal component of gravitational force
C_P	Specific heat capacity at constant pressure
D	Pipe diameter
E	Total energy
e	Internal energy
F_b	Body forces
F_n	Normal forces
F_s	Surface forces
F_t	Tangential forces
f_f	Fanning friction factor
f_D	Darcy friction factor
g	Gravitational constant
H	Total enthalpy
h	Specific enthalpy
l	Pipe length
k	Isothermal coefficient of volumetric expansion
P	Pressure
Q_h	Heat transfer term
R	Gas constant
Re	Reynolds number
s	Specific entropy
T	Fluid temperature
T_∞	Ambient temperature
t	Time
u	Fluid velocity
U_h	Overall heat transfer coefficient
V	Volume
x	Distance along pipe
Z	Compressibility factor
z	Height from the reference point

Greek letters

θ	Angle of inclination
μ	Fluid viscosity
υ	Specific volume
ρ	Fluid density
γ	Ratio of specific heats
Ω	Angle of approach between two non uniform diameter pipelines
ξ	Isobaric coefficient of volumetric expansion

CHAPTER 1
INTRODUCTION

Pipelines are the most common method for conveying highly flammable pressurised hydrocarbons across the world. Generally, this method of transportation represents an efficient and safe means of conveying large amounts of hydrocarbons. However pipeline breaks and ruptures can and do occur. In recent years, the Piper Alpha tragedy (Cullen, 1990), as well as numerous other incidents involving pipeline rupture have provided ample examples of the disastrous consequences associated with such types of accidents. According to data reported by the Office of Pipeline Safety in the Unites States, during 1986 to 2000, there were 3116 natural gas pipeline incidents. These resulted in 309 fatalities, 1398 injuries and 478 million dollars of damage to property.

Of these incidents, distribution pipelines (those running in cities for domestic supply) gave rise to 1954 incidents, 267 fatalities 1189 injuries and 227 million dollars in property damage. Transmission pipelines, usually running across miles of woodland and farmland, account for 1162 incidents, 42 deaths, 209 injuries, and 251 million dollars in damages.

The above is equivalent to an average of an incident every two days, an injury every four days, and a fatality every seventeen days. It is alarming to note that such stark statistics are for natural gas pipelines only. They do not account for numerous pipelines scattered across the globe containing other flammable hydrocarbons.

Table 1.1 presents examples of some recent pipeline rupture accidents along with their consequences.

Date	Location	Nature of accident	Consequences
12 June 2003	Cold spring Minnesota USA	Gas pipeline rupture and gas ignition	A gas pipeline worker was hospitalised and 60 customers lost gas service
22 August 2000	Near Ebute-Oko Nigeria	Fuel pipeline explosion	The explosion caused the death of more than 50 people
19 August 2000	Pecos River near Carlsbad New Mexico USA	Natural gas transmission pipeline rupture	12 people, including 5 children, died as a result of the explosion and two nearby steel suspension bridges for gas pipelines crossing the river were extensively damaged
23 October 1999	1.5 km from Toba Singh, Pakistan	Gas pipeline explosion	The explosion killed 13 people and injuring 35
10 June 1999	Bellingham Washington USA	Pipeline rupture	3 people including 2 children were killed. 237000 gallon of gasoline was released into a creek that flowed through Whatcom Falls park in Bellingham
22 January 1999	Bridgereport Alabama	Natural gas pipeline rupture and explosion	3 people were killed and 6 people were injured
February 1998	Near Esmeraldas Refinery Ecuador	Pipeline rupture	Spill of 16,000 barrels of crude oil into a river near the city, and a blaze in neighbouring areas. The disaster killed 14 people and injured more than 52 people
21 July 1997	Indianapolis Indiana USA	Natural gas pipeline rupture and fire	1 people was killed and 1 was injured
24 August 1996	Lively Texas	LPG pipeline rupture	2 people were killed
September 1993	Next to a major highway Venezuela	Natural gas pipeline rupture	At least 50 people were killed

Table 1.1 A listing of some of the most recent accidents relating to pipeline rupture

Pipeline failure may be in the form of full bore rupture, a simple puncture or longitudinal tear. Of these, full bore rupture (FBR) in which the pipeline is split into two across its circumference is by far the most serious due to the ensuing massive release rate. This is particularly important in view of the fact that a typical natural gas pipeline (0.7 m diameter and 150 km long) in the North Sea for example may contain over 750,000 kg of inventory at a normal operating pressure of 150 bar. The energy released following its full bore rupture and subsequent ignition is equivalent to a 100 MW nuclear reactor working continuously over 40 days. Apart from the very likely possibility of undermining the structural integrity of the production platform, FBR can also lead to loss of life as well as significant environmental pollution.

Pipeline ruptures are therefore not isolated events, and such incidents frequently result in serious public safety and environmental consequences. The population density along the oil or gas pipelines is increasing, as a result the number of people and property affected by pipeline accidents is increasing too (Zhu, 1998).

In the recent years, various governments have paid more attention to safety and environmental protection. For instance in the UK until 1996, the health and safety aspects of onshore and offshore pipelines were covered by several sets of regulations of varying scope set by Health and Safety Executive (HSE).

However as a result of formal enquiry following the Piper Alpha disaster, safety legislations were reviewed by HSE. The Pipelines Safety Regulation 1996 (PSR) (HSE, 1996) was introduced under Hazardous and Solid Waste Act (HSWA), as a single set of goal-setting, risk based regulations enveloping health and safety aspects of both onshore and offshore pipelines.

The purpose of the new regulations is to ensure that a pipeline is designed, constructed and operated safely, thereby reducing risks to the environment and personnel. Notably, the new legislation includes guidelines that pay special attention to the need to evaluate the likelihood and consequences of pipeline failure, in order to assist and inform local authorities when preparing emergency plans. Pipeline risk analysis is a vigorous means for safety management authorities to scientifically judge the risk level for existing or proposed pipelines.

In carrying out the appropriate risk analysis particularly when forecasting the consequences of pipeline rupture, the first stage involves the estimation of the release rate and its variation in time (Montiel et al., 1998). However the highly transient nature of the release process as well as the large number of interacting processes involved during the discharge render an analytical solution to this problem impossible (Flatt, 1985a,b; Swaffield, 1993).

In recent years, a number of numerically based models for predicting release rates following FBR of long pipelines containing high pressure hydrocarbon mixtures have been reported. Of these, those reported by Chen et al. (1995a, b) and Mahgerefteh et al. (1997-2000) have been most successful in predicting release rates when compared to real data. However, an important drawback of these models is their limitation to horizontal and uniform diameter pipelines. Pipelines often cross terrains with different inclination. Also, pipeline networks comprising different diameter pipelines are often connected to one another using enlargement sections or joints. The precise effects of such factors on the release process following FBR is unknown.

The aim of this project is to develop a numerical simulation based on the Method of Characteristics (MOC) for investigating the effects of inclination as well as pipeline enlargement on the release process following the FBR of long pipelines containing two-phase hydrocarbon mixtures. The use of pipeline enlargement as a means of reducing the failure hazard following FBR is also investigated.

Two types of accidents scenarios, one based on the rupture at the top end of the inclined pipeline and the other, rupture at the bottom end are investigated. The effect of some key factors such as curved and linear characteristics, time step and pipeline's friction factor on the model's predictions are also examined.

This thesis is divided into 6 chapters. Chapter 2 first describes a review of how the governing conservation equations have been considered in other works followed by the derivation of the appropriate basic equations governing flow, such as momentum, energy and mass conservation incorporating the effect of pipeline inclination. Chapter 3 is a critical review of the various models proposed in recent years for simulating

pipeline rupture. The MOC as the numerical technique employed in this study is also described in the same chapter.

Chapter 4 describes the appropriate compatibility equations and their solution based on the Euler predictor-corrector technique (Zucrow and Hoffman, 1976). The characteristic pathways can be approximated as straight lines (linear characteristics) or as part of parabolas (curved characteristics). Solution methods based on the both assumptions are also discussed in the same chapter. This is followed by the description of the mathematical algorithms used to develop a computer code to model the FBR of inclined and enlarged pipelines.

Chapter 5 deals generally with a discussion of the results of the application of the model to both real and hypothetical failure scenarios, highlighting the salient features. In the first part, the sensitivity of the model's simulations following changes in some key parameters such as linear or curved characteristics, time step and friction factor are investigated and discussed. In the second part, the results of the simulations for inclined and enlarged pipelines are presented. The latter data are used to investigate the potential of using pipeline enlargement as an effective means for reducing the failure hazard following FBR. This is followed by validation of the model against available experimental data. Chapter 6 presents the general conclusion and suggestions for future work.

CHAPTER 2

BASIC EQUATIONS DEFINING TRANSIENT FLOW PROPAGATION IN A PIPELINE FOLLOWING RUPTURE

2.1 INTRODUCTION

The rupture of pressurised pipeline is usually characterised by an enormous discharge rate at the rupture plane followed by a highly transient flow along the rest of the pipeline. The aim of this study is to develop a mathematical model to simulate the fluid's unstable behaviour at any time and space along the pipeline under a variety of pipeline configurations.

Development of such a model necessitates accomplishing three main steps. The first involves formulating the basic equations governing the flow, the thermodynamics, and the pertinent boundary conditions. The next stage requires the solution of derived equations using an accurate and efficient mathematical technique. Finally from a practical point of view, the results of the model should be validated against any available experimental data. An important precursor to the above is the formulation of the pertinent conservation equations relating to mass, momentum or energy.

Solving the full system of the equations is the ultimate goal of a numerical flow simulation but the numerical discretisation necessary to accomplish this for a whole range of fluid flows is extremely difficult requiring substantial computer resources. In fact, only very simplified flow systems are computed at present and these involve a high level of approximation. In undertaking such a task, it is always necessary to consider if it is indeed always required to resolve every term in the Navier-Stokes conservation equations. Depending on the type of flow scenario that needs resolving, certain terms in the equations will have a negligible outcome on the final solution and may therefore effectively be ignored without any serious loss of accuracy.

The final form of these equations, ready for numerical discretisation, can be derived through many assumptions and simplifications. Accordingly, the equations may, in the more general classification, be linear, quasi-linear or non-linear, parabolic or hyperbolic, and first or second-order.

Significant simplifications to the governing equations can greatly reduce computer run times, but this might well be at a cost to accuracy of the final solution. For example, Bell (1978) used a simple exponential model that approximated the mass flow rate by the sum of two exponentials. This however took no account of either the highly non-linear nature of the discharge process, the type of flow or the length of the pipeline. The frictional losses in the pipeline will have important effects on the flow and are of course dependent on the pipeline length. FBR modelling, especially for two-phase flows when thermodynamic computations such as vapour liquid equilibria are important, demands powerful computing resources.

This chapter first describes a review of how the governing conservation equations have been considered in other works. This is then followed by a presentation of the assumptions employed in order to derive the specific governing conservation equations utilised in the present work for simulating both steady and unsteady state flows.

Following the above derivation of conservation equations taking into account the effect of pipeline inclination for both steady and unsteady conditions will be presented.

2.2 REVIEW OF LITERATURE RELATING TO THE GENERAL SYSTEM OF CONSERVATION EQUATIONS ADOPTED FOR SIMULATING TRANSIENT FLOWS

The unsteady flow of compressible fluids in pipelines is described by a set of three partial differential equations derived from the principles of conservation for mass (continuity equation), momentum (Newton's second law of motion) and energy (the first law of thermodynamics). The fluid properties may in turn be described by an

appropriate equation of state. These together with appropriate auxiliary conditions, determine the mathematical state of the fluid. The most complete formulation to describe any fluid flow situation is given by the Navier-Stokes equations which allow for variation of fluid properties in four dimensions, i.e. the three dimensions of space, x, y, and z, and also time, t. In order to resolve these equations numerically closure relations need to be provided to account for both the diffusive and source terms, thus yielding a system of relatively complicated equations.

In most of the studies reviewed here, researchers have made various assumptions and simplifications for different terms, such as friction and inertia force, in the conservation equations in order to simplify these complex equations and consequently to suit a particular method of solution or application. As previously mentioned, appropriate simplifications to the governing equations can greatly reduce computer run times, but this might well be at a cost to accuracy of the final solution. The following is a general overview of these various assumptions. A more detailed description of their effects on the accuracy of the results will be given later.

Van Deen and Reintsema (1983) for example developed a technique, which reduces the energy equation to a single parameter-in-mass equation without the assumption of isothermal or isentropic flow.

Osiadacs (1983,1984) neglected the inertia forces in the equations thereby using a finite difference method for solving a linear model.

Bisgard et al., (1987) accounted for elevation but used a finite element method, which has difficulty in handling the choking condition at the rupture plane. The authors assumed that the pipe is an insulated system without energy exchange with the surroundings. Thus, the law of conservation of energy was not included in their mathematical model and the gas flow was assumed isothermal. Saha (1997) shows that this assumption significantly affects the accuracy of the results.

Fannelop and Ryhming (1982) studied the unsteady flow in a natural gas pipeline in which a break occurred at the high-pressure end. However the authors ignored inertia terms in the conservation equations to obtain a set of parabolic equations.

Levenspiel (1984) and Crowl and Louvar (1990) describe a model for the case of a guillotine rupture of the pipe, assuming adiabatic flow thereby ignoring the important effects of heat transfer from the pipeline to the flowing fluid.

Montiel et al. (1998) reported a model for rupture of gas distribution systems operating at medium and low pressure in which ideal gas behaviour may be assumed using a steady state model. The rupture of the pipeline results in a significant drop in the fluid temperature due to the rapid expansion of the gaseous inventory. In the majority of cases, this will result in the formation of a two-phase mixture for which the behaviour of the inventory will be far from ideal.

Zhou et al. (1997) developed a three-dimensional computational model for natural gas releases from high-pressure pipelines. The authors carried out simulations for obstructed natural gas releases from a pipeline over a range of operating pressures from 8 - 75 bar. In this study no attempt has been made to model the detailed shock within the pipeline or time dependent behaviour, such as expansion-wave propagation in the pipeline and the subsequent decay in mass flow rate. Although the model gives exhaustive description of the fluid physical and thermodynamic properties, the steady state assumption renders it unsuitable for use in modelling the transient release process that characterises pipeline failure.

Sand et al. (1996) modelled a pipeline, subject to a full guillotine break at the low-pressure end. The flow model was divided into two problems. The pipe flow, and the dispersion flow problem, and both were solved using a finite difference control volume scheme. The authors made some simplifying assumptions in order to reduce the complexity of the problem. Firstly they avoided the counter flowing field, which would occur if the pipeline breaks at the high-pressure end. Secondly the authors assumed that the compressible fluid is always in the gas phase, although they included real gas effects in their model. This latter assumption would require the calculation of two-phase flow and also handling the difficulty of phase transition. Finally they assumed that the pipe wall is smooth thus ignoring the important effect of friction on flow.

Jo and Ahn (2002) in their attempt to analyse the hazard areas associated with high-pressure natural gas pipelines briefly studied the rupture of such pipelines. The authors solved very simple steady state equations for an ideal gas to calculate the discharge rate a few minutes after the rupture. They justified the steady state assumption based on the assumption or theory that the highly transient flows prevail for only the first few seconds following the relatively long duration discharge and may therefore be conveniently ignored. A serious drawback of this assumption is due to the fact based on field data (Cullen, 1990) that the majority of the pipeline inventory is lost during the first few seconds of the highly transient flow regime.

2.3 GENERAL ASSUMPTIONS PERTAINING TO THE DERIVATION OF THE CONSERVATION EQUATIONS

In this study, the flow is assumed to be one-dimensional, that is the rate of change of fluid properties normal to the streamline direction is negligible compared with the rate of change along the streamline.

Transient flows encountered during pipeline rupture are frequently two-phase flow even if the initial state of the fluid is single phase. This is in the main a consequence of the quasi-adiabatic decompression process that often follows full-bore rupture. In this study, we assume the homogeneous equilibrium model (HEM) where the two phases move at the same velocity and always at thermodynamic equilibrium with one another. Recent studies (Chen et al., 1993,1995), using field trails conducted by British Gas on the Isle of Grain, have demonstrated the validity of this assumption in the case of FBR of long pipelines (> 100 m). As such separate momentum conservation for each phase are not considered in this study.
Since the aim of this study is to model the rupture of straight pipelines, losses due to bends and obstacles will be neglected.

We assume rupture in long straight pipes that are rigidly anchored and that elasticity of the pipe walls is negligible compared with the compressibility of the fluid. As such fluid structure interactions may be assumed to be negligible compared with frictional and two-phase equilibrium effects (Tiley, 1989).

The equations governing the fluid flow in a pipe must address both steady and unsteady flow conditions. Flow in the pipeline is assumed to be steady state isothermal prior to rupture; however this becomes unsteady due to the highly transient nature of the flow after pipeline rupture. In the following section, the unsteady form of the conservation equations taking into account the effect of inclination will be derived. This will be followed by the derivation of corresponding equations for the specific case of steady state flow for an inclined pipeline prior to rupture. The enlarged pipeline is briefly discussed in this chapter and in more detail in chapter 4.

2.4 CONSERVATION EQUATIONS FOR AN INCLINED PIPELINE: UNSTEADY FLOW

2.4.1 Conservation of Mass

According to figure 2.1, the mass of fluid contained inside the control volume, V is given by

$$\int_V \rho dV$$

The corresponding mass crossing through each surface at time, t is given by

$$\int_A \rho u dA$$

Hence the mass conservation equation can be written as

$$\int_V \frac{\partial \rho}{\partial t} dV + \int_A \rho \cdot u \cdot dA = 0 \qquad (2.1)$$

where

ρ = density

A = cross section area

u= fluid velocity

V = volume

Applying the above equation to the flow model illustrated in figure 2.1 gives the differential form of the conservation of mass.

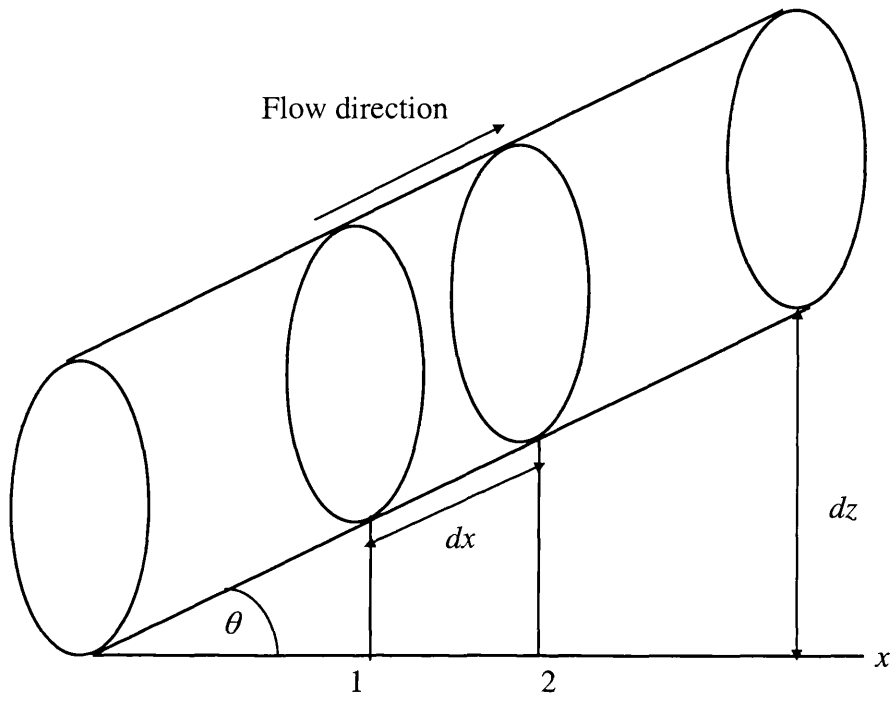

Figure 2.1 Schematic representation of flow model in an inclined pipeline with respect to conservation of mass.

At point 1

The mass flow across the surface = $A \cdot (\rho \cdot u)_{x1}$

At point 2

The mass flow across the surface = $A \cdot (\rho \cdot u)_{x1} + \dfrac{A \cdot \partial(\rho \cdot u)}{\partial x} dx$

The net change of mass because of fluid flowing across the boundary = $A \cdot dx \dfrac{\partial(\rho \cdot u)}{\partial x}$

The unsteady term in equation (2.1) is, ρ_t hence the equation in differential form can be written as

$$\frac{\partial \rho}{\partial t} \cdot dx \cdot A + \frac{\partial(\rho \cdot u)}{\partial x} \cdot dx \cdot A = 0$$

Dividing the above equation by "$dx \cdot A$" yields

$$\rho_t + (\rho \cdot u)_x = 0 \tag{2.2}$$

Expanding equation (2.2) gives

$$\rho_t + \rho \cdot u_x + u \cdot \rho_x = 0 \tag{2.3}$$

Equation (2.3) is the differential form of the mass conservation equation.

2.4.2 Conservation of Momentum

The application of the Newton's second law of motion to the control volume results in the momentum equation. This equation relates the sum of the forces acting on a fluid element to its acceleration or rate of change of momentum in the direction of the resultant force. Moreover the rate of change of momentum within a control volume plus the rate of change of momentum due to fluid flow across the boundary is equal to the external and internal forces acting on the control volume.

Hence the integral form of the momentum equation can be written as

$$F_b + F_s = \int_V \frac{\partial(\rho \cdot u)}{\partial t} dV + \int_A \frac{\partial(\rho \cdot u^2)}{\partial x} dA \tag{2.4}$$

where

F_b = Body forces

F_s= Surface forces

The most common body force is gravitational attraction. So the integral form of body forces, F_b is given by

$$F_b = \int_V B \cdot \rho \cdot dV$$

where, B is the x (horizontal) component of gravity, which acts in the opposite direction of flow and is given by

$$B = g \cdot \sin\theta$$

where, θ is the angle of pipeline inclination with respect to the horizontal plane. Hence

$$F_b = \int_V g \cdot \sin\theta \cdot \rho dV \tag{2.5}$$

The surface forces are those that act on the boundaries of the system by virtue of their contact with the surroundings. Surface forces may be subdivided into normal forces, F_n and tangential forces, F_t, such that

$$F_s = F_t + F_n$$

In the case of the flow of an inviscid fluid, the normal forces are caused by pressure. Thus

$$F_n = \int_A PdA \tag{2.6}$$

The shear and friction forces make up the tangential forces. In the case of an inviscid flow the shear force is zero. The friction force acts in the opposite direction to flow. Thus

$$F_t = F_{friction} = -\int_V \frac{u^2 \cdot \rho}{2} \frac{4 \cdot f_f}{D} dV \tag{2.7}$$

where

f_f = Fanning friction factor

D = pipe diameter

Substituting equations (2.5-2.7) into equation (2.4) produces

$$-\int_V \frac{u^2 \cdot \rho}{2} \frac{4 \cdot f_f}{D} dV - \int_V g \cdot \sin\cdot\theta \cdot \rho dV + \int_A PdA = \int_V \frac{\partial(\rho \cdot u)}{\partial t} dV + \int_V \frac{\partial(\rho \cdot u^2)}{\partial x} dV \tag{2.8}$$

Application of equation (2.8) to the flow diagram illustrated in figure 2.2, gives the differential form of the conservation of momentum shown below.

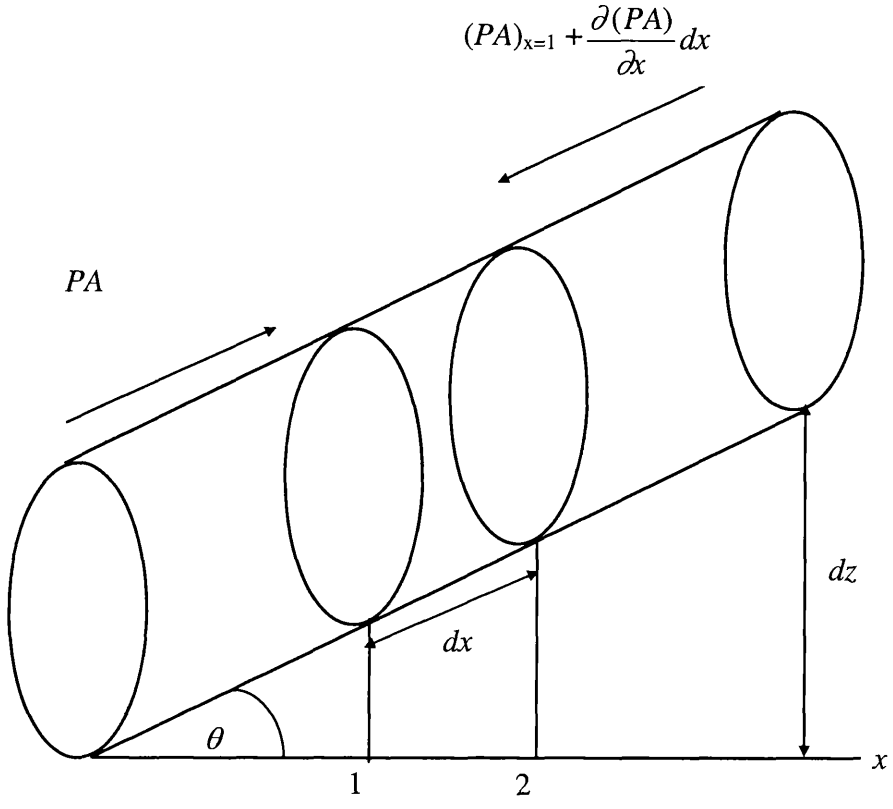

Figure 2.2 Schematic representation of a flow model in an inclined pipeline with respect to conservation of momentum

Referring to figure 2.2 at point 1 the normal force F_n can be written as

$$\int_A PdA = (P \cdot A)_{x=1}$$

At point 2 the normal force F_n can be written as:

$$\int_A PdA = -(P \cdot A)_{x=1} + \frac{\partial(P \cdot A)}{\partial x}dx$$

The negative sign accounts for the force being in the opposite direction of flow. Hence the net amount of normal forces acting on the control volume can be written as

$$-\frac{\partial(P \cdot A)}{\partial x}dx = -A\frac{\partial P}{\partial x}dx \qquad (2.9)$$

Substituting equation (2.9) into equation (2.8) yields

$$-\frac{\rho \cdot u^2}{2}\frac{4 \cdot f_f}{D}dx \cdot A - \rho \cdot g \cdot \sin\theta \cdot dx \cdot A - \frac{\partial P}{\partial x}dx \cdot A = \frac{\partial(\rho \cdot u)}{\partial t}dx \cdot A + \frac{\partial(\rho \cdot u^2)}{\partial x}dx \cdot A \tag{2.10}$$

Dividing equation (2.10) by, Adx produces

$$-\frac{\rho \cdot u^2}{2}\frac{4 \cdot f_f}{D} - \rho \cdot g \cdot \sin\theta = \frac{\partial(\rho \cdot u)}{\partial t} + \frac{\partial(\rho \cdot u^2)}{\partial x} + \frac{\partial P}{\partial x}$$

Rearranging the above equation gives

$$-\frac{\rho \cdot u^2}{2}\frac{4 \cdot f_f}{D} - \rho \cdot g \cdot \sin\theta = (\rho \cdot u)_t + (\rho \cdot u^2)_x + P_x \tag{2.11}$$

Expanding the differential terms in equation (2.11) using the product rule (Stroud, 1990) gives

$$-\rho \cdot g \cdot \sin\theta - \frac{\rho \cdot u^2}{2}\frac{4 \cdot f_f}{D} = P_x + \rho \cdot u_t + \rho_t \cdot u + u^2 \cdot \rho_x + 2 \cdot u \cdot u_x \cdot \rho \tag{2.12}$$

The last term in the RHS of the above equation can be expanded as

$$2 \cdot u \cdot u_x \cdot \rho = (u \cdot u_x \cdot \rho + u \cdot u_x \cdot \rho)$$

Hence equation (2.12) can be written as

$$-\rho \cdot g \cdot \sin\theta - \frac{\rho \cdot u^2}{2}\frac{4 \cdot f_f}{D} = P_x + \rho \cdot u_t + u \cdot u_x \cdot \rho + u \cdot (\rho_t \cdot + u \cdot \rho_x + u_x \cdot \rho) \tag{2.13}$$

The term inside the bracket in the above equation is the same as the continuity equation (equation 2.3). Hence substituting this equation into equation (2.13) produces

$$-\rho \cdot g \cdot \sin\theta - \frac{\rho \cdot u^2}{2}\frac{4 \cdot f_f}{D} = P_x + \rho \cdot u_t + u \cdot u_x \cdot \rho$$

The above equation can be rearranged as

$$P_x + \rho \cdot u_t + u \cdot u_x \cdot \rho = \alpha + \beta \tag{2.14}$$

Or it can be written as

$$P_x + \rho \cdot u_t + u \cdot u_x \cdot \rho = \varpi$$

where

$\varpi = \alpha + \beta$

$\alpha = -\rho \cdot g \cdot \sin\theta$

$$\beta = -\frac{\rho \cdot u \cdot |u|}{2}\frac{4 \cdot f_f}{D}$$

The modulus of the velocity, $|u|$ is introduced so that the friction force opposes the direction of the flow at any given time.

Equation (2.14) is the differential form of the momentum equation for an inclined pipeline.

2.4.3 Conservation of Energy

The first law of thermodynamics states that the sources for the variation of the total energy of a system are the work of the forces acting on the system plus the heat transmitted to this system. The total energy to be considered in a fluid when deriving the conservation equation is the sum of its internal, kinetic and potential energies per unit mass. Therefore based on the first law of thermodynamic we have

$$W_{shaft} + W_{shear} + W_n - Q_h + \int_V \frac{\partial}{\partial t}\left[\rho \cdot \left(e + \frac{u^2}{2} + g \cdot z\right)\right] dV + \int_A \left(e + \frac{u^2}{2} + g \cdot z\right)(\rho \cdot u) dA = 0 \tag{2.15}$$

where:

e = internal energy

z = the inclination height

Q_h = the rate of heat transfer to the fluid

W_{shaft} and W_{shear} are the mechanical work and the shear work respectively. These are assumed to be zero for the present case.

W_n is the work done by normal forces (i.e. pressure). It is given by

$$W_n = \int_A P \cdot u dA \tag{2.16}$$

Substituting equation (2.16) into equation (2.15) yields

$$\int_A P \cdot u dA + \int_V \frac{\partial}{\partial t}\left[\rho \cdot \left(e + \frac{u^2}{2} + g \cdot z\right)\right] dV + \int_A \left(e + \frac{u^2}{2} + g \cdot z\right)(\rho \cdot u) dA = Q_h \qquad (2.17)$$

The work done by pressure forces is positive for mass flowing out of the control volume and negative for mass flowing into it. Application of equation (2.17) to the flow model illustrated in figure 2.3, gives the differential form of the conservation of energy in the following form

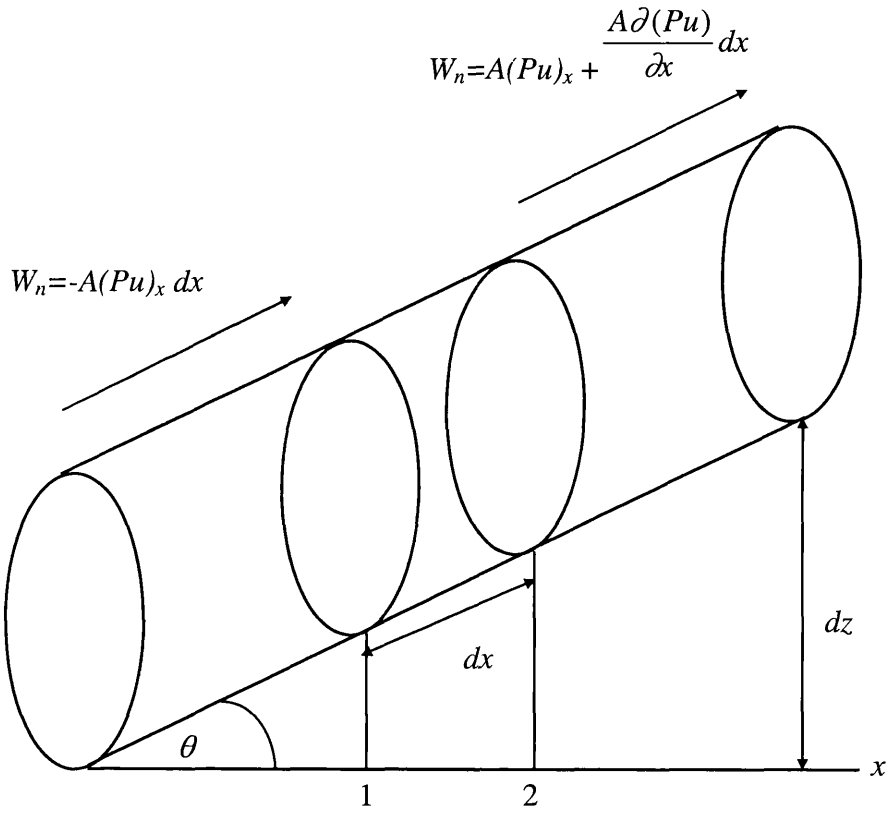

Figure 2.3 Schematic representation of a flow model in an inclined pipeline with respect to conservation of energy

At point 1

$$W_n = -A \cdot (P \cdot u)_x$$

At point 2

$$W_n = A \cdot (P \cdot u)_x + A \cdot \frac{\partial (P \cdot u)}{\partial x} dx$$

Hence the net work of the forces, W_n acting on the system is

$$W_n = A \cdot \frac{\partial (P \cdot u)}{\partial x} dx \tag{2.18}$$

The variation of the total energy of the system with distance can be expressed as the deviation of total energy across the surface at point 1 and 2 and at time, *t*.

Returning to figure 2.3, at point 1 the total energy across the surface may be written as

$A \cdot (\rho \cdot u \cdot E)$

And for point 2 the corresponding total energy is given by

$$A \cdot (\rho \cdot u \cdot E) + A \cdot \frac{\partial (\rho u E)}{\partial x} dx$$

where

E = total energy

So the net rate change of total energy because of fluid flowing across the boundary can be written as

$$A \cdot \frac{\partial (\rho \cdot u \cdot E)}{\partial x} dx \tag{2.19}$$

The unsteady term of the energy equation (equation 2.15), which is the rate of the change of the total energy inside the control volume, can be written as:

$$\frac{\partial (\rho \cdot E)}{\partial t} \cdot dx \cdot A \tag{2.20}$$

Substituting equations (2.20,2.19,2.18) into equation (2.15) produces

$$\frac{\partial (\rho \cdot E)}{\partial t} \cdot dx \cdot A + \frac{\partial (\rho \cdot u \cdot E)}{\partial x} \cdot dx \cdot A + \frac{\partial (P \cdot u)}{\partial x} \cdot dx \cdot A = Q_h \tag{2.21}$$

where, the rate of heat transfer to the fluid from the surrounding is given by

$$Q_h = \frac{4}{D} \cdot U_h \cdot (T_\infty - T) \cdot A \cdot dx$$

where

U_h = overall heat transfer coefficient

T_∞ = surrounding's temperature

T = fluid temperature

The above equation can be written as

$$Q_h = q_h \cdot dx \cdot A \tag{2.22}$$

where

$$q_h = \frac{4}{D} \cdot U_h \cdot (T_\infty - T)$$

Substituting equation (2.22) into equation (2.21) and dividing it by *dxA* produces

$$\frac{\partial(\rho \cdot E)}{\partial t} + \frac{\partial(\rho \cdot u \cdot E)}{\partial x} + \frac{\partial(P \cdot u)}{\partial x} = q_h \tag{2.23}$$

Expanding the differential terms in above equation, using the product rule (Stroud, 1990) gives

$$E\frac{\partial \rho}{\partial t} + E \cdot \rho \frac{\partial u}{\partial x} + E \cdot u \frac{\partial \rho}{\partial x} + \rho \cdot u \frac{\partial E}{\partial x} + \rho \frac{\partial E}{\partial t} + P \cdot u_x + u \cdot P_x = q_h \tag{2.24}$$

Factorising E in equation (2.24) yields

$$E \cdot (\rho_t + \rho \cdot u_x + u \cdot \rho_x) + \rho \cdot u \frac{\partial E}{\partial x} + \rho \frac{\partial E}{\partial t} + P \cdot u_x + u \cdot P_x = q_h \tag{2.25}$$

Replacing the first term in equation (2.25) with the continuity equation (equation 2.3) gives

$$\rho \cdot u \frac{\partial E}{\partial x} + \rho \frac{\partial E}{\partial t} + P \cdot u_x + u \cdot P_x = q_h \tag{2.26}$$

The total energy, E in equation (2.26) may be expressed as

$$E = e + \frac{u^2}{2} + gz = h + \frac{u^2}{2} + gz - \frac{P}{\rho} \tag{2.27}$$

where, h is the specific enthalpy.

Substituting equation (2. 27) into equation (2.26) gives

$$\frac{\partial}{\partial t}\left[\rho\left(h + \frac{u^2}{2} + gz\right) - P\right] + \frac{\partial}{\partial x}\left(\rho u\left(h + \frac{u^2}{2} + gz\right)\right) = q_h \tag{2.28}$$

Introducing the total enthalpy, H

$$H = h + \frac{u^2}{2} + gz \tag{2.29}$$

And substituting equation (2.29) into equation (2.28), gives

$$\frac{\partial}{\partial t}[(H\rho - P)] + \frac{\partial}{\partial x}[\rho u H] = q_h$$

Expanding the differential terms in above equation gives

$$H\frac{\partial \rho}{\partial t} + \rho\frac{\partial H}{\partial t} - \frac{\partial P}{\partial t} + \rho u\frac{\partial H}{\partial x} + H\rho\frac{\partial u}{\partial x} + Hu\frac{\partial \rho}{\partial x} = q_h$$

Factorising the total enthalpy (H) in above equation yields

$$H\left(\frac{\partial \rho}{\partial t} + \rho\frac{\partial u}{\partial x} + u\frac{\partial \rho}{\partial x}\right) + \rho\frac{\partial H}{\partial t} + \rho u\frac{\partial H}{\partial x} - \frac{\partial P}{\partial t} = q_h \qquad (2.30)$$

The first bracket in equation (2.30) can be replaced by the continuity equation (equation 2.3). Hence equation (2.30) can be written as

$$\rho\frac{\partial H}{\partial t} + \rho u\frac{\partial H}{\partial x} - \frac{\partial P}{\partial t} - q_h = 0$$

Substituting for H from equation (2.29)

$$\rho\frac{\partial}{\partial t}\left[h + \frac{u^2}{2} + gz\right] + \rho u\frac{\partial}{\partial x}\left[h + \frac{u^2}{2} + gz\right] - \frac{\partial P}{\partial t} - q_h = 0$$

Expanding the terms in the above equation we have

$$\rho\frac{\partial h}{\partial t} + \rho u\frac{\partial u}{\partial t} + \rho u\frac{\partial h}{\partial x} + \rho u^2\frac{\partial u}{\partial x} + \rho u g\sin\theta - \frac{\partial P}{\partial t} - q_h = 0 \qquad (2.31)$$

Rearranging equation (2.31) we have

$$\rho\frac{Dh}{Dt} + u\left[\rho\frac{\partial u}{\partial t} + \rho u\frac{\partial u}{\partial x} + \rho u g\sin\theta\right] - \frac{\partial P}{\partial t} - q_h = 0 \qquad (2.32)$$

Substituting equation (2.14) into equation (2.32) we have

$$\rho\frac{Dh}{Dt} - u\frac{\partial P}{\partial x} + u\beta - \frac{\partial P}{\partial t} - q_h = 0 \qquad (2.33)$$

$$\rho\frac{Dh}{Dt} - \frac{DP}{Dt} - (q_h - u\beta) = 0$$

For any fluid the following thermodynamic relationship holds

$$dh = Tds + \upsilon dP \qquad (2.34)$$

where, s is the specific entropy and, υ is the specific volume.

Expressing equation (2.34) in substantial derivative form,

$$\frac{Dh}{Dt} = T\frac{Ds}{Dt} + \frac{1}{\rho}\frac{DP}{Dt} \tag{2.35}$$

Substituting equation (2.35) into equation (2.33) we have

$$\rho\left[T\frac{Ds}{Dt} + \frac{1}{\rho}\frac{DP}{Dt}\right] - \frac{DP}{Dt} - (q_h - u\beta) = 0$$

$$\rho T\frac{Ds}{Dt} - (q_h - u\beta) = 0 \tag{2.36}$$

The fluid pressure, P can be expressed as a function of density and entropy, i.e. $P = f(\rho, s)$. Expressed in partial differential form we have,

$$dP = \left(\frac{\partial P}{\partial \rho}\right)_s d\rho + \left(\frac{\partial P}{\partial s}\right)_\rho ds \tag{2.37}$$

where,

$$\left(\frac{\partial P}{\partial s}\right)_\rho = \varphi \tag{2.38}$$

and

$$\left(\frac{\partial P}{\partial \rho}\right)_s = a^2 \tag{2.39}$$

where a = speed of sound.

Equation (2.37) can be expressed in substantial derivative form, that is

$$\frac{DP}{Dt} = a^2\frac{D\rho}{Dt} + \varphi\frac{Ds}{Dt} \tag{2.40}$$

Substituting for Ds/Dt from equation (2.40) into equation (2.36) and re-arranging

$$\frac{DP}{Dt} - a^2\frac{D\rho}{Dt} - \varphi\left[\frac{q - u\beta}{\rho T}\right] = 0 \tag{2.41}$$

If

$$\varphi\left[\frac{q - u\beta}{\rho T}\right] = \psi \tag{2.42}$$

Then equation (2.41) may be expressed as

$$\frac{DP}{Dt} - a^2\frac{D\rho}{Dt} - \psi = 0 \tag{2.43}$$

The above equation, in terms of partial derivatives can be expressed as

$$P_t + u \cdot P_x - a^2(\rho_t + u \cdot \rho_x) = \psi \tag{2.44}$$

Equation (2.44) is the derivative form of energy conservation equation.

The speed of sound, a and the thermodynamic function φ, for real multi-component single-phase fluids are given by (Picard and Bishnoi, 1987)

$$a^2 = \frac{\gamma}{k \cdot \rho} \tag{2.45}$$

$$\varphi = \frac{\rho \cdot \xi \cdot T \cdot a^2}{C_p} \tag{2.46}$$

where, γ is the ratio of specific heats, k and ξ are the isothermal and isobaric coefficients of volumetric expansion, respectively. C_p, is the specific heat capacity at constant pressure.

For two phase flows, the analytical determination of γ and C_p becomes complex (Mahgerefteh et al., 1999). Hence the parameters a and φ are evaluated numerically at a given temperature and pressure. Accordingly

$$a^2 = \left(\frac{\Delta P}{\Delta \rho}\right)_S \tag{2.47}$$

$$\varphi = \rho^2 \cdot \left(\frac{\Delta T}{\Delta \rho}\right)_S \tag{2.48}$$

The Peng-Robinson equation of state (Peng and Robinson, 1976) is employed here in order to obtain the appropriate thermodynamic and phase equilibrium data. This equation has been shown to be particularly applicable to high-pressure hydrocarbon mixtures (see for example de Reuck et al., 1996 and Assael et al., 1996). The number and the appropriate fluid phase(s) present at any given temperature and pressure are determined using the stability test based on the Gibbs tangent plane criterion developed by Michelsen (Michelsen, 1982a, b, Michelsen, 1987). For unstable systems, the same technique also provides the composition of a new phase, which can be split off to decrease the Gibbs energy of the mixture.

Pseudo-fluid properties for mixtures are calculated from the pure liquid and gas properties obtained from the equation of state. Moreover the equation of state is solved for the compressibility factors from which the density of a two-phase mixture can be calculated according to the equation

$$\rho = \frac{\rho_g . \rho_l}{\rho_g . (1 - X) + (\rho_l . X)}$$

Where the subscripts, g and l denote gas and liquid phase respectively. The term, X refers to the fluid quality and is the mass of vapour per unit mass of bulk fluid. The values of respective phase densities can be calculated according to the following equations

$$\rho_g = \frac{P.M_g}{Z_g.R.T}$$

$$\rho_l = \frac{P.M_l}{Z_l.R.T}$$

The mixture viscosity is given by

$$\frac{1}{\mu_m} = \frac{X}{\mu_g} + \frac{(1 - X)}{\mu_l}$$

The gas and liquid viscosities are calculated according to the Ely and Henley scheme for non-polar gaseous mixtures, and Dymond and Assael scheme for liquid mixtures (Assael et al., 1996).

In summary therefore, the following equations are the complete set of equations governing the unsteady flow in an inclined pipeline

$$\rho_t + \rho \cdot u_x + u \cdot \rho_x = 0 \qquad \text{Conservation of mass} \qquad (2.3)$$

$$P_x + \rho \cdot u_t + u \cdot u_x \cdot \rho = \varpi \qquad \text{Conservation of momentum} \qquad (2.14)$$

$$P_t + u \cdot P_x - a^2 (\rho_t + u \cdot \rho_x) = \psi \qquad \text{Conservation of energy} \qquad (2.44)$$

The above equations are just as valid for a non-ideal multi-phase, multi-component fluid as for a perfect gas, providing the following assumptions are always applied:

- Homogeneous flow where the multi-phase mixture moves at the same velocity

- Thermodynamic and phase equilibrium is maintained at each x-t increment.

The equations, which have been derived so far, are a set of conservation equations for fluid flow in an inclined pipeline under unsteady condition. The exceptional cases of steady state and pipeline enlargement will be described in subsequent sections of this chapter.

2.5 CONSERVATION EQUATIONS FOR AN INCLINED PIPELINE: STEADY FLOW

It is assumed that the flow is isothermal steady state prior to rupture. Hence only two conservation equations (mass and momentum) are solved in order to determine the flow properties prior to rupture.

The conservation of mass in an inclined pipeline for steady state flow condition between any two consequent segments may be expressed by

$$\rho_{i-1} \cdot u_{i-1} = \rho \cdot u \tag{2.49}$$

Rearranging the above equation for, u gives

$$\frac{1}{u} = \frac{\rho}{\rho_{i-1} \cdot u_{i-1}} \tag{2.50}$$

Derivation of above equation is given by

$$du = \frac{-d\rho \cdot \rho_{i-1} \cdot u_{i-1}}{\rho^2} \tag{2.51}$$

Conservation of momentum or Newton's second law for an element of fluid flowing in an inclined pipeline, taking into account the effect of friction is presented by:

$$dP + \rho \cdot u \cdot du + \rho \cdot g \cdot dz + \frac{\rho \cdot u^2}{2} \cdot \frac{4 \cdot f_f \cdot dx}{D} = 0 \tag{2.52}$$

Dividing the above equation by, u gives

$$\frac{dP}{u} + \rho \cdot du + \frac{\rho}{u} \cdot g \cdot dz + \rho \cdot u \cdot \frac{2 \cdot f_f \cdot dx}{D} = 0 \tag{2.53}$$

Assuming

$dz = \sin\theta .dx$

And substituting it in equation (2.53) produces:

$$\frac{dP \cdot \rho}{\rho_{i-1} \cdot u_{i-1}} - \frac{d\rho \cdot \rho_{i-1} \cdot u_{i-1}}{\rho} + \frac{\rho^2}{\rho_{i-1} \cdot u_{i-1}} \cdot g \cdot \sin\theta \cdot dx + \rho_{i-1} \cdot u_{i-1} \cdot \frac{2 \cdot f_f \cdot dx}{D} = 0 \tag{2.54}$$

From the equation of state, density in terms of pressure and temperature can be expressed as:

$$\rho = \frac{P}{ZRT} \tag{2.55}$$

Substituting equation (2.55) into equation (2.54) followed by factorising the common terms gives

$$dx \cdot \left(\frac{D \cdot p^2 \cdot g \cdot \sin\theta + (Z \cdot R \cdot T\rho_{i-1} \cdot u_{i-1})^2 \cdot 2 \cdot f_f}{D \cdot Z \cdot R \cdot T}\right) = \frac{dP}{P}((\rho_{i-1} \cdot u_{i-1})^2 \cdot Z \cdot R \cdot T - P^2)$$

Solving the above equation for dx yields

$$dx = \frac{dP}{P}\left[\frac{D \cdot (Z \cdot R \cdot T \cdot \rho_{i-1} \cdot u_{i-1})^2 - D \cdot Z \cdot R \cdot T \cdot P^2}{P^2 \cdot D \cdot g \cdot \sin\theta + (Z \cdot R \cdot T\rho_{i-1} \cdot u_{i-1})^2 \cdot 2 \cdot f_f}\right] \tag{2.56}$$

When u_{i-1}, the initial velocity, is zero, then equation (2.56) becomes

$$-dx = \frac{dP}{P} \cdot \frac{Z \cdot R \cdot T}{g \cdot \sin\theta}$$

Integrating the above equation between points *i*, *i-1* gives

$$\Delta x = \frac{-Z \cdot R \cdot T}{g \cdot \sin\theta} \cdot \ln \frac{P_i}{P_{i-1}}$$

However if compressibility factor is not taken as constant over each segment, applying the trapezoidal rule (Perry, 1973) gives

$$\Delta x = \frac{-Z \cdot R \cdot T}{g \cdot \sin\theta} \cdot \ln \frac{\frac{P_i}{Z_i}}{\frac{P_{i-1}}{Z_{i-1}}} \tag{2.57}$$

The above equation can be used to calculate pressure drop along an inclined pipeline, where the fluid's initial velocity is equal to zero. However if the initial velocity, u_{i-1}, is not equal to zero equation (2.56) must be solved numerically. This equation may be written as:

$$dx = \frac{dP}{P}\left[\frac{A_A - B_B \cdot p^2}{p^2 \cdot H_H + M}\right] \tag{2.58}$$

where

$$A_A = D \cdot \left(Z \cdot R \cdot T \cdot \rho_{i-1} \cdot u_{i-1}\right)^2$$
$$B_B = D \cdot Z \cdot R \cdot T$$
$$H_H = D \cdot g \cdot \sin\theta$$
$$M = (Z \cdot R \cdot T \cdot \rho_{i-1} \cdot u_{i-1})^2 \cdot 2 \cdot f_f$$

Expanding equation (2.58) gives

$$dx = \left(\frac{dP}{P} \cdot \frac{A_A}{P^2 \cdot H_H + M}\right) - \left(\frac{dP \cdot B_B \cdot P}{P^2 \cdot H_H + M}\right) \tag{2.59}$$

And the expression in the first bracket of equation (2.59) by omitting dP and using method of partial fractions (Stroud, 1990) may be expressed as

$$\frac{A_A}{P\cdot(H_H\cdot P^2+M)}=\frac{a_a}{P}+\frac{m_m+n_n\cdot P}{(H_H\cdot P^2+M)} \tag{2.60}$$

Solving equation (2.60) for the coefficients gives

$$A_A=a_a\cdot H_H\cdot P^2+a_a\cdot M+P\cdot m_m+P^2\cdot n_n$$

$$\left.\begin{aligned} &a_a\cdot H_H+n_n=0\Rightarrow n_n=-a_aH_H\\ &A_A=a_a\cdot M\Rightarrow a_a=\frac{A_A}{M}\\ &m_m=0 \end{aligned}\right\}\Rightarrow n_n=-\frac{A_A.H_H}{M}$$

Therefore substituting the above coefficients for n_n and m_m into equation (2.60) produces

$$\frac{A_A}{P\cdot\left[H_H\cdot P^2+M\right]}=\frac{A_A}{M\cdot P}-\frac{A_A\cdot H_H}{M}\cdot\frac{P}{H_H\cdot P^2+M}$$

Multiplying the above equation by dP (which was omitted before) gives

$$dP\cdot\frac{A_A}{P\cdot\left[H_H\cdot P^2+M\right]}=\frac{A_A}{M}\cdot\frac{dP}{P}-\frac{A_A\cdot H_H}{M}\cdot\frac{dP\cdot P}{H_H\cdot P^2+M} \tag{2.61}$$

Applying the quotient rule (Stroud, 1990) to equation (2.61) we have

$$H_H\cdot P^2+M=P^* \tag{2.62}$$

$$dP^*=2\cdot P\cdot H_H\cdot dP \tag{2.63}$$

Substituting equations (2.62) and (2.63) into equation (2.61) gives

$$dP\cdot\frac{A_A}{P\cdot\left[H_H\cdot P^2+M\right]}=\frac{A_A}{M}\cdot\frac{dP}{P}-\frac{A_A}{M}\cdot\frac{1}{2}\cdot\frac{dP^*}{P^*} \tag{2.64}$$

The RHS of equation (2.64) can be replaced by the first term in the RHS of the equation (2.59).

Applying the quotient rule again and substituting equations (2.62), (2.63) into the second term of right hand side of equation (2.59) produces

$$\frac{dP \cdot P \cdot B_B}{H_H \cdot P^2 + M} = \frac{dP^*}{P^*} \cdot \frac{B_B}{2 \cdot H_H} \tag{2.65}$$

Combining equations (2.64) and (2.65) and substituting into equation (2.59) produces

$$dx = \frac{A_A}{M} \cdot \frac{dp}{p} - \frac{A_A}{2 \cdot M} \cdot \frac{dP^*}{P^*} - \frac{B_B}{2 \cdot H_H} \cdot \frac{dP^*}{P^*} \tag{2.66}$$

Reverting to the main expression (equation 2.56) and cancelling out the common terms gives

$$dx = \frac{D}{2 \cdot f} \cdot \frac{dp}{p} - \frac{D}{4 \cdot f} \cdot \frac{dP^*}{P^*} - \frac{Z \cdot R \cdot T}{2 \cdot g \cdot \sin\theta} \cdot \frac{dP^*}{P^*} \tag{2.67}$$

Integrating the above equation produces

$$\Delta x = \frac{D}{2 \cdot f_f} \cdot \ln \frac{P_i}{P_{i-1}} - \left[\frac{D}{4 \cdot f_f} + \frac{Z \cdot R \cdot T}{2 \cdot g \cdot \sin\theta} \right] \cdot \ln \frac{P_i^*}{P_{i-1}^*} \tag{2.68}$$

Substituting for P^* into equation (2.68) yields

$$\Delta x = \frac{D}{2 \cdot f_f} \cdot \ln \frac{P_i}{P_{i-1}} - \left[\frac{D}{4 \cdot f_f} + \frac{Z \cdot R \cdot T}{2 \cdot g \cdot \sin\theta} \right] \cdot \ln \left[\frac{D \cdot g \cdot \sin\theta \cdot P_i^2 + (Z \cdot R \cdot T \cdot \rho_{i-1} \cdot u_{i-1})^2 \cdot 2 \cdot f_f}{D \cdot g \cdot \sin\theta \cdot P_{i-1}^2 + (Z \cdot R \cdot T \cdot \rho_{i-1} \cdot u_{i-1})^2 \cdot 2 \cdot f_f} \right] \tag{2.69}$$

In this study, the compressibility factor (Z) is assumed not to be constant over each segment along the pipeline. Applying the trapezoidal rule (Perry, 1973) and following the same techniques employed above gives

$$\Delta x = \frac{D}{2 \cdot f_f} \cdot \ln \frac{\frac{P_i}{Z_i}}{\frac{P_{i-1}}{Z_{i-1}}} - \left[\frac{D}{4 \cdot f_f} + \frac{Z_{av} \cdot R \cdot T}{2 \cdot g \cdot \sin\theta} \right] \cdot \ln \left[\frac{D \cdot g \cdot \sin\theta \cdot \left(\frac{P_i}{Z_i} \right)^2 + (Z_{av} \cdot R \cdot T \cdot \rho_{i-1} \cdot u_{i-1})^2 \cdot 2 \cdot f_f}{D \cdot g \cdot \sin\theta \cdot \left(\frac{P_{i-1}}{Z_{i-1}} \right)^2 + (Z_{av} \cdot R \cdot T \cdot \rho_{i-1} \cdot u_{i-1})^2 \cdot 2 \cdot f_f} \right] \tag{2.70}$$

where

$$Z_{av} = \left(\frac{Z_i + Z_{i-1}}{2} \right)$$

Equation (2.70) must be solved numerically to obtain the steady state pressure drop along an inclined pipeline. The method has been used in this study to solve the above equation will be discussed in chapter 4.

For horizontal pipelines ($\theta = 0$), there is a discontinuity in the third term of the equation (2.70). This singularity at $\theta = 0$ can be removed by applying L'Hopital's Rule (Stroud, 1990)

$$\lim_{\theta \to 0} \frac{Z_{av}.R.T}{2.g.\sin\theta} \cdot \ln \left[\frac{D \cdot g \cdot \sin\theta \cdot \left(\frac{P_i}{Z_i}\right)^2 + (Z_{av} \cdot R \cdot T \cdot \rho_{i-1} \cdot u_{i-1})^2 \cdot 2 \cdot f_f}{D \cdot g \cdot \sin\theta \cdot \left(\frac{P_{i-1}}{Z_i - 1}\right)^2 + (Z_{av} \cdot R \cdot T \cdot \rho_{i-1} \cdot u_{i-1})^2 \cdot 2 \cdot f_f} \right] =$$

$$\lim_{\theta \to 0} \frac{Z_{av}.R.T}{2.g.\cos\theta} \cdot \frac{B\cos\theta \cdot (C\sin\theta + A) - [C\cos\theta \cdot (B\sin\theta + A)]}{(C\sin\theta + A) \cdot (B\sin\theta + A)}$$

where

$$A = (Z_{av} \cdot R \cdot T \cdot \rho_1 \cdot u_1)^2 \cdot 2 \cdot f_f$$

$$B = D \cdot g \cdot \left(\frac{P_i}{Z_i}\right)^2$$

$$C = D \cdot g \cdot \left(\frac{P_{i-1}}{Z_{i-1}}\right)^2$$

Hence

$$\lim_{\theta \to 0} \frac{Z.R.T}{2.g.\cos\theta} \cdot \frac{B\cos\theta \cdot (C\sin\theta + A) - [C\cos\theta \cdot (B\sin\theta + A)]}{(C\sin\theta + A) \cdot (B\sin\theta + A)} = \frac{ZRT}{2.g} \cdot \frac{B - C}{A}$$

Substituting A,B and C in the above equation gives

$$\frac{Z_{av}RT}{2.g} \cdot \frac{B - C}{A} = \frac{D \cdot \left(\left(\frac{P_i}{Z_i}\right)^2 - \left(\frac{P_{i-1}}{Z_{i-1}}\right)^2 \right)}{4.f_f.Z.R.T.(\rho_i u_i)^2} \qquad (2.71)$$

Hence, substituting $\theta = 0$ and equation (2.71) in to equation (2.70) yields

$$\Delta x = \frac{D}{2 \cdot f_f} \cdot \ln \frac{\frac{P_i}{Z_i}}{\frac{P_{i-1}}{Z_{i-1}}} - \frac{D \cdot \left(\left(\frac{P_i}{Z_i} \right)^2 - \left(\frac{P_{i-1}}{Z_{i-1}} \right)^2 \right)}{4.f_f.Z_{av}.R.T.(\rho_i u_i)^2} \tag{2.72}$$

However if the compressibility factor is assumed to be constant over each segment equation (2.72) is reduced to its simpler form (equation 2.73)

$$\Delta x = \frac{D}{2 \cdot f_f} \cdot \ln \frac{P_i}{P_{i-1}} - \frac{D \cdot \left(P_i^2 - P_{i-1}^2 \right)}{4.f.Z.R.T.(\rho_i u_i)^2} \tag{2.73}$$

Either equation (2.72) or (2.73) has to be solved numerically to determine the steady state pressure drop along a horizontal pipeline.

2.6 ENLARGED PIPELINE

Enlarged pipeline can be treated as two uniform pipelines, which are connected via an enlarged section (see figure 4.7). The governing equations for the two uniform pipelines have already been discussed. These include equation 2.71 for steady state flow and the set of conservation equations (equations 2.3,2.14 and 2.44) for unsteady state flow ignoring the gravitational term. The enlarged section can be treated as two different boundary conditions, which will be discussed in detail in chapter 4.

2.7 CONCLUSION

In order to study the behaviour of fluid flow in a pipeline following rupture it is necessary to first develop the basic conservation equations relating to mass, momentum and energy. Since the condition in the pipe is steady state prior to rupture and highly transient following rupture, it is necessary to study both the steady and the unsteady state flow phenomena.

Generally the conservation equations adopted for modelling pipeline rupture are derived by making some assumptions. This chapter first described a review of how the governing conservation equations have been formulated in other works.

Following to the above, the basic fluid flow conservation equations for pipeline inclination for both steady and unsteady state conditions were derived in this chapter. These together with equations presented in section 4.6 will also be used in modelling the rupture of an enlarged pipeline. The corresponding solution techniques and algorithms for modelling both scenarios will be extensively discussed in chapter 4.

The conservation equations, which have been derived in this chapter, are partial differential equations, which are hyperbolic in nature. There is no analytical solution for these equations so a numerical method must be utilized to solve these equations. The numerical methods available for the solution of these equations will be briefly illustrated in the following chapter. Thereafter, the method employed in this study to solve these equations will be explained in detail. A comprehensive literature survey on the study of modelling pipeline rupture is presented in the same chapter.

CHAPTER 3

REVIEW OF NUMERICAL METHODS FOR THE SOLUTION OF CONSERVATION EQUATIONS

3.1 INTRODUCTION

The partial differential equations pertaining to conservation of mass, momentum and energy, derived in chapter 2, are a set of quasi-linear hyperbolic partial differential equations that must be solved numerically.

This chapter deals with a review of available numerical methods for the above followed by a brief history of development of Method of Characteristics (MOC). Particular attention is paid to the description of the mathematical formulation of MOC and its different methods of application as it is ultimately the selected numerical solution technique utilised in this work for the simulation of the special case involving fluid flow following the rupture of enlarged or inclined pipelines described chapter 4.

Finally a literature review of previous work relating to the application of different numerical solution techniques for the problem of pipeline rupture, and where applicable, the evaluation of their performance against available experimental data is presented.

3.2 REVIEW OF THE NUMERICAL METHODS OF SOLUTION

Since the basic equations of momentum and continuity are quasi-linear, hyperbolic partial differential equations, a closed-form solution of the equations is impossible. However by neglecting or linearising the non-linear terms various graphical (see for example Parmakian, 1963; Bergeron, 1961; Pickford, 1969 and Enever, 1970) and analytical (see for example Allievi, 1903; Rich, 1963 and Wood, 1938) methods have

been developed. These methods are approximate and cannot be used to analyse systems incorporating complex boundary conditions.

Other techniques are more suitable for computer simulation, such as the implicit finite-difference method (see for example Perkins et al., 1964), and the method of characteristics (see for example Lister, 1960; Evangelisti, 1969; Abbot, 1966; Swaffield, 1972; Streeter, 1967; Boldy, 1975; Chaudhry, 1987; Fox, 1977,1989; Wylie and Streeter, 1978, 1983).

In the implicit finite-difference method, the partial derivatives are replaced by finite differences and the resulting algebraic equations for the whole system are then solved simultaneously. Depending upon the size of the system, this involves the simultaneous solution of a large number of non-linear equations. The analysis by this method becomes even more complicated for systems, which incorporate complex boundary conditions, which must be solved by an iterative technique. The method has the advantage of being unconditionally stable; therefore large time steps may be used resulting in a reduction in the computational demand. However the time step cannot be increased arbitrarily since this will result in a smoothing of the transient pressure peaks.

In MOC the partial differential equations are converted into ordinary differential equations, which are then solved using an explicit finite-difference technique. Because each node point and boundary condition is analysed individually at each time step, the method is particularly suitable for systems containing complex boundary conditions.

The disadvantage of MOC is that small time steps must be used in order to satisfy the stability criterion, but this is now less of a problem due to the rapid advances in the speed of operation of modern computers.

The method of characteristics is generally accepted as the most appropriate technique for developing computer simulation programs for transient flow in internal fluid flow systems (Swaffield, 1993).

3.3 DEVELOPMENT OF THE METHOD OF CHARACTERISTICS; A HISTORICAL REVIEW

The method of characteristics is a general mathematical technique that is particularly suited to the solution of pairs of quasi-linear hyperbolic partial differential equations linking two dependent and two independent variables.

Rieman (Swaffield, 1993) first proposed the method in 1860 while studying finite amplitude sound wave propagation. Massau (1900) employed the method in a study of unsteady flow in open channels. The first application to pressure transient analysis was due to Lamoen (1947), while later contributions by Gray (1953,1954) received wider attention. Both authors works were limited by the unavailability of computers. Following Gray's, work a considerable number of publications appeared in the USA employing this technique; among the first being Ezekial and Paynter (1957) and most significantly Streeter with a number of co-authors, (1962,1966,1967,1969). Much of the published work rested on the presentation of the MOC by Lister (1960), which remains the basis for the analytical techniques in this work.

In the UK and Europe interest in the use of MOC developed rapidly with papers by Fox (1968), Evangelisti (1969), Swaffield (1970) and by the early 1970s, this technique was established as the standard method for transient analysis; a fact clearly evident in the wide range of international papers presented at the first BHRA Pressure surge conference in 1972.

Streeter and Lai (1962) claimed that MOC was equivalent of treating the frictional loss as an uniformly distributed loss along the whole pipeline. However this is strictly not the case, rather the method extends and improves upon the graphical technique's (see for example Parmakian, 1963; Bergeron, 1961; Pickford, 1969 and Enever, 1970) friction joint approach by utilising the computer's ability to introduce as many friction joints as the analyst would wish, thus allowing the model to approach the continuously distributed friction loss effect. This discussion was active in the 1960s, particularly supported by the last users of the graphical method and a comparison to MOC solution will reveal more similarities than differences between the two

approaches; Enever (1970). Both methods rely on the modelling of the transmission of changes in flow conditions through the pipe network along lines in the time–distance plane whose slopes are determined by fluid velocity and wave speed. Likewise both represent frictional losses at discrete locations based upon the application of steady uniform flow values of friction factor to the local unsteady flow condition.

3.4 THE METHOD OF CHARACTERISTICS; ITS MATHEMATICAL DESCRIPTION

The method of characteristics is essentially an explicit finite difference scheme with a sufficiently different approach to warrant separate treatment. It is based on the principle of the propagation of characteristic waves and is therefore well suited to handling fast transient flows where each disturbance is captured along the propagating wave. These characteristics, which are schematically presented in figure 3.1 can handle any type of discontinuity in fluid flow such as a shock wave, contact surface or expansion fan. The speed of propagating of these waves known as Mach lines, are given by $(u+a)$ corresponding to the right running characteristics or C_+ and $(u-a)$ corresponding to the left running characteristic or C_-. The path line characteristic or C_0 is given by (u).

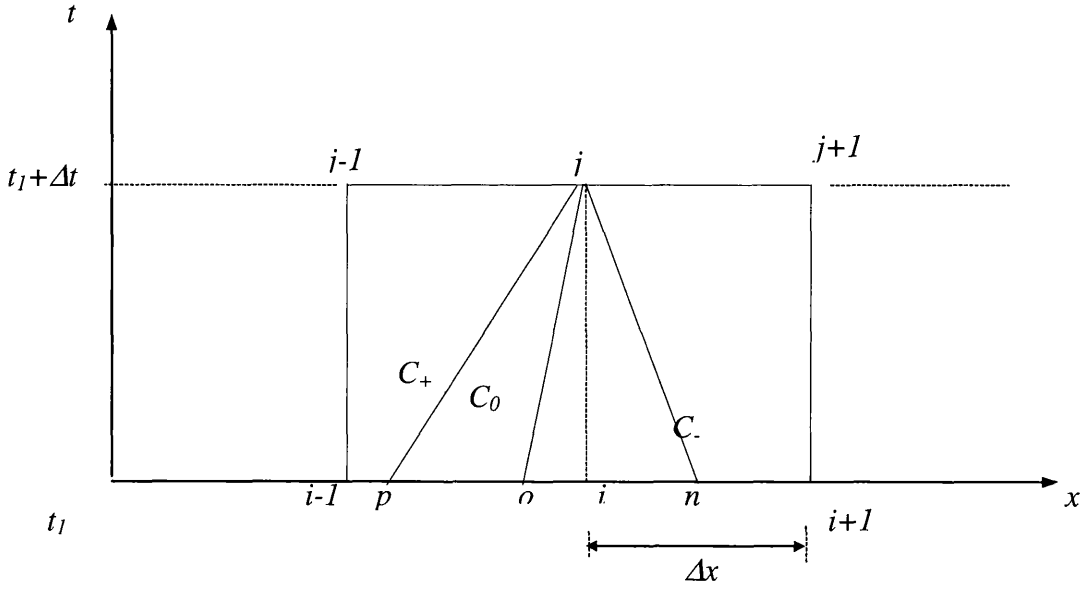

Figure 3.1 Schematic representations of path line (C_0) and Mach lines (C_+, C_-) characteristics at a grid point along the time (t) and space (x) axes

By an appropriate choice of co-ordinates, the characteristic lines can be defined such that the system of partial differential equations, which were derived in chapter 2, may be converted into ordinary differential equations. These are termed as the compatibility equations and may be solved by standard single step finite-difference methods for ordinary differential equations.

There are two main grid discretrisation methods for MOC. These include Characteristic Grid method (CG) which is also known as natural method of characteristics, and the Inverse Marching method or the method of Specified Time Intervals (ST) (Flat, 1986).

In the Characteristic Grid method, characteristic co-ordinates are applied to two equations in two dependent variables and this is often the case when isothermal flow assumption is made (see for example Wylie and Streeter, 1993). Applying the method of characteristics in this way makes it particularly simple. However Chen et al. (1993) extended this method to the three characteristics model necessary to describe non-isothermal transient fluid flow and this is referred to as the Wave Tracing method.

In any characteristic grid method, the position of the new solution point is not specified a priori, but is determined from the intersection of left and right running characteristics with origins located at known solution points or initial data. Hence a free-floating grid is developed in the x-t plane as shown in figure 3.2. This method of characteristics is particularly accurate since the solution progresses naturally along the characteristic lines. However, when more than two characteristic lines are present, i.e. when an energy equation is solved in addition to the mass and momentum conservation equations, a path line (C_0 characteristic with velocity, u) is present in addition to the two Mach lines (C_+ and C_- with velocity $u+a$ and $u-a$ respectively) and this requires some interpolation to locate the path line intersection between known initial points.

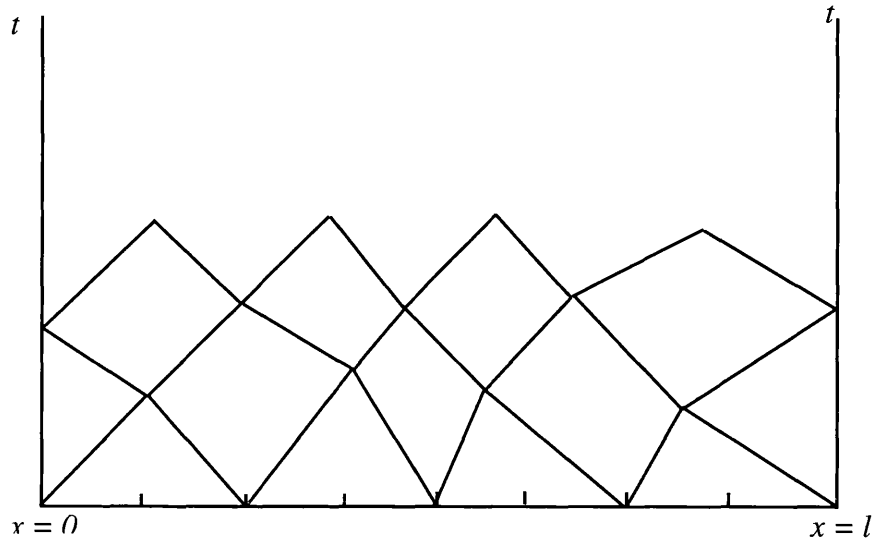

Figure 3.2 Schematic representation of The Characteristic Grid method

The main advantage of the CG (Characteristic Grid) method or natural method of characteristics is that discontinuities can be handled and that large time steps are possible since they are not restricted by a stability criterion (Thorley and Tiley, 1987). However this method has two main disadvantages when dealing with rapid gas transients. As mentioned earlier, the first is that if more than two dependent variables are required to describe the system then the complexity of the computation increases. The second major drawback is that if the solutions of variables are required at fixed time intervals, then two-dimensional interpolation in the characteristic net is required and this can be very complicated. To overcome this second complication the Mesh method of characteristics, which is also called Inverse Marching, method or method of Specified Time Intervals was developed (Courant et al., 1952)

In this method (see figure 3.3) the location of the solution points in the space-time grid is specified a priori and the characteristic lines are extended backwards in time to intersect a time line on which initial-data points are known from a previous solution. This necessitates interpolation to locate the intersection of all three characteristic lines and as a result can lead to a greater loss of accuracy than the CG method.

As previously shown in this section, the MOC has many advantages compared with other numerical methods of solution. Discontinuities in the initial value may propagate along the characteristics, making it easy to handle. The boundary conditions are properly posed. The method of characteristics is relatively accurate but requires the choice of a suitable time step. The method can be readily adapted to solve for three dependant variables required for analysis of non-isothermal transient fluid flow.

The MOC is chosen as the numerical scheme in this work on the basis that it has the great advantage of being conceptually descriptive of the transmission of the fluid flow transients through a pipeline (Douglas, 1995). It has been proven to be an accurate tool for the solution of hyperbolic equations and is relatively simple to program (Saha, 1997). As previously mentioned the CG method becomes very complicated when dealing with all three conservation equations. In addition, it does not permit both the easy modelling of an enlarged section as a fixed point within the pipe and the inclusion of pumping as a boundary condition. Based on the above findings, the ST method is adopted for the purpose of this study.

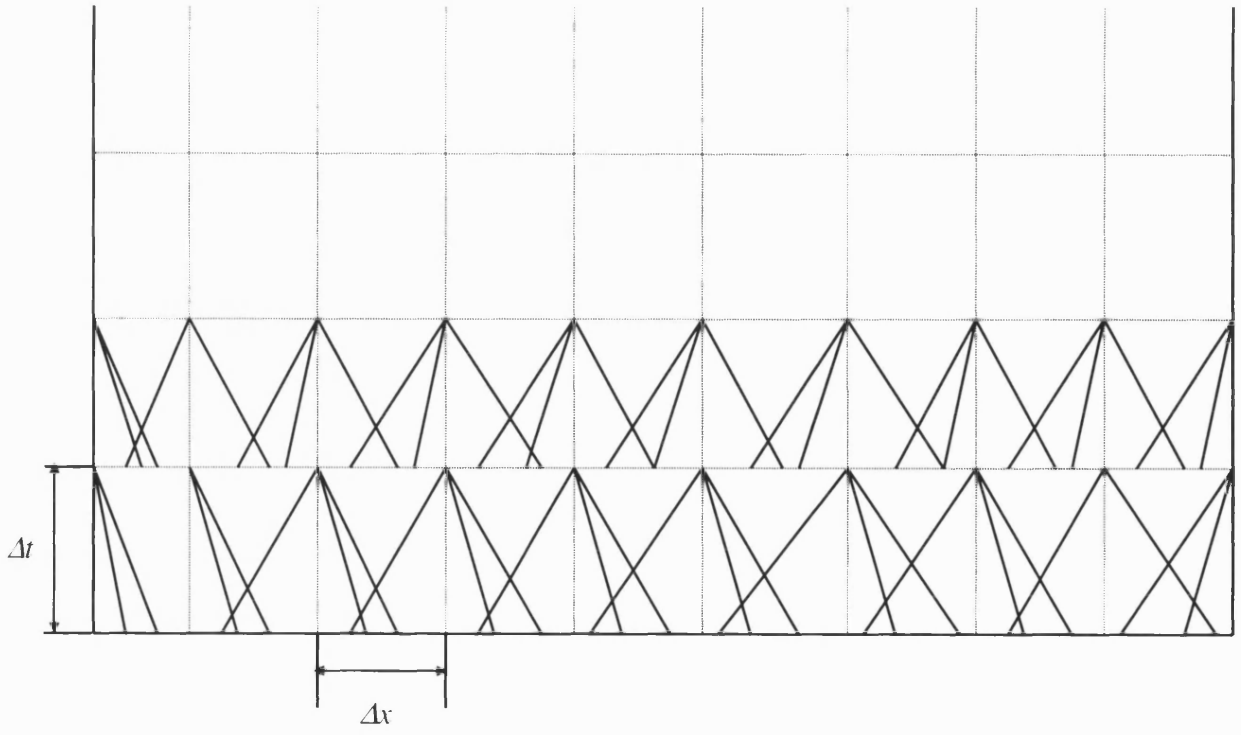

Figure 3.3 Schematic Representation of the Method of Specified Time Intervals

3.5 LITERATURE REVIEW OF WORK RELATING TO THE SIMULATION OF PIPELINE RUPTURE

The literature relating to fluid pressure transient propagation is extensive and covers the last 100 years. Contributions range from the purely theoretical, such as early attempts to use Laplace transforms, discussions of analytical methods, to reports of particular transient conditions in individual plant or fluid systems.

The scope of this review is restricted to the works related to the formulation of the governing equations for transient flow wave propagation, the mathematical methods employed to solve those equations as well as, where appropriate, comparison of the model results with experimental data.

As explained in chapter 2, the partial differential equations pertaining to conservation of mass, momentum and energy together with an equation of state (EOS) constitute a system of equations that are Euler equations. These incorporate stiff source terms due to the friction and heat transfer terms in the momentum and energy equations respectively. The Euler equations constitute the most complete description of inviscid, non-heat conducting flows and hence, is the highest level of approximation for non-viscous fluids. Obviously the inviscid flow models are not applicable on a universal basis, but the importance of their accurate numerical simulation resides in the dominating convective character of the Navier-Stokes equations at high Reynold numbers. Therefore most numerical methods developed for the Euler equations are also valid for the Navier-Stokes equation. It is only at very low Reynolds numbers, when the flow is diffusion dominated, that specific methods for the Navier-Stokes equations have to be defined.

The majority of the techniques for modelling pipeline rupture and blowdown are based on the method of characteristics (MOC). The rest are either based on various finite element or finite difference schemes. The following is a review of work reported employing these methods.

Sens et al. (1970) used an explicit finite difference method for the numerical solution of partial differential equations to simulate transient flow in a gas pipeline a few seconds after rupture. The model is intrinsically one-dimensional and assumes perfect gas behaviour. The latter ignores the highly probable condensation of the fluid inventory due to its rapid expansion induced cooling at the rupture plane. This will inevitably affect the fluid dynamics, particularly the discharge rate.

In 1978, a study was funded and conducted by the Alberta Petroleum Industry, Government Environmental Committee (APIGEC, 1978) to evaluate and improve the H_2S isopleth prediction techniques. All three phases involved in gas release and dispersion from a pipeline following failure were considered. These are: blowdown phase, atmospheric dispersion phase and plume rise phase. The last two phases are not of interest to this current study, hence only the blowdown phase is herein discussed. Two blowdown models were employed to create the common blowdown curves, which were later used for dispersion calculations. These were INTERCOMP TRANSFLOW blowdown model and a simplified exponential blowdown model. The INTERCOMP TRANSFLOW model is based on momentum; mass and energy balances in a numerical simulator and these were used to calculate the time curve defining the rate of gas blowdown from the pipeline. Among other things, the model has the capability of including valve closure time, frictional effects, and gas flow rate in the line before rupture in the calculations. No more information about the model in the report is supplied, and the reader has been referred to the INTERCOMP program documentation (APIGEC, 1978) for more details about the TRANSFLOW model. The results from the TRANSFLOW blowdown model were presented in graphical format as reproduced in figures 3.4-3.11. Based on these results, the following observations may be made:

1. The blowdown curve for the base case shows the typical high initial flow rate with rapid decline, which is characteristic of pipeline ruptures. The slight bump or "knee" in the curve is caused by closure of the block valves; figure 3.4 (APIGEC, 1978).

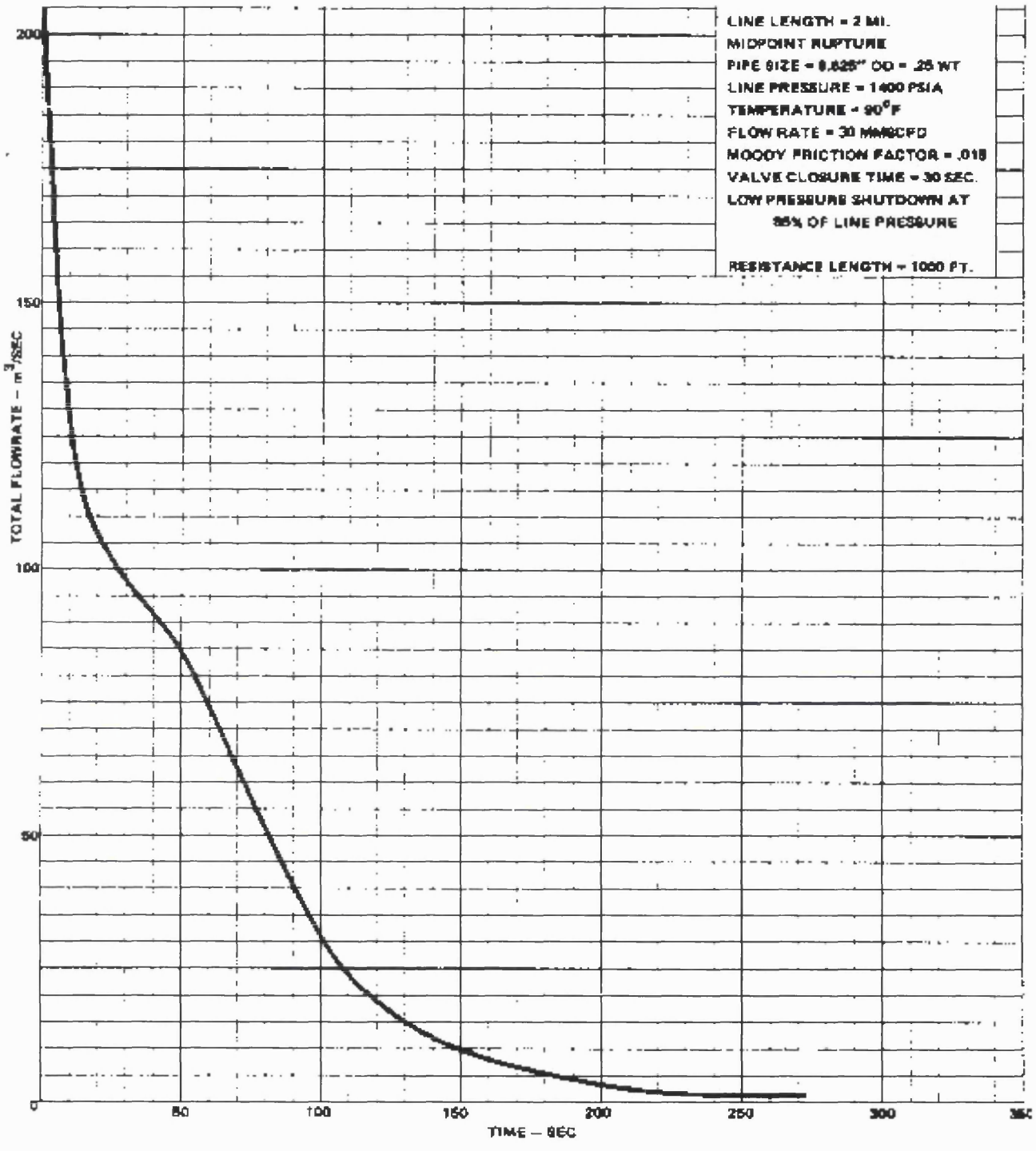

Figure 3.4 Blowdown model sensitivity test, flow rate variation with time (APIGEC, 1978)

2. Replacing the downstream block valve with a check valve reduces the "knee" but does not significantly affect the overall curve; figure 3.5 (APIGEC, 1978).

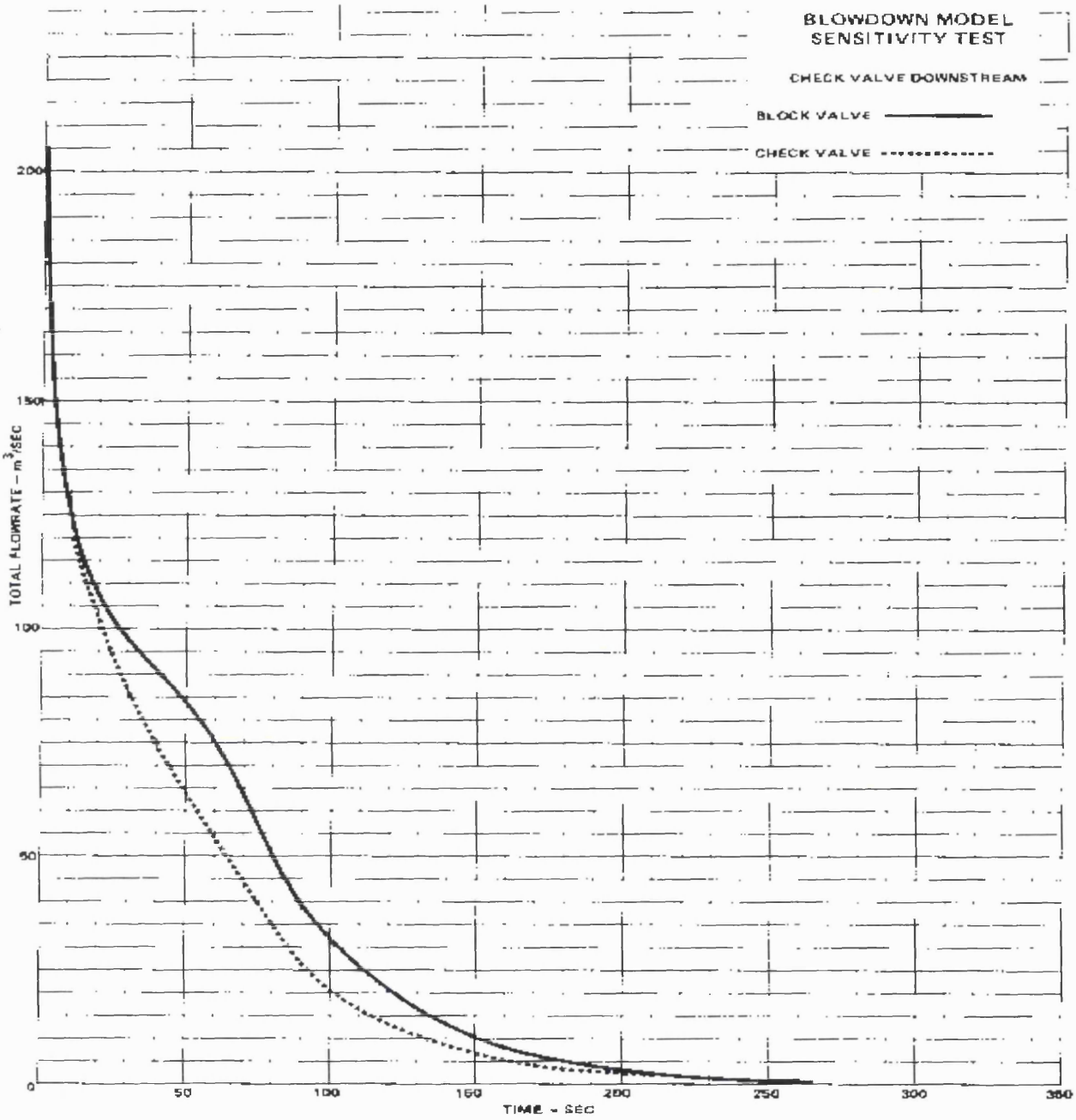

Figure 3.5 The effect of replacing the downstream block valve with a check valve on blowdown rate (APIGEC, 1978)

3. As predicted by theory, the long pipeline length strongly affects the shape of the decline portion of the curve, but has no effect on the initial release section; figure 3.6 (APIGEC, 1978).

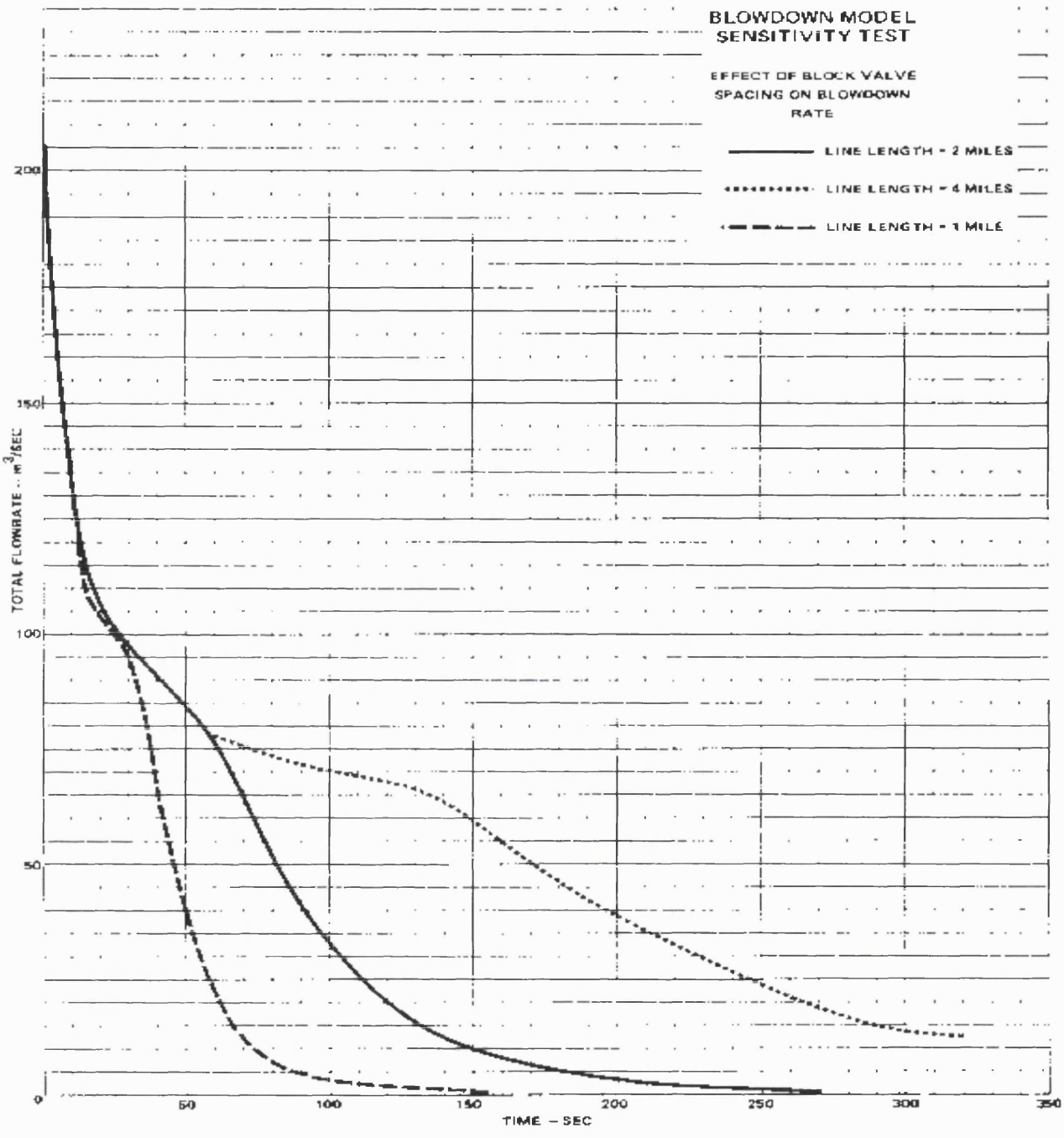

Figure 3.6 The effect of line length on blowdown rate (APIGEC, 1978)

4. As expected, that initial flow is directly proportional to pressure, the initial release portion of the curve is shown to be strongly influenced by the line pressure; figure 3.7 (APIGEC, 1978).

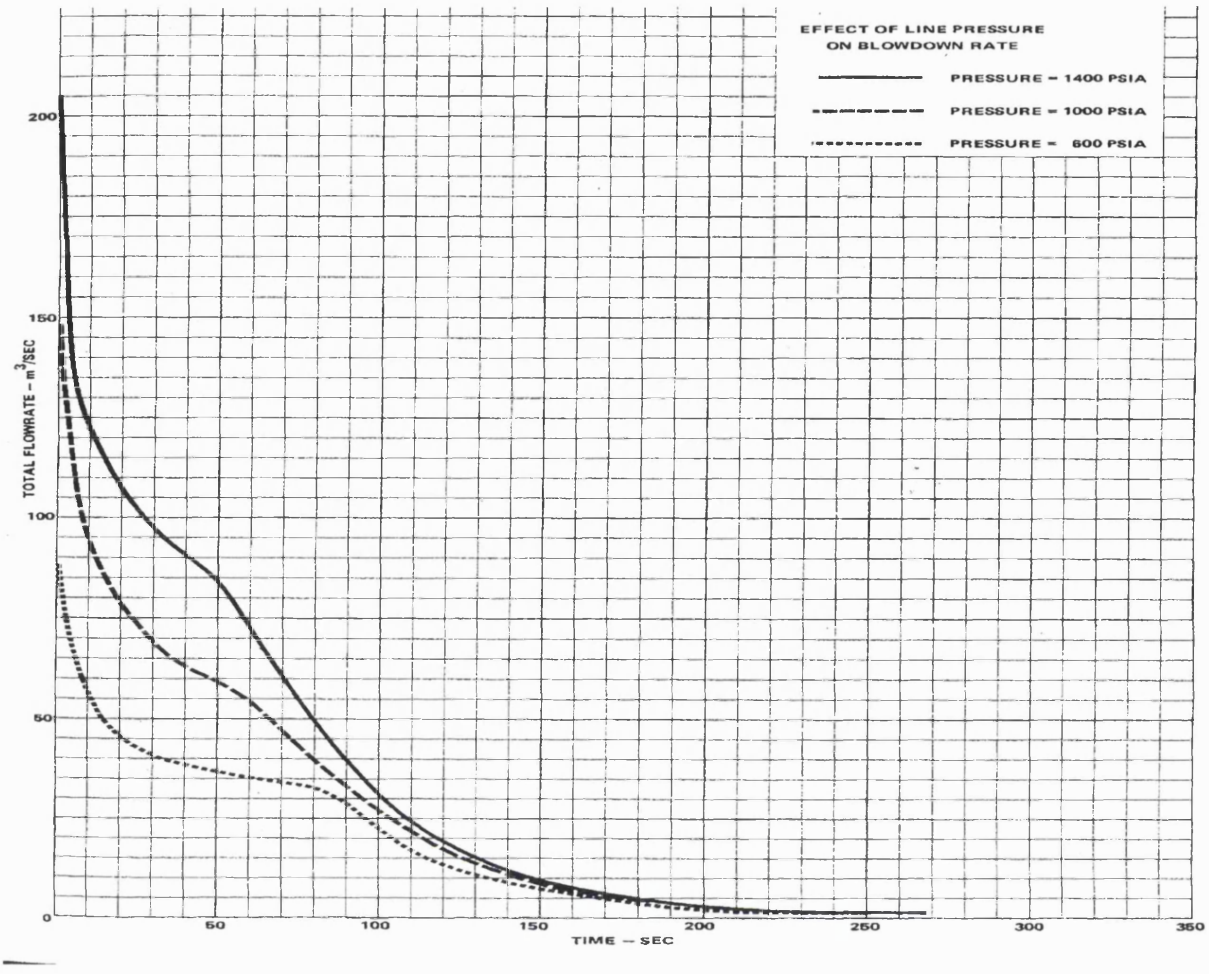

Figure 3.7 Effect of line pressure on blowdown rate (APIGEC, 1978)

5. The initial gas temperature has little effect on the blowdown; figure 3.8 (APIGEC, 1978).

6. Gas flow rate in the line before rupture, for the same diameter line has little effect on the blowdown curve. This is to be expected since the gas velocity immediately after rupture is two orders of magnitude higher than that before rupture. However line diameter has a strong influence on blowdown rates. This is shown in figure 3.9 and to be expected since the discharge rate is proportional to the square of the line diameter; figure 3.9 (APIGEC, 1978).

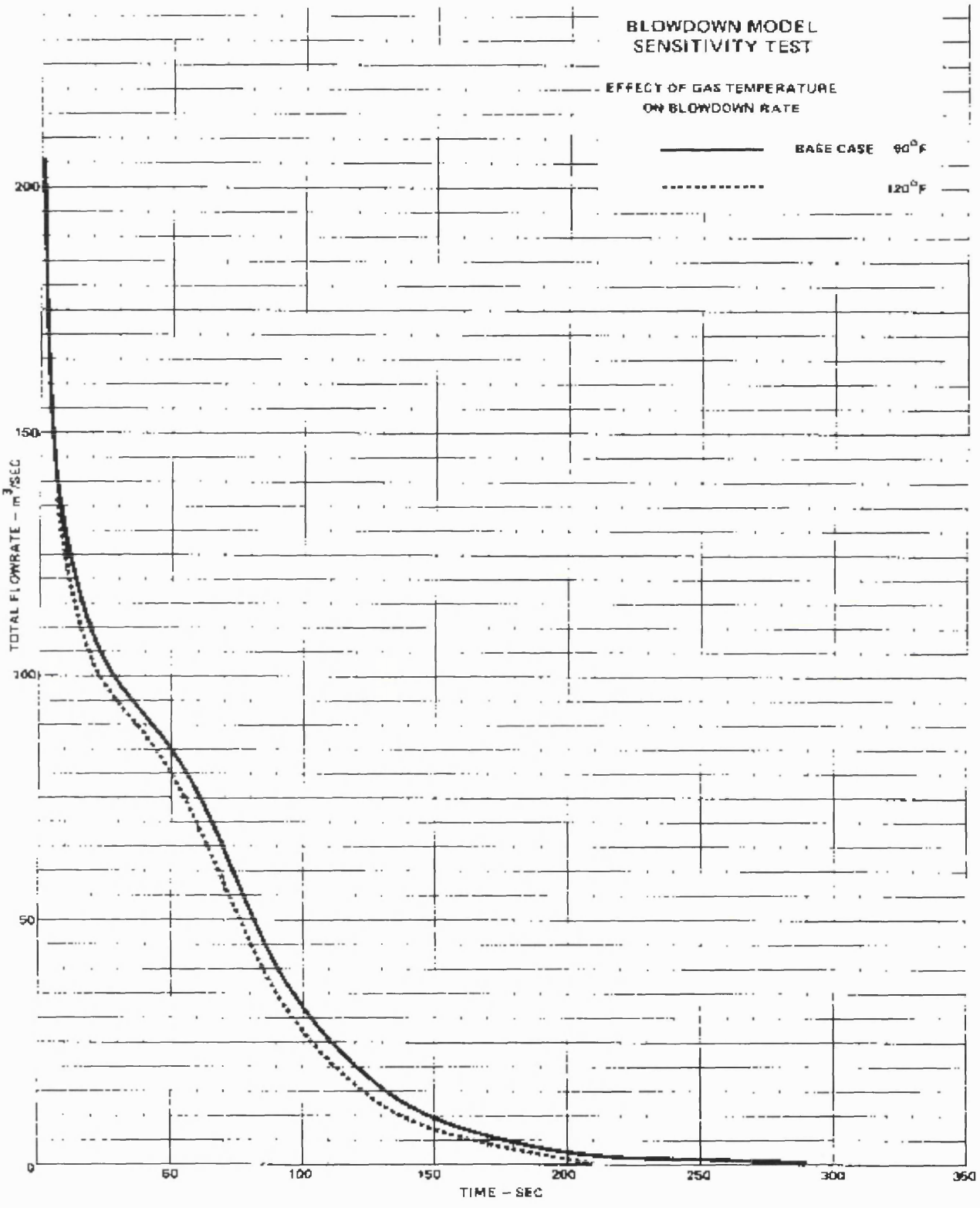

Figure 3.8 The effect of line temperature on blowdown (APIGEC, 1978)

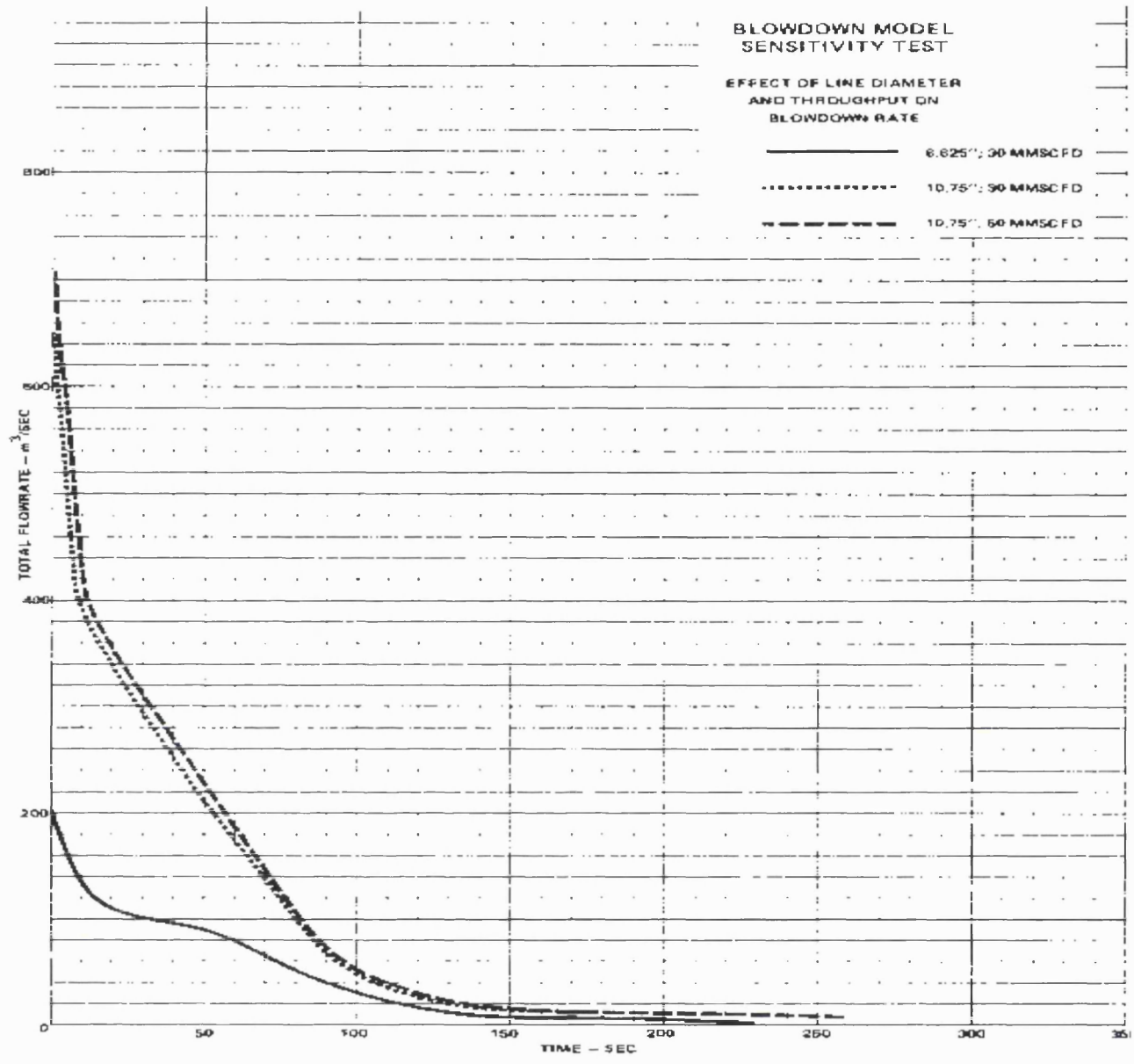

Figure 3.9 The effect of line diameter and throughput on blowdown rate (APIGEC, 1978)

7. Valve closure time is shown to have a minor effect on the blowdown curve; figure 3.10 (APIGEC, 1978).

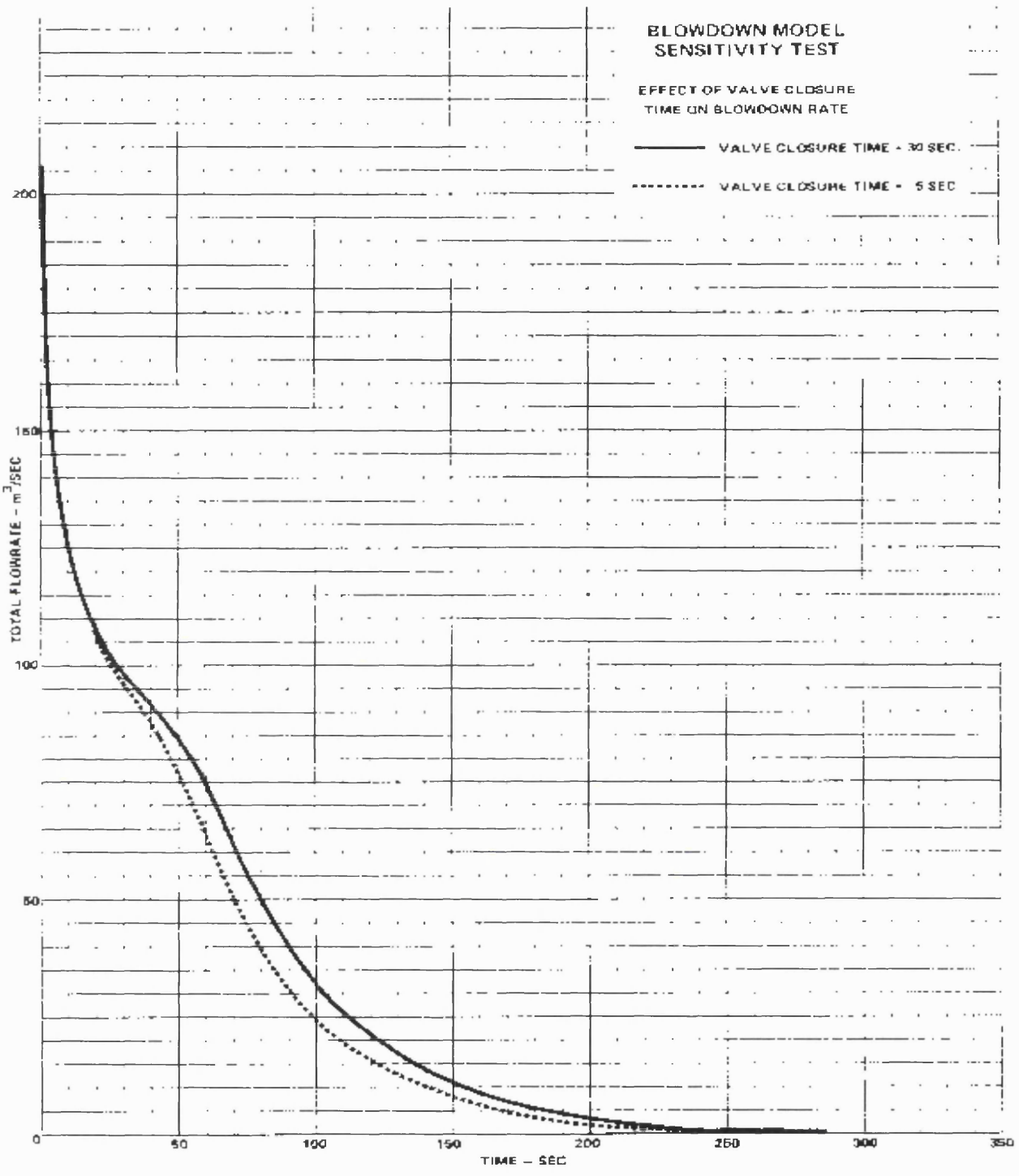

3.10 The effect of valve closure time on blowdown rate (APIGEC, 1978)

8. The resistance length (fl/d) is shown to have a significant effect on both the initial blowdown rate and the rate of the decline; figure 3.11 (APIGEC, 1978).

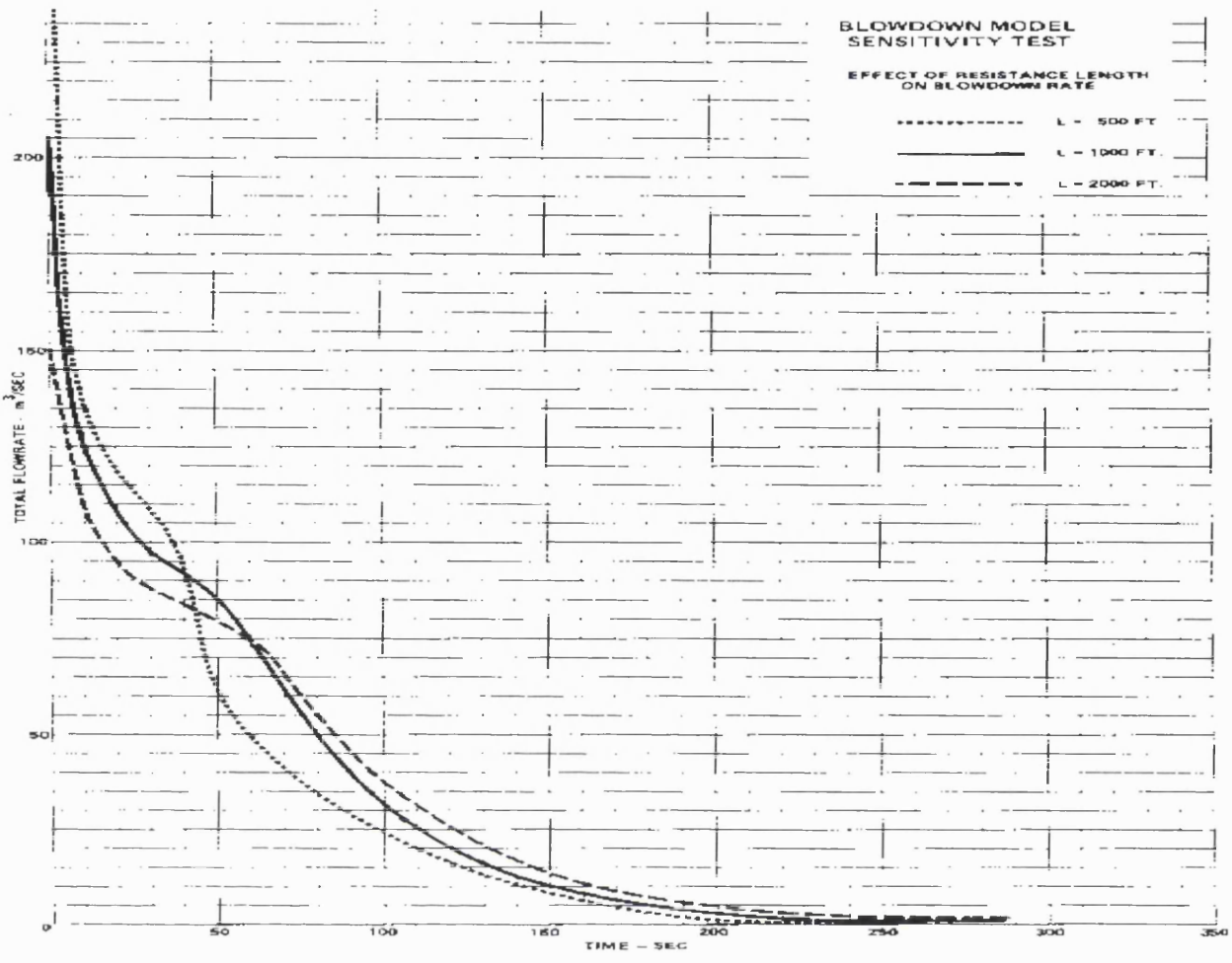

Figure 3.11 The effect of resistance length on blowdown rate (APIGEC, 1978)

The other blowdown model, which APIGEC employed, was a simplified exponential model based on the following equation

$$Q_q = A_q.\exp(-B_q.T)$$

where:

$$A_q = \frac{161.5.\left(\frac{T}{M}\right)^{0.5}.C_qP}{\left(T.Z.(1+K)^{0.5}\right)}$$

$$B_q = \frac{42.3.\left(\frac{T}{M}\right)^{0.5}.C_q P}{\left(L.(1+K)^{0.5}\right)}$$

C_q = rupture area (usually cross section area of the pipe) m^2

K = friction coefficient

= 0 , no friction

= 1, sudden expansion

= (f.N)/D , for other friction losses where f is based on 64/Re charts and is about 0.015 for this study.

l= physical line length, m

M = gas molecular weight

P = initial line pressure, kPa

Q_q = gas deliverability, m^3/s

T = initial gas temperature, ^0K

t = time since rupture, s

Z = gas compressibility factor

The above equation does not allow for valve closure or gas flow rate in the line. To compensate for this, the coefficient, B_q has been modified such that the total volume of gas released (q_q= A_q/B_q) is 30% larger than the volume of gas in the section of line under consideration. This modification gives the simple model about the same total gas release as the TRANSFLOW model. It should be noted that this expression assumes the rupture occurs at the end of the line whereas in the TRANSFLOW model, the rupture occurred in the middle. The group compared the results produced by the two blowdown models and conclude that they compared remarkably well, considering the simplicity of the exponential model. The results are shown in figure 3.12. Based on the above findings APIGEC main concern was the sensitivity of the blowdown models to different parameters such as pipe length, initial temperature and initial pressure. There is no information in the report on the thermodynamic formulation of the models, however it is mentioned that a constant gas compressibility factor and constant friction factor have been employed. There is also no validation against experimental data.

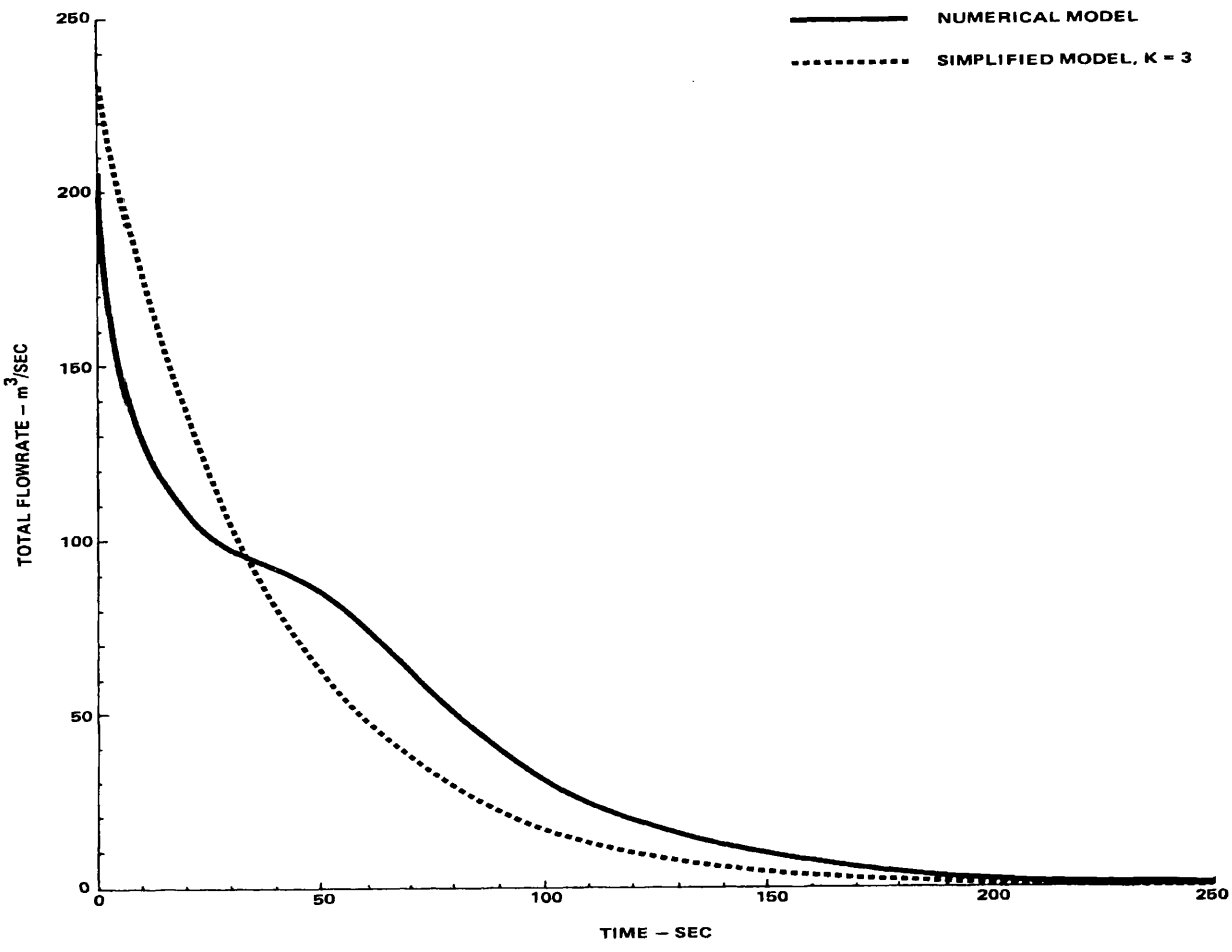

Figure 3.12 Total mass flow rate versus time, comparison of numerical blowdown model and simplified model (APIGEC, 1978)

Following the above study, the Alberta Petroleum Industry Government Committee in 1979 (APIGEC, 1979) carried out a full-scale field study to observe the source configuration of gaseous emissions resulting from a pipeline rupture. The purpose was to observe and record the nature of pipeline ruptures and gather data to evaluate the validity of the assumptions used in calculating hazardous areas, which could result from uncontrolled release of sour natural gas. They conducted a series of tests with three basic objectives in mind. One of the objectives was to obtain flow measurement data with which to correlate the transient blowdown models, which they used in their previous study in 1978. In order to carry out measurement of the transient flow rate from a ruptured pipeline four potential techniques were identified. Among these techniques the "critical flow" and "surface shear head loss" techniques were found to be acceptable for the purpose of their study. The critical flow technique assumes that

critical flow (sonic velocity) occurs at the exhaust point; which is only valid when the ratio between atmospheric pressure and the exit pressure is less than 0.53 (i.e. the critical pressure ratio corresponding to conditions for chocked flow (Perry, 1973)). The mass flow rate is shown to be directly proportional to the static pressure at the exit. The surface shear head loss technique uses the assumption that the flow in the pipe is fully developed; this appears to be valid 3 seconds after the rupture. Figure 3.13 shows mass flow rate from the ruptured 168.3 mm diameter pipeline at an initial pressure of 6900 kPa. Both the critical flow and surface shear head loss were employed simultaneously to estimate the mass flow rate for the entire duration of rupture. Depletion time was approximately 170 seconds with critical flow existing for the first 70 seconds. The theoretical mass flow rate curve shown in the graph is obtained using Intercomp Resource Development and Engineering's Thermal Transflow blowdown model. Total measured mass released from the pipe is very close to the calculated mass released during the rupture (less than 1%). With respect to the validation of Thermal TRANSFLOW blowdown model it is evident that the model underestimates the flow rate during the early stages and overestimates during the latter with the total predicted mass released being approximately 12% lower than the actual value.

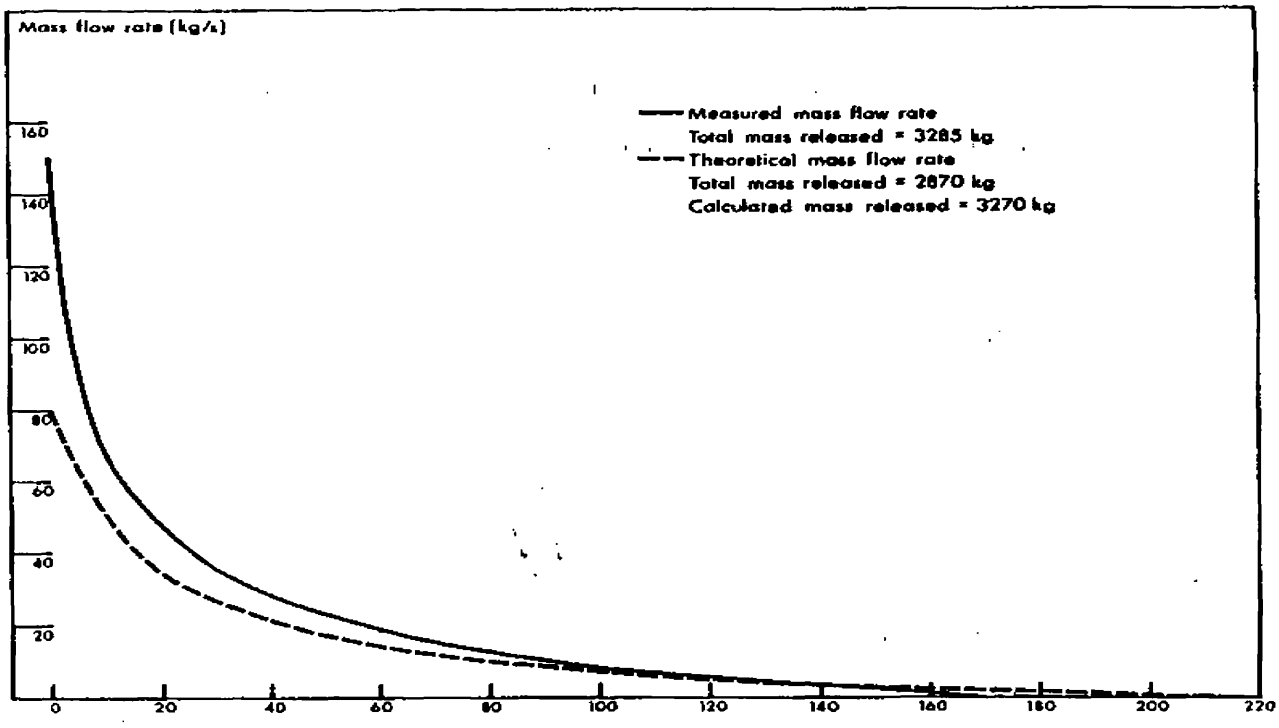

Figure 3.13 Mass flow rate from 168.3 mm ruptured pipe at initial pressure 6900kpa and gas temperature 10^{O}C(APIGEC, 1979)

Figure 3.14 shows the measured mass flow rate curve based on the critical flow technique data and calculated mass flow rate based on the blowdown model. This figure shows that the total measured mass released is approximately 15% greater than the calculated value. It can also been observed from the graphs in figure 3.14 that the blowdown model underestimates the mass flow rate with the total mass released roughly 20% less than the expected value.

APIGEC (1979) concluded that mass flow rates computed by the critical flow method were valid for times after rupture greater than 0.01 seconds for un buried tests and for times after rupture greater than 1.0 second for buried pipeline tests. It is also mentioned in the report that for the final stages of the blowdown, the exit pressure drops below the necessary value for the critical flow and the mass flow calculation using the critical flow method becomes inaccurate.

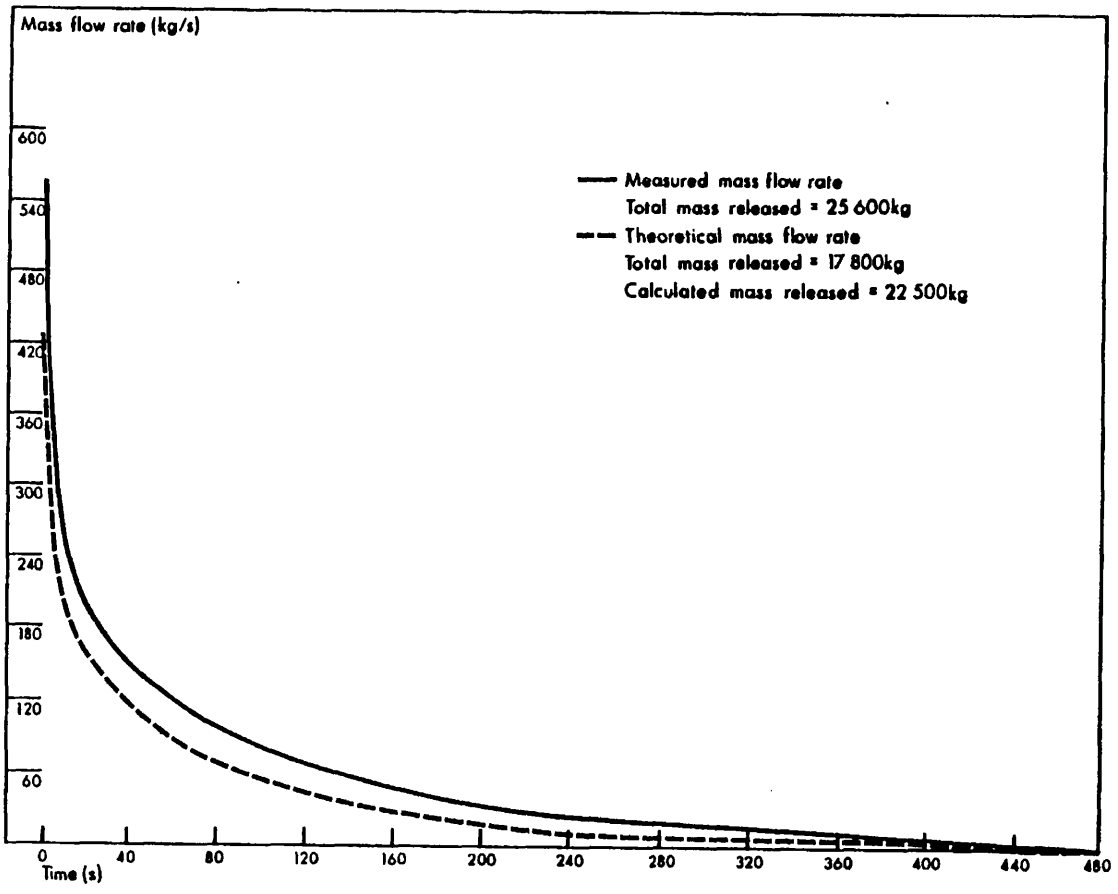

Figure 3.14 Mass flow rate from a 329 mm ruptured pipe at initial pressure 6900kpa and gas temperature 50 ^{O}C (APIGEC, 1979)

Lyczkowski et al. (1978) investigated explicit finite difference numerical schemes for the solution of homogeneous equations of change for one-dimensional fluid flow and heat transfer. In particular two methods were chosen and employed in simulating pipeline blowdown. The two methods are the two-step Lax-Wendroff (LW) scheme (Richtmyer and Morton, 1967) and the Alternating Gradient Method (AGM) (proposed by the same authors). Both methods are based on the basic Lax method (Lax, 1954). The Alternating Gradient Method (AGM) derives its name from the numerical scheme, which is a two-step method with predictor and corrector equations. Their main interest was the loss of coolant accident in a nuclear power reactor. Based on their interest three different scenarios were simulated to validate their model. The first one was an ideal gas shock tube problem. Lyczkowski et al. carried out some simulations with both AGM and LW schemes and compared the results from both schemes with analytical solutions. They found that the AGM is more accurate than the Lax-Wendroff scheme, probably due to greater numerical damping in the AGM (see figure 3.15).

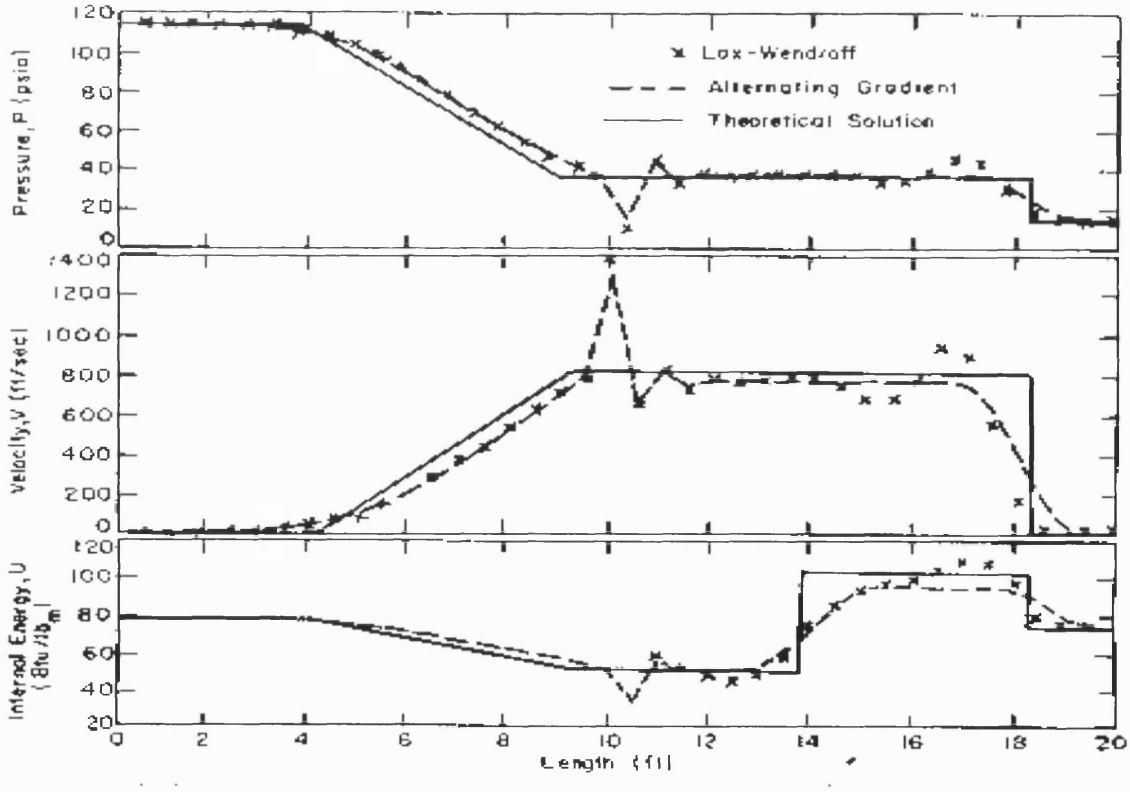

Figure 3.15 Comparison of the Lax-Wendroff and Alternating Gradient methods with the theoretical solution (Lyczkowski et al., 1978)

The second problem which Lyczkowski et al. (1978) studied was the blowdown of an ideal diatomic gas. The numerical results obtained with the AGM were compared with an analytical wave diagram solution obtained by Rudinger (1969). The AGM method showed good agreement with the results presented by Rudinger (1969). The results of the comparison are shown in figures 3.16 and 3.17.

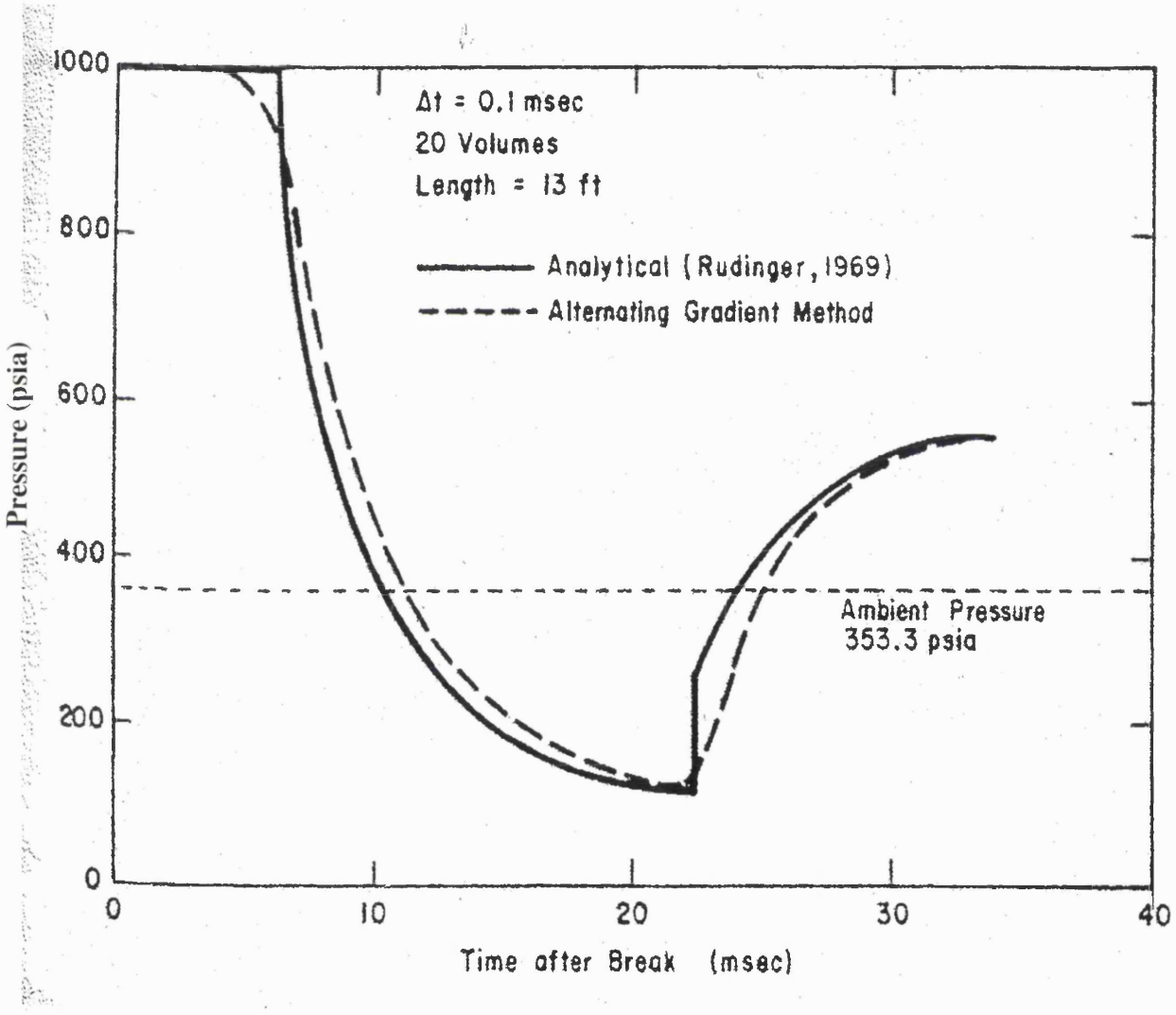

Figure 3.16 Ideal gas blowdown pressure results (Lyczkowski et al., 1978)

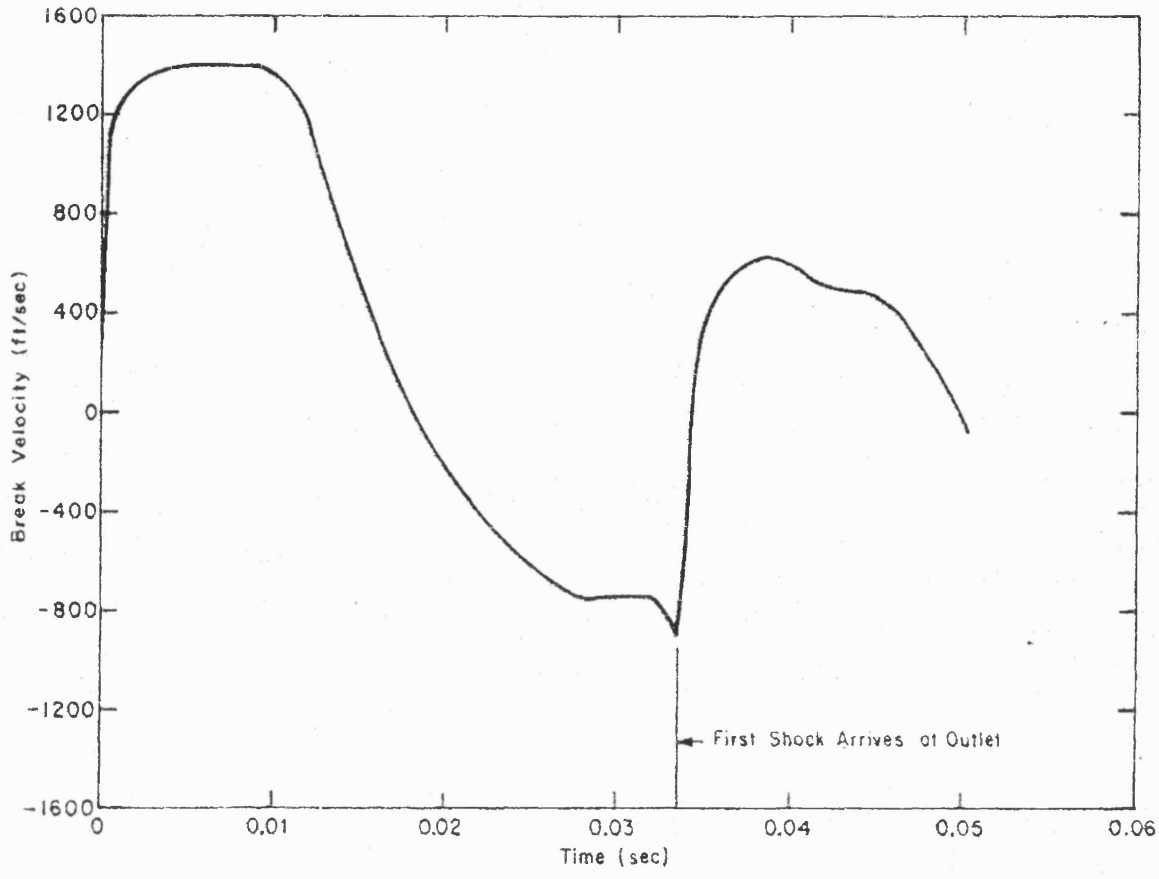

Figure 3.17 Ideal gas blowdown velocity results (Lyczkowski et al., 1978)

Finally the third problem analysed was the blowdown of a steam-water mixture. The results computed using the Alternating Gradient Method (AGM) was compared with results from experimental runs 51 through 53 from Edwards (1970). Again agreement between code results and experimental data was excellent. The corresponding results are presented in figures 3.18 and 3.19. The authors point out that although the AGM is restricted by a time-step limitation, which is slightly smaller than the standard Courant condition for a given time-step and mesh size, it is at least as accurate as implicit schemes. Since only two cycles per time step are needed, the AGM is faster than a fully implicit scheme. In addition, the AGM is simple to programme. Their assertions were based on the depressurisation of pipelines conveying steam-water mixtures or, ideal gas and as such remains to be tested with two-phase hydrocarbon mixtures.

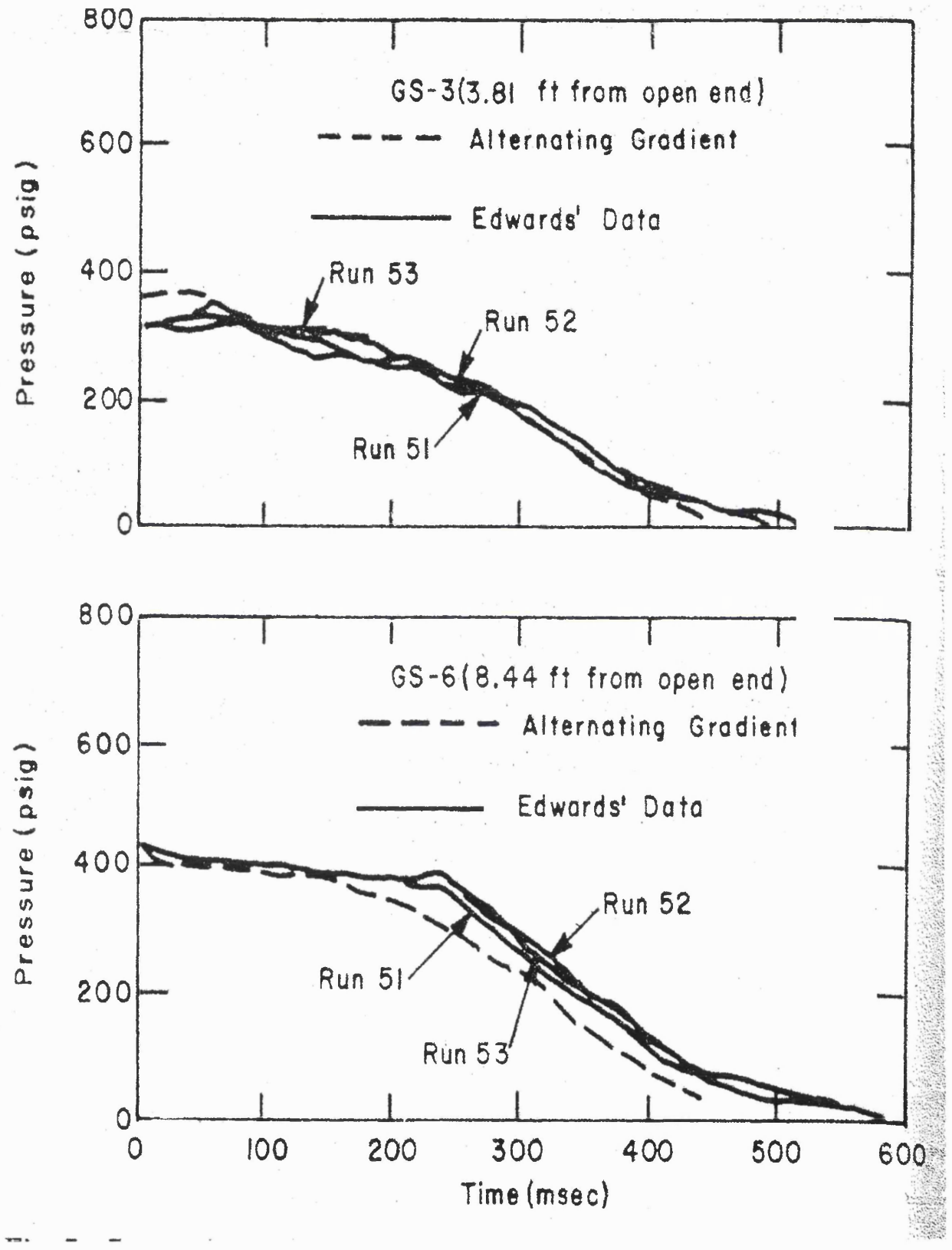

Figure 3.18 Comparison of Alternating Gradient long-term pressure transient response computations with Edwards' data (Lyczkowski et al., 1978)

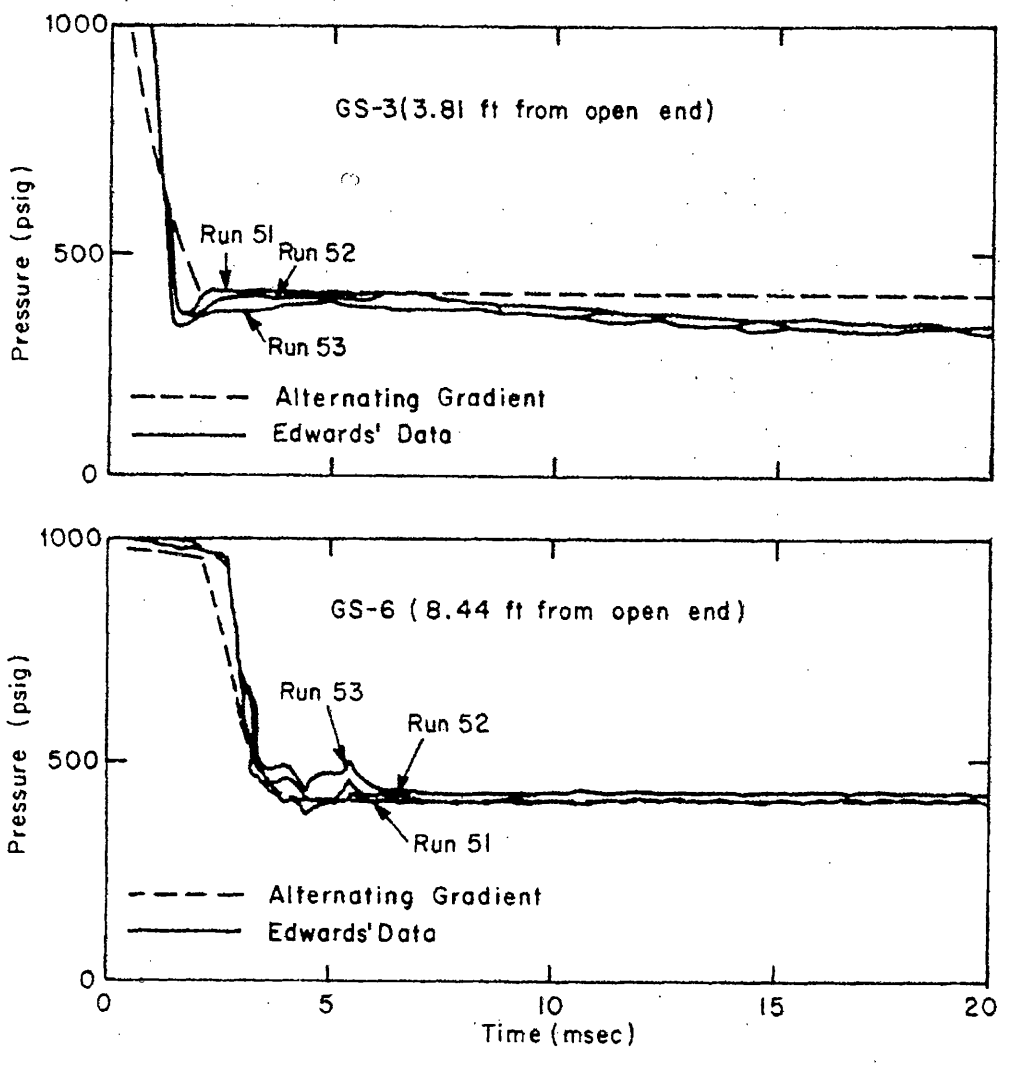

Figure 3.19 Comparison of alternating gradient short-term pressure transient response computations with Edwards' data (Lyczkowski et al., 1978)

Shin (1978) discussed the extension of the one-dimensional MOC to two space dimensions. The extended method uses the same simplifications and retains the similar simplicity and efficiency as in the conventional one. The two-dimensional method is applicable to both the Cartesian and axi-symmetric systems and includes the conventional method as a special case.

An important aspect of the effect of two-phase flow was reported by Maxey et al. (1972) who investigated ductile fracture propagation (DFP) along the pressurised pipeline. It was demonstrated that in the case of two-phase flow, a greater ductile

fracture resistance is required for fracture arrest than if only a single-phase was present. This is due to the formation of higher crack-tip pressure levels in the presence of a second phase.

Cronje et al. (1980) described a procedure to solve the equations for single-phase, one-dimensional, unsteady, compressible, frictional flow with heat transfer. The procedure is based on Hartree's hybrid method (Hartree, 1958) for solving the governing hyperbolic partial differential equations. In this numerical method, a rectangular grid is superimposed on the characteristic mesh in the time-distance plane. The values of the variables at points lying on the characteristics at time, t are calculated by linear interpolation from their known values prevailing at the rectangular grid points at the same time, t. The governing equations are integrated along their characteristics over a time step, δt in time, to obtain the new values of these variables at the grid points at time, $t + \delta t$, and the process is repeated until the required time interval is covered. The method was applied to shock tube data that simulate a gas pipeline rupture. The authors compared the results obtained by their model with experimental data and theoretical simulation presented by Groves (1978). Figure 3.20 shows this comparison. From the figure the authors conclude that the theoretical predictions by both methods compare well with experimental values down to a pressure ratio of approximately 0.47. At lower pressure ratios, the author's model better approximates the experimental values due to the fact that it accounts for the friction and heat transfer effects. They also performed some simulations for pure Argon for various combinations of friction factor and Stanton number. The results are shown in figure 3.21. The theoretically predicted curves compare favourably with the experimental data down to a pressure ratio of approximately 0.7. Below this ratio the adiabatic prediction of both methods deviate considerably in nature from the experimental results. Finally figure 3.22 illustrates the computed effects of friction with and without heat transfer. The authors conclude that the effect of friction is considerably more important than the effect of heat transfer. For large elapse times the effect of friction is significant and their numerical model predicted well the available experimental values at these times. However the model, similar to the most cases reviewed in this study, assumes ideal gas behaviour and fails to consider the effect of pipeline inclination.

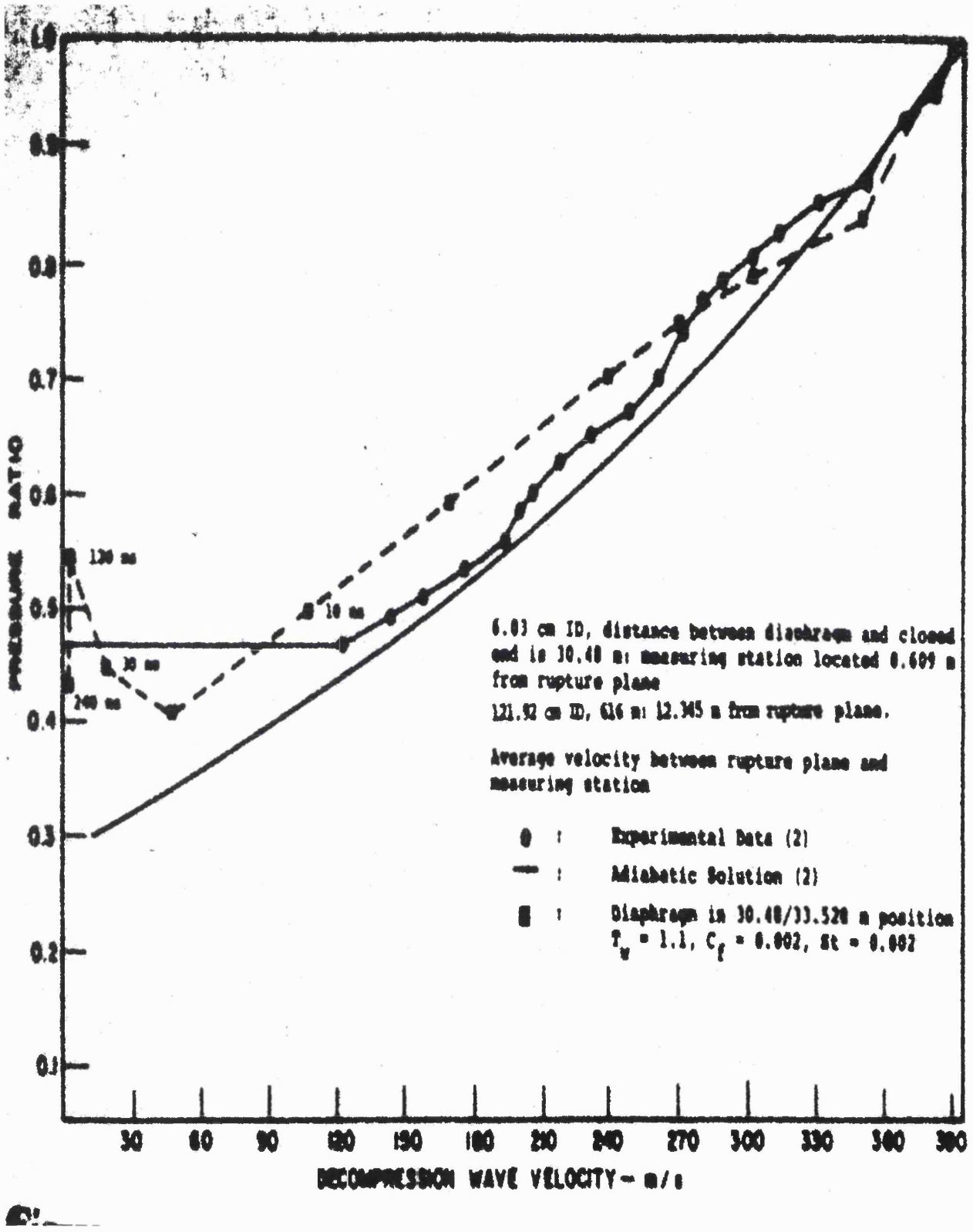

Figure 3.20 Pure methane gas decompression wave velocity. Initial condition p_o = 7743 kPa, T = 264 K (Cronje et al., 1980)

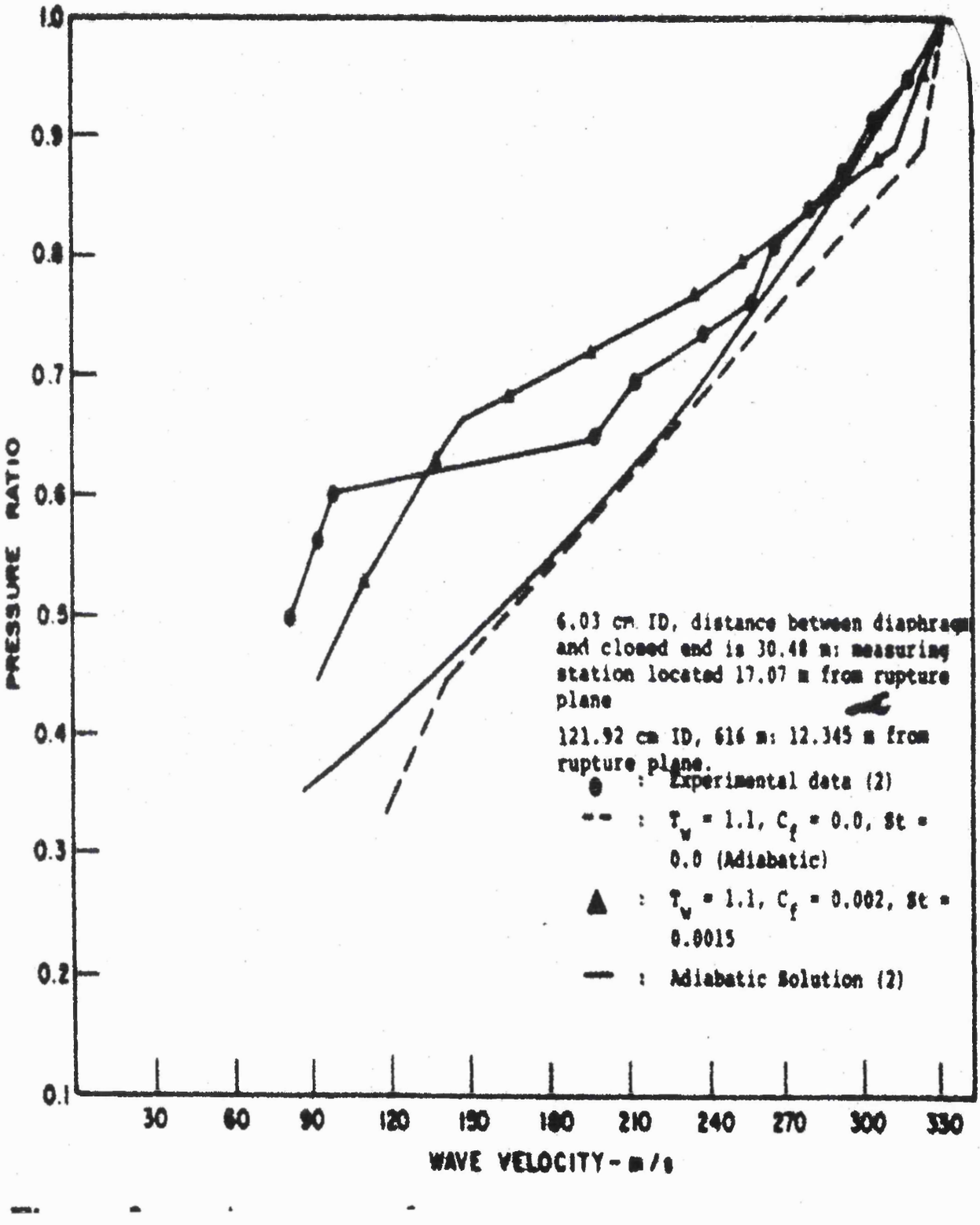

Figure 3.21 Argon gas decompression wave velocity. Initial condition p_o= 9200 kpa, T=296K (Cronje et al., 1980)

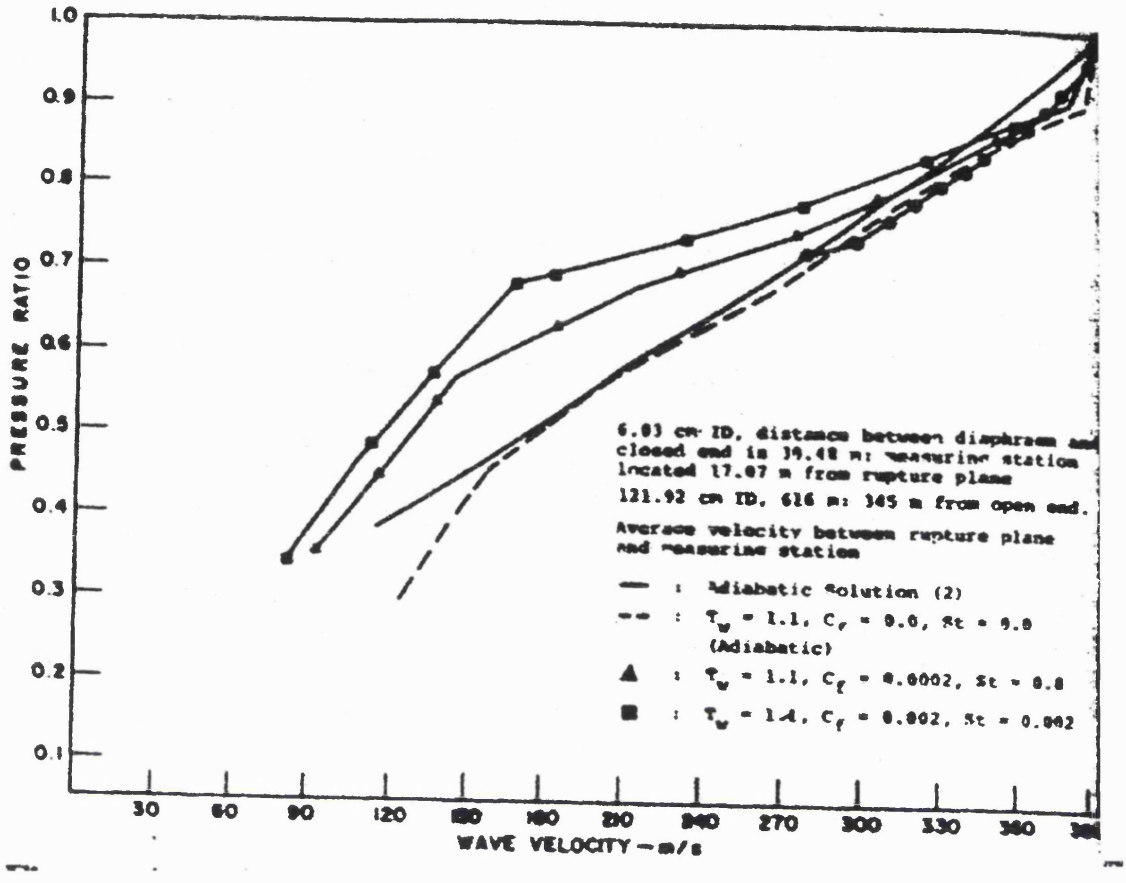

Figure 3.22 Pure methane gas decompression wave velocity. Initial condition p_o= 7743 kPa, T = 264 K (Cronje et al., 1980)

Knox et al. (1980) presented a summary on the study conducted by the Alberta Petroleum Industry Government Environment Committee (APIGEC; 1978,1979). In their report, all aspects of the earlier study were covered. The authors conclude that uncertainty analysis for the results obtained indicate that the measured instantaneous mass flow rates have accuracies of plus and minus 7 percent for the critical flow rate technique and plus or minus 17 percent for the surface shear head loss data.

Jones and Gough (1981) reported on rich gas decompression behaviour following pipeline rupture. The author studied a theoretical model, named after British Gas who developed it. They incorporated the British Gas model in a computer program called DECAY. The model is based on isentropic and homogeneous equilibrium fluid flow. The pipeline has also been assumed to be horizontal with no heat transfer occurring between the fluid and the ambient. In order to confirm the validity of their computer

program, DECAY, Jones and Gough (1981) carried out a series of shock tube experiments. They concluded that their model shows a good agreement with experimental data as shown in figures 3.23 and 3.24. Jones and Gough (1981) also reported that other organisations such as Exxon Production Research and the University of Calgary, were involved in studies on high-pressure gas decompression behaviour and that they had developed similar models to that of British Gas. The only difference between all these models is the equation of state, which has been applied in each model. The University of Calgary used Redlich_Kwong-Soave equation of state (Walas, 1985). However Exxon Production Research Company used the BWRS equation of state (Walas, 1985). Finally the three models were shown to exhibit similar performance in comparison to one another.

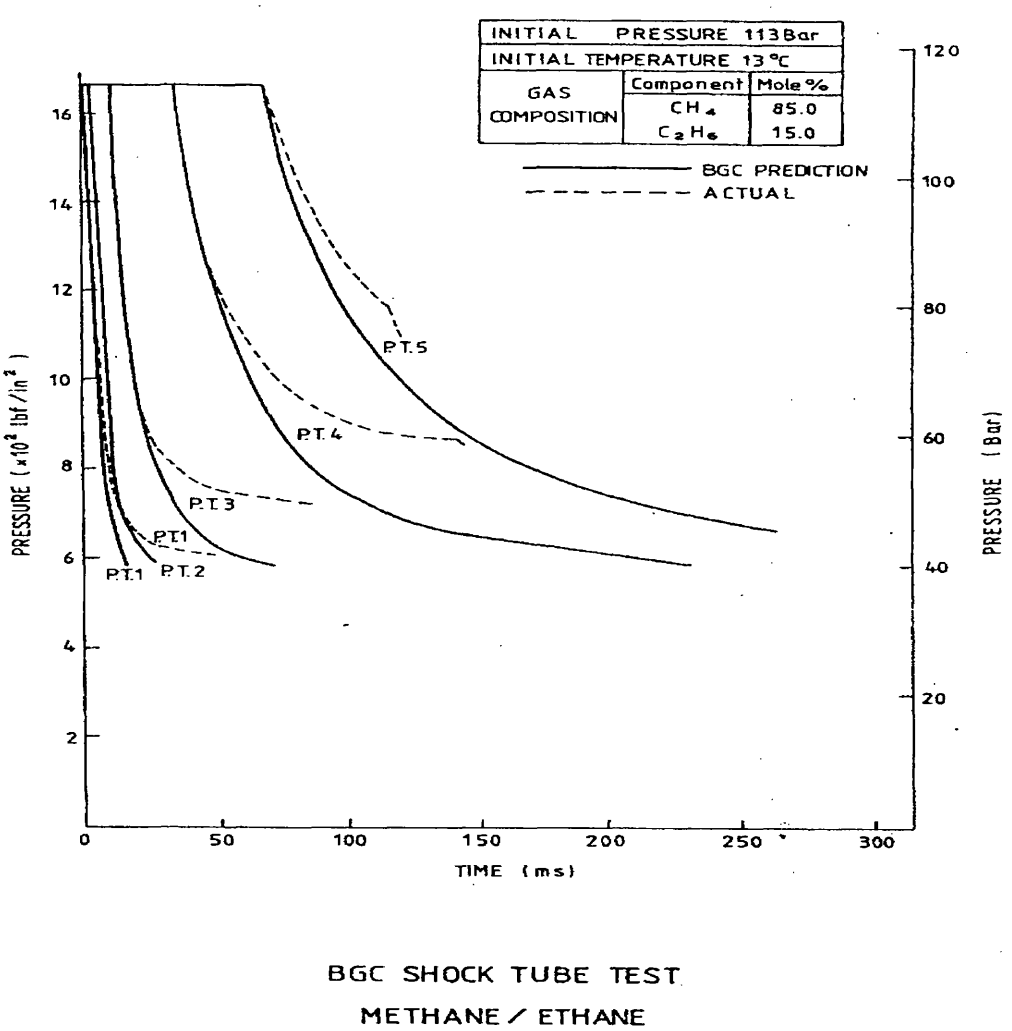

Figure 3.23 Comparison between British Gas model and experimental data (Jones and Gough, 1981)

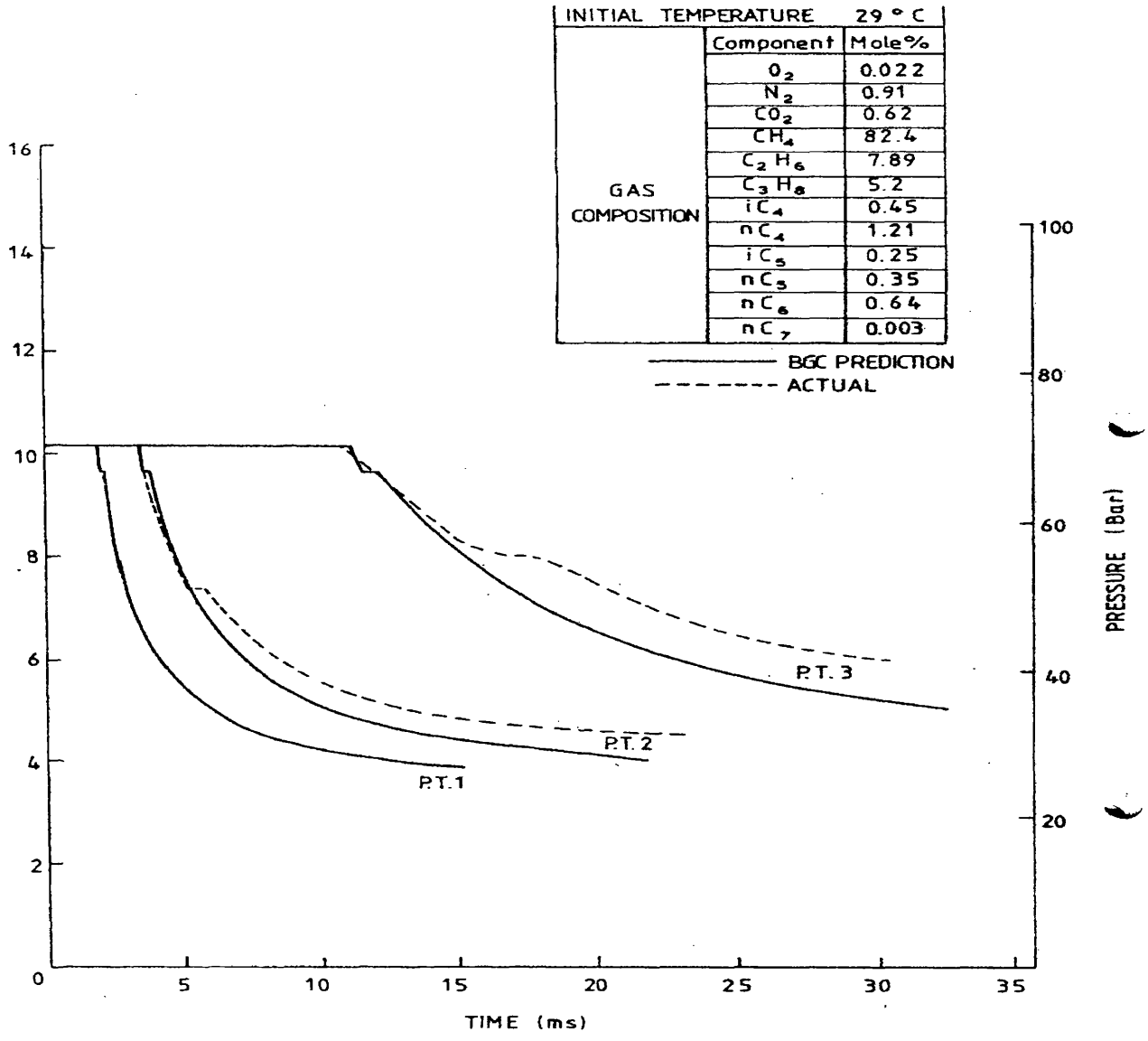

Figure 3.24 Comparison between British Gas model and experimental data (Jones and Gough, 1981)

Fannelop and Ryhming (1982) focused their research on the unsteady characteristic of long, large-diameter natural gas pipelines. They presented the equations of motion for steady state and unsteady conditions. The authors categorised the flow after the rupture based on three different time regimes and employed an individual method of solution for each regime. When the rupture occurs, flow will be chocked at the rupture plane (inviscid chocking condition). This is followed by a viscous expansion process in which wave and dissipation processes are both important and in which the pressure at the break approaches the ambient value. The combined inviscid and viscous expansion phase were categorised as the early time regime. The intermediate time regime is defined as the time, following the early regime, and it lasts until the pressure peak reaches to the low-pressure end (closed end) of the pipeline. The time regime when the pressure decreases monotonically towards the open end was referred to as the late time regime. The flow is considered to be isothermal thus removing the need for an energy equation. The authors have proposed the integral method to solve this problem. This involves integrating the conservation equations over the length of the pipeline by approximating the fluid property variation along the pipeline with a suitable function (flow profile). Although the method of integrals has been used in many engineering problems, however the choice of an approximate function could be very critical. The authors have compared the results of using different approximated functions, and the sensitivity of the integral method (in the simulated results obtained) to the profile/function employed. Results obtained show that the integral method is relatively insensitive to the type of profile employed, and consistently gives similar trends in its predictions. Consequently, the authors conclude by recommending the integral method as a tool for the analysis of engineering problems involving pipeline rupture and the ensuing release process.

Van Deen and Reinstema (1983) developed a computer model for high-pressure gas transmission lines based on the method of characteristics (MOC) and compared it with experimental data from the Gasunie in Netherlands transmission system. A leak was simulated by the fast opening of a valve connecting the pipeline to a nearby parallel pipeline at a lower pressure. Pressure responses at a point 10 km downstream of the leak were investigated. Lack of agreement in the magnitude of the reflected pressure waves was observed and attributed to imperfect modelling of the boundary

conditions. It was also observed that changes in the numerical values of the resistance factor of the pipeline have only a slight influence on the value of the result.

Flatt (1985-1989), studied the use of MOC for analysis of unsteady compressible flow in long pipelines following rupture. In his model, the simplifying assumptions of isothermal and low Mach number, often applied in the case of unsteady compressible flow in pipelines, were not used. To achieve improved accuracy, higher-order polynomials and an assumption of curved characteristic lines were also utilised. The algorithms used were limited to shock free flows. An accuracy criterion showed that higher numerical accuracy might be obtained if the number of grid points was sufficiently large and if a special modified form of the boundary conditions at the broken section was used. The major difficulty encountered was due to the singularity, which resulted from the combined effects of friction and choking (Ma = 1), occurring at the broken end. The results confirmed conclusions established earlier (Fannelop and Ryhming, 1982) that viscous flows with large values of $f\ell$/D (order of magnitude of 1000) behave very differently from flows without friction. In particular the simulated mass flow escaping through the broken section, and the corresponding pressure fall to much smaller values. On the other hand, at some distance from the broken section, the pressure stays at high values much longer than in the case without friction. The study concluded that MOC is more suited to problems with relatively low values of the parameter, $f\ell$/D. Cases with important frictional effects are advised to be carefully checked regarding the accuracy of the results, and require many more grid points than those without friction.

Bisgard et al. (1987) reported on a finite-element method developed for transient compressible flow in pipelines. A weighted residual method with a one-dimensional straight-line element with two nodes was combined with an implicit Euler method and applied to the basic equations without making any major simplifying assumptions. Higher-order polynomials were used as interpolating functions, since derivatives must be specified at the nodes in addition to the variable itself. The Galerkin finite-element method (Rachford and Dupont, 1974) was used to discretise the equations. The Galerkin method is a two-step method, which reduces the partial differential equations to ordinary differential, but it is generally unpopular for this type of analysis because of its lengthy execution (Thorley, 1987). Gauss quadrature was used for the

integration, where the order of the Gauss quadrature was adjusted to the order of the polynomial. A fully implicit Euler integration method was used for time integration after a third-order Runga-Kutta method had failed the stability criterion. The method was used to describe blowdown and to determine the performance of a leak detection system. The first derivative of density and the first and second derivatives of velocity were included since small leaks are more easily recognised from derivatives of specified variables than from the variables themselves. A comparison was made between full-scale measurements carried out on a 77.33 kilometres gas transmission line from Neustadt through Sorzen to Unterfohring, in Germany, and corresponding finite element calculations. In the rupture simulation, the fluid was assumed to behave like an ideal gas with constant specific heat flowing through a convergent nozzle and calculations were carried out with 21 elements and a time step length of 0.5 seconds. The authors claim that results from the computer model have been previously successfully compared with process data from a full-scale pipeline. However, the data was not shown in the paper for the case of a pipe rupture. It therefore remains doubtful as to whether the method could accurately and efficiently be used for the analysis of pipe rupture problems.

Lang and Fannelop (1987) reported on a method for the efficient computation of the pipeline break problem. In their method, partial differential equations were reduced to a set of ordinary differential equations by means of procedures in the family of the method of weighted residuals (Finalyson, 1972). The reduced equations were integrated by standard numerical techniques. The finite element method, the spectral Galerkin method and the spectral collocation method were all used and results compared. It was demonstrated that stable, accurate and efficient solutions to the pipeline break problem could be obtained by the method of weighted residuals. Although the approximate functions used with the spectral collocation method would appear to be suited primarily for elliptic problems, it was possible to apply them to the hyperbolic equations by modifying one of the coefficients. Good results were obtained, and it was recommended that the computer time required by this method could be further reduced without loss of accuracy when the number of polynomials in the approximate solutions is reduced successively during the course of the calculation, as the gradients of pressure and velocity become smaller. It was concluded that the

best results in terms of stability, accuracy and computing time were obtained with the collocation method.

Picard and Bishnoi (1988) expanded the earlier work of Maxey et al. (1972), and investigated the importance of real-fluid behaviour during the rapid decompression of dense natural gas mixtures using one-dimensional models for real-fluid isentropic decompression (RID) and perfect-gas isentropic decompression (PID). Two different real-fluid equations of state were used to determine the thermodynamic properties of the fluid when using the RID model; the Soave-Redlich-Kwong (SRK) and the Peng-Robinson (PR) equation of state. Overall, the PR equation of state proved to be the most reliable as it performs better in the single phase region and predicts slightly higher values of expansion wave pressure levels in both fluid-phases, resulting in a more conservative pipeline design when conducting ductile fracture propagation and arrest analysis.

The results showed that the assumption of perfect-gas behaviour may result in significant errors, as the calculated fracture-tip pressure was shown to be underestimated by as much as 20%. Also, in order to investigate the importance of non-isentropic effects a real-fluid non-isentropic decompression (RND) model was developed, which showed that non-isentropic effects can be neglected for pipe sizes above approximately 510 mm O.D.

Picard and Bishnoi (1989) building on their previous work, reinforced the importance of modelling using real-fluid behaviour in the prediction of release rates from ruptures in high-pressure pipelines. The authors realised that the previously developed non-isentropic decompression model (Picard and Bishnoi, 1988) was prone to numerical instability at the rupture plane for problems involving non-isentropic flow if the selected distance between grid nodes was too large in the high gradient region immediately upstream of the rupture plane. This problem was overcome by imposing a short isentropic region at the rupture plane, which was assumed valid if the isentropic region was small relative to the total pipe length. This was achieved by setting the non-isentropic terms of the path line and left and right running characteristics to zero when evaluating the flow conditions at a zero axial distance upstream from the open-end. However, to completely eliminate this numerical

stability similar terms of the right running characteristic of the next upstream grid were set to half their normal value.

As a result, it was demonstrated that perfect gas theory could underestimate the release rate by 30 to 45%, mainly due to its low estimate of fluid density. It was also shown that the total amount of gas released could be underestimated by as much as 50%. Furthermore, perfect gas theory cannot consider condensation effects. However the authors mentioned that more reliable approximation could be obtained by slightly modifying the model. This involves determining the initial mass of fluid based on real fluid theory. Overall, it was demonstrated that a conservative approximation can be made of the depressurisation process if real fluid theory is used to predict the initial mass of fluid in the pipeline.

Botros et al. (1989) discussed some computational models and solution methods for gas pipeline blowdown and assessed the significance of the various assumptions involved. Two physical models, namely a volume model where a pipe is considered as a volume with stagnation conditions inside, and a pipe model where a pipeline section is considered as a pipe with velocity increasing towards the exit were considered. The pertinent equations for each model were solved analytically and numerically. The volume model was represented by a set of quasi-linear ordinary differential equations, which were solved by a variable order backward differentiation formula method (Gear's method). The pipe model was governed by a set of non-linear first-order parabolic partial differential equations, which were solved by a first-order Euler implicit finite-difference scheme. It was concluded that the accuracy of results obtained from the various models and solution methods depended greatly on the ratio $f_d l/D$ of the pipe section under blowdown and the stack relative size with respect to the main pipe size. Generally as $f_d l/D$ increases predictions using all models tend to become inaccurate. For relatively low $f_d l/D$ values all models provide reasonable predictions and therefore the simple analytical volume calculations can be used effectively.

Tiley (1989) used MOC for pressure transients in a ruptured gas pipeline with friction and thermal effects included. A real gas equation of state, Berthelot equation (Walas, 1985) was used and the "small terms" in the basic equations were neglected. A

reducing grid size was used in the vicinity of the break to enable rarefaction waves to be modelled following a rupture. The friction term was represented by a second-order approximation. The values at an initial condition at the base of the characteristic were found by interpolating between known grid points. Hence by solving these equations, a first-order approximation was obtained for the predicted pressure, temperature and flow velocity. Since the required stability and accuracy were not achieved using the first-order approximation, this solution was used as an initial estimate in a second-order procedure. Although the exact procedure of this second order model is dependent on the type of grid point being examined, in principle, new values for the variable at the initial condition were found using quadratic interpolation. The coefficients in the characteristic equations were then calculated using these values. These were then averaged with the previous initial condition coefficients, and the results were substituted back into the characteristic equations. By this method, new values for the predicted pressure, temperature and flow velocity were obtained. Results were obtained by performing a number of computer simulations for a set of data and comparing the results with shock tube and full-size pipeline experimental data. Problems were encountered with numerical stability and accuracy of results. For certain grid size and initial conditions, the solution became unstable at random points along the pipeline. It was concluded that although this type of instability could be controlled to an extent by varying the grid size and break boundary conditions, the problem may be totally alleviated by using an alternative numerical method for solving the theoretical equations.

Lang (1991) reported on the computation of gas flow in pipelines following a rupture using the spectral method in which the governing partial differential equations were converted into a scheme suitable for solution by a computer using a two step procedure. In the first step, the collocation version of the spectral method was used to calculate the space derivatives. The remaining ordinary differential equations were then integrated by standard numerical techniques in the second step, where the unknown are the time dependant physical variables at the collocation points. To test the accuracy and the validity of his calculations, Lang checked how well the global conservation of mass is satisfied. This method of validation was first introduced by Fannelop and Ryhming (1982). Lang compared his results with those reported by Battara et al. (1985) and good agreement was obtained. The author also compared his

results to data from Fannelop and Ryhming (1982), and only very small differences were found. The author claimed that stable, accurate and efficient solutions to the problem of pipeline flow following a sudden rupture can be obtained using the spectral method. However he made some simplifications and assumptions, which undermines the validity of his claim. These assumptions include isothermal or adiabatic flow and the treatment of the conveying fluid as a perfect gas. In addition, no attempts have been made to validate the results with experimental data.

Kameswara and Eswaran (1993) have developed a model for flow transients in complex pipeline networks based on the method of characteristics. The authors claim that their model is applicable to all forms of transients that can be encountered. However, there is no information about the equation of state, which has been used in their program. The authors in their concluding remarks claim that the model would give accurate predictions when applied to a dry system or an ideal gas pipeline.

Olorunmaiye and Imide (1993) presented a mathematical model based on unsteady isothermal flow theory and solved using MOC. It was reported that the model predicted results for natural gas pipeline rupture problems consistent with predictions of other workers. The accuracy of the numerical scheme when using linear characteristics with quadratic interpolation was found to be adequate. It was found that the curvature of the characteristics is not as pronounced in isothermal flow as it is in adiabatic flow and therefore it is not necessary to include the effect of curvature of the characteristics in the computation of unsteady isothermal flows. It was concluded that the model is useful in analysing other unsteady flows associated with pipeline operation, such as controlled venting to the atmosphere prior to shutdown or repair, and sudden changes in pressure at either end of the pipeline. The waves generated in these operations cannot be as strong as waves associated with pipeline rupture.

Kunsch et al. (1995) observed that a precise knowledge of the coefficient of friction and other losses coefficients is not necessary in simulating outflow following pipeline rupture. They demonstrated that the mass flow rates are insensitive to the exact geometric shape and contraction ratio of the break resulting from an accidental rupture. They also compared their model results with those obtained by Flatt (1985b). The authors admitted that the results from Flatt's model (based on MOC) were

probably more accurate than theirs, for the inertia dominated early time regime. The authors observed that the ideal gas assumption overestimated the mass flow rate. Flatt (1985b) observed the opposite effect when the perfect gas assumption was used.

The Southwest Research Institute (SwRI) [Morrow, (1997)] conducted a study to simulate venting of natural gas pipelines for the Gas Research Institute. The computer model, which was reported, by Olorunmaiye and Imide (1993) was used. One of the aspects, which was considered was whether a leak detection system could distinguish between a signal caused by a pipeline leak and other transient signals caused by normal operation, such as compressor start-up and shutdown and deliveries of gas through branched lines. Initially, the computed transient results overestimated the gas outflow and pressure drop. In order to match the computed results to experimental data, the throat area of the relief valve was reduced below its physical size. This empirical adjustment, which is called "exit loss factor", resulted in a fairly good agreement between computed and measured pressures.

Richardson and his co-workers (Haque and Saville) at Imperial College started their work on blowdown of pressure vessels in early 1990's. They developed a computer model, BLOWDOWN for simulating the quasi-adiabatic expansion process following the blowdown of pressure vessels. However, later on in order to simulate the depressurisation of pipelines, Richardson and Saville (1991) modified the BLOWDOWN model in order to predict the internal fluid, and wall temperatures in a pipeline conveying hydrocarbons and the efflux flow-rate, composition and phase. They point out that the distinction between blowdown of a vessel and blowdown of a pipeline is that there is a significant pressure difference within the latter but not for the former. Thus for blowdown of a vessel, the only significant pressure drops are across the orifice and also between the exit of the orifice (or choke) and the atmosphere if the flow is choked at the orifice. On the other hand, for pipeline blowdown, there are significant pressure drops along the line, across the orifice if the orifice is small enough (clearly if there is a full bore rupture there is no pressure drop across the orifice) and between the exit of the orifice and the atmosphere if the flow is choked at the orifice.

The authors point out that depressurisations of pipelines may be considered to occur in different stages depending on the contents of the line. A line containing non-volatile liquid (e.g. dead oil) can be regarded to occur in two stages;

Stage 1: An expansion wave travels from the ruptured end of the line to the intact end, where at the ruptured end flow is considered to be initially choked and the initial pressure at the intact end remains constant.

Stage2: Here, quasi-steady frictional flow occurs. Pressure starts to fall at the intact end due to the arrival of the expansion wave. This pressure drop is a result of friction at the wall.

When the line contains a gas, a third stage is seen to develop with the first two stages remaining unchanged. The dominant flow regime in this stage is quasi-steady unchoked frictional flow. Here, the ruptured end becomes unchoked when the pressure in the line falls significantly. However, when the line contains a volatile liquid (e.g. condensate or live oil), again three-stages of depressurisation are considered. Stage 1 remains unchanged, stage 2 now contains a compressed liquid of quasi-steady frictional flow and stage 3 contains a two-phase flow of liquid and gas with quasi-steady frictional flow. In this instance, gas is evolved from the liquid when the pressure falls significantly. In the case of full-bore rupture, gas evolution starts immediately at the ruptured end resulting in stage 2 being subsumed within stage 1. Also, when considering a line containing two-phase flow, there is two-phase flow in stage 1 and stage 2 does not exist.

The pipeline is modelled as a horizontal line with a short vertical riser at one end, at the top of which the rupture is assumed to take place. Axial discretisation is achieved by dividing the line into a number of elements, for each one, mass, momentum and energy balances are performed.

When the above balances are being performed, the mass flow-rate is assumed to be constant in every element (quasi-steady approximation) and in the case of two-phase flow, a homogeneous or non-slip condition is assumed to occur. This latter assumption limits the program to the modelling of blowdown scenarios occurring at

high velocity in the case of two-phase flow. The balances are then interfaced to satisfy the boundary condition for a full-bore rupture, that is a pressure of 1 bar at the ruptured end or choking pressure if the flow becomes choked. Execution of the balances in such a manner gives a clear insight of the conditions along the pipe in terms of pressure, temperature, phase split, volume fraction and speed, along with total mass in the line and efflux rate.

In addition to the quasi-steady approximation assumption, Richardson and co-workers also ignored the wave motion up and down the line, which according to them is rather complex but usually irrelevant. Other assumptions made during the development of the program are that the material approaching the orifice is always in thermodynamic and phase equilibrium. While the material within the orifice is subject to the same assumption except when in the presence of a volatile liquid where a flashing flow algorithm is used.

The proposed model was validated against data gathered from the FBR of the gas line between the Piper Alpha and MCP-01 platforms. The results are shown in figure 3.25, which show good agreement between the two sets of data.

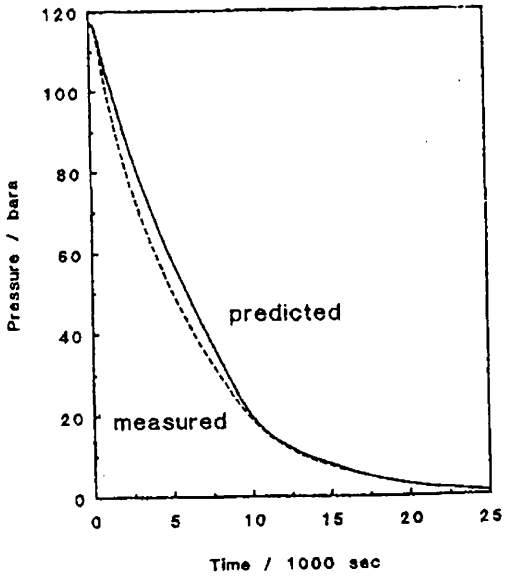

Figure 3.25 Variation at intact (MCP-01) end of line with time (Richardson & Saville, 1991)

Richardson and Saville (1996) later extensively validated their computer model, BLOWDOWN against tests conducted by Shell and BP using LPG carried out on the Isle of Grain. The results showed that predictions made by BLOWDOWN on a whole are generally at least adequate and often show good agreement with measured data.

Temperature predictions based on BLOWDOWN are generally good with discrepancies less than $10^{o}C$ at any given instant, with the largest discrepancies arising towards the end of the depressurisation. It is also shown that the predicted inventory is consistently greater than the measured one with the resulting efflux rate lower than the measured value. This maybe as a result of the quasi-steady and homogeneous flow assumption made in BLOWDOWN.

Chen et al. (1992) simulated the blowdown of pipelines containing perfect gases following a full-bore rupture using MOC with four different algorithms: the hybrid method, the hybrid method with multigrid system, wave-tracing and multiple wave-tracing. In modelling a rupture containing high-pressure gas, the one-dimensional Euler equations of gas dynamics must be solved. This generally involves one of two methods; one being the finite difference method (FDM) and the other is the method of characteristics (MOC). MOC is the more superior of the two since it can handle the choking condition intrinsically via the characteristics and since it is based on the characteristics of wave propagation where numerical diffusion associated with FDM of partial derivatives is avoided.

The four algorithms mentioned above stem from the two main methods of solving one-dimensional unsteady flow problems. The hybrid method is where a rectangular grid is prescribed in advance in the time and space domains and the other is the wave-tracing method. Both the multigrid system and the multiple wave-tracing methods evolved in order to minimise the computational load while resolving the initial transient for very long pipelines. The multigrid system involves the use of fine grids near the open end in order to resolve the fast transients and the use of coarser grids elsewhere, thereby reducing the calculation time. The multiple wave-tracing method uses the same analogy by tracing more waves with smaller wave spacing near the pipe exit in order to resolve the fast transients.

Figure 3.26 illustrates the importance of choosing appropriate time-step and space-steps in order to resolve the fast transient, as if this is improperly modelled, it will lead to an underestimate of the release rate. This model was then validated against measured data that was logged at the MCP-01 platform after rupture of the pipeline at Piper Alpha. Figure 3.27 compares the intact end pressure during the blowdown of the Piper to MCP-01 pipeline with the predictions made by the perfect gas blowdown model. The results show that the proposed model overestimates the intact end pressure, which may be due to the fluid deviating from prefect gas behaviour.

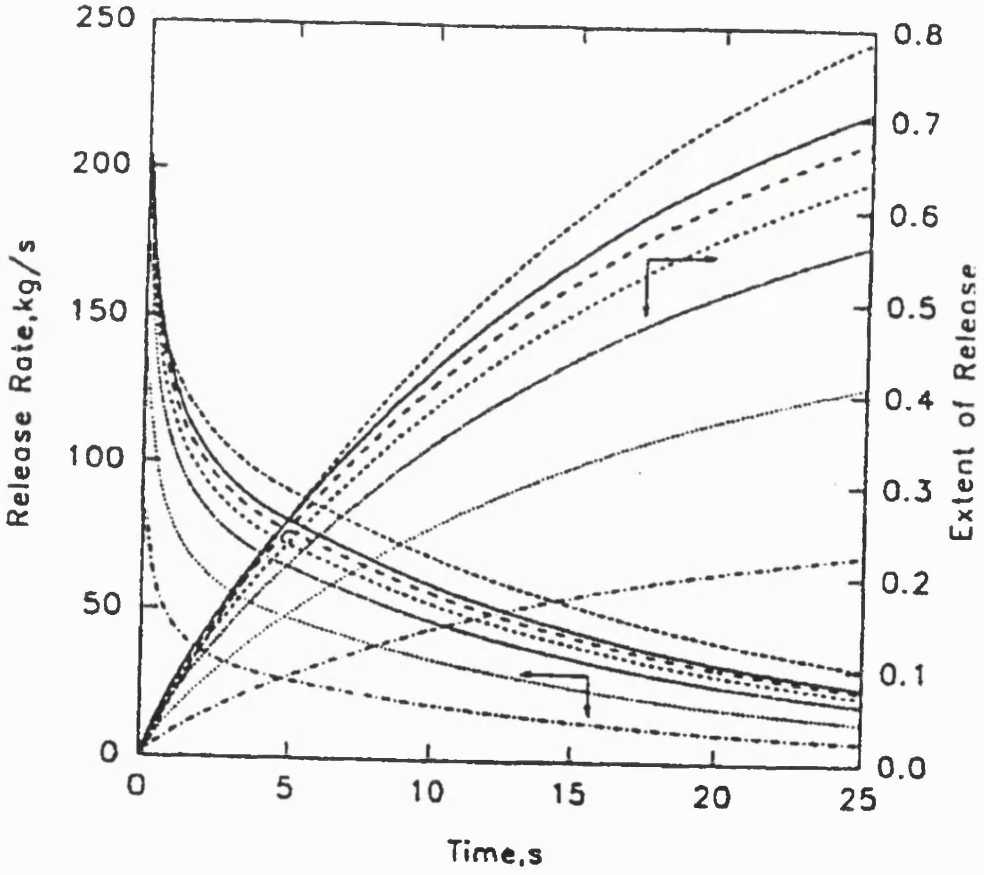

Figure 3.26 Comparisons of predicted release rate and extent of release for hybrid method with different space-steps and time-steps (Chen et al., 1992)

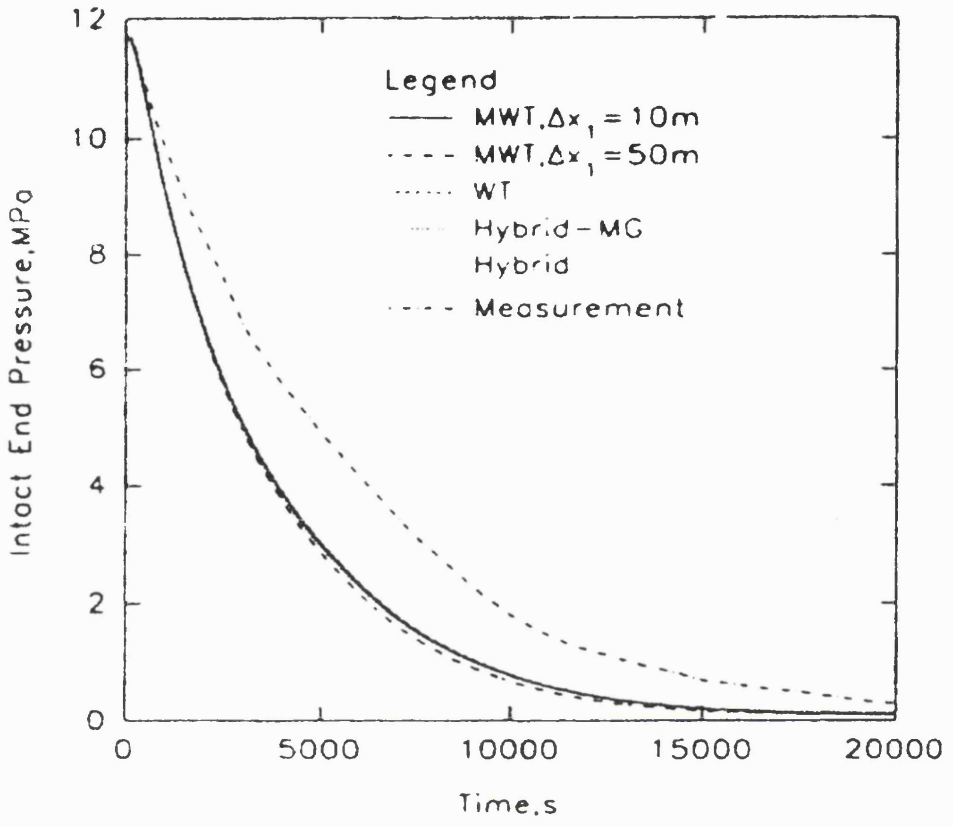

Figure 3.27 Comparison of measured intact end pressure during the blowdown of the Piper to MCP-01 pipeline with the predicted results of the four algorithms (Chen et al., 1992)

The multiple wave-tracing methods was found to be the most appropriate for solving very long gas line blowdown problems, as it is less prone to numerical oscillation. The only drawback of such a model is that it is incapable of modelling real fluids, however its speed and ease of use can give a quick and reasonably accurate estimation of the consequences of a full-bore rupture.

Chen et al. (1993) reported the development of a finite difference method for solving transient two-phase flow in pipes. The work was based on the ICE scheme of Harlow and Amsden (1971), which treats pressure and mass convection terms implicitly and momentum and energy convection terms explicitly. Such a semi-implicit approach reduces the computational time by reducing the size of the Jacobian matrices.

Chen et al. proposed to express the flow velocity in terms of pressure and the momentum convection term explicitly.

By using a locally linearised equation of state, the mass conservation equation was eliminated so that the discretised conservation laws were reduced to two difference equations in terms of mixture enthalpy and pressure only. This method assumes that equilibrium exists between the two phases; as a result a pressure-enthalpy flash calculation can be performed for each cell to obtain the void fraction, density and enthalpy of each phase. Using the calculated pressures, the flow velocities can then be calculated from the momentum equations. The model uses the Peng-Robinson equation of state to calculate the thermophysical properties of the system and to perform the pressure-enthalpy flashing. The proposed model was then used to solve a homogeneous two-phase flow depressurisation problem and the results compared with the experimental data of Tam and Cowley (1988). The results show (see figure 3.28 a,b) that the model over-predicts the discharge rate and the associated pressure drop.

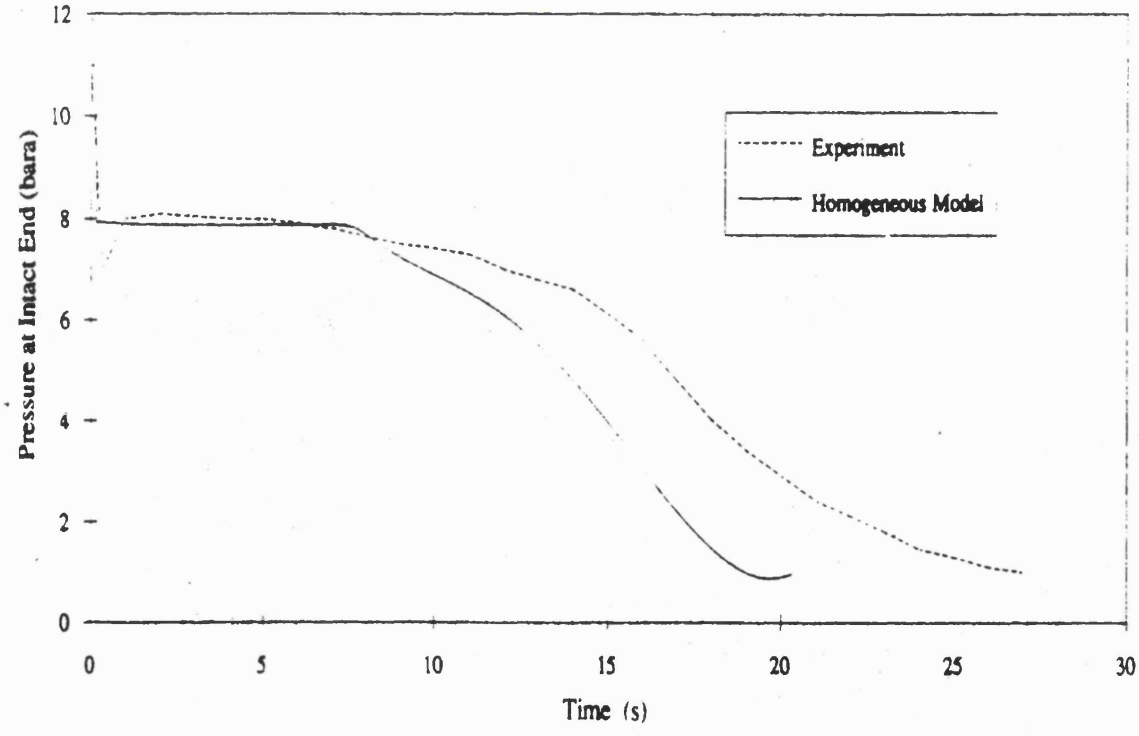

Figure 3.28a Pressure at the intact end of the pipeline (Chen et al., 1993)

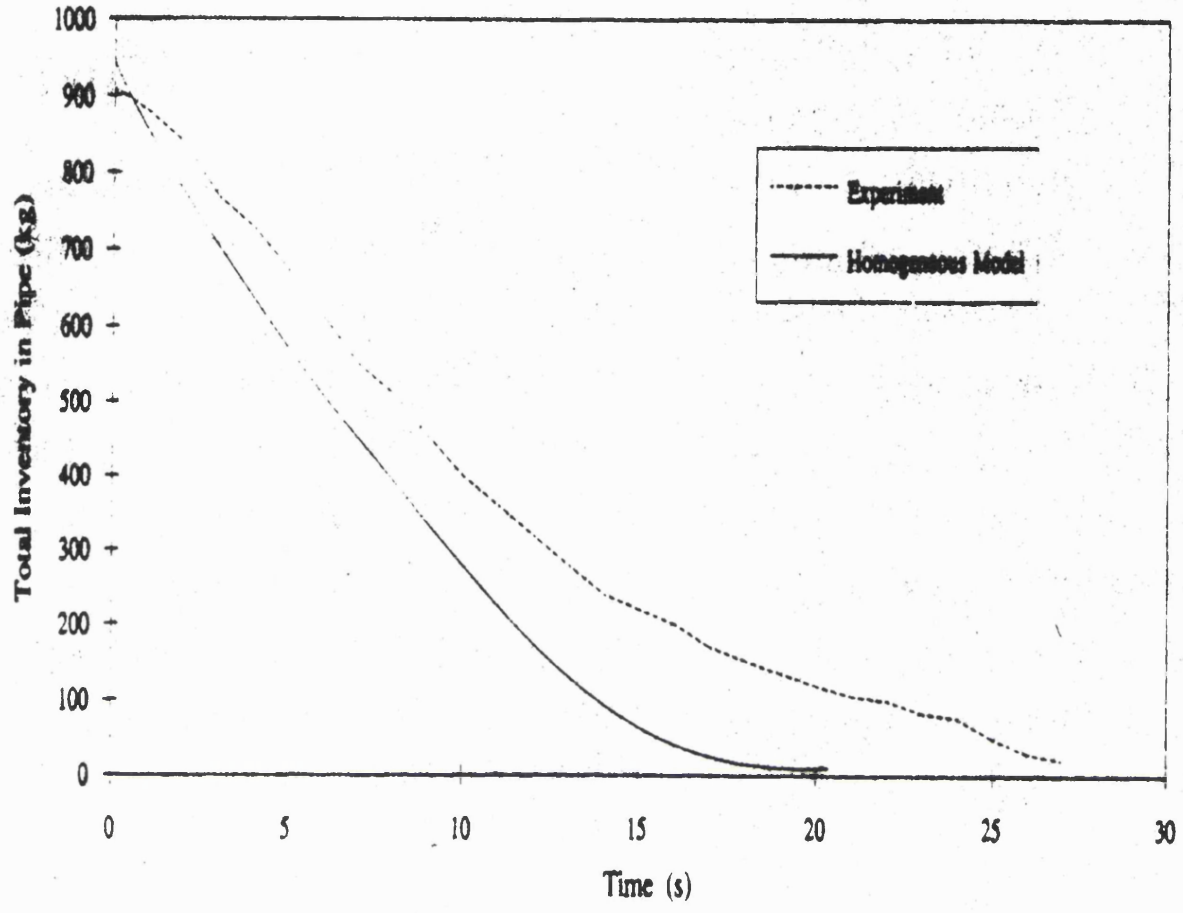

Figure 3.28b Inventory of the line (Chen et al., 1993)

Chen et al. (1995a) extended Geurst's variational principle (Geurst; 1986) for bubbly flow to generalised multi-component two-phase dispersion. In the development of the two-phase model, the two-phases are assumed to be in thermodynamic equilibrium when the flow is homogeneous but non-equilibrium effects are retained when the flow is non-homogeneous. The assumption of thermodynamic equilibrium will ensure the maximum possible mass transfer rate during any phase change, while it will also simplify the modelling at the interfacial heat/mass transfer process to a simple phase equilibrium calculation. Provided that the relaxation time of thermodynamic equilibrium is shorter than the relaxation time of the overall system, the thermodynamic equilibrium assumption is justified.

However, when the flow is non-homogeneous, the averaged thermodynamic state for each phase may differ from each other. Some types of dynamic effects, non-uniform phase distribution and local velocity slip between the two phases can cause this non-homogeneity. It is seen that the departure from equilibrium can be expressed explicitly in terms of the flow non-homogeneity or U_G-U_L, where U_G and U_L are the cross-sectionally averaged velocities of the vapour and liquid phases.

The kinetic energy of two-phase flow described in this model follows that of Geurst. However, this representation may not represent the true kinetic energy of the system due to the relative motion in other flow regimes such as annular or stratified flow. However, the two phases are strongly coupled under fast transient conditions and such flow patterns do not usually occur. The energy conservation equation of two-phase mixtures is derived from Noether's invariant theorem (Logan, 1977;Geurst 1985a,b) and is shown to be comparable with the averaging formulation. In order to achieve equations that are in hyperbolic form, the flow is forced to be marginally stable. This is achieved by assuming that the void wave propagates at the gas velocity whatever the flow regime.

The flow regime transitions are specified empirically by using a flow regime map. This approach avoids the problem of complex characteristics that would render the model ill posed and arrives at a flow that is marginally stable for the void wave characteristics. Under the marginally stable condition, all information related to the structure of the flow is found to be embedded in an inertial coupling constant and an expression for this constant is obtained based on critical flow data. This model can give correct sonic characteristics up to a void fraction of 0.8.

Chen et al. (1995b) present a simplified numerical method to solve general two-phase flow equations for multi-component mixtures. Mixture properties such as density, velocity and enthalpy are based on the mass centre average of the two phases and the momentum equations for each phase are added to give a single mixture momentum equation. When the gas phase velocity is equal to that the liquid, these equations reduce to the HEM (Homogeneous Equilibrium Model). This model is simpler to solve than a two-fluid model because the convection terms can be readily expressed in terms of mixture variables. Also developed was a heterogeneous equilibrium model

called META (Multi-component Equilibrium Two-phase Analyser) incorporating both the HEM and the marginal stability two-fluid model.

The predictions of both models were investigated using pipeline depressurisation data obtained from experiments using both short and long pipes. The short pipeline was 4m in length and was that used by Necmi and Hancox (1978). It can be seen from figure 3.29 that the predicted pressure of the HEM always drops more quickly than the measured values. This is a result of HEM predicting a lower critical flow than the actual flow out of the line. It can be concluded from the data presented that either model is not very accurate where the measured values lie somewhere between the predictions made by the two models. The long pipeline field data was obtained from the Isle of Grain tests where the pipe was 100m in length. Figure 3.30 compares the predicted and measured values, while this time it can be seen that the predictions made by HEM are reasonably good.

The prediction of temperature, void fraction and inventory histories are relatively the same as the measured values. The only deviation of HEM is the rapid increase in void fraction predicted after 7s while this is not realised in the measured void fraction until after 10s. It can be seen that the Marginal Stability Model (MSM) predicts a lower pressure and temperature at both ends of the pipe than the HEM predictions and measurements, while the void fraction is higher at both ends. This suggests that the out flow is over-predicted by MSM. Except for the first second of blowdown, the predicted release of MSM and HEM are very similar. This shows that HEM is a good approximation for strongly coupled two-phase flow in long and large diameter pipelines.

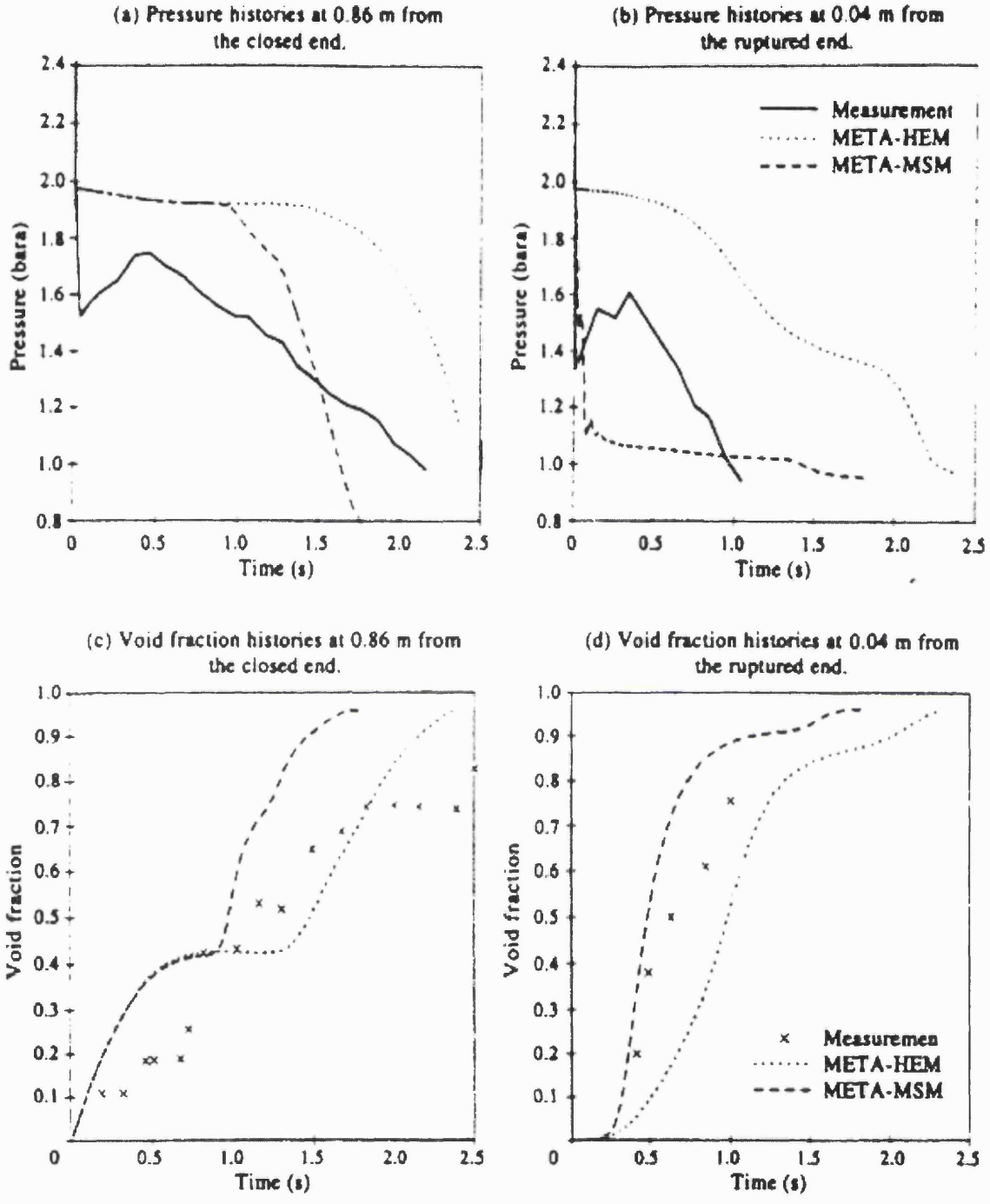

Figure 3.29 (a-d) Results of one-component systems for a 'short' pipeline (Chen et al., 1995)

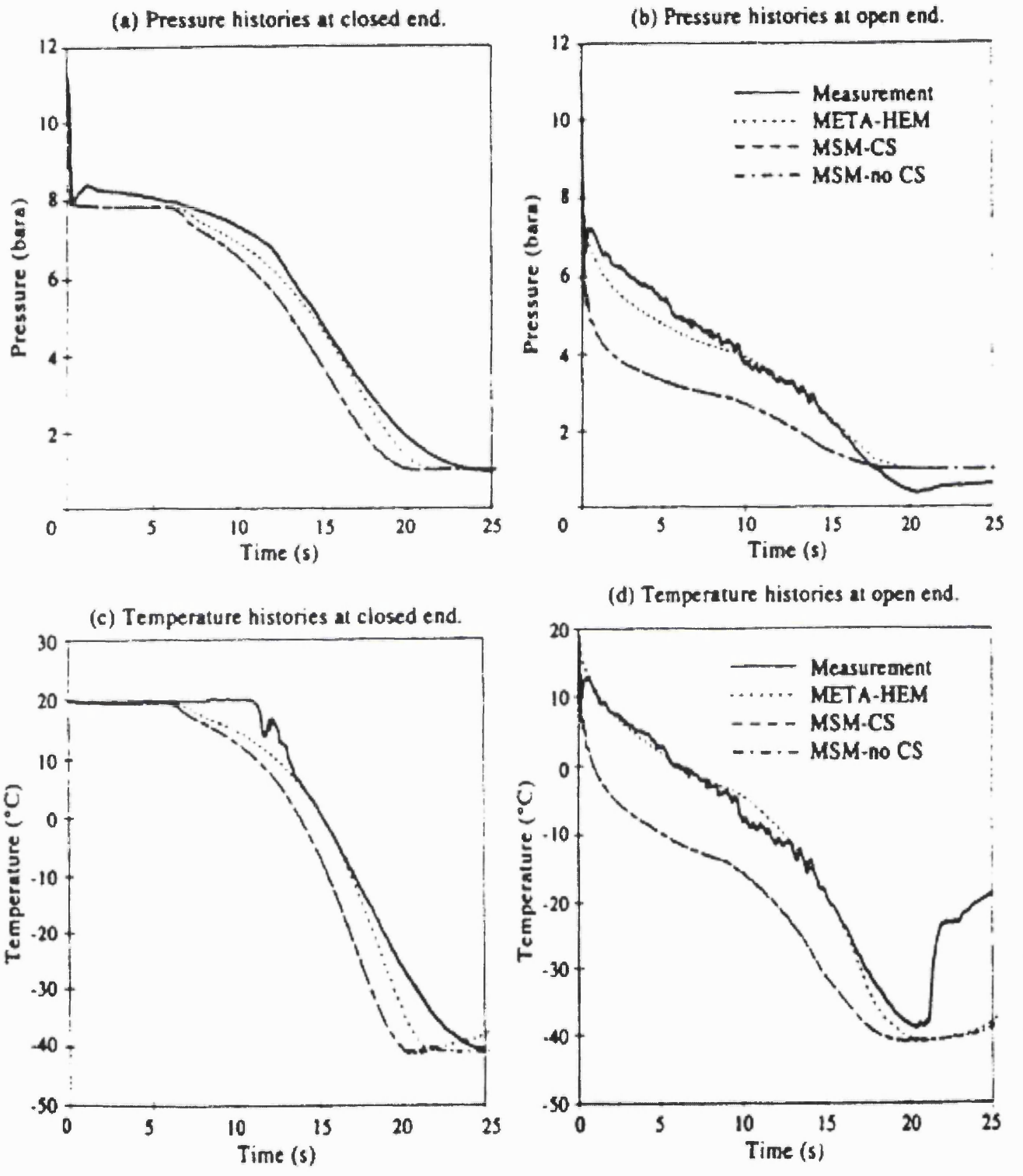

Figures 3.30 (a-d) Results of two-component systems (Chen et al., 1995)

It can also be concluded that the effects of concentration stratification can be ignored when modelling multi-component transient blowdown of long pipelines. Overall, the results show that the Marginal Stability Model performs better than the Homogeneous Equilibrium Model for blowdown of short pipelines, while both models are quite similar when modelling the blowdown of long pipelines.

The Peng-Robinson equation of state was used for all calculations of thermodynamic and phase behaviour in the above models by Chen et al. (1995b). The Marginal Stability Model took approximately 20h to execute a simulation, while the Homogeneous Equilibrium Model only took approximately 8h to run the same simulation. During these runs 95% of the CPU time was spent on the thermodynamic and phase equilibrium calculations.

An important drawback of the above model is however its inability to simulate the pertinent fluid dynamic profiles along the pipeline in particular the motion of the expansion wave from the rupture plane to the intact end of the pipeline. Mahgerefteh et al. (1997-2000) (see later) show that such phenomena critically affect the dynamic response of emergency shutdown valves following pipeline rupture.

Mahgerefteh et al. (1997) studied the dynamic response of ball valves and check valves following full-bore rupture of high-pressure gas pipelines using a numerical simulation based on MOC. The performance of the valves were evaluated on the basis of two main characteristics; namely the activation time, and the closure time. The former is based on the time taken for the fluid disturbances produced as a result of FBR to propagate from the rupture plane to the location of the emergency shut down valve (ESDV). The valve closure time on the other hand is the time it takes the valve to close once initiated to do so. Summation of the above two characteristic times gives the overall performance of the valve in the form of a valve response time.

Mahgerefteh et al.'s model was used to simulate the full bore rupture of a real North Sea pipeline where the inventory was in the gas state and the properties approximated as ideal. The authors used the same approach as that employed by Richardson et al. in solving the flow problem by expressing the compatibility equations in finite difference form, in conjunction with a nested grid system in which increasingly finer

grid were employed near the rupture. Some of the assumptions made in the development of the model were a zero closure time for the check valves and a ball valve closure rate of 2.54 cm s^{-1} As seen in figure 3.31, after rupture an expansion wave is produced that causes rapid changes in pressure and velocity of the fluid at the ruptured end. This results in a sudden pressure loss producing a flow of gas in opposite directions while conditions remain unchanged downstream of the expansion waves. The assumption of instantaneous closure of the check valve means that no pressure surges will be produced when using such a valve.

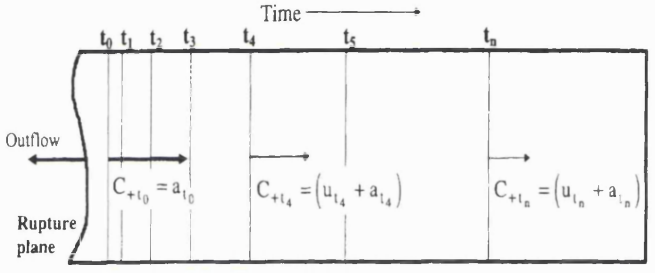

Figure 3.31 A Schematic representation of expansion wave propagation with time following full bore pipeline rupture (Mahgerefteh et al., 1997)

However, this research has shown (figure 3.32) that the common practise of employing delayed valve closure to avoid damage due to valve slamming, can in the contrary result in the build up of large pressure surges. They arise as a consequence of the reflection of the expansion wave from the closed end of the pipeline. Such effects are expected to occur more frequently in pipelines containing liquids, as the speed of the reflected wave is equal to the local speed of sound relative to the fluid velocity. These pressure surges can also give rise to cavitation in pipelines containing condensable liquids. This occurs when the pressure drop is large enough to allow the fluid to reach its vapour pressure producing a vaporous cavity that can suddenly collapse in response to a reflected pressure wave. This can result in check valves reopening momentarily and hence result in a loss of inventory. However, these surges have been demonstrated to be reduced in intensity with larger closure times (> 2s) due

to the drop in pressure from an increase of inventory loss and in long pipelines as a result of deceleration of the pressure waves due to frictional losses.

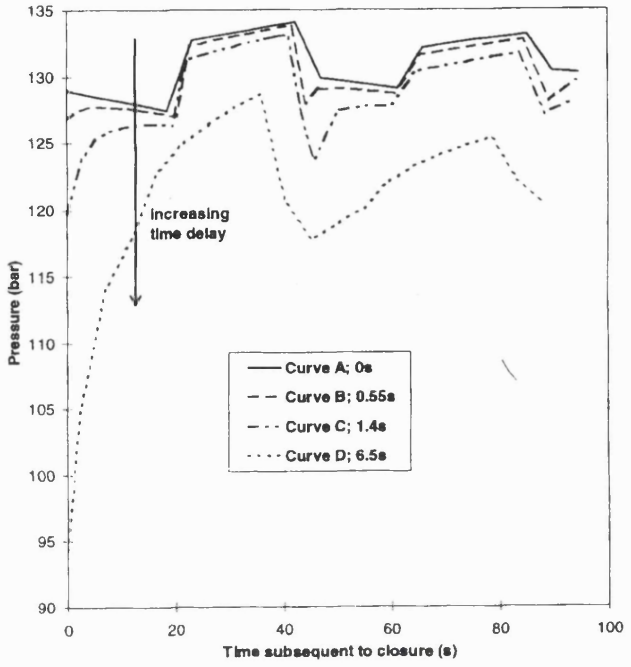

Figure 3.32 The effect of time delay on pressure-time history at the upstream side of a check valve placed 300 m from rupture plane (Mahgerefteh et al., 1997)

Figure 3.33 shows the performance of both valves in limiting the inventory loss depends on their proximity to the rupture plane and the flow reversal propagation speed. The data demonstrate that when in close proximity to the rupture plane, the check valve offers better protection while both valves perform the same at longer distances. Figure 3.34 on the other hand shows that the general consensus regarding the amount of inventory released following FBR is equal to that in the isolatable section of the pipeline prior to ESD can produce gross underestimates, especially in the case of a ball valve in close proximity to the rupture plane.

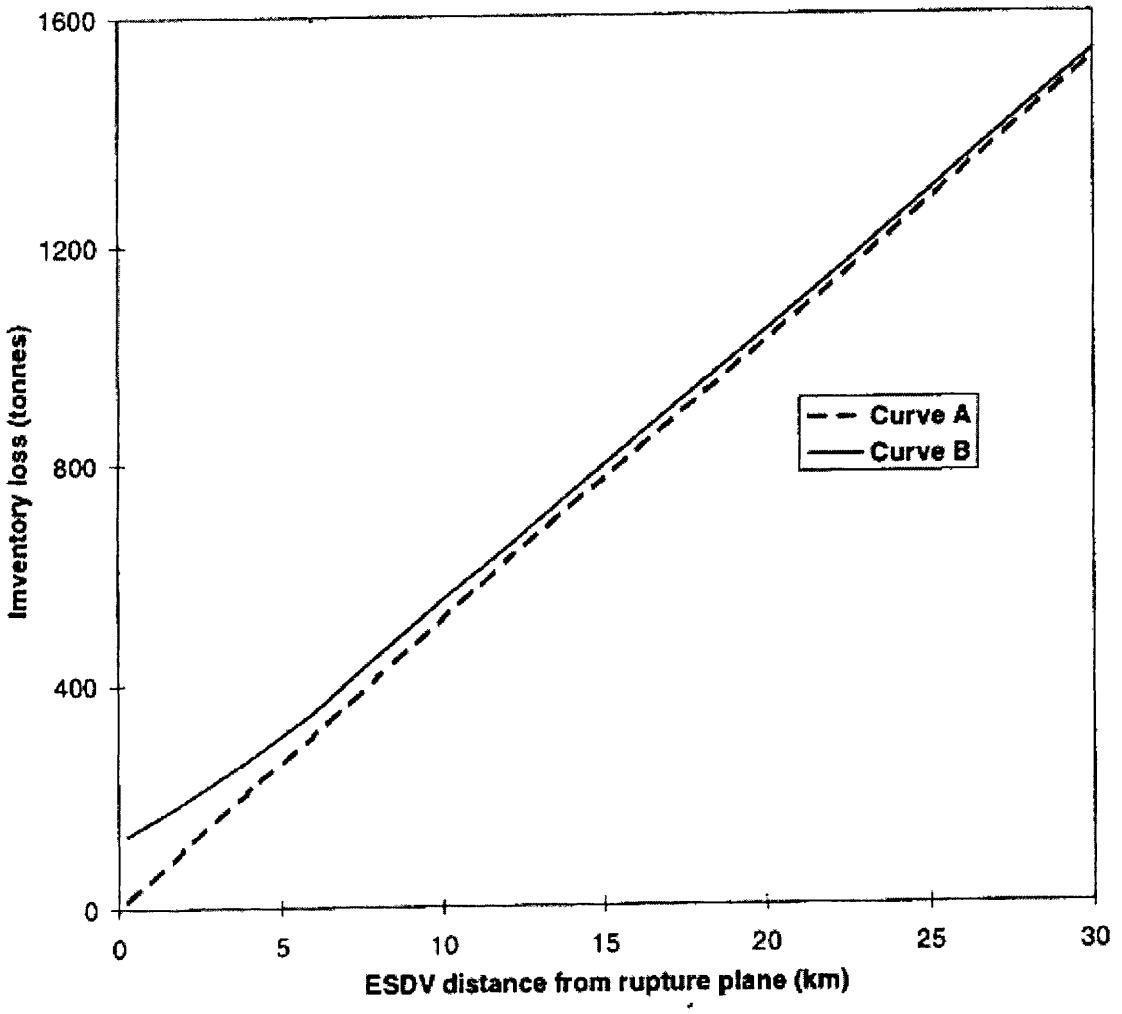

Figure 3.33 The variation of inventory loss as a function of ESDV proximity to the rupture plane

Curve A: check valve

Curve B: ball valve

(Mahgerefteh et al., 1997)

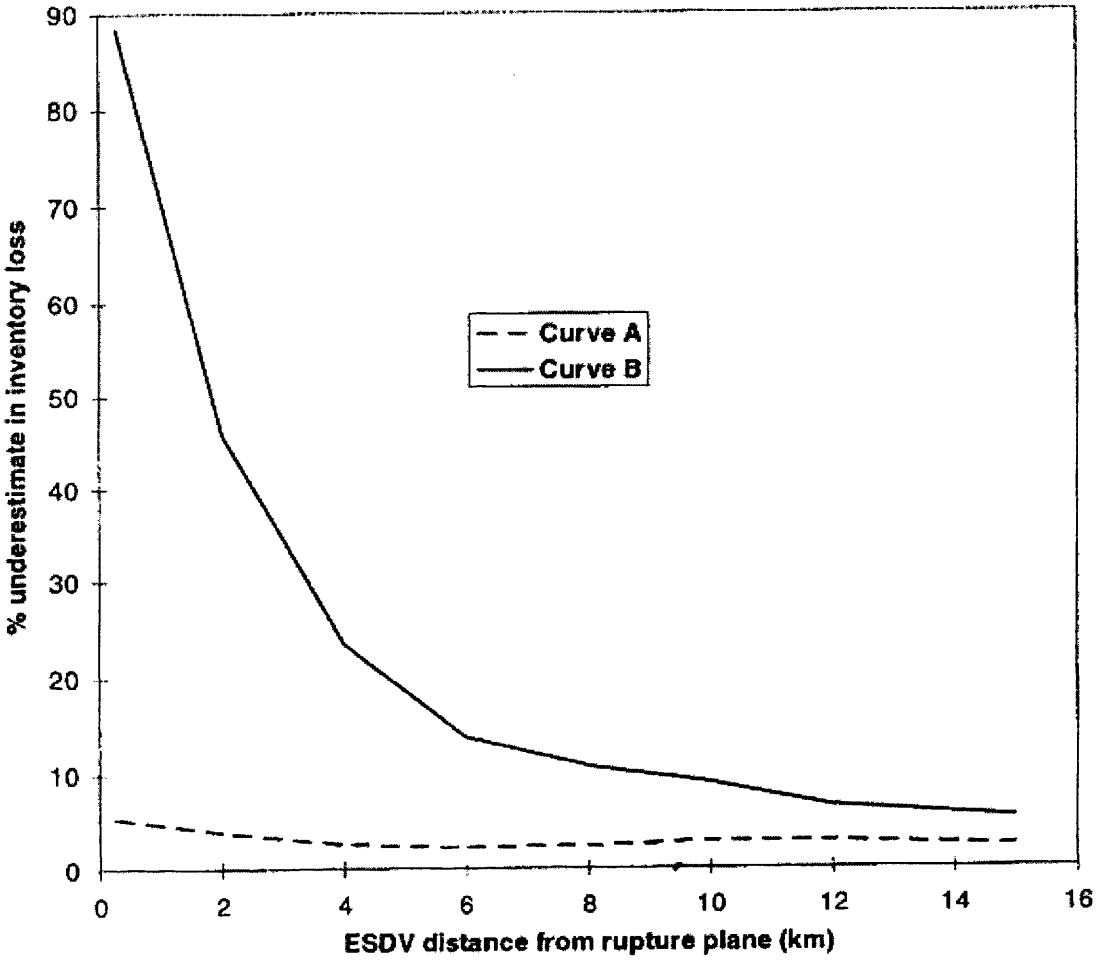

Figure 3.34 Percentage underestimate of total inventory loss based on the simple isolation section approximation
Curve A: check valve
Curve B: ball valve
(Mahgerefteh et al., 1997)

Mahgerefteh et al. (2000) extended the above model to simulate FBR involving two-phase flows and its effect on valve dynamics and associated discharge process. The method of characteristics is again the chosen method of solution with the non-linear variation in fluid properties following FBR dealt with by assuming curved characteristics. The curvature being accounted for by considering them as arcs of parabolas, as reported by Flatt (1986).

When considering a condensable fluid, liquid formation will occur as a result of significant cooling of the gas from the rapid depressurisation process. The front of this two-phase mixture travels from the rupture plane to the closed end of the pipe, where it will eventually return to its gaseous state due to heat transfer from the pipeline walls. The presence of condensate in the line will have a marked effect on reducing the speed of the expansion wave, which in turn will lead to a reduced valve activation time and a delayed emergency isolation. However, figure 3.35 shows that this small difference in the time scale gives a huge difference in the amount of inventory released. It can also be concluded from the presented data that the predicted release rates are much higher in the case of a condensable gas mixture than those for the permanent gas following emergency isolation of the pipeline. This results in more inventory being released when dealing with a two-phase mixture prior to pipeline isolation when compared to a line containing gas.

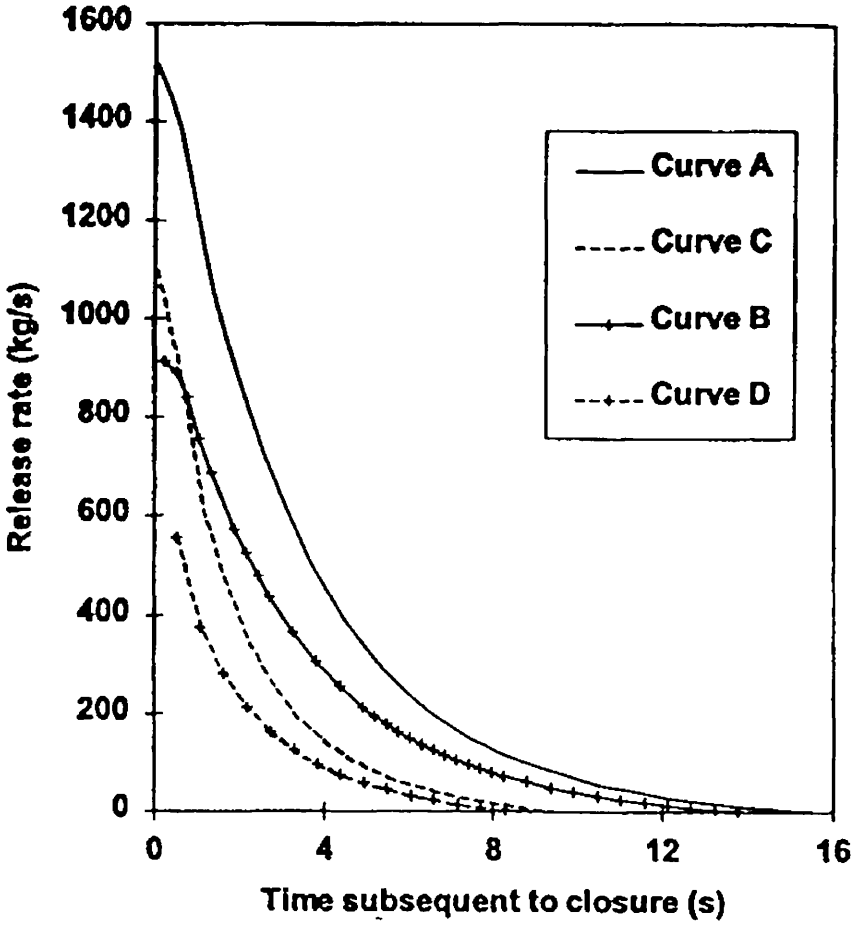

Figure 3.35 Variation of release rate with time subsequent to check valve closure for various arbitrary delays in valve shutdown

Curve A: Two-phase; valve closure delay after passage of flow reversal = 1.37 s;
Curve B: Two-phase; valve closure delay after passage of flow reversal = 6.47 s;
Curve C: Permanent gas; valve closure delay after passage of flow reversal = 1.37 s;
Curve D: Permanent gas; valve closure delay after passage of flow reversal = 6.47 s;
(Mahgerefteh et al., 2000)

On comparison of the permanent gas model and the two-phase fluid model, both models show similar pressure effects upstream of the rupture plane. However, figure 3.36 shows that on the downstream side the condensable gas mixture produces a much slower depressurisation rate as a result of the smaller pressure drop across the closing

valve due to the evaporation taking place. Also, as can be seen from figure 3.37 the condensable gas mixture has a smaller pressure surge when compared to the gas model due to the increased friction forces leading to a substantial reduction in flow velocity.

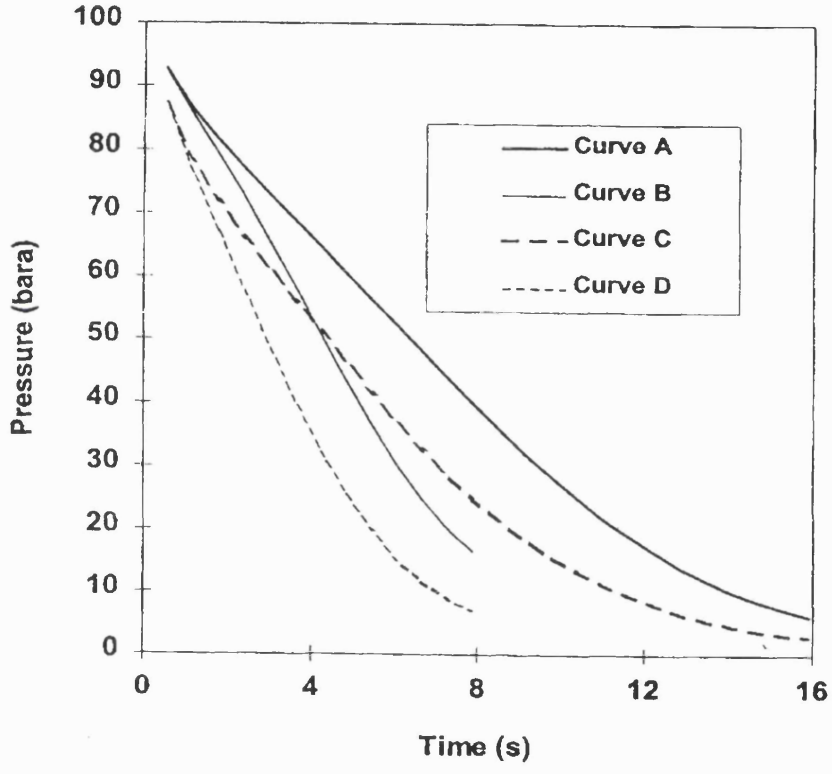

Figure 3.36 Downstream pressure-time histories at the downstream side of a closing ball valve for different closure rates

Curve A: Two-phase, 2.54 cm/s

Curve B: Two-phase, 5.08 cm/s

Curve C: Permanent gas, 2.54 cm/s

Curve D: Permanent gas, 5.08 cm/s

(Mahgerefteh et al., 2000)

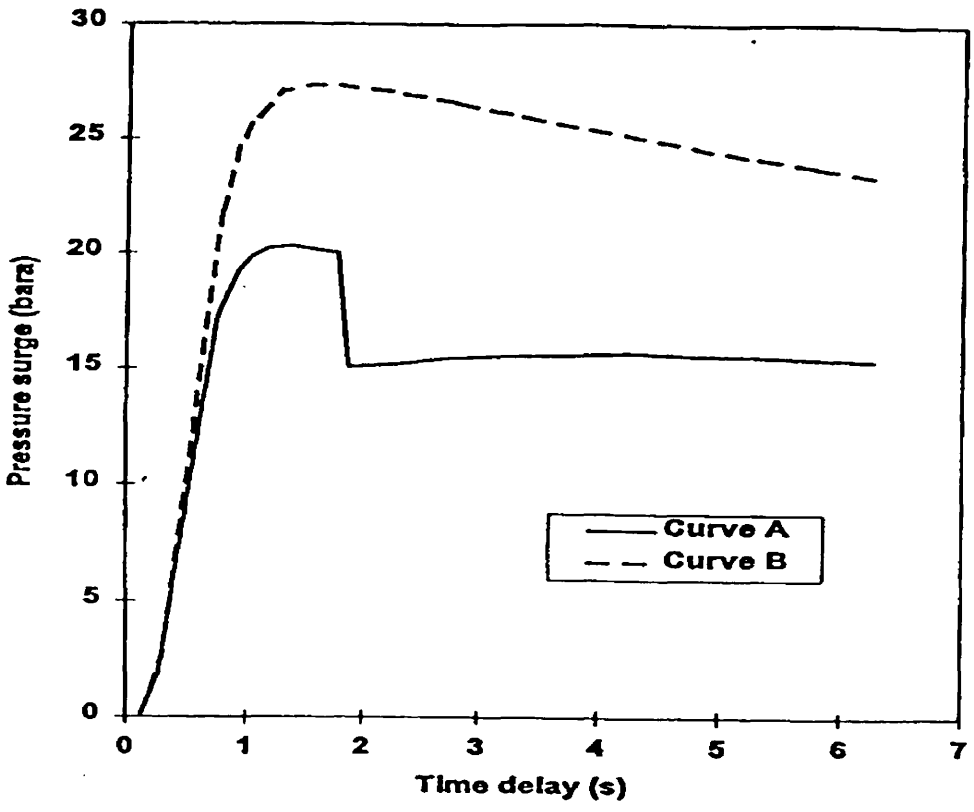

Figure 3.37 Variation of pressure surge at various check valve closure time delays following the passage of flow reversal
Curve A: Two-phase; Curve B: Permanent gas.
(Mahgerefteh et al., 2000)

One of the main problems associated with FBR simulations is the long CPU time required to reach a converged result. As simulations become increasingly complex, one of the main distinguishing characteristics in the future will be their execution time as industrial demands intensify. Mahgerefteh et al. (1999) addressed this problem by developing an efficient numerical simulator (CNGS-MOC) that produces a reduction in CPU time and a surprising improvement in accuracy. This is achieved by using the method of characteristics and solving a system of simultaneous equations. As discussed earlier, this model also uses a nested grid system and second order or curved characteristics, which improve the global accuracy and allow the use of larger discretisation grids.

The model assumes that all phases are at thermal and phase equilibrium where each simulation is based on the homogeneous equilibrium model. Such an assumption

ensures that all hydrodynamic constitutive relations pertaining to momentum exchange between two phases are non-existent. Isothermal steady-state flow is also assumed in the pipeline prior to rupture.

This model was validated with data gathered during the Piper Alpha disaster as well as FBR experiments using LPG at the Isle of Grain and compared against other models namely BLOWDOWN, META-HEM, PLAC and MSM-CS. The reduction in CPU time when simulating FBR is demonstrated in figure 3.38. All simulations were carried out on a DEC Alpha server 8400 5/440 and it can be seen that both second order solutions (curve B & C) provide the best results, while the first order CNGS solution (curve D) underestimates the release rate. Overall, the results of the Mahgerefteh et al. model show an approximate 75-fold reduction in CPU time (cf. 250 h; curve A with 3.75; curve B) when using second order characteristics along with a CNGS without any loss in accuracy.

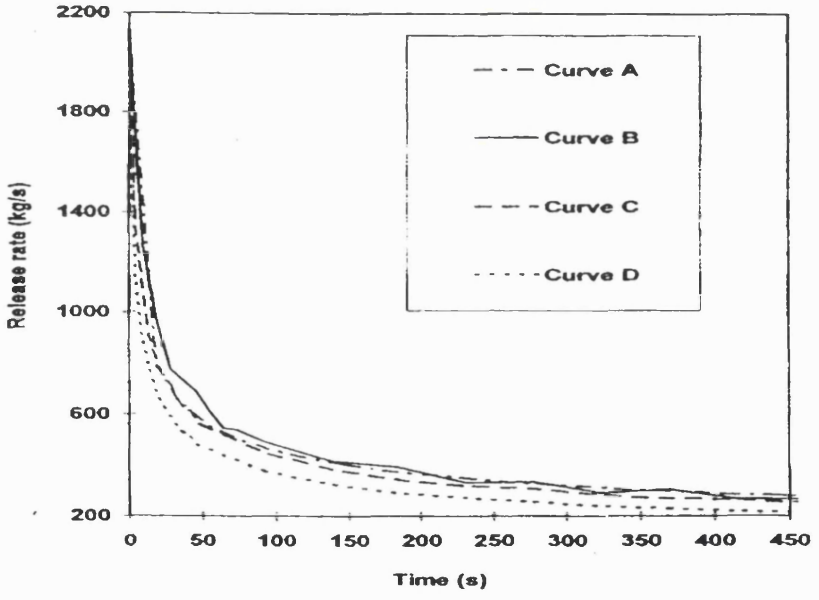

Figure 3.38 Piper Alpha: MCP line release rate profiles for different grid settings

Curve A: First Order simple grid system (SGS), Δx = 10 m, CPU time = 250 h;
Curve B: Second-order (CNGS-MOC), Δx = 500 m, CPU time = 3.75 h;
Curve C: Second-order (CNGS-MOC), Δx = 250 m, CPU time = 12.2 h;
Curve D: First-order (CNGS-MOC), Δx = 250 m, CPU time = 12.1 h.
(Mahgerefteh et al, 1999)

Figure 3.39 shows the measured intact end pressure/time history following the FBR of Piper Alpha to MCP-01 subsea line. The results reinforce the importance of accounting for real fluid behaviour when executing such simulations. It can be seen that curve B that used the second order CNGS-MOC model is in good agreement with the measured data shown by curve A. The gross inaccuracy can then be seen when comparing curve B to curve C, which employ first order characteristics in conjunction with the ideal gas assumption.

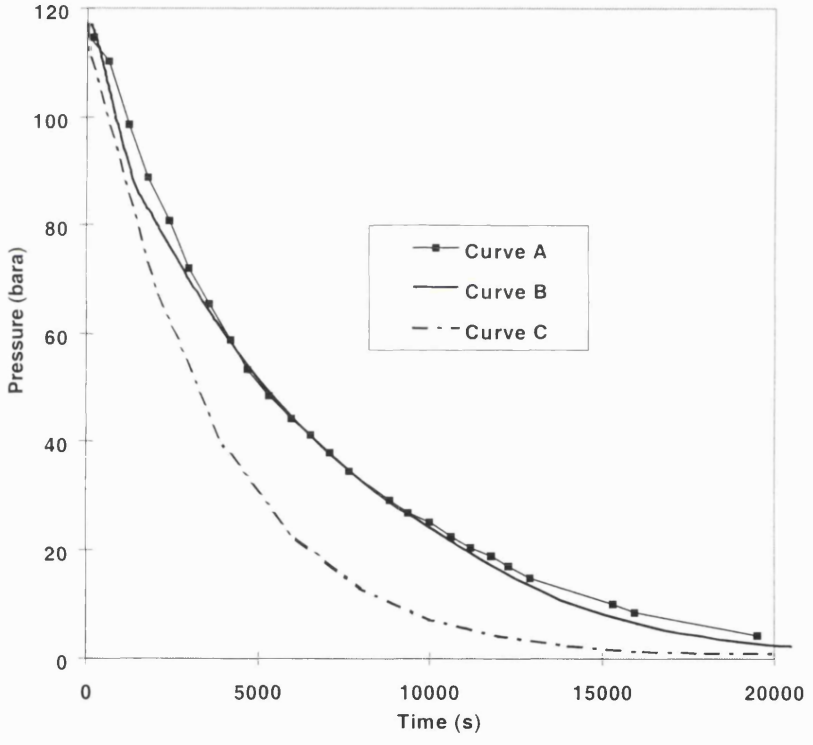

Figure 3.39 Comparison of intact end pressure (Piper Alpha-MCP line)
Curve A: Measurement
Curve B: CNGS, CPU time = 6days
Curve C: CNGS-ideal, CPU time = 1.5 minutes
(Mahgerefteh et al., 1999)

Figures 3.40 and 3.41 show the predictions for both pressure-time and temperature-time profiles at the closed and open ends based on the CNGS-MOC model compared to measurements taken during the P40 tests using LPG at the Isle of Grain. It can be seen from figure 3.40 that the predicted results represented by curves C and D are in good agreement with the measured data represented by curves A and B. The same is true for the temperature-time profiles presented in figure 3.41, where the open-end predictions being slightly higher and the closed end being slightly lower than the measured data. However, the slight differences in both sets of predicted results may be attributed to factors such as the uncertainty associated with the measurement of pressure, the inaccuracies associated with the prediction of VLE data, the uncertainty in the selected pipe roughness and the exact knowledge of the fluid composition.

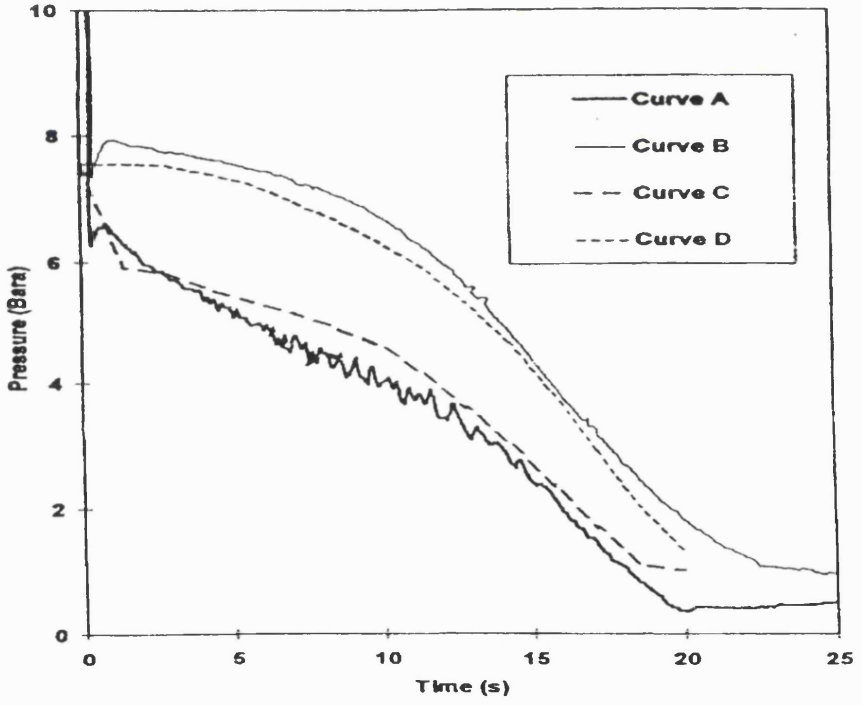

Figure 3.40 Pressure-time profiles at closed and open ends for the P40 (LPG) test
Curve A: Field data (open end); Curve B: Field data (closed end)
Curve C: Open end, CNGS-MOC; Curve D: closed end, CNGS-MOC.
(Mahgerefteh et al., 1999)

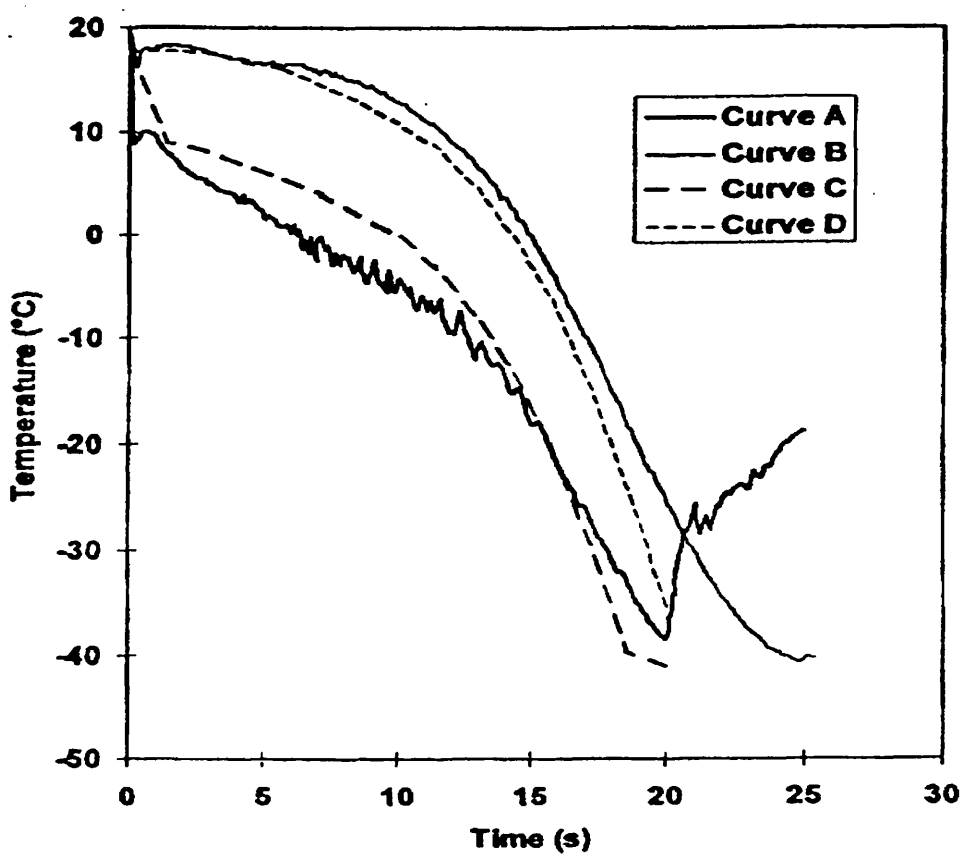

Figure 3.41 Temperature-time profiles at the open and closed ends for the P40 (LPG) test

Curve A: Field data (open end); Curve B: Field data (closed end)

Curve C: CNGS-MOC (open end); Curve D: CNGS-MOC (closed end)

(Mahgerefteh et al., 1999)

The performances of CNGS-MOC and META-HEM (Chen et al., 1993, 1995; Chen, 1995) to predict the total line inventory during depressurisation were compared with data gathered during test run P40. It can be seen from figure 3.42 that both models slightly overestimate line inventory, but give very similar results.

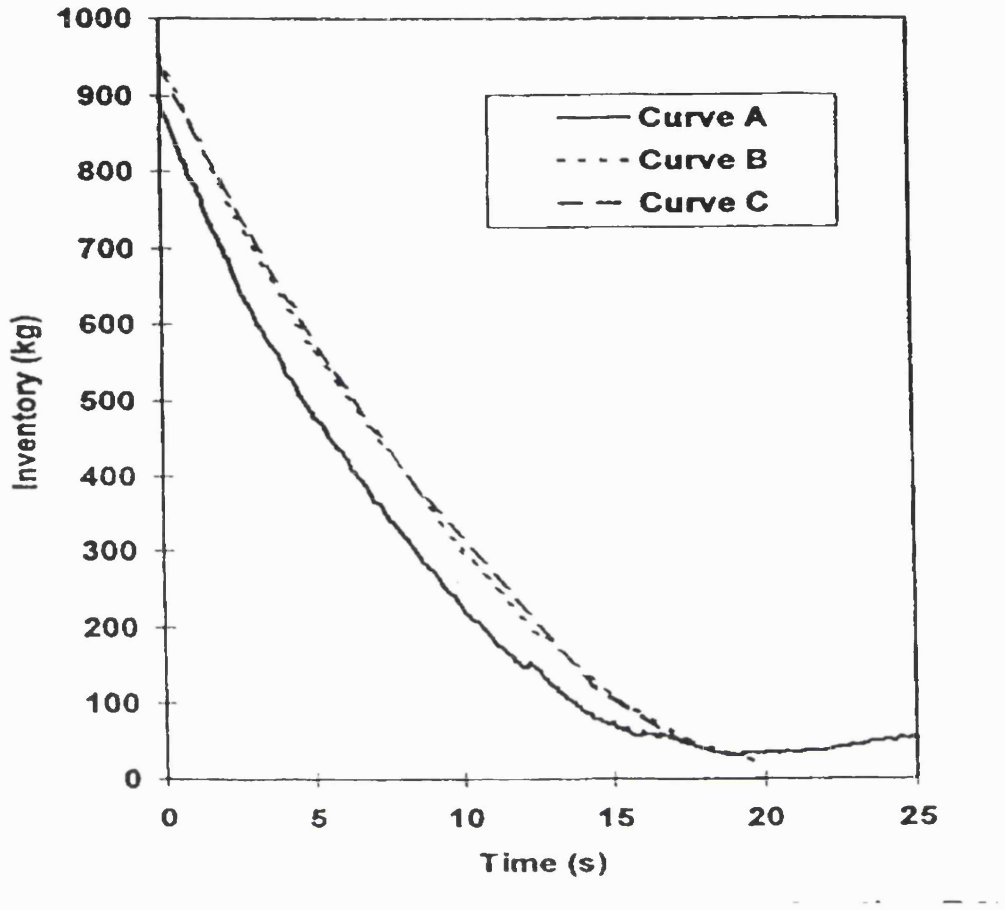

Figure 3.42 Total line inventory predictions for the P40 test (LPG)
Curve A: Field data; Curve B: META-HEM; Curve C: CNGS-MOC
(Mahgerefteh et al., 1999)

However, the true strength of the CNGS-MOC model (curve B) is demonstrated in figure 3.43 where it is compared with experimental data of the pressure-time profiles at the open end for the P42 test and other models namely: META-HEM (curve C), MSM-CS (curve D), BLOWDOWN (curve E) and PLAC (curve F). Both CNGS-MOC and META-HEM give the best predictions, while the others perform relatively poorly mainly due to some assumptions, such as the quasi steady-state flow assumption in BLOWDOWN.

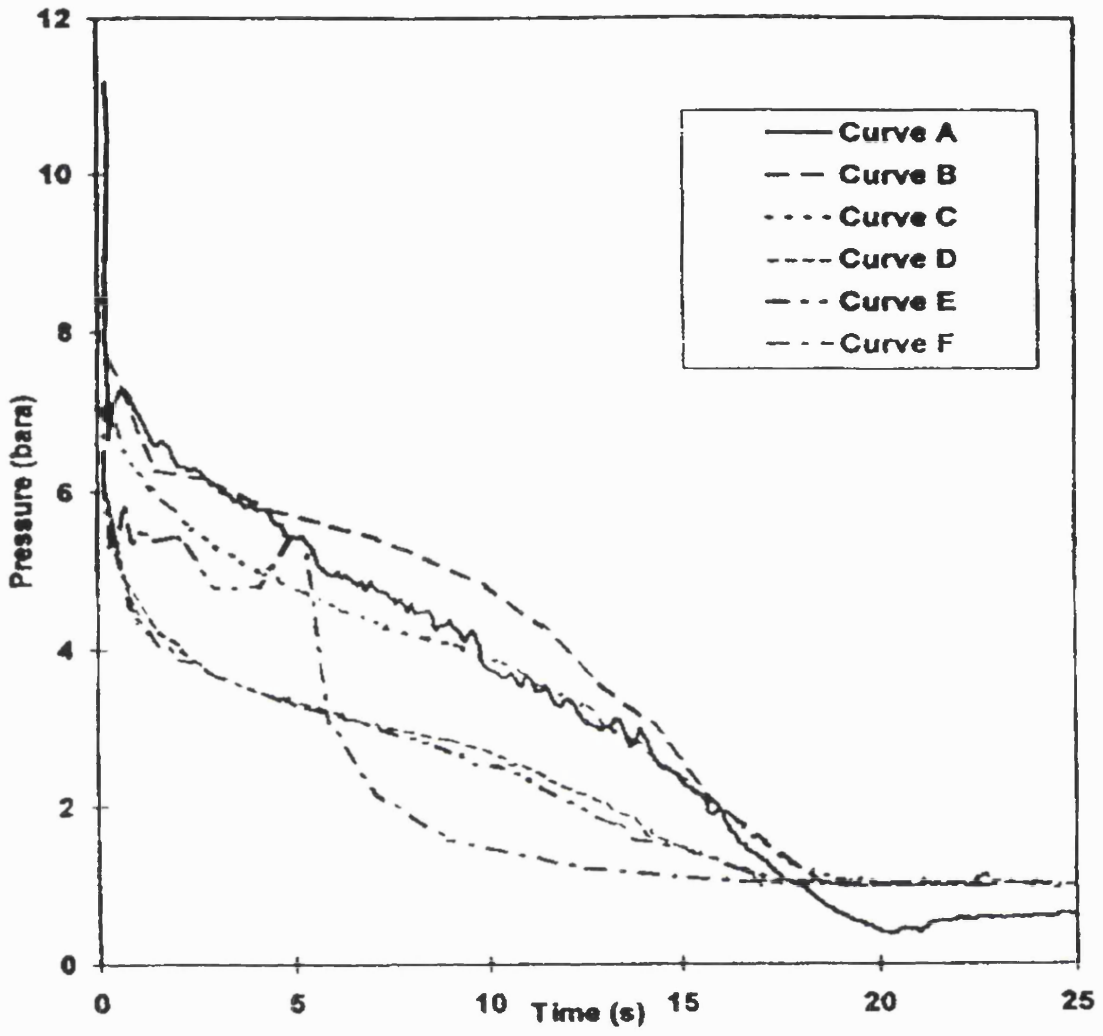

Figure 3.43 Pressure-time profiles at the open end for the P42 (LPG) test
Curve A: Field Data; Curve B: CNGS-MOC; Curve C: META-HEM
Curve D: MSM-CS; Curve E: Blow down; Curve F: PLAC
(Mahgerefteh et al., 1999)

Figure 3.44 shows the same data as for figure 3.43, but for the closed end. This time CNGS-MOC, META-HEM and BLOWDOWN show very similar results with MSM doing less well and PLAC performing very poorly. PLAC again predicts a large pressure drop at ca. 5 s and continues to drop much faster than the other models.

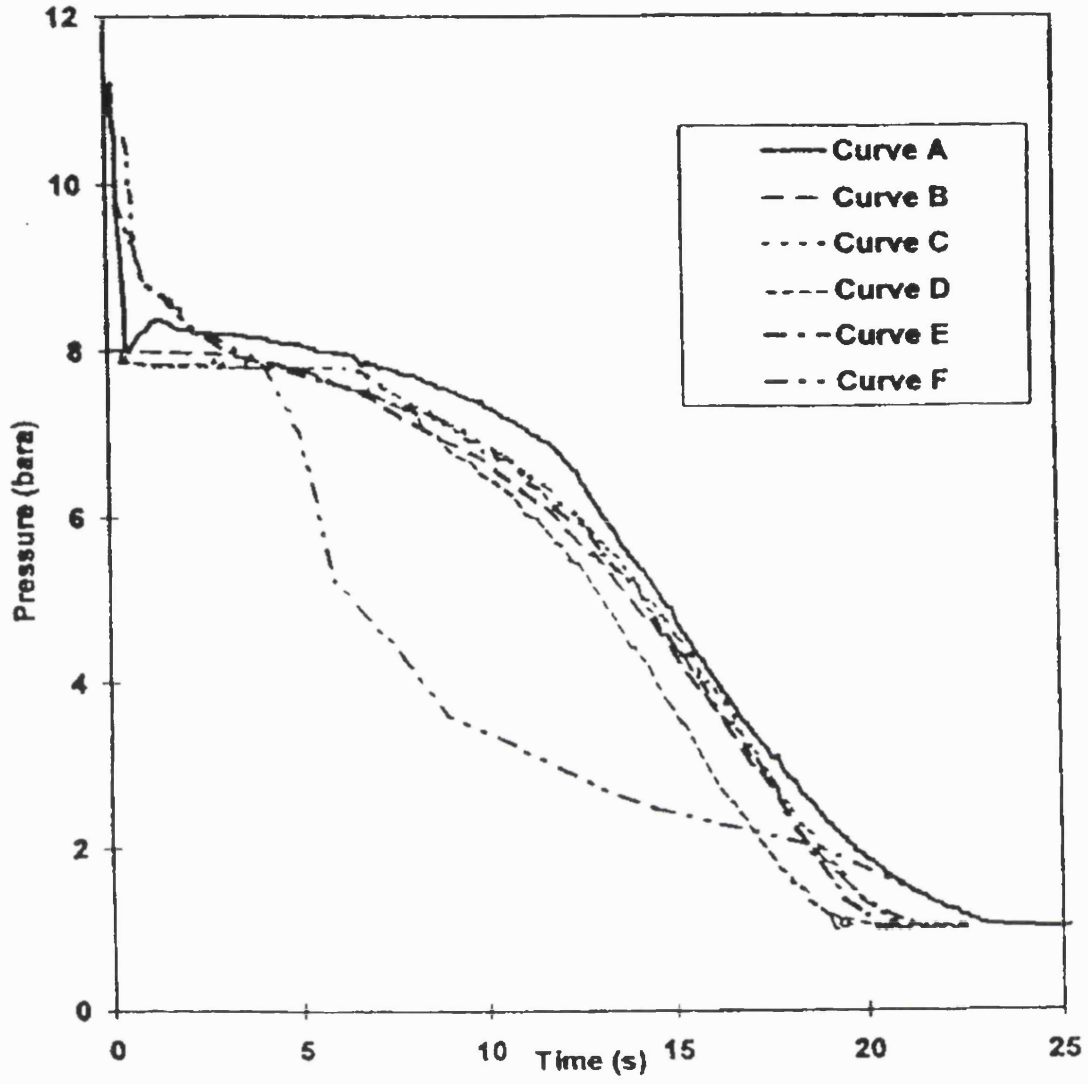

Figure 3.44 Pressure-time profile predictions at the closed end for the P42 (LPG) test

Curve A: Field data; Curve B: CNGS-MOC; Curve C: META-HEM

Curve D: MSM-CS; Curve E: BLOWDOWN, Curve F: PLAC

(Magerefteh et al., 1999)

Tao and Ti (1998) and Ke and Ti (2000) utilised a unique approach in the transient analysis of gas pipeline network. The authors used the electric analogy method for the computation of solutions to the transient gas transmission problem. Instead of having to handle the original partial differential equations, a set of first order ordinary

differential equations were solved in their place. Again the above authors employed the isothermal flow and ideal gas assumptions both of which are highly unrealistic.

Dukhovnaya and Adewumi (2000) used the TVD scheme (Total Variation Diminishing) to integrate the system of equations governing two-phase transient flow in pipelines. The TVD scheme is based on the determination of real eigenvalues for the system of equations, and their consequent use in obtaining the final solution. In deriving of their scheme, the author employed several simplifying assumptions, which limit the applicability of his model in simulating real rupture scenarios. Firstly it is assumed that the speed of sound for each fluid phase is constant along the flow direction. Secondly, as a boundary and initial condition, it is assumed that the inlet/outlet pressure is maintained at a constant value, while the outlet /inlet flow rate of the mixture and temperature are known functions of time (or a constant value) respectively.

3.6 CONCLUSION

Since the partial differential equations, which were derived in chapter 2, are not analytically solvable, an appropriate numerically based mathematical method is required for their solution. In this chapter a summary of existing mathematical methods developed for this purpose was presented. Based on the above review, an accurate and appropriate solution method is chosen for the purpose of this study.

A comprehensive literature survey on work relating to the modelling of outflow following pipeline rupture is also presented. This survey has highlighted the key attributes and limitations of the proposed models, while also emphasising the importance of taking into account real-fluid behaviour. This survey has also demonstrated the importance of the validation of reported models by comparison against experimental data. Much of the experimental data available is taken from either small-scale tests or short-tube experiments, which are important at certain stages in the development of a computer model. The pipeline rupture tests conducted by BP and Shell on the Isle of Grain may be considered as the benchmark for validation purposes. These have been conducted using fully instrumented pipelines

under controlled conditions. However, these are limited to relatively short pipelines. The ultimate test of the accuracy and robustness of pipeline rupture models require validation against full-scale experiments, for which there very little data is available.

The field experiments conducted by the Alberta Petroleum Industry to evaluate and improve H_2S isopleth prediction techniques are very useful in that they provide an important insight into the effects of various parameters affecting outflow following pipeline rupture. An interesting and potentially important observation based on these tests is that at least in the early stages of depressurisation, the pipeline length has little effect on the discharge rate. However, more tests in conjunction with condensable hydrocarbon mixtures are required before establishing such finding as a general rule. A positive outcome would largely address the problem of modelling outflow in long pipelines where long computation run times are a severe limitation.

All the models reviewed in this chapter are limited to modelling release following pipeline rupture in horizontal and uniform diameter pipelines. No models relating to outflow simulation for at inclined or enlarged pipelines have been reported.

Among the models, which have been reviewed in this chapter, the homogenous equilibrium based models by Mahgerefteh et al. (1999, 2000), and Chen et al. (1995a, b) have been the most extensively validated against field data. Mahgerefteh et al.'s model performs better in terms of computational run time, simulates in-line dynamic effects following valve closure, and is based on a more robust numerical solution technique (MOC).

In the next chapter, the application of the method of characteristics and the derivation of compatibility equations will be addressed in detail. This is followed by the details of the procedure involved in the solution of flow transients throughout the length of the pipeline. This covers the method utilised in the solution of the compatibility equations, and the definition of the nature and type of the initial and boundary conditions employed.

CHAPTER 4
APPLICATION OF THE MOC FOR THE MODELLING OF PIPELINE RUPTURE

4.1 INTRODUCTION

As highlighted in chapter 2, no analytical solution for the partial differential equations, characterising the transient flow in a pipeline following its FBR is available. The method of characteristics chosen as the numerical solution tool for the above was fully discussed in chapter 3. In this chapter, the characteristic lines and corresponding compatibility equations are presented based on the methods developed by Zucrow and Hoffman (1976). In the absence of an analytical solution, this is followed by a description of the numerical technique for the solution of the compatibility equations for inclined pipelines. The above, in conjunction with the use of the appropriate boundary conditions at the pump inlet and the rupture plane allow the simulation of the ensuing transient fluid dynamics within the pipeline following FBR. This is then followed by the presentation of the corresponding outflow calculation algorithm for an enlarged pipeline. The modelling for simulating the steady state flow is also presented, as this is an important pre-requisite for establishing the conditions within the inclined pipeline prior to its FBR.

4.2 COMPATIBILITY EQUATIONS

The first step in any method of characteristics solution is to convert the basic partial differential equations of flow into ordinary differential equations. The two most common methods of achieving this are the matrix transformation method, such as that used by Tiley (1989), and that of multiplying the basic equations by an unknown parameter and subsequent summation. The latter method is used by Lister (1960), Wylie and Streeter (1978) for isothermal flow and by Zucrow and Hoffman (1976) for non-isothermal flow. The method used by Zucrow and Hoffman (1976) is adapted for this study because of its simplicity and mathematical rigour. In this method, the three

conservation equations (equations 2.3,2.14,2.44) may be replaced by the following characteristic

$$\lambda = \frac{d_0 t}{d_0 x} = \frac{1}{u} \qquad \text{Path line} \qquad (4.1)$$

$$\lambda_+ = \frac{d_+ t}{d_+ x} = \frac{1}{u+a} \qquad \text{Positive Mach line} \qquad (4.2)$$

$$\lambda_- = \frac{d_- t}{d_- x} = \frac{1}{u-a} \qquad \text{Negative Mach line} \qquad (4.3)$$

where

λ = slope of the characteristic line

dt = time step

dx = distance step

The corresponding compatibility equations along the above characteristic lines can be presented as (Zucrow and Hoffman, 1976)

$$d_0 P - a^2 d_0 \rho = \psi d_0 t \text{ along } \frac{d_0 t}{d_0 x} = \frac{1}{u} \qquad (4.4)$$

$$d_+ P + \rho a d_+ u = [\psi + a\varpi] d_+ t \text{ along } \frac{d_+ t}{d_+ x} = \frac{1}{(u+a)} \qquad (4.5)$$

$$d_- P - \rho a d_- u = [\psi - a\varpi] d_- t \text{ along } \frac{d_- t}{d_- x} = \frac{1}{(u-a)} \qquad (4.6)$$

All the symbols have been defined in chapter 2.

The compatibility equations (4.4-4.6) stipulate the way in which information is propagated through a flow field. As such, they play a fundamental role in dictating the discharge process.

To apply the characteristic and compatibility equations, a characteristic grid or network must be devised. Figure 4.1 represents a schematic presentation of a

characteristic network. The three characteristic lines intersect at a common point (j), and the flow properties (ρ, p and u) at that point are solved simultaneously with the aid of the three compatibility equations.

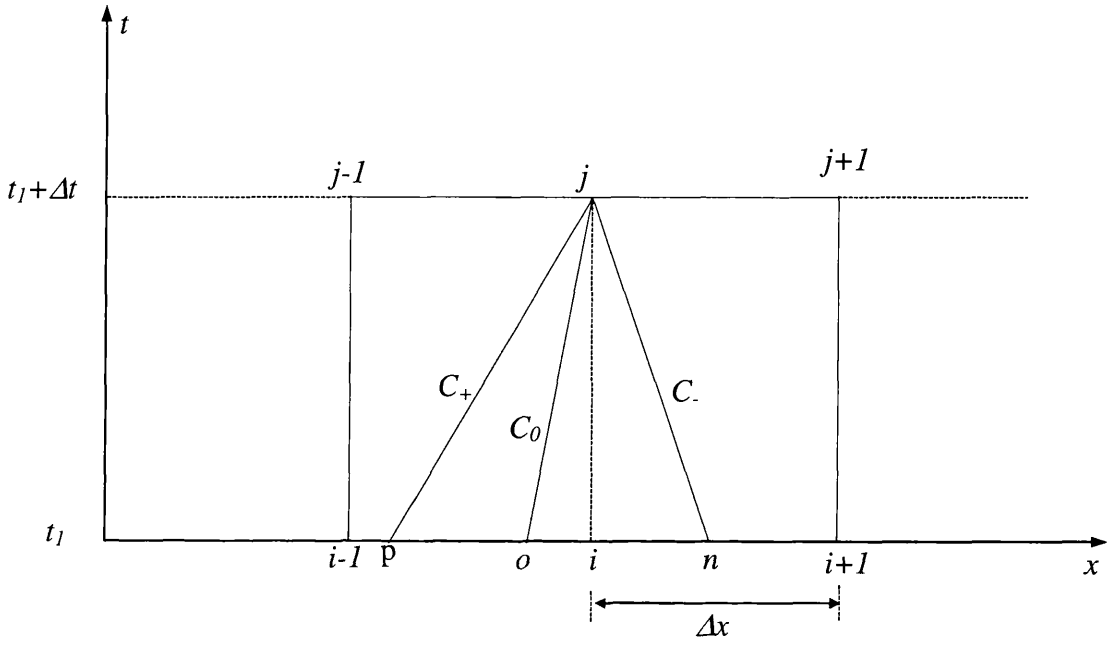

Figure 4.1 Schematic representation of a characteristic network

In order to apply the compatibility equations along the characteristic grid networks it is initially necessary to determine the conditions at p, o and n at time t_1. Assuming that initial conditions are known at all nodes at time t_1, then the most common solution to this situation is to interpolate linearly between $i+1$, i, $i-1$.

Knowing the condition at points p, o and n, the compatibility equations can be solved via a finite difference method. In order to reduce the error introduced by first order finite difference solution, the Euler predictor-corrector technique, which will be discussed in detail in section 4.3, is employed in this study.

The characteristic lines used in the solution of compatibility equations (equations 4.4-4.6) can be approximated either as straight lines (figure 4.1) or curves as indicated in figure 4.2. The methods of solving the solution point based on both assumptions are presented in the following sections. These involve the solution of the interior point in conjunction with the pertinent boundary conditions.

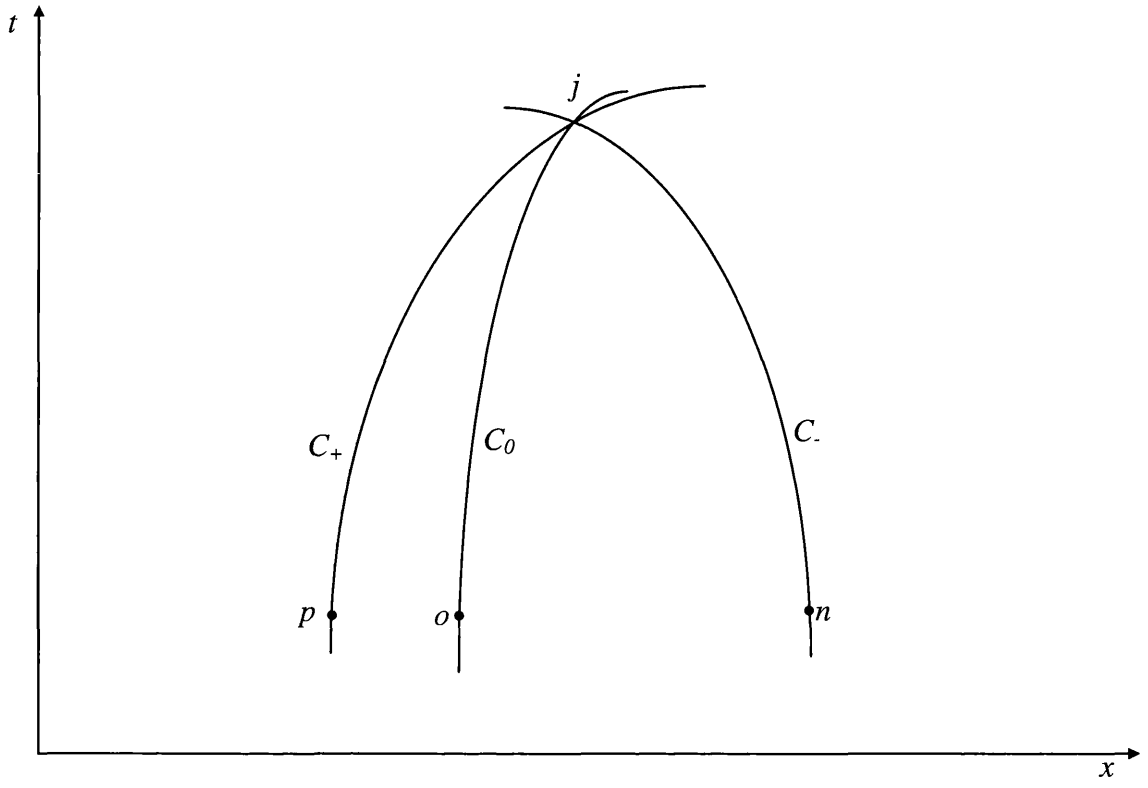

Figure 4.2 Schematic representation of characteristic network: curve characteristics pathway

4.3 THE INTERIOR POINT CALCULATION BASED ON THE LINEAR CHARACTERISTIC ASSUMPTION

The compatibility equations (equation 4.4-4.6) are total differential equations, which must be solved numerically. This rests on how to approximate the flow properties in space and in time, $f(x, t)$ within the given interval.

The common practice in the method of characteristics solution is to use first-order approximation to calculate values at the next time level based on convergence of some iteration criteria. However this might lead to a substantial error in the results. Some workers (see for example Kimambo and Thorley, 1995) have done just one calculation using the first order approximation to obtain an initial guess of flow variables at the solution point followed by a second order approximation. Adopting this procedure makes the solution more like the Euler Predictor-Corrector method (Zucrow and Hoffman, 1976), which is also used in this study.

The Euler predictor-corrector technique as its name implies comprises of the predictor and the corrector steps. In the predictor step the linear finite difference method is used to calculate the initial approximate value. While in the corrector step, the first estimate from the predictor step is enhanced by a second order approximation of the compatibility equations.

The first order or linear finite difference approximation, is expressed by the formula

$$\int_{x_2}^{x_1} f(x)dx \approx f(x_0)(x_1 - x_0) \tag{4.7}$$

From the application of the first order finite difference approximations, the characteristic lines (figure 4.1) equations and corresponding compatibility equations can be shown as

Path line characteristic

$$x_j - x_o = \frac{1}{(\lambda_0)_o}(t_j - t_o) \tag{4.8}$$

Path line compatibility

$$P_j - P_o - (a^2)_o(\rho_j - \rho_o) = \psi_o(t_j - t_o) \tag{4.9}$$

Positive Mach line or right running characteristic

$$x_j - x_p = \frac{1}{(\lambda_+)_p}(t_j - t_p) \tag{4.10}$$

Positive Mach line compatibility

$$P_j - P_p + (\rho a)_p(u_j - u_p) = (\psi + a\varpi)_p(t_j - t_p) \tag{4.11}$$

Negative Mach line or left running characteristic

$$x_j - x_n = \frac{1}{(\lambda_-)_n}(t_j - t_n) \tag{4.12}$$

Negative Mach line compatibility

$$P_j - P_n - (\rho a)_n (u_j - u_n) = (\psi - a\varpi)_n (t_j - t_n) \tag{4.13}$$

The subscripts to the various properties in equations (4.8) to (4.13) denote the location on the characteristic grids.

The second order approximation, which is used in the corrector step, can be expressed as

Path line characteristic

$$x_j - x_o = \frac{1}{2\left((\lambda_0)_o + (\lambda_0)_p\right)}(t_j - t_o) \tag{4.14}$$

Path line compatibility

$$P_j - P_o - \frac{1}{2}\left(\left(a^2\right)_o + \left(a^2\right)_j\right)\left(\rho_j - \rho_o\right) = \frac{1}{2}\left(\psi_o + \psi_j\right)\left(t_j - t_o\right) \tag{4.15}$$

Positive Mach line or right running characteristic

$$x_j - x_p = \frac{1}{2\left((\lambda_+)_p + (\lambda_+)_j\right)}(t_j - t_p) \tag{4.16}$$

Positive Mach line compatibility

$$P_j - P_p + \frac{1}{2}\left((\rho a)_p + (\rho a)_j\right)(u_j - u_p) = \frac{1}{2}\left((\psi + a\varpi)_p + (\psi + a\varpi)_j\right)(t_j - t_p) \tag{4.17}$$

Negative Mach line or left running characteristic

$$x_j - x_n = \frac{1}{2\left((\lambda_-)_n + (\lambda_-)_j\right)}(t_j - t_n) \tag{4.18}$$

Negative Mach line compatibility

$$P_j - P_n - \frac{1}{2}\left((\rho a)_n + (\rho a)_j\right)(u_j - u_n) = \frac{1}{2}\left((\psi - a\varpi)_n + (\psi - a\varpi)_j\right)(t_j - t_n) \tag{4.19}$$

In order to work out the conditions at the solution point, j, the fluid properties at points p,o and n need to be calculated initially. However their location must be computed first. This is performed by making the initial approximation such that,

$u_o=u_{i-1}$, $u_p=u_{i-2}$, $u_n=u_i$ so that the characteristic slopes given by equations (4.1) to (4.3) can be written as

$$\lambda_o = \frac{1}{u_o} = \frac{1}{u_i} = \frac{\Delta t}{x_i - x_o} \Rightarrow x_o = x_i - \Delta t u_i \tag{4.20}$$

$$\lambda_+ = \frac{1}{u_p + a_p} = \frac{1}{u_{i-1} + a_{i-1}} = \frac{\Delta t}{x_i - x_p} \Rightarrow x_p = x_i - \Delta t\left(u_{i-1} + a_{i-1}\right) \tag{4.21}$$

$$\lambda_- = \frac{1}{u_n - a_n} = \frac{1}{u_{i+1} - a_{i+1}} = \frac{\Delta t}{x_i - x_n} \Rightarrow x_n = x_i - \Delta t\left(u_{i+1} - a_{i+1}\right) \tag{4.22}$$

Once the positions of the points *p,o* and *n* are known, the variables at these points can be calculated by linear interpolation along the spatial axis, between points *i-1*, *i*, and *i+1* (figure 4.1). Therefore

$$\mathrm{Y}_p = \mathrm{Y}_{i-1} + \frac{\mathrm{Y}_i - \mathrm{Y}_{i-1}}{x_i - x_{i-1}}\left(x_p - x_{i-1}\right) \tag{4.23}$$

$$\mathrm{Y}_n = \mathrm{Y}_i + \frac{\mathrm{Y}_{i+1} - \mathrm{Y}_i}{x_{i+1} - x_i}\left(x_n - x_i\right) \tag{4.24}$$

$$\mathrm{Y}_o = \begin{cases} \mathrm{Y}_{i-1} + \dfrac{\mathrm{Y}_i - \mathrm{Y}_{i-1}}{x_i - x_{i-1}}\left(x_o - x_{i-1}\right) \text{if } \lambda_o > 0 \\ \mathrm{Y}_i + \dfrac{\mathrm{Y}_{i+1} - \mathrm{Y}_i}{x_{i+1} - x_i}\left(x_o - x_i\right) \text{if} \lambda_o < 0 \end{cases} \tag{4.25}$$

where: Y = *u*, *P*, ρ, and *a*.

The above yields tentative values for the location and flow properties at points *p,o* and *n*. These values can be improved by repeating the above steps iteratively, each time using the most recent values as calculated from the interpolation equations. Once a specified tolerance for the values at x_p, x_n, and x_o have been satisfied, the solution point (*j*) flow variables can be calculated from the compatibility equations (4.9), (4.11) and (4.13) for the predictor step followed by equations (4.15), (4.17), and (4.19) for the corrector step.

Thus the solution point flow variables are evaluated, first using the initial estimate to get tentative solutions and then repeated using the average values of *u*, *p*, ρ, and *a* along each characteristic. This procedure is repeated until another convergence

tolerance is satisfied for the solution point, *j*. This is the established procedure for the method of specified time intervals.

A modification to this method is proposed by Saha (1997), which has been used in this study. In this method the location of the initial points is immediately found without the need for any iteration thus significantly reducing the computational workload.

For the predictor step

$$\frac{d_o t}{d_o x} = \frac{1}{u_o} = \frac{\Delta t}{x_i - x_o} \Rightarrow x_o = x_i - \Delta t u_0 \tag{4.26}$$

$$\frac{d_+ t}{d_+ x} = \frac{1}{u_p + a_p} = \frac{\Delta t}{x_i - x_p} \Rightarrow x_p = x_i - \Delta t\left(u_p + a_p\right) \tag{4.27}$$

$$\frac{d\_t}{d\_x} = \frac{1}{u_n - a_n} = \frac{\Delta t}{x_i - x_n} \Rightarrow x_n = x_i - \Delta t\left(u_n - a_n\right) \tag{4.28}$$

In equations (4.26) to (4.28), expressions for the velocity and speed of sound can be obtained from the first order interpolation formulas. These expressions can then be substituted back into the above characteristic equations, (4.26) to (4.28) to give

$$\begin{aligned} u_p &= u_{i-1} + \frac{u_i - u_{i-1}}{x_i - x_{i-1}}\left[x_i - x_{i-1} - \Delta t\left(u_p + a_p\right)\right] \\ &= u_i - \frac{u_i - u_{i-1}}{x_i - x_{i-1}} \Delta t\left(u_p + a_p\right) \end{aligned} \tag{4.29}$$

Rearranging the above, we can write

$$u_p\left(1 + \frac{u_i - u_{i-1}}{x_i - x_{i-1}} \Delta t\right) + \frac{u_i - u_{i-1}}{x_i - x_{i-1}} \Delta t a_p = u_i \tag{4.30}$$

Carrying out the same manipulation for a_p, we obtain

$$a_p\left(1 + \frac{a_i - a_{i-1}}{x_i - x_{i-1}} \Delta t\right) + \frac{a_i - a_{i-1}}{x_i - x_{i-1}} \Delta t u_p = a_i \tag{4.31}$$

Equations (4.30) and (4.31) can be solved simultaneously for u_p and a_p.

Similarly a 2×2 system of equations can be set up for u_n and a_n based on the same mathematical manipulation to yield

$$u_n\left(1+\frac{u_{i+1}-u_i}{x_{i+1}-x_i}\Delta t\right)-\frac{u_{i+1}-u_i}{x_{i+1}-x_i}\Delta t a_n = u_i \tag{4.32}$$

$$a_n\left(1+\frac{a_{i+1}-a_i}{x_{i+1}-x_i}\Delta t\right)-\frac{a_{i+1}-a_i}{x_{i+1}-x_i}\Delta t u_n = a_i \tag{4.33}$$

For u_o, the solution depends on whether the slope of the pathline characteristic is positive or negative. The nature of the sign determines which way the fluid is flowing. Positive denotes flow towards ruptured end whilst negative denotes flow towards the intact end.

If $\lambda_o > 0$ then

$$u_o = u_{i-1} + \frac{u_i - u_{i-1}}{x_i - x_{i-1}}\left(x_i - \Delta t u_o - x_{i-1}\right)$$

Expanding the second term in the above equation gives

$$u_o = u_{i-1} + u_i - u_{i-1} - \frac{u_i - u_{i-1}}{x_i - x_{i-1}}\Delta t u_o$$

$$= u_i - \frac{u_i - u_{i-1}}{x_i - x_{i-1}}\Delta t u_o \tag{4.34}$$

Rearranging equation (4.34) we can write

$$u_o = \frac{u_i}{\left(1+\frac{u_i - u_{i-1}}{x_i - x_{i-1}}\Delta t\right)} \tag{4.35}$$

If $\lambda_o < 0$, a similar equation for u_o can be derived

$$u_o = \frac{u_i}{\left(1+\frac{u_{i+1} - u_i}{x_{i+1} - x_i}\Delta t\right)} \tag{4.36}$$

The locations of x_p, x_n, and x_o can now be calculated directly from equations (4.26) to (4.28) by substituting the calculated values for u_p, a_p, u_n, a_n, and u_o from the above equations.

The values of P (pressure) at the three initial points are then calculated using the interpolation equations, (4.23) to (4.25). The density, ρ and temperature, T can then be calculated from the equation of state.

All the initial point flow variables are now available to compute the flow conditions at the solution point *j*.

From equations (4.11) and (4.13), we obtain

$$P_j = K_1 - (\rho a)_p (u_j - u_p) + P_p \tag{4.37}$$

$$P_j = K_2 + (\rho a)_n (u_j - u_n) + P_n \tag{4.38}$$

where

$$K_1 = (\psi + a\varpi)_p \Delta t \tag{4.39}$$

and,

$$K_2 = (\psi - a\varpi)_n \Delta t \tag{4.40}$$

Solving the above two equations simultaneously for u_j we can write

$$u_j = \frac{K_1 - K_2 + (\rho a)_p u_p + (\rho a)_n u_n + P_p + P_n}{(\rho a)_n + (\rho a)_p} \tag{4.41}$$

Once the velocity is known, the pressure at the solution point, P_j can be calculated by direct substitution for u_j into either equation (4.37) or (4.38).

The density at the solution point can now be obtained from the pathline compatibility, i.e. equation 4.9

$$\rho_j = \frac{(P_j - P_o) + a_o^2 \rho_0 - \psi_o \Delta t}{a_o^2} \tag{4.42}$$

Once the pressure and density are known, the temperature at the solution point can be obtained through an iterative numerical scheme to solve the following equation

$$\rho_j - \rho(T_j^\gamma, P_j) = 0 \tag{4.43}$$

The subscript, j denotes conditions at the solution point, and the superscript, γ relates to the unknown temperature.

Solution of equation (4.43) becomes a root finding problem where a temperature is sought to match the density obtained from the compatibility equations to that calculated from an isothermal pressure-temperature flash.

This is achieved using a bracketing routine coupled with the Brent iterative method (Press et al., 1992). This method combines bisection and inverse quadratic interpolation to converge from the neighbourhood of a zero crossing.

Once the temperature is obtained at the solution point, the speed of sound and the parameter, φ is found by a flash calculation.

The above steps are the predictor steps. For the corrector steps, these solution point parameters are now re-evaluated using the average values of *u, p, ρ,* and, a along each characteristic.

The procedure for the implementation of the corrector steps based on average values is summarised below

For calculation of u_o, the characteristic path line is rearranged as:

$$\frac{d_o t}{d_o x} = \frac{1}{\left(\frac{u_o + u_j^r}{2}\right)} = \frac{\Delta t}{x_i - x_o} \Rightarrow x_o = x_i - \frac{\Delta t}{2}\left(u_o + u_j^r\right) \tag{4.44}$$

If $\lambda_o > 0$ then

$$u_o = u_{i-1} + \frac{u_i - u_{i-1}}{x_i - x_{i-1}}\left(x_i - \frac{\Delta t}{2}\left(u_o + u_j^r\right) - x_{i-1}\right)$$

In the above equation taking u_o to the one side gives

$$u_o\left(1 + \frac{u_i - u_{i-1}}{x_i - x_{i-1}}\frac{\Delta t}{2}\right) = u_i - \frac{u_i - u_{i-1}}{x_i - x_{i-1}}\frac{\Delta t}{2}u_j^r$$

Solving the above equation for u_o gives

$$u_o = \frac{u_i - \frac{u_i - u_{i-1}}{x_i - x_{i-1}}\frac{\Delta t}{2}u_j^r}{\left(1 + \frac{u_i - u_{i-1}}{x_i - x_{i-1}}\frac{\Delta t}{2}\right)} \tag{4.45}$$

Where the subscript, *j* together with superscript, *r* refer to the solution condition at the previous iteration step, *r*.

For calculation of u_p and a_p, the positive Match line is rearranged as

$$\frac{d_+ t}{d_+ x} = \frac{1}{\frac{1}{2}\left(u_p + u_j^r\right) + \frac{1}{2}\left(a_p + a_j^r\right)} = \frac{\Delta t}{x_i - x_p} \Rightarrow x_p = x_i - \frac{\Delta t}{2}\left(u_p + a_p + u_j^r + a_j^r\right) \tag{4.46}$$

By applying the linear interpolation u_p can be written as

$$u_p = u_{i-1} + \frac{u_i - u_{i-1}}{x_i - x_{i-1}}\left[x_i - x_{i-1} - \frac{\Delta t}{2}\left(u_p + a_p + u_j^r + a_j^r\right)\right]$$

Substituting u_i in the above equation gives

$$u_p = u_i - \frac{u_i - u_{i-1}}{x_i - x_{i-1}}\frac{\Delta t}{2}\left(u_p + a_p + u_j^r + a_j^r\right) \tag{4.47}$$

Rearranging equation (4.47) for the unknowns, u_p and a_p, gives

$$u_p\left(1 + \frac{u_i - u_{i-1}}{x_i - x_{i-1}}\frac{\Delta t}{2}\right) + \frac{u_i - u_{i-1}}{x_i - x_{i-1}}\frac{\Delta t}{2}a_p = u_i - \frac{u_i - u_{i-1}}{x_i - x_{i-1}}\frac{\Delta t}{2}\left(u_j^r + a_j^r\right) \tag{4.48}$$

Doing the same manipulation for a_p, we obtain

$$a_p = a_{i-1} + \frac{a_i - a_{i-1}}{x_i - x_{i-1}}\left[x_i - x_{i-1} - \frac{\Delta t}{2}\left(u_p + a_p + u_j^r + a_j^r\right)\right]$$

$$= a_i - \frac{a_i - a_{i-1}}{x_i - x_{i-1}}\frac{\Delta t}{2}\left(u_p + a_p + u_j^r + a_j^r\right) \tag{4.49}$$

Rearranging equation (4.49) gives

$$a_p\left(1 + \frac{a_i - a_{i-1}}{x_i - x_{i-1}}\frac{\Delta t}{2}\right) + \frac{a_i - a_{i-1}}{x_i - x_{i-1}}\frac{\Delta t}{2}u_p = a_i - \frac{a_i - a_{i-1}}{x_i - x_{i-1}}\frac{\Delta t}{2}\left(u_j^r + a_j^r\right) \tag{4.50}$$

As for the predictor step, equations (4.48) and (4.50) can be solved simultaneously for u_p and a_p.

Similarly a 2×2 system of equations can be set up for u_n and a_n in the corrector step

$$\frac{d\_t}{d\_x} = \frac{1}{\frac{1}{2}\left(u_n + u_j^r\right) - \frac{1}{2}\left(a_n + a_j^r\right)} = \frac{\Delta t}{x_i - x_n}$$

$$\Rightarrow x_n = x_i - \frac{\Delta t}{2}\left(\left(u_n - a_n\right) + \left(u_j^r - a_j^r\right)\right) \tag{4.51}$$

$$u_n = u_i + \frac{u_{i+1} - u_i}{x_{i+1} - x_i}\left[x_i - x_i - \frac{\Delta t}{2}\left(u_n - a_n + u_j^r - a_j^r\right)\right]$$

$$= u_i - \frac{u_{i+1} - u_i}{x_{i+1} - x_i}\frac{\Delta t}{2}\left(u_n - a_n + u_j^r - a_j^r\right) \tag{4.52}$$

$$u_n\left(1 + \frac{u_{i+1} - u_i}{x_{i+1} - x_i}\frac{\Delta t}{2}\right) - \frac{u_{i+1} - u_i}{x_{i+1} - x_i}\frac{\Delta t}{2}a_n = u_i - \frac{u_{i+1} - u_i}{x_{i+1} - x_i}\frac{\Delta t}{2}\left(u_j^r - a_j^r\right) \tag{4.53}$$

$$a_n\left(1+\frac{a_{i+1}-a_i}{x_{i+1}-x_i}\Delta t\right)-\frac{a_{i+1}-a_i}{x_{i+1}-x_i}\frac{\Delta t}{2}u_n=a_i-\frac{a_{i+1}-a_i}{x_{i+1}-x_i}\frac{\Delta t}{2}\left(u_j^r-a_j^r\right) \tag{4.54}$$

The locations of x_p, x_n, and x_o can now be calculated directly from equations (4.44), (4.46) and (4.51) by performing the relevant substitutions. The dependent flow variables at the solution point can now be calculated at the next $r+1$ iteration step

$$P_j^{r+1}=K_1-\frac{1}{2}\left[(\rho a)_p+(\rho a)_j^r\right]\left(u_j^{r+1}-u_p\right)+P_p \tag{4.55}$$

$$P_j^{r+1}=K_2+\frac{1}{2}\left[(\rho a)_n+(\rho a)_j^r\right]\left(u_j^{r+1}-u_n\right)+P_n \tag{4.56}$$

where K_1 is given by

$$K_1=\frac{1}{2}\left[(\Psi+a\varpi)_p+(\Psi+a\varpi)_j^r\right]\Delta t \tag{4.57}$$

and K_2 by

$$K_2=\frac{1}{2}\left[(\Psi-a\varpi)_n+(\Psi-a\varpi)_j^r\right]\Delta t \tag{4.58}$$

Solving the equations (4.55) and (4.56) simultaneously for u_j we can write

$$u_j^{r+1}=\frac{K_1-K_2+\frac{1}{2}\left[(\rho a)_p+(\rho a)_j^r\right]u_p+\frac{1}{2}\left[(\rho a)_n+(\rho a)_j^r\right]u_n+P_p-P_n}{\frac{1}{2}\left[(\rho a)_p+(\rho a)_j^r\right]+\frac{1}{2}\left[(\rho a)_n+(\rho a)_j^r\right]} \tag{4.59}$$

Once u_j^{r+1} is calculated, P_j^{r+1} can be calculated from either equation (4.55) or equation (4.56). The density is given by

$$\rho_j^{r+1}=\frac{\left(P_j^{r+1}-P_o\right)+\frac{1}{2}\left(a_o^2+a_j^{r2}\right)\rho_0-\psi_o\Delta t}{\frac{1}{2}\left(a_o^2+a_j^{r2}\right)} \tag{4.60}$$

The temperature is then calculated with the Brent method (Press et al., 1992). Once the temperature is solved, carrying out a flash calculation gives the speed of sound.

The above calculation procedure is repeated until a certain tolerance is satisfied for the three dependent variables, i.e. P, u, and ρ. The advantage of this process is that only one iteration calculation is involved since the location of the initial points p, o and n are computed directly without any iteration and results in considerable savings in calculation time without any loss of global accuracy. The calculation flow chart for the solution of interior point is shown in figure 4.3.

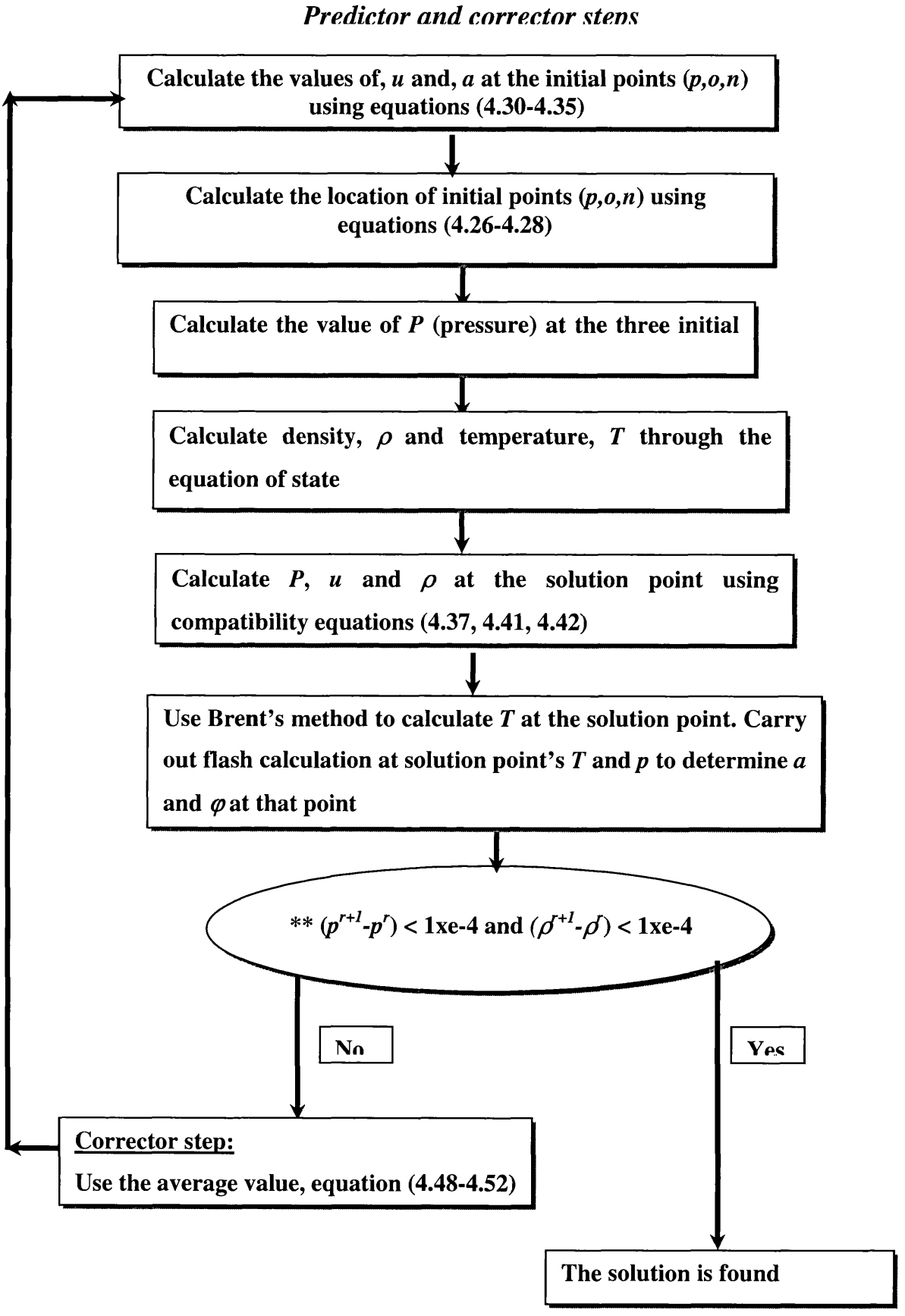

Figure 4.3 The interior point calculation algorithm; corrector and predictor steps

** r is the iteration step

4.4 THE INTERIOR POINT CALCULATION BASED ON THE CURVED CHARACTERISTIC

The linear approximation does not account for the curvature of the characteristics in regions where fluid properties change dramatically in a non-linear manner. This is usually the case for two-phase mixtures or condensable gases where the linear approximation can lead to a significant global error. The adoption of other approximations in place of the linear approximation, which account for the curvature of the characteristic line, may offer better accuracy in simulation results. However, this speculation is subject to further investigation to be presented in chapter 5.

Flatt (1985 a) proposed a singly-iterative second order method of characteristics, which accounts for the curvature of the characteristics by considering them as arcs of parabolas. In this method only a single iteration is needed for the solution point properties. The previous time line properties are calculated directly from the solution of the quadratic interpolation formulas for spatial discretisation.

The schematic representation of the interior grid point in the method proposed by Flat (1985 a) as applied in this study is shown in figure 4.4.

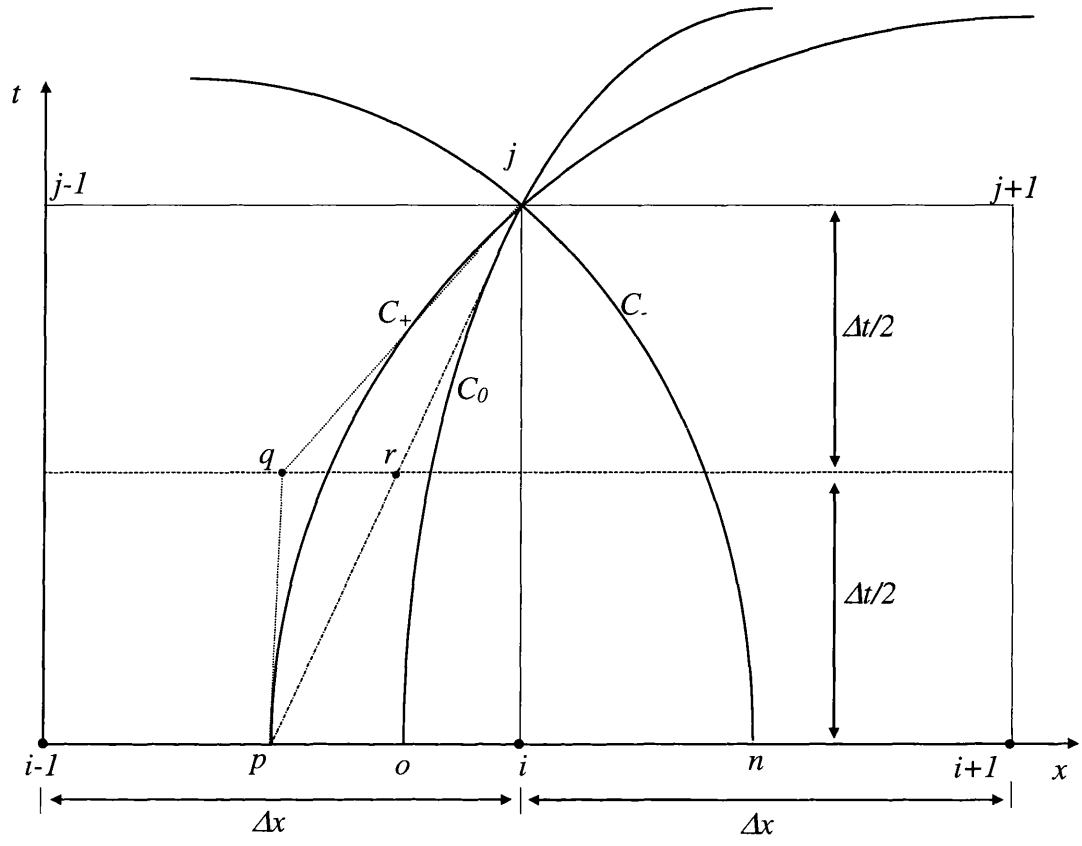

Figure 4.4 Schematic representation of an interior grid point for curved characteristic lines

The approximation of the characteristics lines with arcs of a parabola allows the use of a well-known geometric property such that the tangents to points, j and p meet halfway along the time axis at point q, so that

$$t_q = \frac{1}{2}\left(t_p + t_j\right) = t_p + \frac{\Delta t}{2} = t_j - \frac{\Delta t}{2} \tag{4.61}$$

Introducing the parameter, L so that at any point along the pathline characteristic,

$$L = \frac{1}{\lambda} = u \tag{4.62}$$

Hence, along the positive characteristic

$$L_{(+)} = \frac{1}{\lambda_+} = u + a \tag{4.63}$$

And along the negative characteristic

$$L_{(-)} = \frac{1}{\lambda_-} = u - a \tag{4.64}$$

Considering only the positive Mach line characteristic, the slope of the tangent at the node point j can be written as

$$\frac{\frac{\Delta t}{2}}{x_j - x_q} = \frac{1}{L_{j(+)}}$$

Solving the above equation for, x_q gives

$$x_q = x_j - \frac{\Delta t}{2} L_{j(+)} \tag{4.65}$$

Similarly for the tangent at point, p on the same positive characteristic we have

$$\frac{\frac{\Delta t}{2}}{x_q - x_p} = \frac{1}{L_{p(+)}}$$

Solving the above equation for x_q gives

$$x_q = x_p + \frac{\Delta t}{2} L_{p(+)} \tag{4.66}$$

Equating equation (4.65) to (4.66) and eliminating x_q, gives

$$x_p = x_j - \frac{\Delta t}{2}\left(L_{p(+)} + L_{j(+)}\right) \tag{4.67}$$

$L_{p(+)}$ falls on the same time line as points *i-1* and *i* where conditions are known, so interpolation is needed to evaluate conditions at point *p(+)*. To maintain a coherent second order scheme, a quadratic interpolation is needed based on the three point stencil, *i-1*, i, and *i+1*.

$$L_{p+} = C_1\left(x_p - x_i\right)^2 + C_2\left(x_p - x_i\right) + L_{i+} \tag{4.68}$$

where

$$C_1 = \frac{L_{i-1(+)} - 2L_{i(+)} + L_{i+1(+)}}{2(\Delta x)^2} \tag{4.69}$$

and

$$C_2 = \frac{L_{i+1(+)} - L_{i-1(+)}}{2\Delta x} \tag{4.70}$$

From equation (4.63)

$$L_{p(+)} = (x_j - x_p)\frac{2}{\Delta t} - L_{j(+)} = -(x_p - x_i)\frac{2}{\Delta t} - L_{j(+)} \tag{4.71}$$

Equating equation (4.71) to equation (4.68)

$$C_1 X^2 + \left(C_2 + \frac{2}{\Delta t}\right)X + L_{i(+)} + L_{j(+)} = 0$$

Rearranging the above equation gives

$$C_1 X^2 + 2C_3 X + C_4 = 0 \tag{4.72}$$

where

$$X = (x_p - x_i) \tag{4.73}$$

$$C_3 = \left(\frac{C_2}{2} + \frac{1}{\Delta t}\right) \tag{4.74}$$

$$C_4 = L_{i(+)} + L_{j(+)} \tag{4.75}$$

The solution to the quadratic equation (4.72) can be expressed in the special form

$$X = x_p - x_i = -\frac{C_4}{C_3 \pm \sqrt{C_3^2 - C_1 C_4}} \tag{4.76}$$

Expressing the solution in this form has been shown (Saha, 1997) to give better numerical results than the conventional form if the coefficient, C_1 becomes very small.

Considering equation (4.72) for $C_1 = 0$, the physically correct solution of equation (4.76) will be the one with the upper sign if $C_3>0$, or lower sign if $C_3<0$. Both cases can be expressed in the single form

$$X = x_p - x_i = -\frac{C_4}{C_3\left[1 + \sqrt{\left(1 - \frac{C_1 C_4}{C_3^2}\right)}\right]} \tag{4.77}$$

Using the above technique, the positions of the points of intersection of pathline, positive Mach line and negative Mach line can be determined without the need for any iteration. The conditions at these points are then calculated using quadratic interpolation formulas as shown by equation (4.68).

The conditions at the solution point are obtained by solving the relevant compatibility equations using a second order finite difference scheme as proposed in section 4.3 (corrector step). The calculations are continued until convergence is reached for the dependent variables at the solution point in the same way as outlined for the first order solution, section 4.3 (predictor step).

4.5 BOUNDARY CONDITIONS

Solving a series of total differential equations involves imposing appropriate boundary conditions to enable closure. Modelling pipeline outflow involves the imposition of boundary conditions at the intact end, rupture plane and pump or high-pressure inlet. Considering the characteristics as lines or curves does not affect the solution algorithm for any of the boundary conditions discussed below.

4.5.1 Intact End Boundary Condition

The positive characteristic line, λ_+ is meaningless at the intact end since there is no upstream flow at this point. Whilst the negative and path line characteristics, λ_- and λ_0 become operative (see figure 4.5) and also, the solution point velocity, u_j is zero. Therefore there are only two unknowns, P_j and ρ_j, which can be obtained by solving the compatibility equations along their corresponding characteristic lines.

The relevant compatibility equations are

$$P_j - P_o - a_o^2(\rho_j - \rho_o) = (k-1)(q-u\beta)_o \Delta t = \Psi_o \Delta t \tag{4.78}$$

$$P_j - P_n - (\rho a)_n (0 - u_n) = [(k-1)(q-u\beta)_n - (a\beta)_n]\Delta t = [\Psi - a\beta]_n \Delta t \tag{4.79}$$

Equation (4.79) can be rearranged to give an expression for P_j such that

$$P_j = P_n - (\rho a)_n u_n + [\Psi - a\beta]_n \Delta t \tag{4.80}$$

Thus the solution point density is given by

$$\rho_j = \frac{P_j - P_o - \Psi_o \Delta t + a_o^2 \rho_o}{a_o^2} \tag{4.81}$$

The fluid temperature, T is calculated through the Brent iterative method (Press et al., 1992) whilst the speed of sound is obtained from a P-T flash calculation based on the calculated temperature.

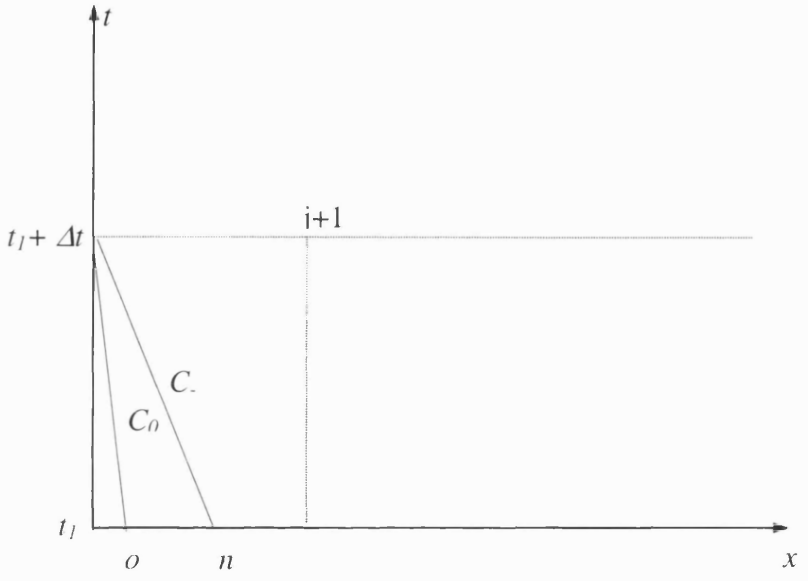

Figure 4.5 Schematic representation of intact end boundary condition

4.5.2 Pump Inlet Boundary Condition

Only the negative and path line characteristics are applicable at the pump or the high-pressure inlet. However, unlike the intact end calculation, the flow pressure and velocity at the solution point (u_j, p_j) are initially specified and remain unchanged for the duration of pump operation.

Thus, the remaining variables to be solved at the solution point are the fluid density ρ_j, and temperature, T_j. These are in turn obtained from the iterative solution of equation (4.81) in conjunction with the equation of state.

4.5.3 Ruptured End Boundary Condition

Outflow at the rupture plane can be divided into two time domains. The first is the choked flow regime, whose duration depends on the time it takes, the discharge pressure to drop to the external pressure. During this transition period, the flow at the rupture point is sonic and no more disturbances can propagate upstream. Once the external pressure is reached, outflow is subsonic (Picard and Bishnoi 1988).
The state of the fluid affects the choked flow calculation. If the fluid is in the vapour phase or in the two-phase region, the speed of fluid is equal to speed of sound at the rupture point, which can be shown as:

$$\mathrm{Ma} = \frac{u}{a} = 1 \tag{4.82}$$

Where Ma is the Mach number.
Therefore at the solution point, we can take $u_j = a_j$. However, if the fluid is in the liquid phase the discharge pressure (pressure at solution point at rupture plane) is equal to ambient pressure. Both release scenarios are modelled in this study.

To account for phase transition at the rupture plane, the first step involves determining the fluid phase prior to rupture. If the fluid is in vapour or two phase, the calculation procedure is the same. However, if the fluid is in the liquid phase a different procedure is followed which both cases are discussed below.

Vapour and two-phase flow

The energy balance at a rupture plane can be written as

$$h_u + \frac{u_u^2}{2} = h_{rup} + \frac{u_{rup}^2}{2}$$

Where subscript "*u*" refers to upstream of the rupture plane and subscript "*rup*" refers to rupture plane. Assuming that the upstream velocity, u_u, is negligible in comparison to the fluid velocity at rupture point, u_{rup} in the above equation can be written as

$$h_u = h_{rup} + \frac{u_{rup}^2}{2} \tag{4.83}$$

As it was mentioned above under the chocking condition, the fluid travels at the same speed as the speed of sound through the mixture. Thus equation (4.83) becomes

$$h_u = h_{rup} + \frac{a_{rup}^2}{2} \tag{4.84}$$

The conditions at rupture plane are calculated based on the conservation of energy at rupture plane equation (4.84) applying the following procedure:

1. Guess the rupture plane pressure (based on the critical pressure), P_{rup}, and perform pressure entropy flash at, P_{rup} and upstream entropy, S_u, to determine the number of phases, bulk enthalpy per unit mass, h_{rup} and rupture temperature, T_{rup}
2. If the fluid is single phase, the speed of sound, a_{rup} is determined analytically from equation (2.45) for a given equation of state. However for a two-phase mixture a_{rup} is numerically calculated through equation (2.47), based on the method recommended by Picard and Bishnoi (1987).
3. Substitute h_{rup} and a_{rup} in equation (4.84). If this equation is not satisfied, repeat steps 2-4 until convergence.As soon as convergence is achieved all the fluid properties at the rupture plane are known.
4. If the ambient pressure is greater than the calculated pressure, P_{rup}, the fluid is not choked. In this case, the fluid temperature at rupture plane, T_{rup}, and fluid enthalpy, h_{rup} are determined by pressure-entropy flash at ambient pressure and upstream entropy S_u. Thereafter the fluid velocity, u_{rup} is determined by solving equation (4.83).

The Brent method (Press et al., 1992) is used to solve for the rupture pressure, P_{rup}.

Liquid Phase Flow

During choked flow, it is not plausible to assume that the speed of fluid is equal to speed of sound. In the case of choked liquid/flashing liquid flows, the discharge rate at the rupture plane is maximum and not necessarily equal to the local speed of sound (Richardson and Saville, 1991; Darby et al., 2001).

In the case of choked liquid flows, the speed of fluid at the rupture plane is determined using the expression given by Simpson (1991):

$$u_{rup} = \rho_n \left(-2 \int_{P_N}^{P_n} \frac{dP}{\rho} \right)^{1/2} \tag{4. 85}$$

The subscripts, n and N refer to final choking condition and the upstream stagnation condition respectively. Based on isentropic flow and homogenous equilibrium assumptions, the above equation has been shown to produce a good degree of agreement (ca. $\leq 4\%$) with experimental data, Simpson (1991).

The integral in equation (4.85) is evaluated numerically using the trapezoidal rule (Perry, 1973). It is noteworthy that the application of Simpson's equation to gaseous or two-phase flows expectedly predicts choking when the speed of the discharging fluid equals the speed of sound through the fluid at the discharge plane.

For subsequent time steps, the ruptured end calculation involves the solution of compatibility equations along the positive Mach, and path lines. However, in order to accommodate the rupture end boundary condition, the concept of a 'ghost cell' is introduced. The addition of an extra ghost cell adjacent to the boundary cell involves the addition of an imaginary characteristic line (see figure 4.6). The conditions at the node $i+1$ are the same as at node i, i.e.

$$Y_{i+1} = Y_i \tag{4.86}$$

where

$Y = P,u,\rho,T,a$

The rest of the calculations are exactly the same as for the interior point, section 4.3.

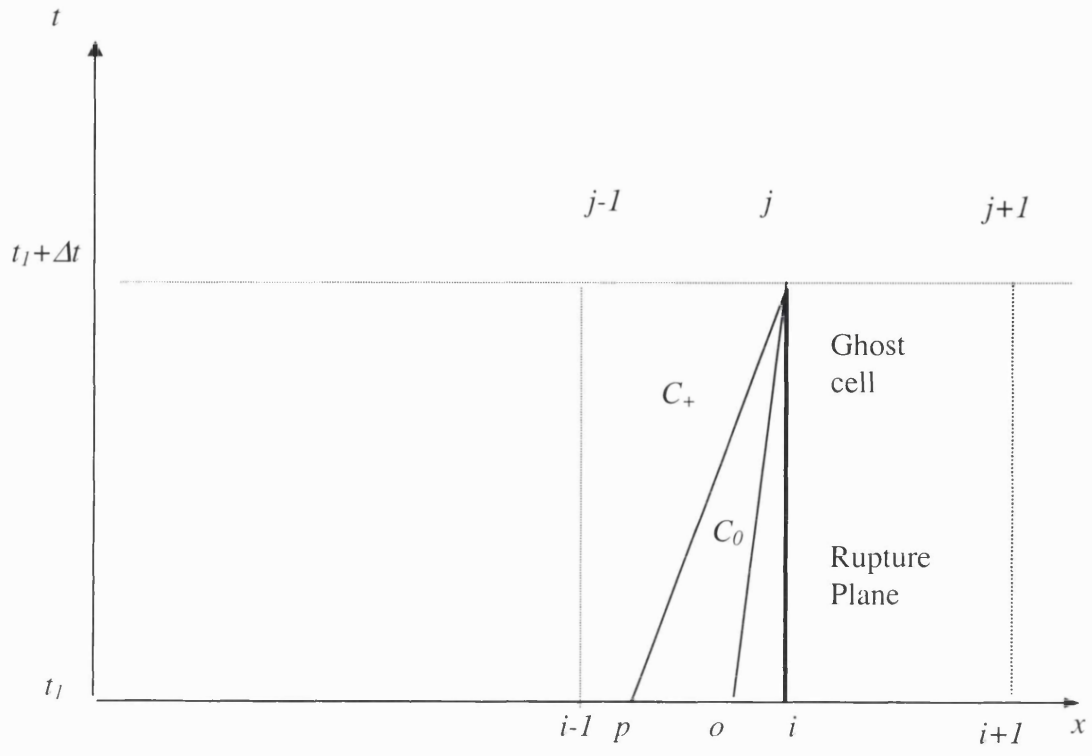

Figure 4.6 Schematic representation of rupture plane boundary condition

4.6 ENLARGED PIPELINE FBR

An enlarged pipeline can be modelled as two non-equal diameter horizontal pipelines, which are connected via an enlarged section as depicted in figure 4.7. The calculation procedure for the grid points along the pipeline other than at the enlarged section are the same as discussed in section 4.3 with the exception of omitting the gravity term. The enlarged part can be treated as two boundary conditions following the rupture, and as a pipe fitting component prior to rupture.

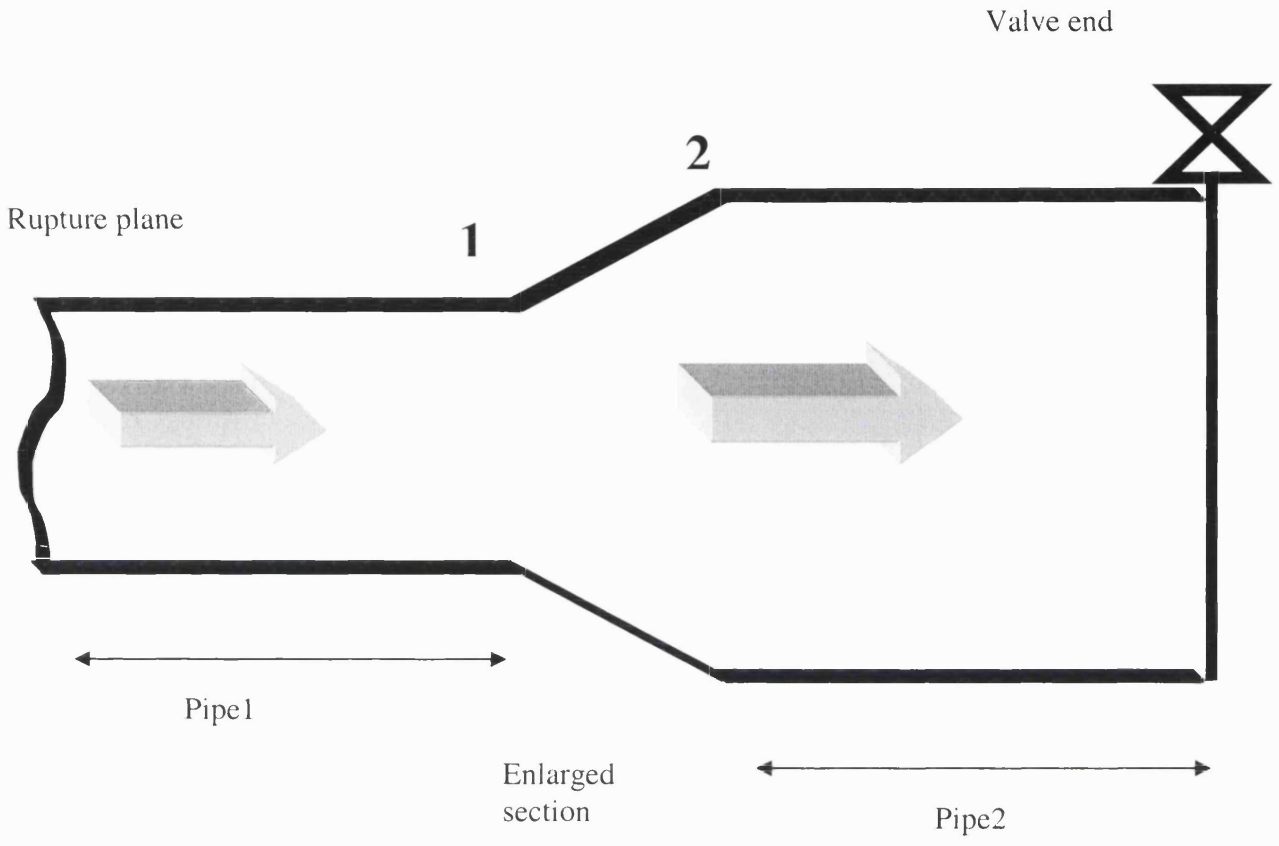

Figure 4.7 Schematic representation of an enlarged pipeline

The Darcy-Weisbach (Perry, 1973) equation has been used to calculate pressure drop across the enlarged section with the appropriate friction term taking into account the effect of contraction/enlargement. Accordingly the pressure drop is given by

$$dP = \rho \cdot f_f \cdot (l/D) \cdot u^2 / 2 \cdot g \qquad (4.87)$$

where:

$$u^2 = (u_1 - u_2)^2$$

$$\rho = (\rho_1 + \rho_2)/2$$

Equation (4.87) can be written as

$$dP = \rho \cdot k \cdot u^2 / 2 \cdot g \qquad (4.88)$$

where

$$k = f_f .(l/D)$$

All other symbols have been defined in chapter 2.

Valve manufacturers have performed experiments on various valves and fittings in order to arrive at empirical pressure drop expressions. Moreover the k value in equation (4.88) for various fittings has been derived through experimentation. One of the most universally used methods is that presented in the Crane Technical Paper 410 (Crane, 1988) also employed in the present study.

Based on this paper, if the flow crosses a contraction, the k value in equation (4.88) can be calculated from the following equations

$$k = 0.8 * \sin(\Omega/2) * (1 - \beta_d{}^2) \qquad (\Omega<45^\circ) \qquad (4.89)$$

$$k = \tfrac{1}{2} * (1 - \beta_d{}^2) * (\sin(\Omega/2))^{\frac{1}{2}} \qquad (45^\circ<\Omega<180^\circ) \qquad (4.90)$$

where

Ω= angle of approach

$\beta_d = D_1/D_2$

However if the flow passes through an enlargement, the k value can be calculated from the following equations

$$k = 2.6 * \sin(\Omega/2) * (1 - \beta_d{}^2) \qquad (\Omega<45^\circ) \qquad (4.91)$$

$$k = (1 - \beta_d{}^2)^2 \qquad (45^\circ<\Omega<180^\circ) \qquad (4.92)$$

Equation (4.88) along with one of the equations (4.89-4.92) have been used to calculate the pressure drop along the connector section. The following describes the calculation algorithm for the simulating flow prior and post rupture through the enlarged section as presented in figures 4.8 and 4.9 respectively.

4.6.1 Enlarged Section Calculation: Prior to Rupture

1 The conditions at the enlargement inlet (point 1 figure 4.6) are determined via the horizontal pipeline steady state calculation (see section 4.7).

2 Density at enlargement exit (point 2, figure 4.6) is calculated through the mass conservation equation (equation, 2.3), with the velocity calculated in step 1 employed as an initial guess.

3 Calculate the pressure drop along the enlargement using equation (4.88) along with equation (4.91) or equation (4.92).

4 Carry out a pressure, entropy flash calculation to determine the corresponding density

5 If the density obtained in step 4 is equal to the one previously found in step 2 (with the tolerance of ±1e-3) the solution is found, otherwise update the velocity by applying mass conservation equation (equation 2.3) and repeat steps 3 to 5.

4.6.2 Enlarged Section Calculation: Post Rupture

For the conditions following rupture, the isentropic flow assumption, which was used for the condition prior to rupture, may not hold due to the highly unsteady conditions. In this case, the starting and terminating points at the enlargement are treated as two boundary conditions. For each of these, only two characteristics lines namely the negative and path line characteristics for the beginning of enlargement and positive and path line characteristics for the terminating point are applicable. The calculation procedure is presented below:

1. Make an initial guess for pressure at enlargement staring point from previous time step and using the two characteristic lines solve the enlargement starting point.
2. Determine the pressure drop across the enlargement by applying equation (4.88) and consequently determine the pressure at the enlargement terminating point.

3. Use the pressure calculated in step 2 along with the two compatibility equations to solve the conditions at the enlargement terminating point.
4. Mass conservation across the connector section is tested. If mass is conserved, the solution is found otherwise the pressure is updated and stages 1 to 4 are repeated until mass in conserved

The pressure drop across the connector section is not a very well behaved function. As a result, algorithms based on bisectioning and root-bracketing methods are incorporated in the algorithms presented above.

Enlarged Section Calculation Algorithm; Prior to rupture

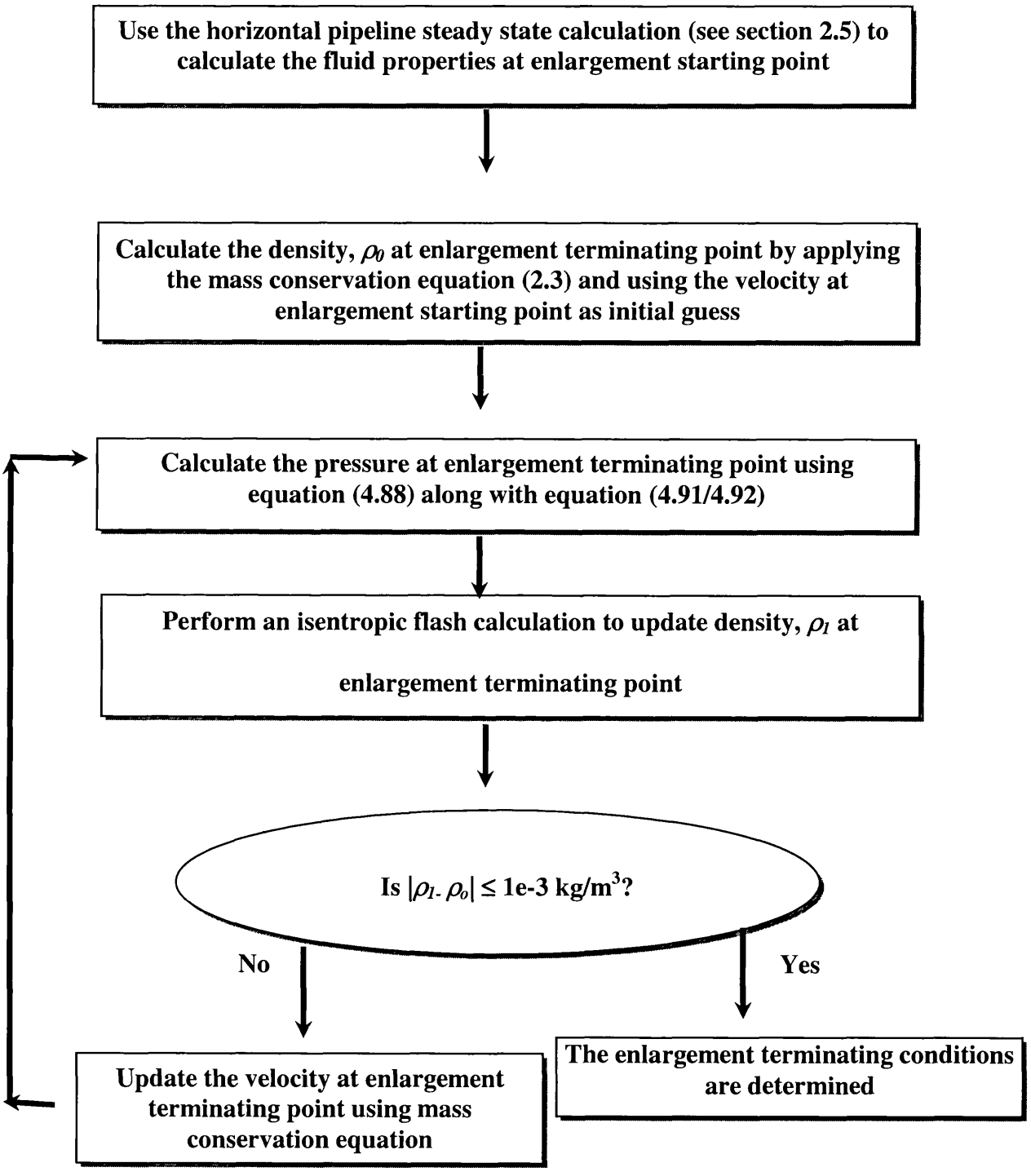

Figure 4.8 Calculation flow algorithm for enlarged section of a non-uniform diameter pipeline, prior to rupture

Enlarged Section Calculation Algorithm; Post Rupture

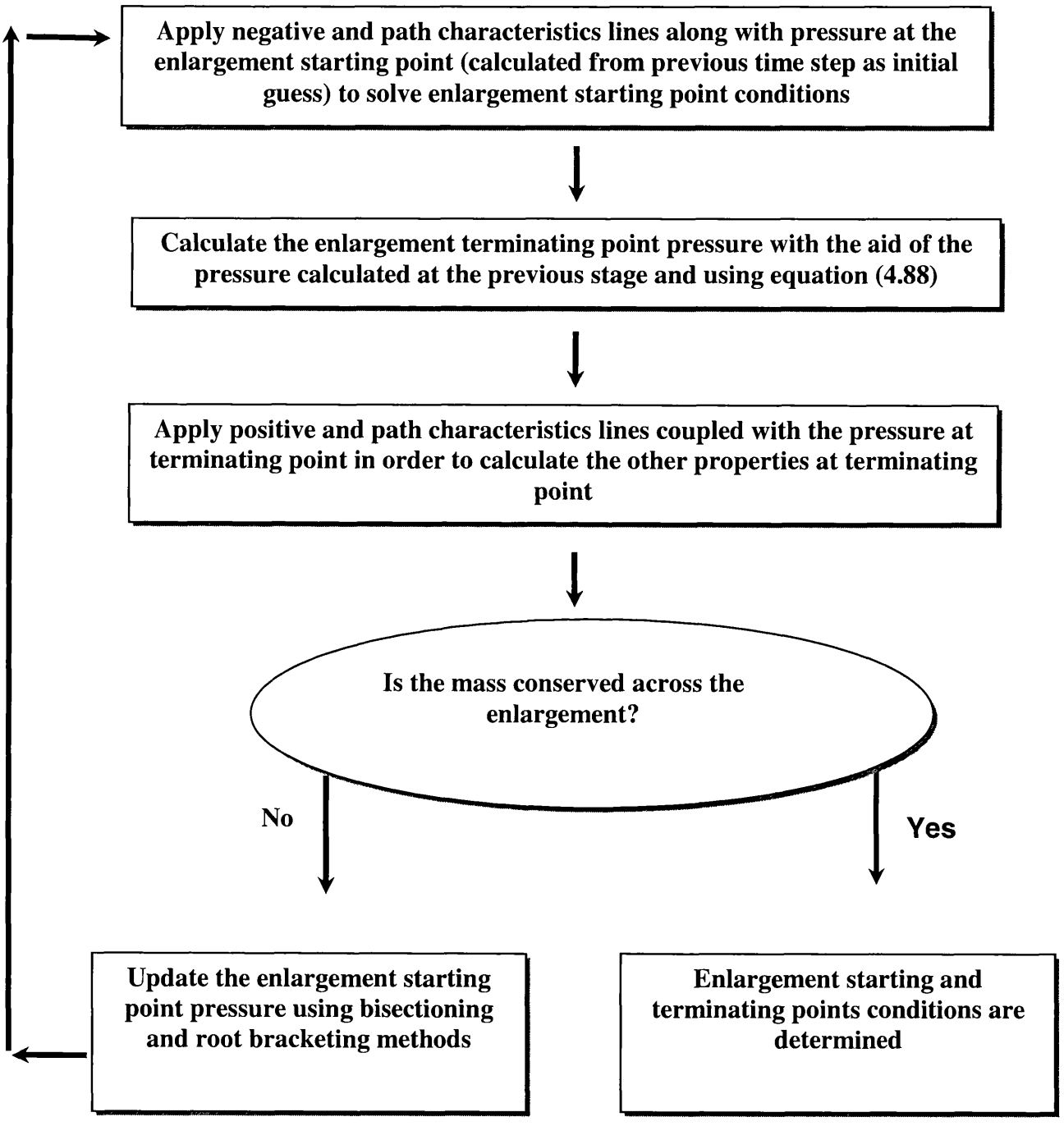

Figure 4.9 Calculation flow algorithm for enlarged section of a non-uniform diameter pipeline; unsteady state flow

4.7 INCLINED PIPELINE FBR: PRIOR TO RUPTURE

The flow in the pipeline prior to rupture (initial condition) can be taken to be isothermal steady state. This can be justified by the fact that flow is relatively slow (Flatt, 1986) and since the pipeline is very long, there is ample opportunity for heat transfer to maintain isothermal conditions. Typically flow velocities in pipelines vary from 10 to 25 m/s and therefore for pipeline lengths of greater than 100 kilometres, a residence time of hours per particle is to be expected.

The simulation of steady state flow along an inclined pipeline conveying real compressible fluid is not trivial. Without simplifications, the differential equations (see chapter 2) describing pressure drop under this flow condition can only be solved numerically. The common practise (Saad, 1985) in steady state pressure drop simulations has involved the simplification of the governing equation in such a way as to avoid the need for an iterative solution. In chapter 2, the analytical expression describing steady state flow behaviour in an inclined pipeline was derived as

$$\Delta x = \frac{D}{2\cdot f}\cdot \ln \frac{\frac{p_2}{Z_2}}{\frac{p_1}{Z_1}} - \left[\frac{D}{4\cdot f} + \frac{Z_{av}\cdot R\cdot T}{2\cdot g\cdot \sin\theta}\right]\cdot \ln\left[\frac{D\cdot g\cdot \sin\theta\cdot\left(\frac{p_2}{Z_2}\right)^2 + (Z_{av}\cdot R\cdot T\cdot \rho_1\cdot u_1)^2\cdot 2\cdot f}{D\cdot g\cdot \sin\theta\cdot\left(\frac{p_1}{Z_1}\right)^2 + (Z_{av}\cdot R\cdot T\cdot \rho_1\cdot u_1)^2\cdot 2\cdot f}\right] \tag{2.70}$$

Considering a pipeline, divided into definite grid points, subscripts *2* and *1* in the above equation relate to the solution point and one grid point upstream of the solution point respectively. Since equation (2.70) is an implicit expression, it can only be solved by numerical techniques.

The classical Secant (Press et al., 1992) method is employed to solve equation (2.70). The algorithm developed to solve the above equation is described below

1. Make two guesses for pressure at solution point and perform P,T flash calculations to find the corresponding densities and compressibility factors.
2. Use the Secant method (Press et al., 1992) to find the root of equation (2.70) between the two initial guesses until the specified tolerance (1e-3) is satisfied.
3. Once the pressure at the solution point is determined, perform a flash calculation to determine solution point density and speed of sound. Consequently, the velocity of fluid, u can be easily obtained by applying the principle of conservation of mass.

The above algorithm has also been used in the current study to calculate the pressure drop along horizontal pipeline, (i.e. $\theta = 0$). However as described in chapter 2, the implicit equation (equation 2.72) to be valuated for pressure drop is different from the above equation.

Zhou and Adewumi (1995) developed a new equation for pressure drop calculation along an inclined pipeline. Although the authors accounted for essential terms in the governing equation, however in the model an approximate value of the compressibility factor was employed over a discrete section of the pipeline. The authors used Newton Raphson algorithm to solve their implicit equation. The results of their works were compared with experimental data.

The experimental data are from tests conducted by American Gas Association (Uhl et al., 1965). The conditions for two tests (F-1 and G-1) are presented in tables 4.1 and 4.2 respectively.

Test index	Inlet pressure (bar)	Inlet temperature (°C)	Inlet velocity (m/s)	Roughness factor (m) e-5
1	35.543	12.961	72.033	2.797
2	41.555	12.961	73.915	2.71
3	56.034	18.517	98.309	2.291
4	35.763	13.517	95.449	2.149
5	42.203	13.517	104.701	2.095
6	55.938	18.794	126.536	2.004
7	42.134	12.961	124.24	1.615
8	55.779	19.072	147.556	1.654
9	56.027	19.35	179.363	1.62
10	56.124	19.35	192.264	1.58
11	56.103	19.35	208.987	1.68

Table 4.1 Tests F-1 specifications

Test index	Inlet pressure (bar)	Inlet temperature (°C)	Inlet velocity (m/s)	Roughness factor (m) e-5
1	35.543	17.294	72.119	2.344
2	41.555	17.572	74.027	2.288
3	56.034	20.183	98.395	2.007
4	35.763	17.016	95.522	1.593
5	42.203	17.405	104.788	1.526
6	55.937	21.294	126.625	1.6
7	42.134	17.127	124.311	1.158
8	55.779	22.294	147.629	1.247
9	56.027	22.405	179.421	1.3
10	56.123	22.795	192.307	1.237

Table 4.2 Tests G-1 specifications

Table 4.3 shows the pipe characteristics for each test. The gas composition is presented in tables 4.4.

Test	Pipe diameter (m)	Pipe length (km)	Angle of inclination (degree)
Test F-1	0.495	245.225	-0.085
Test G-1	0.495	101.5	-0.089

Table 4.3 Pipeline characteristics for tests F-1 and G-1

Component	mole%
CH_4	76.99
C_2H_6	5.21
C_3H_8	2.85
i-C_4H_{10}	0.3
n-C_4H_{10}	0.67
i-C_5H_{12}	0.08
n-C_5H_{12}	0.08
n-C_6H14	0.02
C_7	0.12
N_2	13.28
CO_2	0.3
O_2	0.1

Table 4.4 Fluid compositions in tests F-1 and G-1

Figures 4.10, 4.11 show the deviation of simulated pressure drop along an inclined pipeline from the experimental data for the model developed by Zhou and Adewumi (1995) as compared to that model presented in this study. Although Zhou and Adewumi (1995) model gives relatively good agreement with field data, however better agreement is obtained using the model presented in this study. This can be justified based on the fact that in the model developed in the current study no approximation have been made in the calculation of compressibility factor at each grid point.

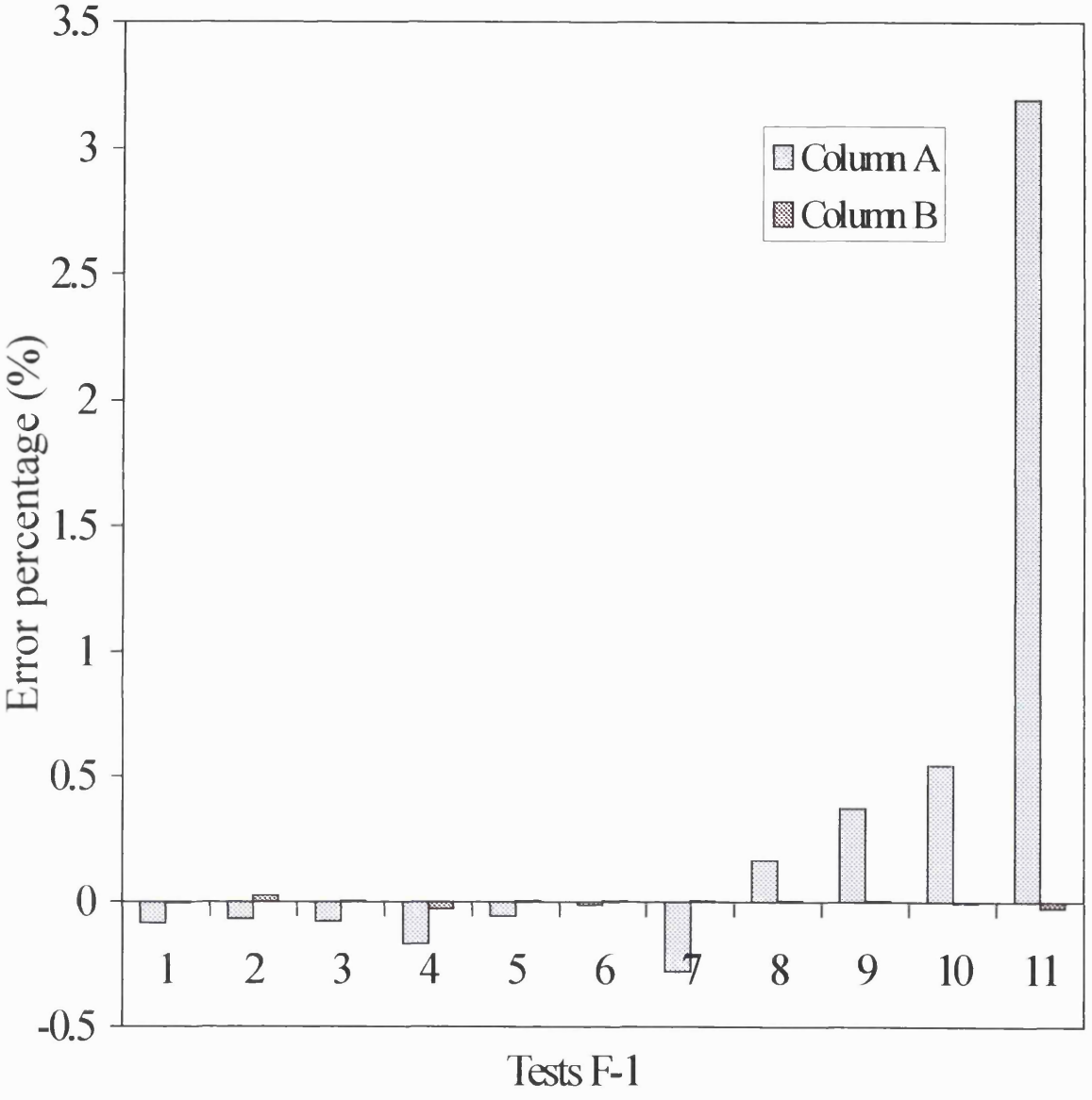

Figure 4.10 The deviation of simulated pressure drop along an inclined pipeline from field data, Tests F-1

Column A: Zhou and Adewumi (1995)

Column B: The present model

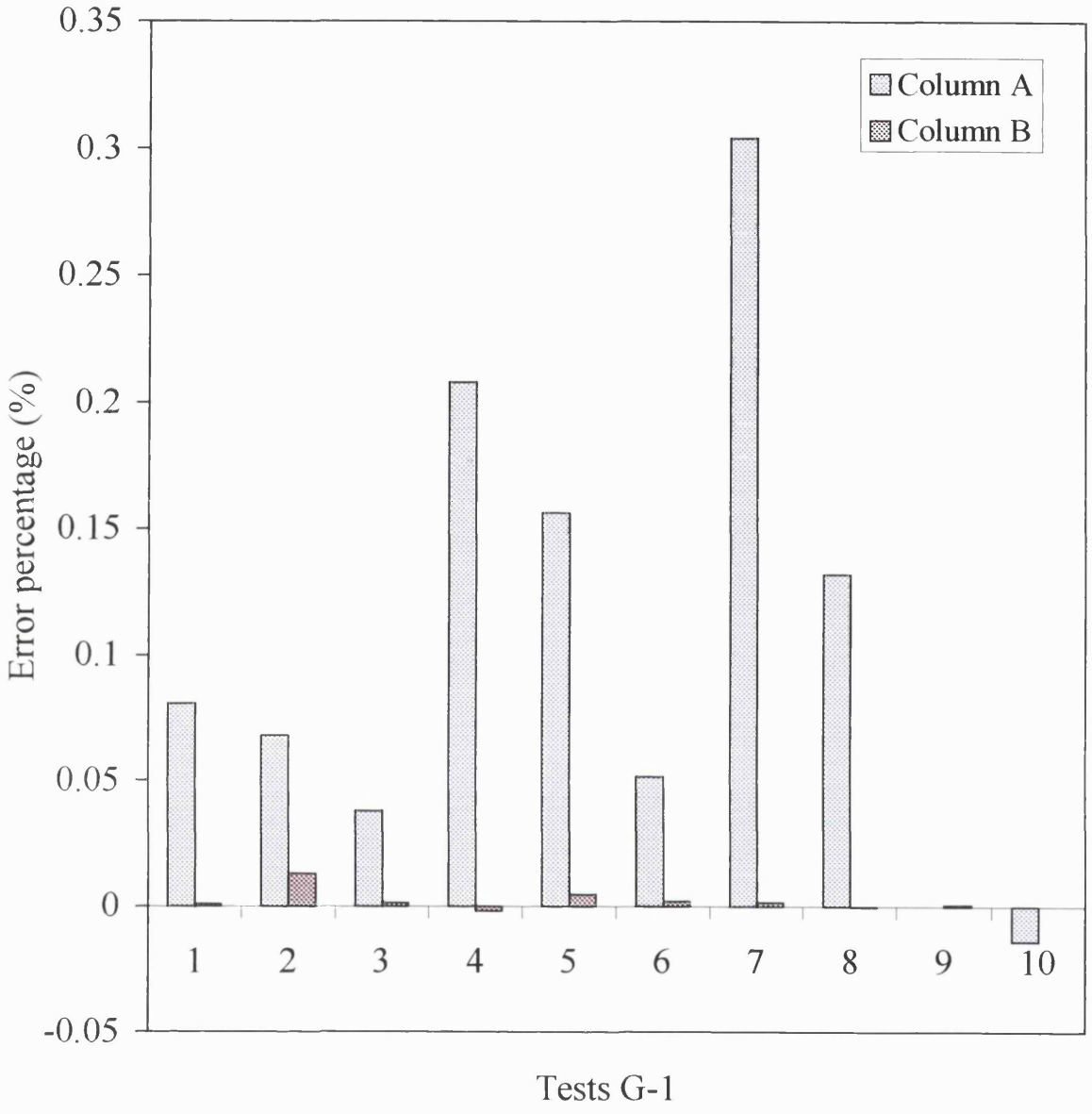

Figure 4.11 The deviation of simulated pressure drop along an inclined pipeline from field data, Tests G-1

Column A: Zhou and Adewumi (1995)

Column B: The present model

4.8 CONCLUSION

The method of characteristics was earlier established as the numerical tool for this study in chapter 3. The application of the method for pipeline rupture has been presented in this chapter. This involved two steps; transformation of the partial differential equations to ordinary differential equations followed by the solution of the latter equations. Following to the description of the methods for pipeline's interior points calculation, the appropriate boundary and initial conditions for different pipeline rupture scenarios were described. The algorithms used to model inclined and enlarged pipeline were also presented. Finally the model presented in this study for calculation pressure drop along an inclined pipeline for steady state condition, was validated against experimental data. The mathematical algorithm presented in this chapter has been used to develop a computer program to simulate pipeline rupture. In the next chapter, the results of the simulation based on the mathematical model derived in this chapter will be presented.

CHAPTER 5
RESULTS AND DISCUSSION

5.1 INTRODUCTION

In chapters 2-4 the problem of outflow following pipeline rupture was mathematically modelled. The governing conservation equations were derived in chapter 2 and the method of characteristic as the numerical tool for solving these equations was presented in chapter 3. The application of method of characteristic and the corresponding algorithm for the numerical solution of the model were discussed in chapter 4.

The predictions obtained from any transient outflow model are highly dependent on the choice of a number of key modelling parameters. This is due to the highly non-linear variation of the physical properties of fluids involved especially if they undergo phase transition during the depressurisation process. This chapter deals with investigating the effects of changing a number of key parameters including choice of curved as opposed to linear characteristic, the discretisation time step and friction factor and on the model's performance. The results are assessed by comparison with available experimental data as well as any reduction in the computation run time.

A major part of this chapter presents and discusses the results of the application of the optimised outflow model to FBR of inclined and enlarged pipelines.

5.2 PERFORMANCE EVALUATION: SENSITIVITY ANALYSIS OF KEY MODEL PARAMETERS

The outflow model's performance is evaluated by comparison with the experimental data of Isle of Grain tests (Tam and Cowly, 1988). These relate to a comprehensive series of experiments on pressurised LPG releases using two horizontal 100m long pipelines of internal diameters of 50mm and 150mm. For these experiments, the rupture of the pipeline was simulated by breaking a glass or graphite diaphragm

installed at the spill end of pipeline. Orifice plates were used to investigate the effect of the size of the rupture on the release rate. The pipeline was suspended at 5 m intervals on hangers connected to load cells. The 20 load cells measured the mass of the fluid in the pipeline. The fluid temperatures and pressures were respectively measured along the whole length of the pipeline using 10 thermocouples (50 ms time constant) and 10 pressure sensors. Further details of these experiments can be found in the work of Chen et al. (1995b). A large number of experiments were carried out during the Isle of Grain pipeline depressurisation tests. In this study tests LPG 40 and LPG 42, are used to verify the model's performance as they relate to discharge diameters closest to full bore. Table 5.1 gives the pertaining conditions for LPG 40 and LPG 42 tests.

Test	LPG 40	LPG 42
Initial fluid temperature (C)	20.0	20.0
Ambient air temperature (C)	19.1	18.6
Initial pressure (bara)	21.013	11.25
Pipe length (m)	100.0	100.0
Pipe diameter (m)	0.15	0.15
Fluid composition	95% Propane 5% Butane	95% Propane 5% Butane
Pipe roughness x 10^{-5} (m)	5	5

Table 5.1 LPG 40 and LPG 42 Isle of Grain test specifications

The above depressurisation tests involve the transition into the two-phase region. For the sake of completeness, further simulations are performed involving the hypothetical rupture of a pipeline containing methane, which remains in the gaseous phase throughout the depressurisation process. Table 5.2 gives the pertaining conditions for methane simulation cases.

Initial temperature (C)	**Ambient temperature (C)**	**Initial pressure (bar)**	**Pipe length (m)**	**Pipe roughness x 10^{-5}(m)**	**Pipe diameter (m)**	**Fluid composition**
20	22	50	1000	5	0.15	100% methane

Table 5.2 Pure methane pipeline rupture case study specification

Unless otherwise specified, all simulations are based on a Compound Nested Grid System (CNGS) in which increasingly finer grids are used at the rupture plane to simulate the rapid transients. This allows the use of relatively coarse grids away from the rupture plane thus significantly reducing the computational workload. Figure 5.1 shows a schematic representation of the grid discretisation system used in this study. Δx, and Δt represent the distance and time grids with the subscripts 1 – 3 representing the three discretisation levels. Unless otherwise specified in the case of all the simulations presented Δx_1= 20 m, Δx_2= 4 m and Δx_3= 0.8 m.

All the simulations in this study were performed using a Pentium 4 PC with a 1.7 GHz processor.

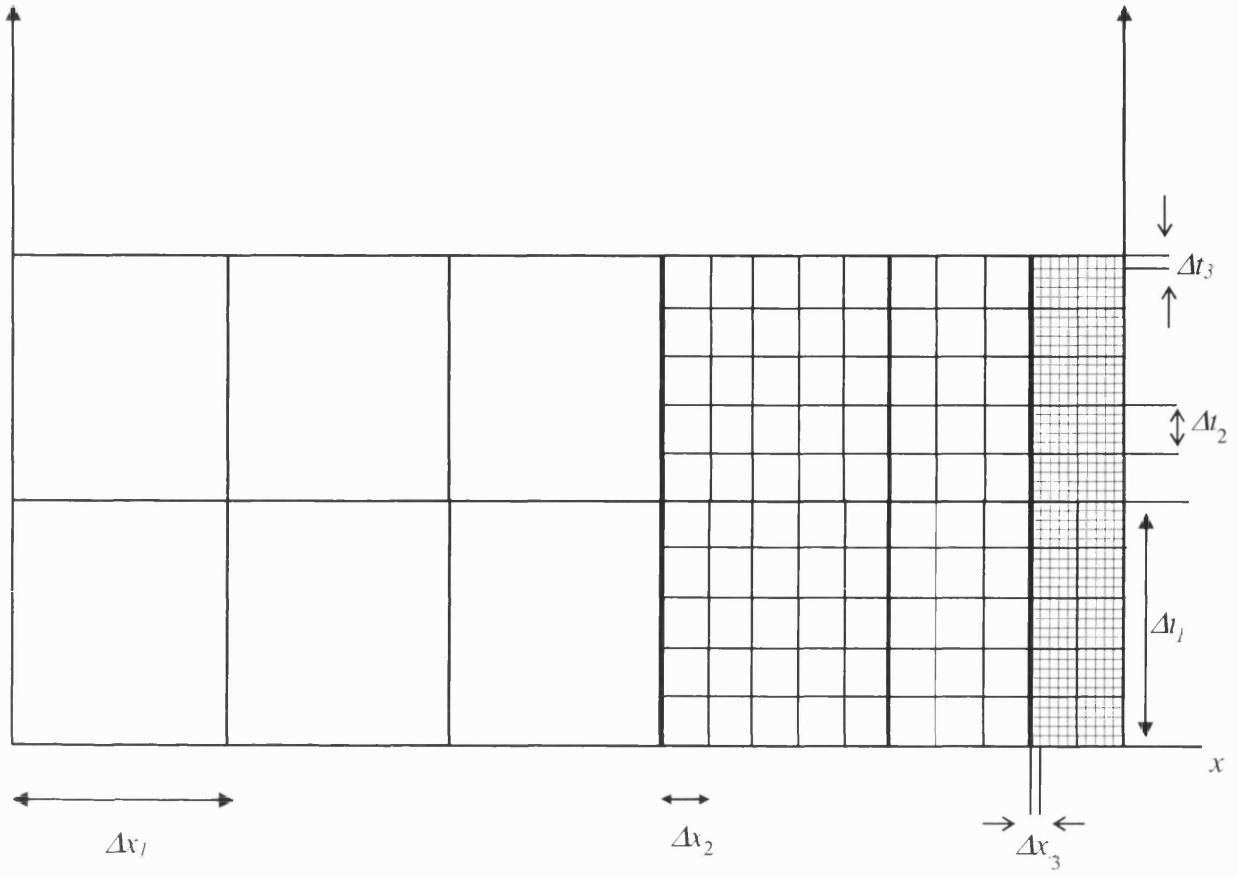

Figure 5.1 Schematic representation of the nested grid formulation

5.2.1 The Comparison of Linear and Curved Characteristics

As described in chapter 4, the method of characteristics is based on the characteristic pathways. The slopes of these pathways determine how information is transferred in time and space along the pipeline. The calculation of properties along these pathways involves interpolation methods. The interpolation method employed may be based on assuming variations along linear (section 4.3) or non-linear (curved; section 4.4) characteristics.

Flatt (1985) describes a procedure based on second order interpolation using curved characteristics within each numerical space-time mesh. In his method, the curvature of the characteristics is taken into account by considering them as arcs of parabolas.

The author claims that his proposed algorithm is more accurate than first order characteristics method.

However, Swaffield (1993) claims that generally, the use of a second order approximation has not found favour in the application of the method of characteristics to pressure transient modelling. Equally valid predictions may be obtained from the first order approximation without the complexity introduced by the need for an iterative solution as the unknown wave speed and velocity at the intersection of characteristic lines appear in the friction term and the characteristic slope. However, no detailed systematic study substantiating the validity of the above has been undertaken.

In order to investigate the effect of curved and linear characteristics, both first order and second order interpolation methods have been applied in the current model. The corresponding effects on the performance of the model are presented below.

Figure 5.2, shows the results of pressure variation with time at rupture plane for LPG 40 test, which undergoes phase transition during the depressurisation process. Curve A shows the simulated results based on the first order interpolation using linear characteristics. Curve B shows the corresponding experimental data. Curve C on the other hand shows the result of second order interpolation based on curved characteristics.

Referring to the data it is clear that the first order linear characteristics (curve A) provides a reasonably good prediction of the experimental results (curve B). However a marked disagreement between the latter and the simulated data based on curved characteristics (curve C) is obtained.

Figures 5.3 and 5.4 respectively show the corresponding variations of inventory and intact end pressure with time following FBR. As it may be seen, the same trends as those with the open-end pressure are obtained. In general, the linear characteristics provide consistently better predictions. In terms of CPU time, the linear characteristic simulation was completed in 5 hours and 20 minutes. This compares with approximately 10 hours in the case of curved characteristics.

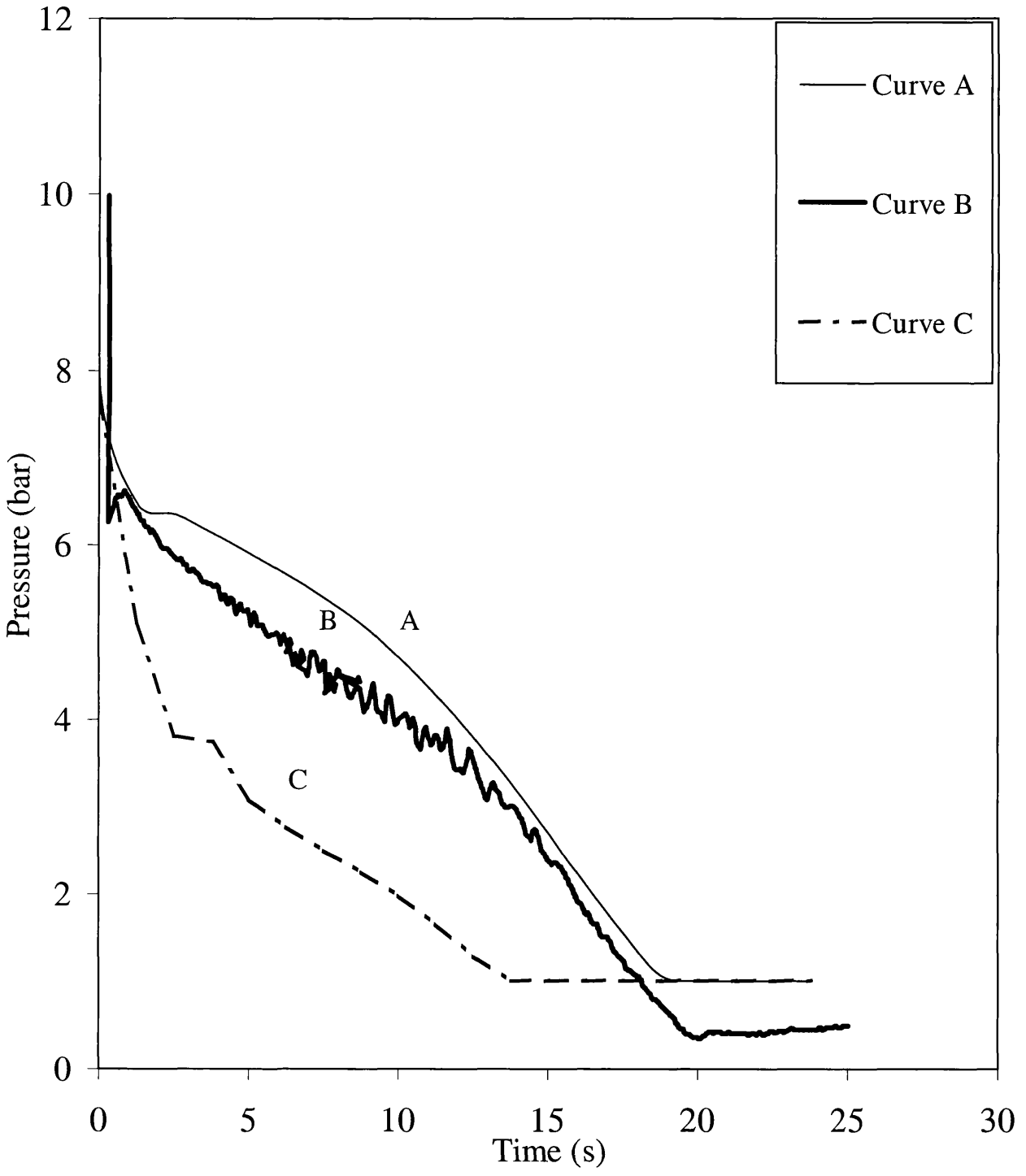

Figure 5.2 Pressure variation with time at rupture plane for LPG40 following FBR

Curve A: Linear characteristics.

Curve B: Experimental data.

Curve C: Curved characteristic

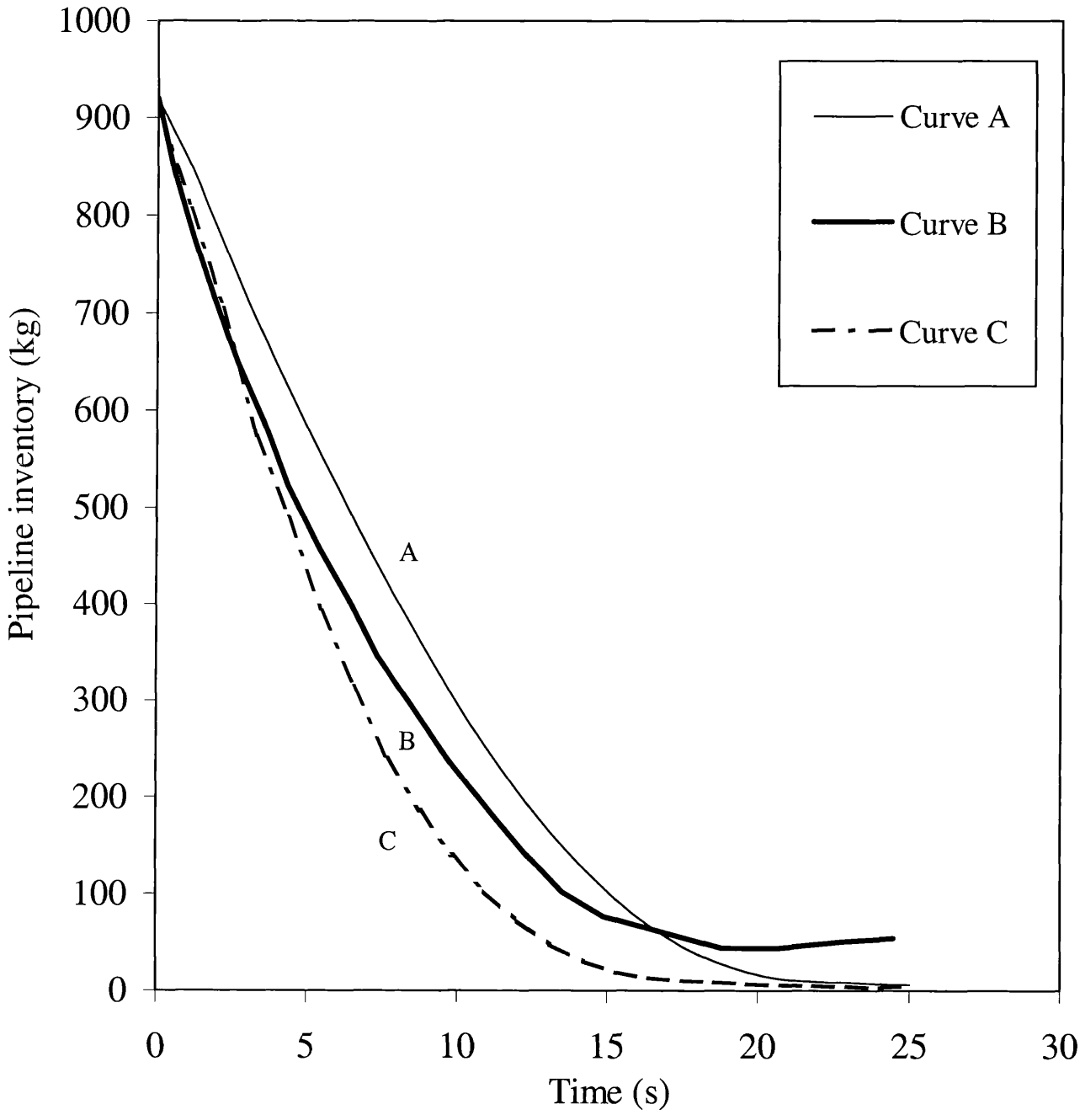

Figure 5.3 Pipeline inventory variation with time for LPG40 following FBR

Curve A: Linear characteristics

Curve B: Experimental data

Curve C: Curved characteristics

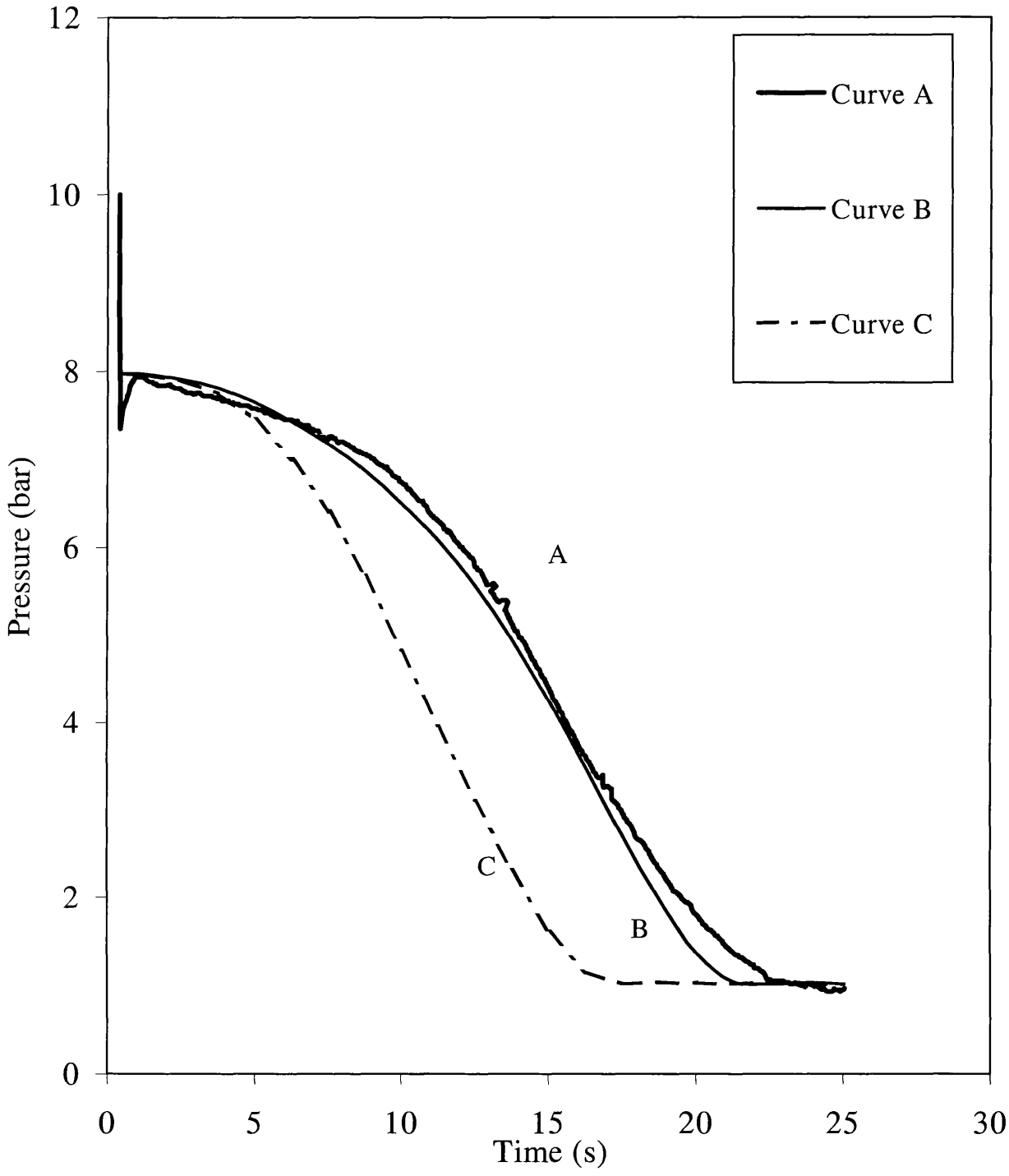

Figure 5.4 Pressure variation with time at intact end, for LPG40 following FBR

Curve A: Experimental data

Curve B: Linear characteristics

Curve C: Curved characteristic

Figures 5.5, 5.6 and 5.7 respectively show the variations of rupture plane pressure, intact end pressure and inventory with time following the FBR of the methane pipeline (table 5.2). In this case methane remains in the gaseous phase throughout the depressurisation process. In all three figures, curve A shows the result of the first order interpolation using linear characteristics and curve B shows the result of second order interpolation using curved characteristics. No experimental data are presented as these tests simulate a hypothetical rupture scenario.

In contrast to the predictions obtained in the LPG 40 case, in this case, the predictions obtained using both the linear and curved characteristics agree closely corresponding to the same CPU time of ca. 35 minutes.

The above simulations show that predictions obtained and the computational run times using either of the two methodologies are greatly influenced by the state of the fluid flowing through the pipeline. LPG remains predominantly in the two-phase region throughout the discharge process. Methane on the other hand remains in the gaseous phase and never crosses into the two-phase region. The reasons for the observed discrepancy between the predictions obtained using the linear as opposed to the curved characteristics in the case of two-phase flow is explained as follows.

In the depressurising fluid following FBR, information is transferred along the characteristic lines. In the case of two-phase flow, discontinuities occur in flow properties due to phase change. This introduces errors in the numerical solution as discussed later (see section 5.2.2). At the discontinuities, the use of curved as against linear characteristics leads to significant errors, as the former approximation would by nature smoothen out such flow related discontinuities. Generally, any such error introduced during flow calculations would naturally propagate with time. Thus, the poor agreement with field data for calculations using curved characteristics seem to suggest that wave propagation along a pipeline, where flow discontinuities are prevalent (e.g., two-phase flow), are better approximated with linear as opposed to curved characteristics. Based on the above findings, linear characteristics are used in the proceeding simulations.

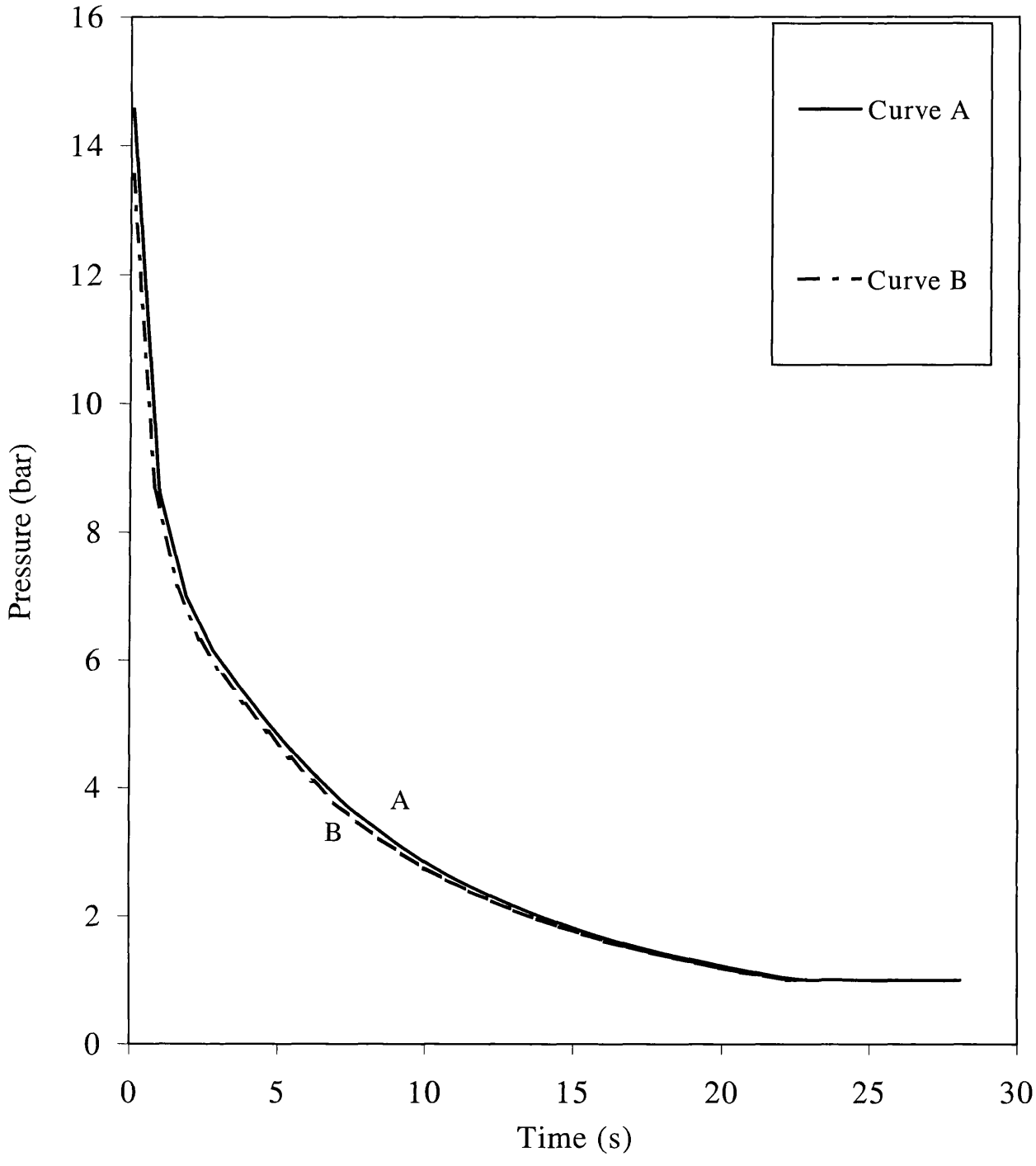

Figure 5.5 Rupture plane pressure variation with time for methane following FBR

Curve A: Curved characteristics

Curve B: Linear characteristics

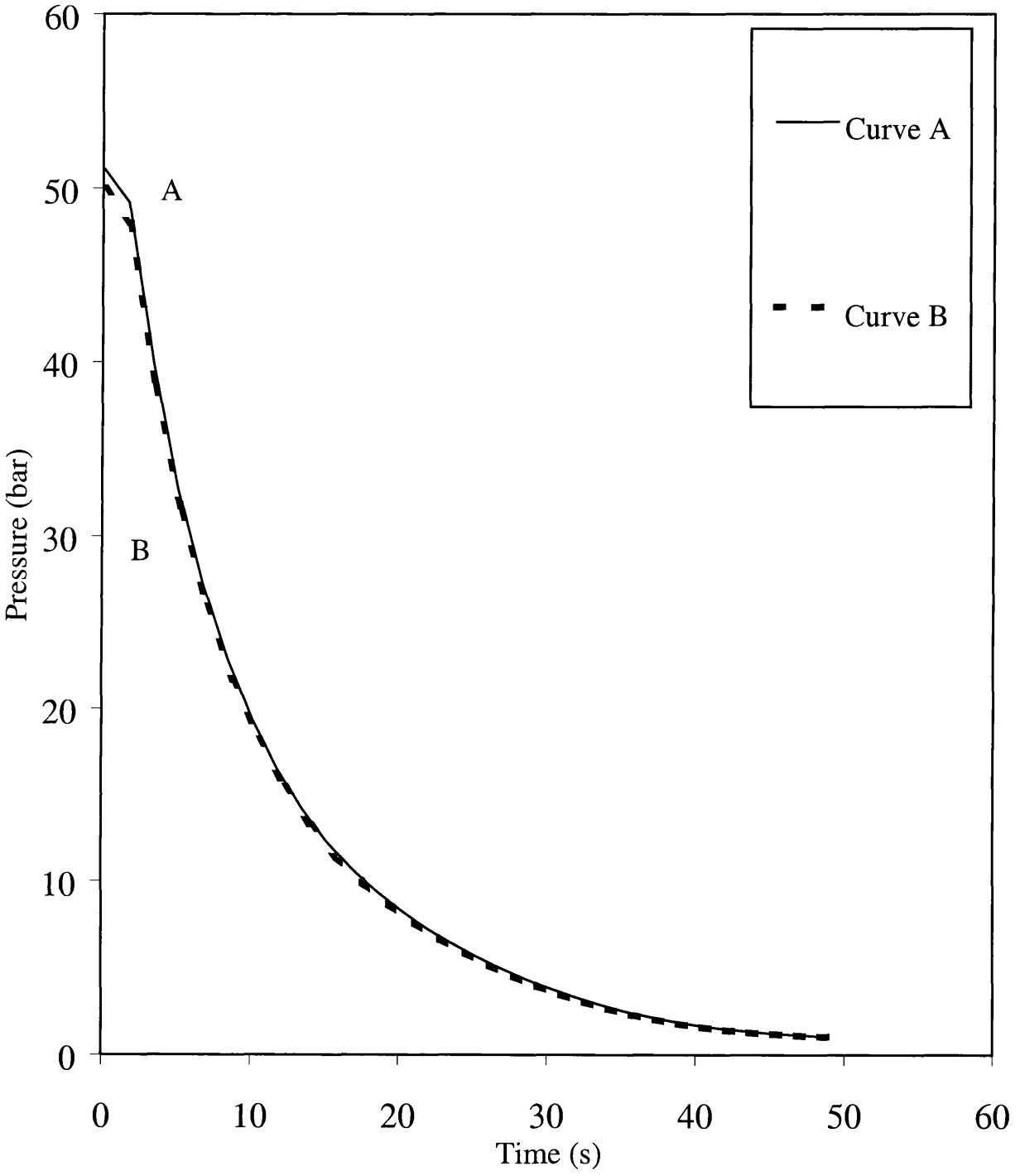

Figure 5.6 Intact end pressure variation with time for methane following FBR

Curve A: Curved characteristics

Curve B: Linear characteristics

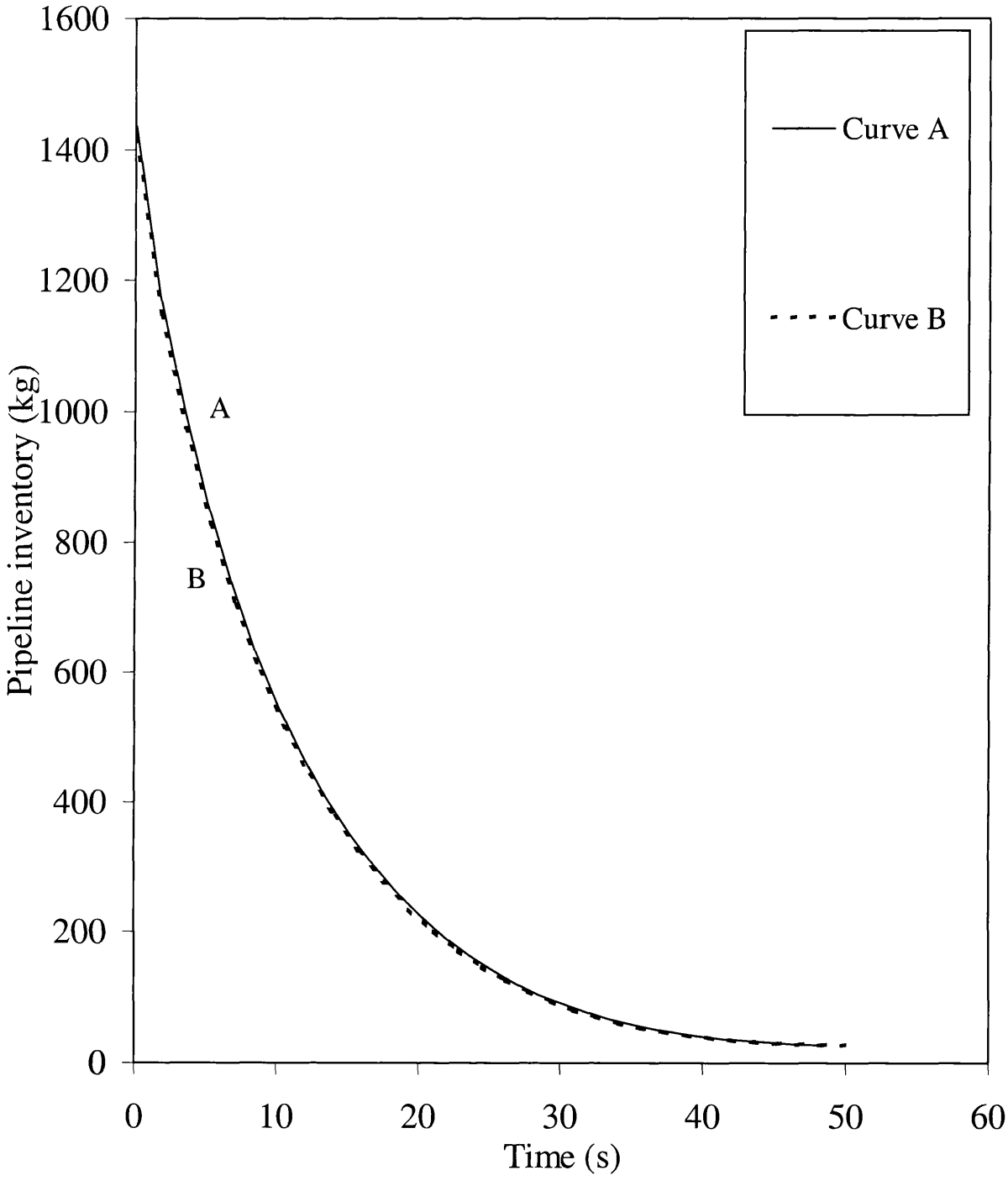

Figure 5.7 Pipeline inventory variation with time for pure methane following FBR

Curve A: Curved characteristics

Curve B: Linear characteristics

5.2.2 Effect of Time Step (Δt) on Outflow Predictions

If a numerical model is to yield useful results, it is essential that the computation scheme on which the model is based should cause the approximation errors in the calculated parameters, to decay rather than to propagate with increasing amplitude as the calculation proceeds forward in time. A computation scheme having the former attribute is said to be stable. In practice, stability imposes upper limits on the space, Δx and time, Δt increments used in the calculation (Swaffield, 1993)

The conditions for stability in computation schemes of the explicit type method of characteristics are generally defined by the relation known as the Courant Criterion (CFL). The CFL is named after Courant, Friedrichs and Lewy who wrote a fundamental paper in 1928 (Courant et al., 1928) that was essentially the first paper on the stability and convergence of finite difference methods for partial differential equations. The CFL is defined as:

$$\Delta t \leq \frac{\Delta x}{u + a} \tag{5.1}$$

where u, is fluid velocity and a, is speed of sound.

Since time step, Δt is inversely proportional to the speed of sound and fluid velocities (see equation 5.1), changes in these variables affect the time step and generally the convergence of the solution. The following describes the ways in which changes in the state of a fluid affects the size of the time step employed and consequently the slope of the characteristics lines.

In a study by Picard and Bishnoi (1987) on a numerical procedure for the prediction of the acoustic velocity in two-phase multi-component fluids, a sudden reduction in speed of sound was observed at approximately the calculated dew point. This may be attributed to the fact that as a second phase forms, the compressibility of the fluid decreases abruptly.

Figure 5.8 shows a plot of variation of predicted speed of sound for a range of temperatures along various isobars for the Piper Alpha mixture (see table 5.3). The

inventory is the same as that contained in the MCP 01 riser following its FBR during the Piper Alpha tragedy (Richardson and Saville, 1989).

Component	mole%
CH_4	73.6
C_2H_6	13.4
C_3H_8	7.4
i-C_4H_{10}	0.4
n-C_4H_{10}	1.0
i-C_5H_{12}	0.08
n-C_5H_{12}	0.07
n-C_6H14	0.02
N_2	4.03

Table 5.3 Composition of Piper Alpha mixture

The speed of sound has been calculated based on equations derived by Picard and Bishnoi (1987). Curves A,B and C shows the isobars at 80, 70 and 60 bar respectively.

The sudden drop in speed of sound coincides with the onset of condensation in the mixture. On either side of the rapid transition however, the variation of speed of sound is linear. Also, the higher the pressure, the greater the drop in sound velocity. During pipeline rupture, the onset of two-phase condensate flows causes a sudden reduction in the expansion wave velocity, the magnitude of which will vary depending on the mixture's composition.

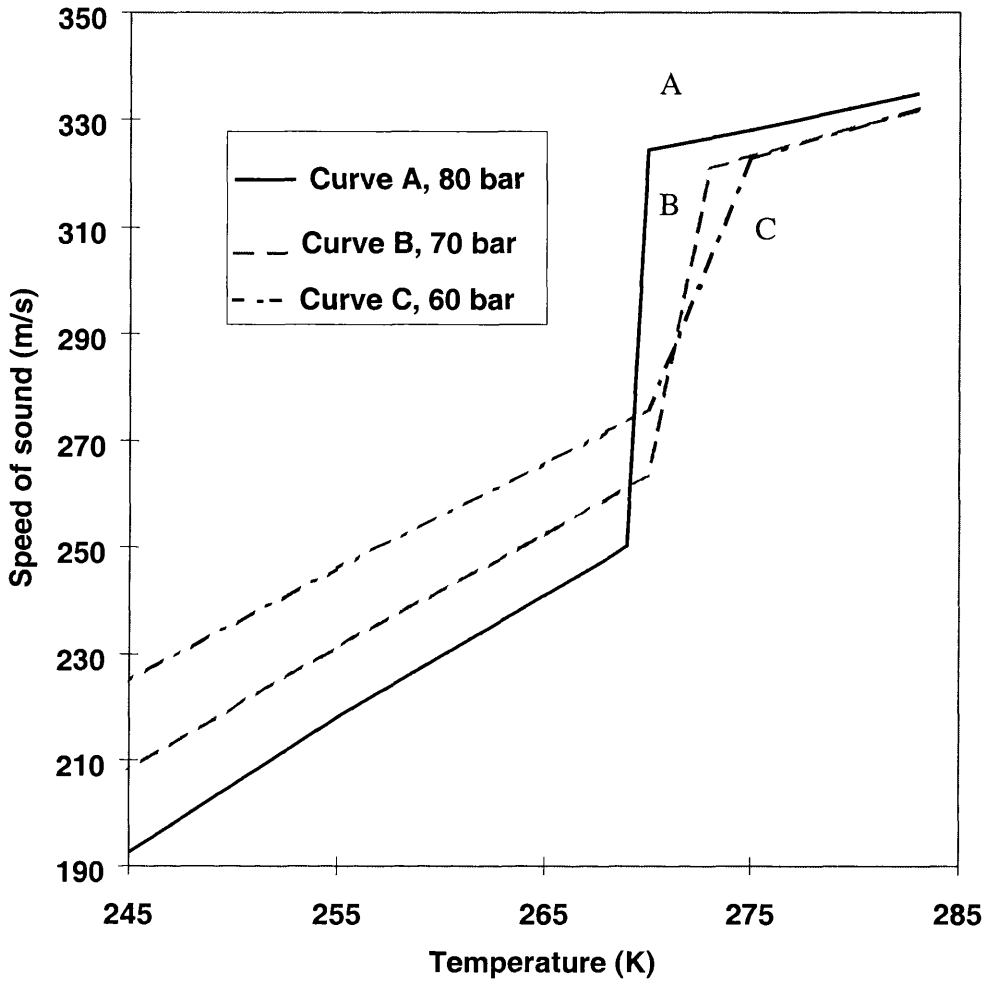

Figure 5.8 Variation of speed of sound with temperature along various isobars for the Piper Alpha mixture

Figure 5.9 shows the variation of predicted fluid density based on Peng Robinson equation of state (Peng and Robinson, 1976) for a range of temperatures along various isobars for the Piper Alpha mixture. Curve A shows the 80 bar isobar, whereas curves B and C show the isobars corresponding to 70 and 60 bar respectively. The data cover the transition from single to two-phase.

Unlike the speed of sound predictions, the variation of density does not exhibit a step change across the phase boundary but the overall behaviour is non-linear.

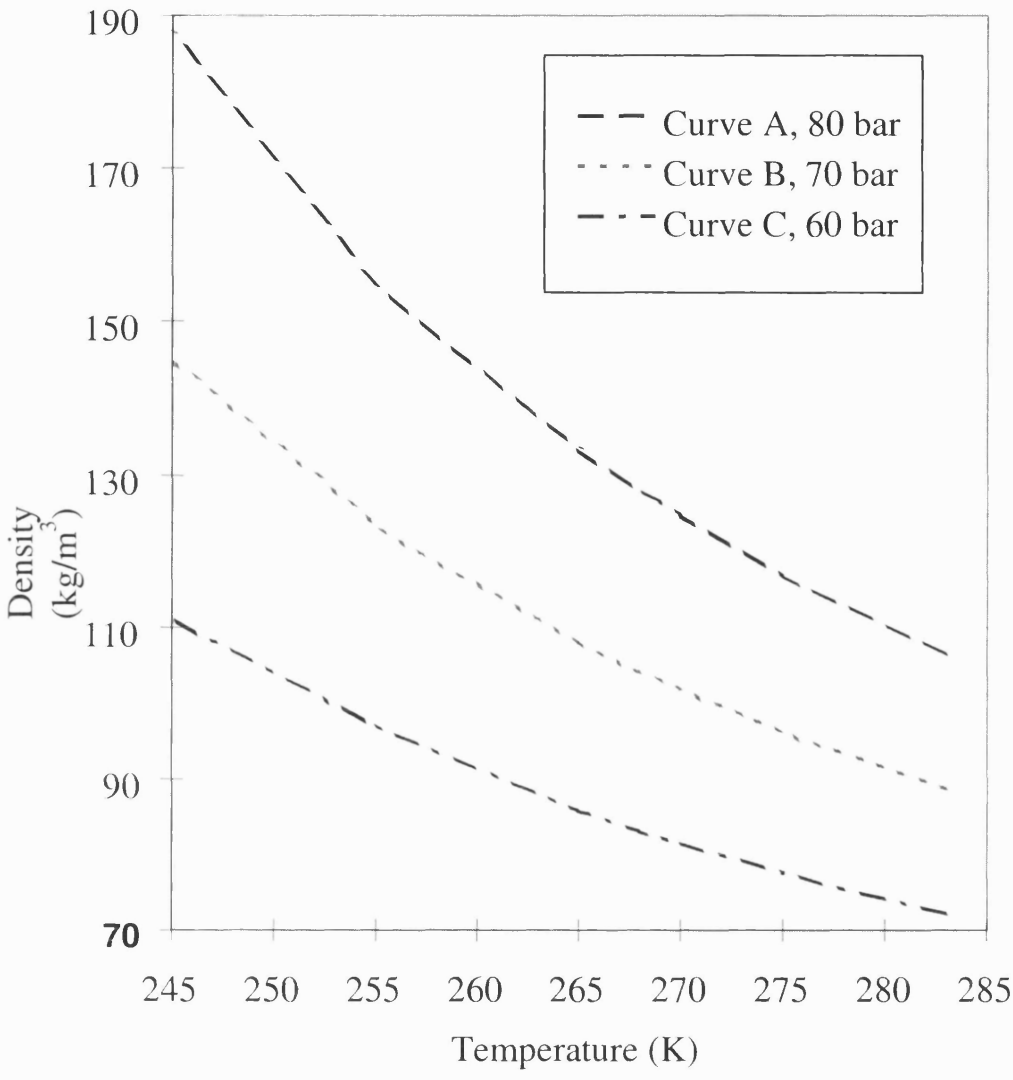

Figure 5.9 Fluid bulk density variation with temperature along various isobars for the Piper Alpha mixture

A boundary between a gas and two-phase can be termed as a condensation boundary whereas that between liquid and two phase is termed as a boiling boundary. Either boundary may propagate along the path of depressurisation in the pipeline and travel at a faster or slower velocity than the local fluid velocity depending on the prevailing conditions. The basic assumptions in dealing with such interfaces are firstly that a distinct interface exists and secondly that no mixing occurs across any such interface. The presence of the interface between a single phase and a two-phase mixture poses problems from a computational viewpoint for two reasons.

Firstly, the propagation velocity of the positive Mach line is greater in a single-phase than in a two-phase mixture so that the gradient ($\Delta t/\Delta x$) will be steeper in two-phase flow than that in single-phase flow. The reverse is true for the negative Mach line. The substantial difference in acoustic velocities between the two different states (depending on the difference in compressibility) means that if the characteristic lines were to cross such an interface, significant refraction would occur as schematically represented in figure 5.10 for a left travelling interface.

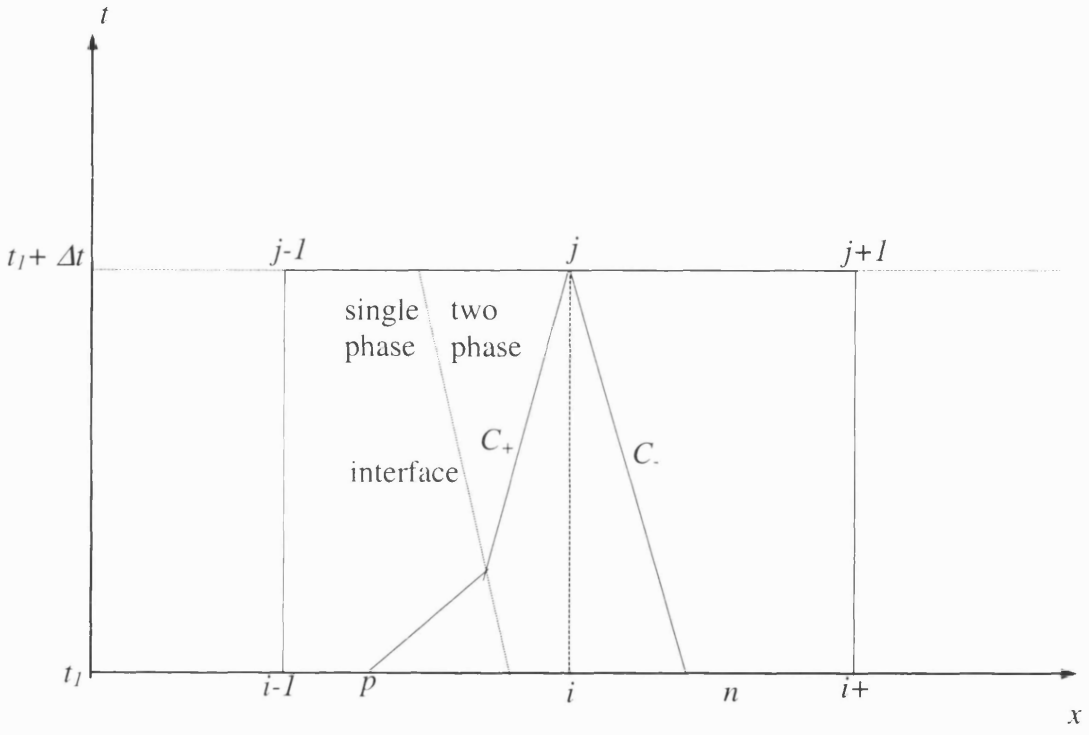

Figure 5.10 Refraction effect of single phase/two phase interface on characteristic lines

Secondly, other fluid properties may change significantly across an interface so the compatibility equations have to account for the presence of an interface (Nakamura et al., 1995). The added complexity of the mathematical modelling that is necessary to fully account for these phenomena is avoided in this study by minimising the discretisation time step, Δt. An explanation demonstrating how a reduction in the value of Δt reduces the error caused by the refraction of the characteristic lines is presented below.

For both first and second order solutions, the values of the fluid velocity, u and speed of sound, a need to be calculated before the locations of points, p and n on the characteristics lines can be determined (see sections 4.3 and 4.4 for the first and second order solutions respectively). In the first order solution for example, in order to calculate the location of point, p (the intersection of the positive Mach line on the previous time line), the following two equations, as shown in chapter 4 but repeated here for reference, are solved simultaneously for u_p and a_p,

$$u_p\left(1+\frac{u_i-u_{i-1}}{x_i-x_{i-1}}\Delta t\right)+\frac{u_i-u_{i-1}}{x_i-x_{i-1}}\Delta t a_p=u_i \tag{4.30}$$

$$a_p\left(1+\frac{a_i-a_{i-1}}{x_i-x_{i-1}}\Delta t\right)+\frac{a_i-a_{i-1}}{x_i-x_{i-1}}\Delta t u_p=a_i \tag{4.31}$$

Once u_p and a_p are known, the location of x_p is calculated from,

$$x_p=x_i-\Delta t\left(u_p+a_p\right) \tag{4.27}$$

Reducing Δt has the effect of pushing the location of x_p closer to that of x_i where the exact conditions are known and so flow values are likely to be close to those at x_i, thus minimising interpolation errors. This effect is illustrated in figure 5.11.

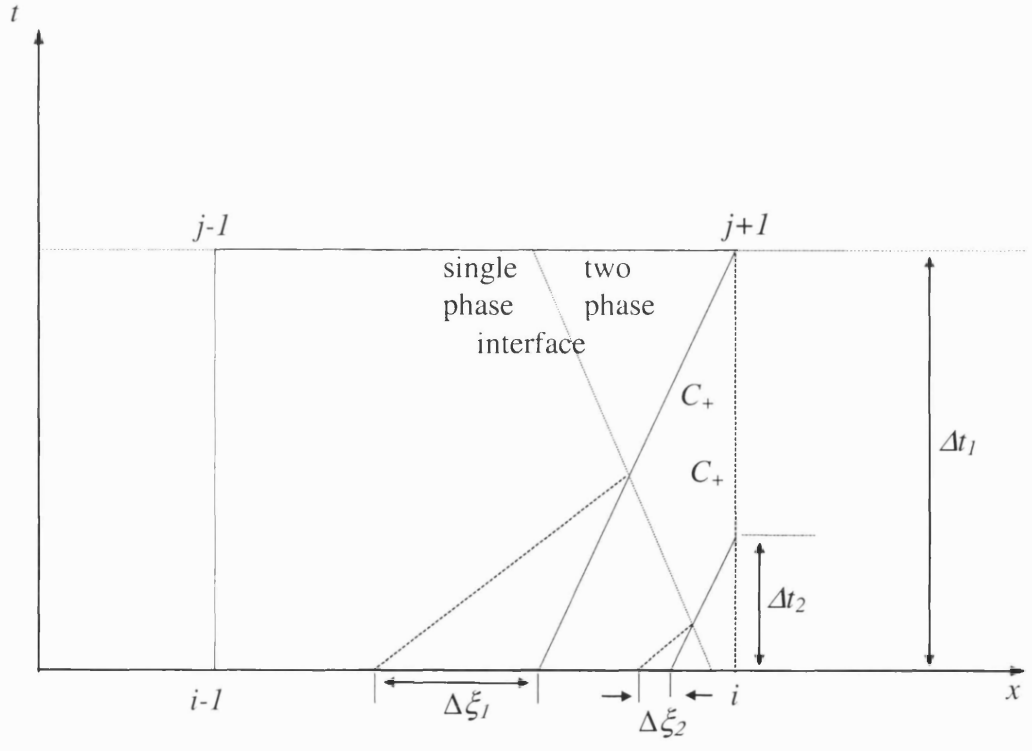

Figure 5.11 Effect of smaller Δt on resulting accuracy of prediction of point p

The broken lines indicate the refracted characteristics whilst the straight characteristic line denotes the first order solution. Δt_2 is smaller than Δt_1 and results in a smaller interpolation error, $\Delta \xi_2$.

Based on the above it is desirable to decide on an appropriate time step while using a numerical method based on time and distance spaces. The selected time step should be determined in such a way that it satisfies the CFL criterion, reduces the error introduced during the calculation and also takes account of the effect of phase transition.

In order to obtain a suitably small time step, which would minimise interpolation errors, the largest permissible time step at any instant along the whole length of the pipeline as computed from the CFL criterion is given as:

$$\Delta t \leq \frac{\Delta x}{u_{max} + a_{max}} \tag{5.2}$$

Where u_{max} and a_{max} are the maximum values of fluid velocity and speed of sound in the fluid, along the pipe at the particular time step. It is worth noting that these maximum values may change at each time step where the same value for u_{max} and a_{max} may not be found at all grid points. Consequently, one and two-dimensional dynamically updated time steps, which are a function of both depressurisation time and distance along the pipeline are used in the simulations. In both methods, Δt is calculated at all grid points in each time step in order to determine the smallest value. In the one-dimensional dynamically updated time step (1DDTS) method, the comparison is only made between the grid points (x axis) of that particular time step. However in two-dimensional method (2DDTS) the comparison is carried out both between the grid points (x axis) and the time steps (t axis).

Figures 5.12 and 5.13 respectively show the results of open-end pressure and pipeline inventory variation with time, for the Isle of Grain LPG 42 FBR (table 5.1). In both figures, curve A shows the results based on 1DDTS. Curve B shows the results based on 2DDTS with curve C representing the experimental data. Figure 5.14 shows the results of pressure variation with time at intact end for the same test. Curve A shows

the experimental data, curves B and C on the other hand show the results based on 1DDTS and 2DDTS respectively.

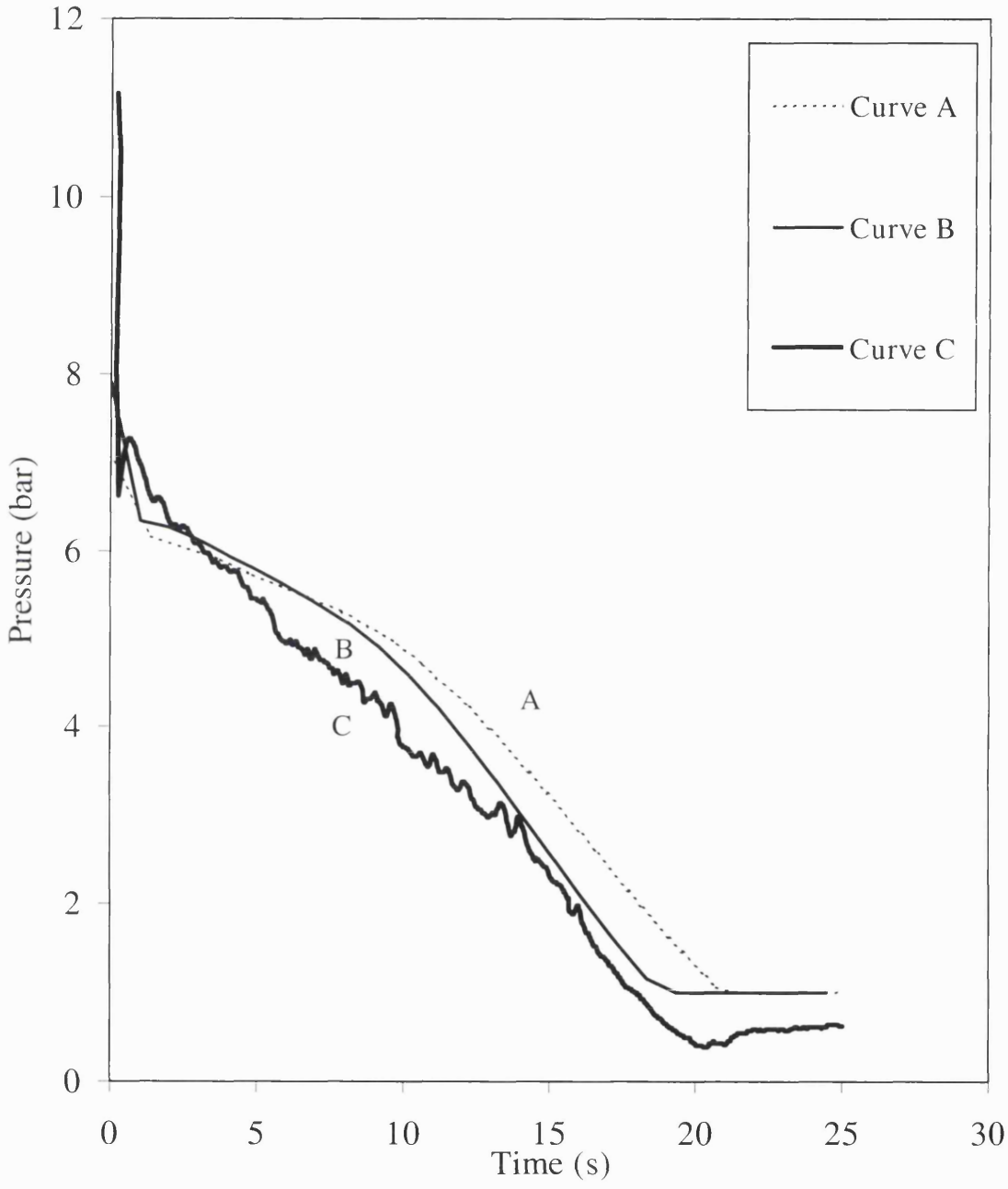

Figure 5.12 Rupture plane pressure variation with time for LPG42 test following FBR

Curve A: Simulated data based on 1DDTS

Curve B: Simulated data based on 2DDTS

Curve C: Experimental data

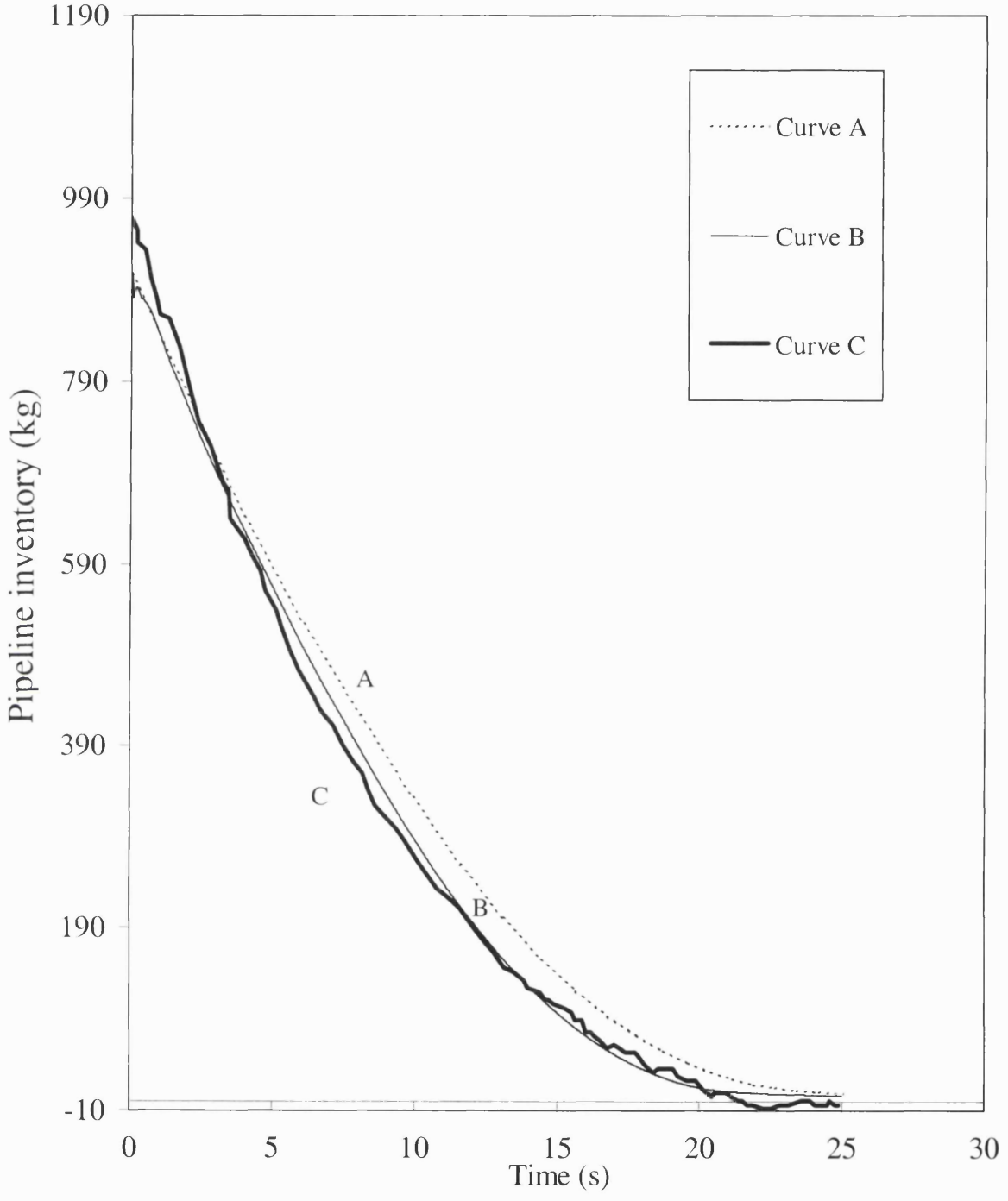

Figure 5.13 Pipeline inventory variation with time for LPG42 test following FBR

Curve A: Simulated data based on 1DDTS

Curve B: Simulated data based on 2DDTS

Curve C: Experimental data

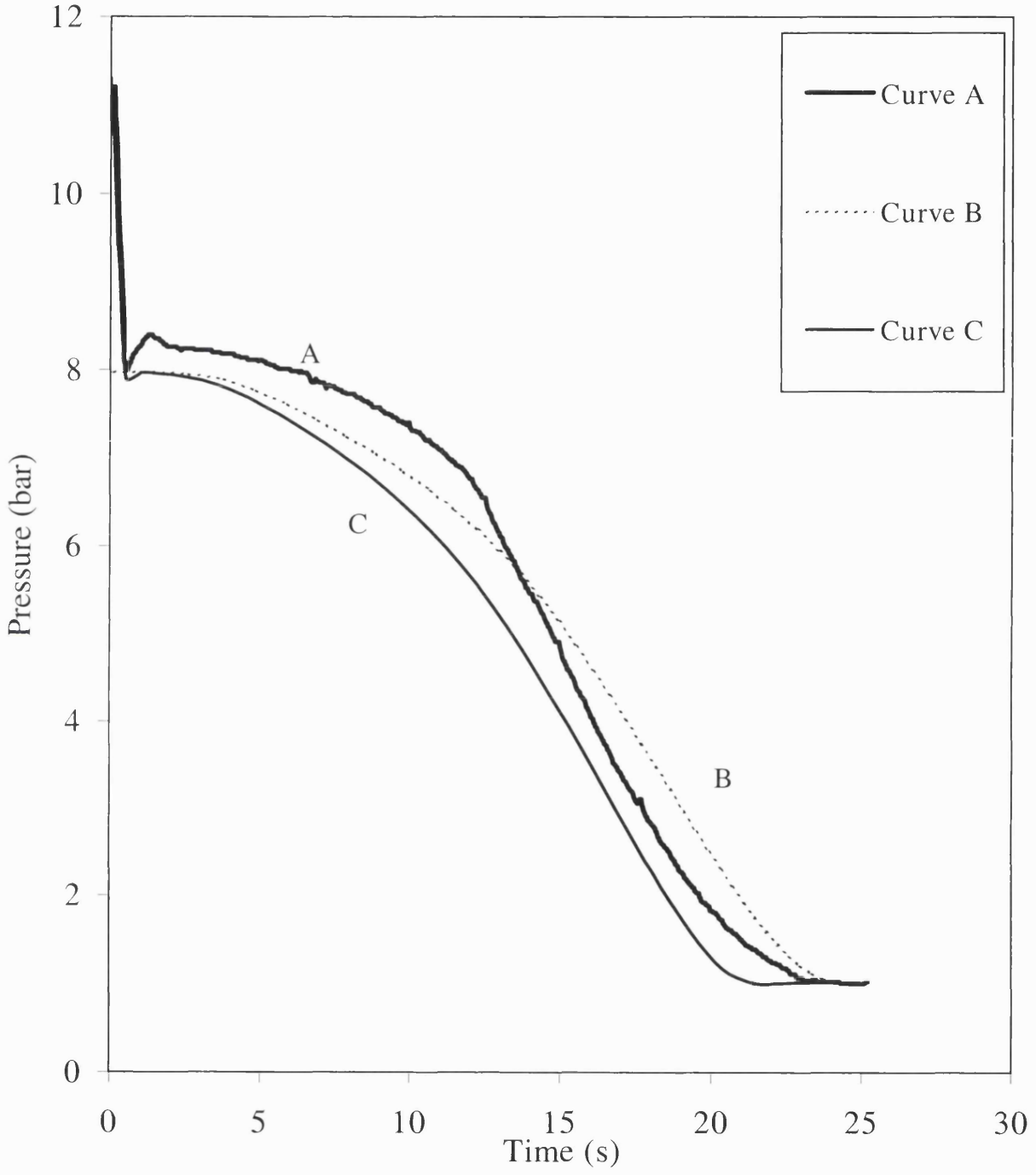

Figure 5.14 Intact end pressure variation with time for LPG42 test following FBR

Curve A: Experimental data

Curve B: Simulated data based on 1DDTS

Curve C: Simulated data based on 2DDTS

The above data show that in all cases, the 2DDTS produces better agreement with experimental as compared to the 1DDTS. However the computational run time for 2DDST is 6 hr and 30 minutes, as compared with 66 minutes for 1DDTS.

The rationale for the two-dimensional dynamically updating the calculated time step is based on the minimisation of the effect of refraction at the single/ two-phase interface occurring during depressurisation. However, when such transition is absent, both methods generate identical results. This is illustrated in the case of the rupture of the same pipeline conveying methane (table 5.2) as indicated in figure 5.15. Curves A and B show simulated results based on 1DDTS and 2DDTS methods respectively. As can be seen, both methods produce the same pressure/time predictions.

It can be concluded here that in the presence of phase transition, it is important to use very small time steps, which are updated both in time and in distance such as that in 2DDTS. However when no such phase transition occurs, larger time steps based on the 1DDTS scheme can be employed without any loss in accuracy and with significant reduction in computational run time.

Unless otherwise stated, the above findings coupled with linear characteristics are employed in the proceeding simulations.

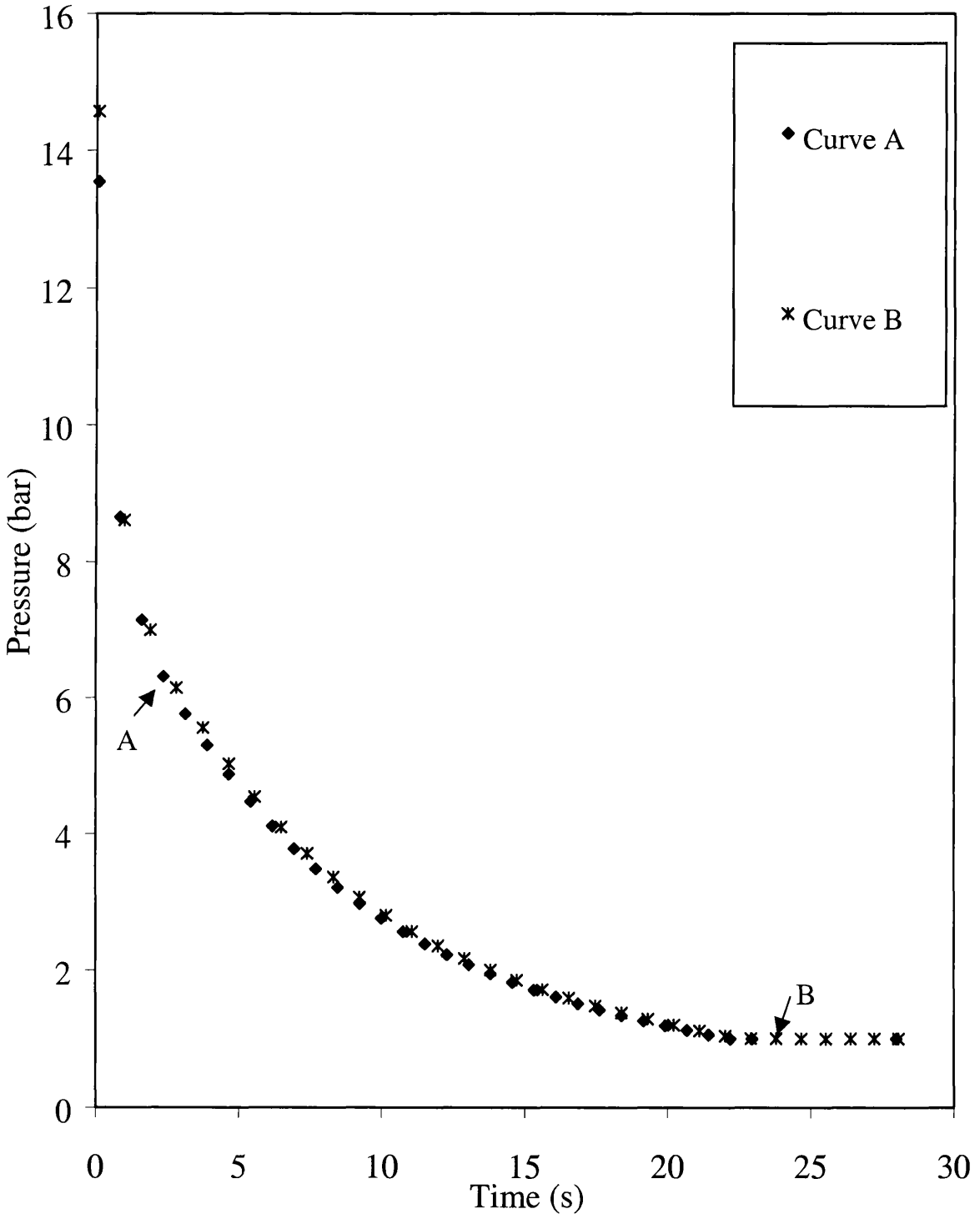

Figure 5.15 Rupture plane pressure variation with time for methane following FBR

Curve A: Simulated data based on 1DDTS

Curve B: Simulated data based on 2DDTS

5.2.3 Frictional Force Effects

In all cases of depressurisation of a pipeline containing non-volatile liquid, volatile liquid or gas, the main contribution to the pressure drop in the pipeline can be attributed to frictional effects at the wall (Richardson and Saville, 1991). The longer the pipeline, the greater is the significance of frictional pressure drop on the transient flow profiles. Therefore an accurate representation of the friction forces acting on the fluid in the pipeline is of primary importance.

Assuming that minor losses are negligible, frictional force for a flowing fluid in a pipeline can be expressed by the empirical relation (Perry, 1973)

$$\beta = -2\frac{f_f}{D}\rho u|u| \tag{5.3}$$

The symbols are all defined in chapter 2.

Despite the importance of pressure drop in transient flow situations, there is still no universally satisfactory method for calculating frictional pressure drop, especially for highly transient two-phase flows.

The most popular methods are often cumbersome, heavily dependent on empirically determined coefficients, and have considerable uncertainty (Thorley and Tiley, 1987). Simpler forms or firmer theoretical bases for predictive methods are applicable at narrow ranges.
The friction factor may be categorised as unsteady and steady types. However the steady friction factor itself can be further categorised as flow independent (constant) and flow dependent.

Saha (1997) undertook an extensive review of the literature on unsteady state friction factor. He concluded that there is still some uncertainty in the accurate prediction of unsteady friction factor in rough pipes where highly turbulent flows prevail. Moreover from the few studies performed to date (see for example Wood and Funk, 1970; Chen, 1993) the effect of the unsteady component in wall shear stress calculations seems to diminish in magnitude the greater the turbulence.

In the absence of any theoretically or experimentally validated transient turbulent friction models for rough pipes, in this study this component for friction has been ignored. However the advantage of using a method of characteristics solution for FBR, as indeed for any transient flow scenario, any unsteady state friction factor correlation can easily be incorporated (see for example Zielke, 1968;Trikha, 1975; Eichinger and Lein, 1992; Vardy and Brown, 1995, 1996). Consequently the friction factor employed in this study is based on steady state friction factor correlations.

Steady state friction factor can be categorised into flow dependent, and flow independent (constant) friction factor. However the flow dependent friction factor itself can be subdivided into single phase and two-phase categories. The correlation employed in friction factor calculation depends on the prevailing flow regime.

For laminar flow (Re<2100) the following well established flow dependent equation for friction factor is employed

$$f_f = \frac{16}{\mathrm{Re}} \tag{5.4}$$

where f_f is the Fanning friction factor and Re is the Reynolds number.

For partially developed turbulent and transition zone flow, the friction factor changes with the Reynolds number (flow dependent). However for fully developed turbulence, the 'rough pipe law' (Perry, 1973) expressed below can be employed:

$$\frac{1}{\sqrt{f_f}} = 2A_1 \log\left(\frac{D}{\varepsilon}\right) B_1 \tag{5.5}$$

where, A_1 and B_1 are constants.

In the above equation it is assumed that the friction factor is solely dependent on the pipe roughness and size used (flow independent).

Typical high-pressure gas pipeline flows, following pipeline failure are characterised by their high Reynolds numbers (Re>4000). As such the key decision to be made for accounting for such flows therefore, is whether it can be assumed that fully developed

turbulence has been achieved. Once the above is established, the appropriate friction factor may be applied.

Both flow independent and flow dependent friction factor have been studied below in the context of outflow following FBR.

Flow Independent Friction Factor

Van Deen and Reintsema (1983) stated that the friction factor is weakly dependent on Reynolds number at high Re ($> 10^7$). The authors used a constant friction factor for their study for modelling high-pressure gas transmission lines. However they did not mention how the friction factor employed was obtained. In their study, the authors highlighted the need to verify whether it suffices to employ a steady state based constant friction factor for highly transient flows.

Flatt (1985) also used Van Deen and Reintsema (1983) justification to employ a constant friction factor. However the value chosen seems to be specific to the author's model, lacks theoretical basis, and thus of limited use in practice.

Issa and Spalding (1972), Cronj et al. 1980, Guy (1967) and Stoner (1969) all claim that at high Reynold's number, the friction factor can be assumed to be constant and support their claim by experimental data.

Thorley and Tiley (1987) also recommend the use of a constant friction factor in the modelling of unsteady transient flow of compressible fluids in relatively short pipelines giving rise to a reasonable degree of accuracy in predicting real data.

In none of the work reviewed so far, an equation for a flow independent (constant) friction factor has been given.

Nikuradse (1933) performed a series of experiments in order to develop a relationship between the friction factor and Reynolds number in pipes under turbulent flow. Based on his experiments he developed two separate equations for smooth and rough pipes. Nikuradse's equation for rough pipes is presented as

$$f_f = \frac{1}{\left(3.48 - \left(1.737 \ln \frac{2\varepsilon}{D}\right)\right)^2} \tag{5.6}$$

where

ε = pipe roughness factor

D = pipe diameter

The above equation is the most universally used equation for calculating friction factor. It is employed in the present work for assessing the effect of using constant friction factor in predicting outflow following FBR.

Single Phase Flow Dependent Friction Factor

The friction factor is dependent on the type of flow, which may vary from point to point in a pipeline, and in addition on pipe roughness. The traditional way of estimating the friction factor for a Newtonian fluid flowing through a pipe is based on the well-known Moody Friction Chart (Perry, 1973). This however is unsuitable for computer simulations and therefore an equation for calculating the friction factor is desirable.

The Colebrooke equation (Colebrooke, 1939) is the universally adopted equation where the use of a Moody chart is impossible. This equation is presented as

$$\frac{1}{\sqrt{f_D}} = -2\log\left(\frac{\varepsilon}{3.7065D} + \frac{2.5226}{\mathrm{Re}\sqrt{f_D}}\right) \tag{5.7}$$

where

f_D= Darcy friction factor; which is four times greater than Fanning friction factor

ε = Roughness factor

Equation (5.7) covers both the transition region as well as the fully developed flow regime for smooth and rough pipes (Chen, 1979). It produces results within 5% of

experimental data, although its major disadvantage is that the solution for the friction factor requires iteration which can be computationally expensive.

A number of authors have attempted to drive approximate explicit expressions to the Colebrook's equation.

Moody (1944) developed the following explicit expression for friction factor:

$$f_f = 0.001375\left[1+\left(20000\frac{\varepsilon}{D}+\frac{10^6}{\mathrm{Re}}\right)^{\frac{1}{3}}\right] \tag{5.8}$$

Which is valid for Re ≥ 2000.

Two other explicit friction factor expressions are those by Churchill (1977) and Chen (1979). The convenience of these correlations are that they cover the whole range of Reynolds numbers and pipe roughness, producing results of almost the same accuracy as those produced by the Colebrooke's equation. Churchill and Chen equations are respectively given by

Churchill:

$$f_D = 8\left[(8/\mathrm{Re})^{12}+1/(A+B)^{3/2}\right]^{1/12} \tag{5.9}$$

where

$$A = \left[2.4547\ln\frac{1}{(7/\mathrm{Re})^{0.9}+0.27\frac{\varepsilon}{D}}\right]^{16}$$

$$B = (37530/\mathrm{Re})^{16}$$

Chen:

$$\frac{1}{\sqrt{f_f}} - 4.0\log\left[\frac{\varepsilon}{3.7065D}-\frac{5.0452}{\mathrm{Re}}\log\left(\frac{1}{2.8257}\left(\frac{\varepsilon}{D}\right)^{1.1098}+\frac{5.8506}{\mathrm{Re}^{0.8981}}\right)\right] \tag{5.10}$$

Chen's equation is simpler in its formulation than the Churchill equation. However both equations produce similar predictions compared to real data (Chen 1979).

The Chen equation was used by Bisgaard et al. (1987) and Saha (1997) in modelling the transients as a result of rupture of high-pressure gas pipelines. However Saha

(1997) also made a comparison between Chen and Moody equations, and concluded that there was negligible difference in their predictions.

Serghides (1984) presented a new approximation by applying Steffenson's accelerated convergence technique (Serghides, 1984) to an iterative, numerical solution of the Colebrook equation. Serghides' equation is shown as

$$f_D = \left(A - \frac{(B-A)^2}{C-2B+A} \right)^{-2} \tag{5.11}$$

where

$$A = -2\log\left(\frac{\frac{\varepsilon}{D}}{3.7} + \frac{12}{\mathrm{Re}} \right)$$

$$B = -2\log\left(\frac{\frac{\varepsilon}{D}}{3.7} + \frac{2.51A}{\mathrm{Re}} \right)$$

$$C = -2\log\left(\frac{\frac{\varepsilon}{D}}{3.7} + \frac{2.51B}{\mathrm{Re}} \right)$$

Serghides compared his equation with seven other well-known high accuracy explicit approximations. The equations examined in his tests were those by Moody (1944), Swamee and Jain (1976), Wood (1966), Churchill(1977), Chen(1979) and Zigrang and Sylvester (1982). The results showed that the maximum deviation of Serghides' equation in calculating friction factor from the numerical solution of Colebrook's equation was only 0.0023%. It was also shown that the average deviation of the friction factor obtained by Serghides is a hundred or more times smaller than those predicted from the other equations studied.

El-Emam et al. (1997) developed a friction factor equation with the help of data fitting techniques. The authors used Haaland's (1983) relation, which itself is an explicit equation to solve Colebrook's equation to give the following expression for the friction factor:

$$\frac{1}{\sqrt{f_f}} = \frac{-1.8}{n}\left[\left(\frac{6.9}{\mathrm{Re}}\right)^n + \left(\frac{\varepsilon}{3.7D}\right)^{1.11n}\right] \tag{5.12}$$

Haalands (1983) recommends different values for the constant, n for different pipelines.

Based on field data El-Emam et al. (1997) introduced a new constant, K in the friction factor equation, which is dictated by flow rate. The corresponding expression is given by

$$\frac{1}{\sqrt{f_f}} = K\log\left[\left(\frac{6.9}{\mathrm{Re}}\right)^{2.8} + \left(\frac{\varepsilon}{3.7D}\right)^{1.11*2.8}\right]$$

The authors compared the results from their equation with some well-known friction factor equations and concluded that their equation performed best in terms of accuracy compared to experimental data.

Two-Phase Flow Dependent Friction Factor

For a two-phase mixture, the wall friction is assumed to arise from the liquid phase only, so that the gas friction part, f_{wg} is zero.

When a two-phase multiplier is used to account for two phase flow, the wall friction pressure drop written in terms of the liquid friction factor given by,

$$\beta = -2\phi_{lo}^2 \frac{f_{fl}}{D}\rho u|u| \tag{5.13}$$

where, f_{fl} is the liquid friction factor and ϕ_{lo}^2 is the two-phase multiplier.

The liquid friction factor can be calculated from any single-phase friction factor equation such as equation (5.10) or (5.11).

ϕ_{lo}^2 is given by the following correlation of Friedel (1979)

$$\phi_{lo}^2 = B + \frac{3.24FH}{Fr^{0.045}We^{0.035}}$$

$$B = (1-X)^2 + X^2 \frac{\rho_l f_{fg}}{\rho_g f_{fl}}$$

$$F = X^{0.78}(1-X)^{0.224}$$

$$H = \left(\frac{\rho_l}{\rho_g}\right)^{0.91}\left(\frac{\mu_g}{\mu_l}\right)^{0.19}\left(1-\frac{\mu_g}{\mu_l}\right)^{0.7}$$

$$Fr = \frac{G^2}{gD\rho_m^2}$$

$$We = \frac{G^2 D}{\sigma\rho_m} \qquad (5.14)$$

Where X, σ and G are the liquid fraction, the surface tension, and the mass flow rate respectively. Fr and We on the other hand are the Froude and Weber numbers respectively. The subscripts g, l and m refer to gas, liquid and mixture properties respectively.

The other alternative to calculating two-phase momentum loss due to friction is based on replacing single-phase properties by mixture properties. This is only suitable for homogeneous flows where both phases move at the same velocity so that

$$\beta = -2\frac{f_{fm}}{D}\rho_m u|u| \qquad (5.15)$$

Where f_{fm} is the two-phase mixture friction factor and can be determined either by equation 5.10 or equation 5.11 where the following substitutions are made for flow parameters

$$\mathrm{Re} = \mathrm{Re}_m = \frac{\rho_m uD}{\mu_m} \qquad (5.16)$$

The mixture density can be calculated from relevant equation, see chapter 2.

The mixture viscosity is given by

$$\frac{1}{\mu_m} = \frac{X}{\mu_g} + \frac{(1-X)}{\mu_l} \tag{5.17}$$

The gas and liquid viscosities are calculated according to the Ely and Hanley scheme for non-polar gaseous mixtures, and the Dymond and Assael scheme for liquid mixtures (Assael et al., 1996).

The merits of either method with regard to accuracy has been tested by Chen (1993) with relation to the depressurisation of Edwards and O'Briens (1970) blowdown experiments of sub cooled water lines. Chen shows that both methods do not vary significantly in their blowdown predictions.

The advantage of the method whereby the single-phase properties are replaced by two-phase mixture properties is that no additional calculation needs to be performed for surface tension. Therefore in this study, the single-phase friction factor is used. Additionally, in order to verify the effect of friction factor in modelling highly transient fluid flows, two sets of simulations are conducted.

The first series show the comparison in results based on using different reported single-phase flow dependent friction factor equations. The second set of simulations show the same results based on comparison between flow independent friction factor and the most suitable flow dependent friction factor identified in the first series of studies. The flow dependent friction factor correlations investigated include those given by Chen (1979), Serghides (1984) and El-Emam et al. (1997). In the case of flow independent friction factor (constant), the Nikuradse (1933) expression is chosen.

Figure 5.16 shows the pressure variation with time at the rupture plane for the LPG40 test. Curves A, B and C respectively show the results obtained by applying the flow dependent correlations proposed by Chen (1979), Serghides (1984) and El-Emam et al. (1997) friction factor correlations. Curve D shows the experimental data.

Figure 5.17 shows the corresponding variation of inventory with time at the rupture plane for the LPG 40 test. Curves A, B and C respectively show the results obtained

by applying the flow dependent correlations proposed by Chen (1979), Serghides (1984) and El-Emam et al. (1997) friction factor correlations. Curve D shows the experimental data. As it may observed, all of the correlations tested produce reasonably degree of accuracies when compared to the experimental data for both pressure at the rupture plane and inventory. Interestingly, the results produced based on Chen and Serighdes friction factor correlations are particularly close to one another.

Figure 5.18 shows the pressure variation with time at the intact end for the same test. Curve A shows the experimental data and curves B, C, D respectively show the results obtained by applying the flow dependent correlations proposed by Chen (1979), Serghides (1984) and El-Emam et al. (1997) friction factor correlations. It is evident that the results obtained by Chen and Serghides correlation show better agreement with experimental data than the one obtained by El-Emam et al.

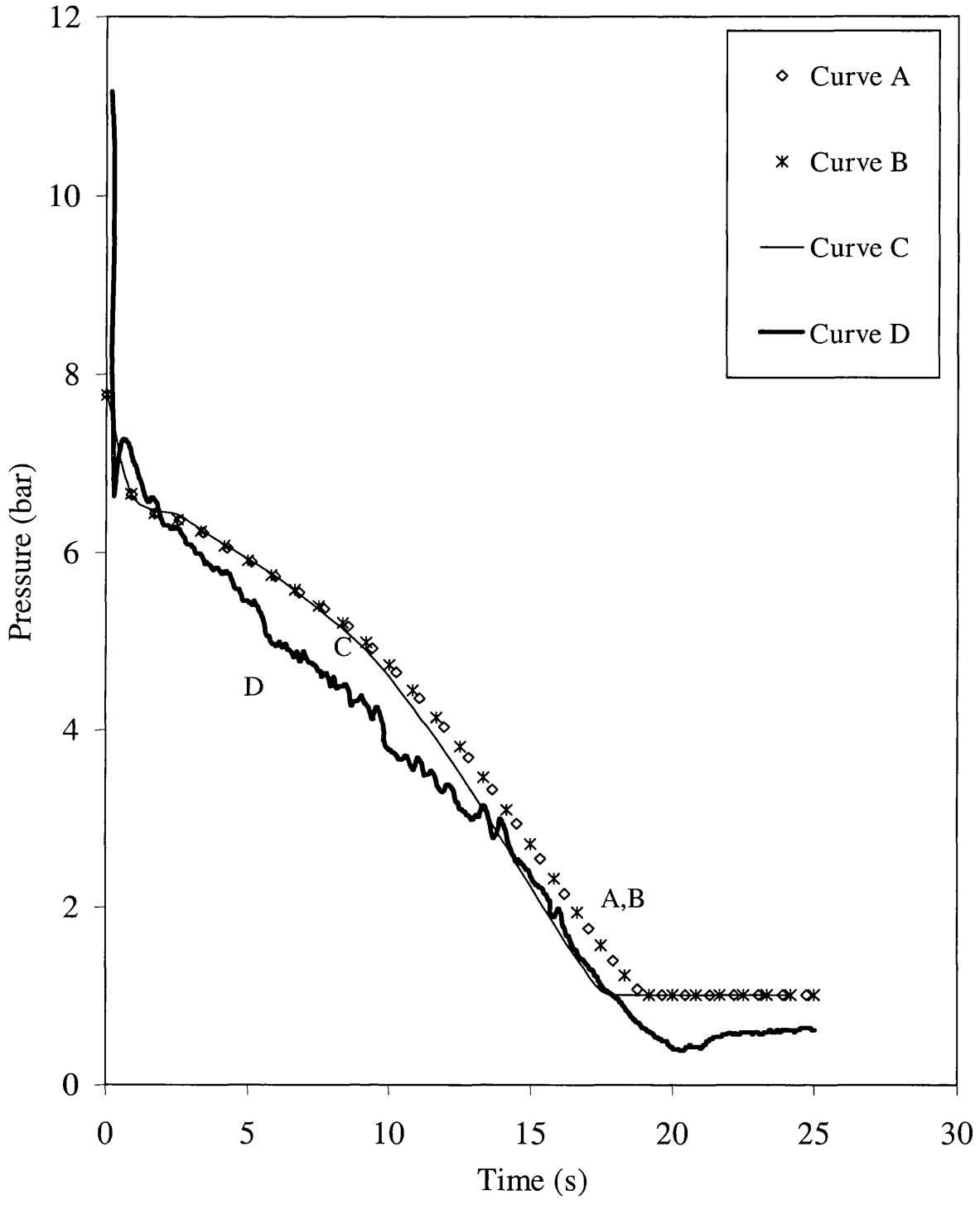

Figure 5.16 Rupture plane pressure variation with time for LPG40 following FBR based on different flow dependent friction factor correlations

Curve A: Chen (1979)

Curve B: Serghides (1984)

Curve C: El-Emam et al. (1997)

Curve D: Experimental data

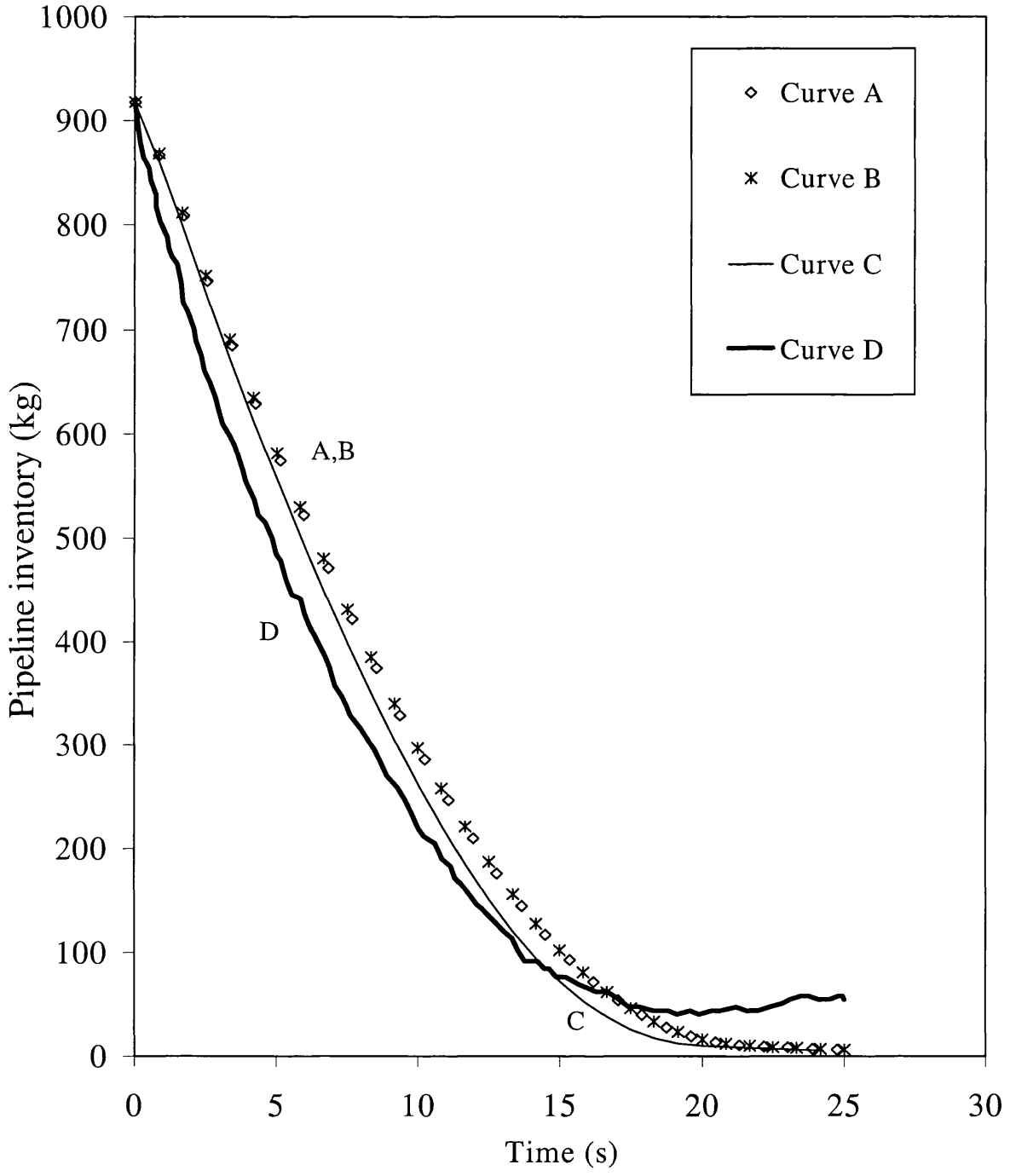

Figure 5.17 Pipeline inventory variation with time for LPG 40 following FBR based on different flow dependent friction factor correlations

Curve A: Chen (1979).

Curve B: Serghides (1984).

Curve C: El-Emam et al. (1997).

Curve D: Experimental data.

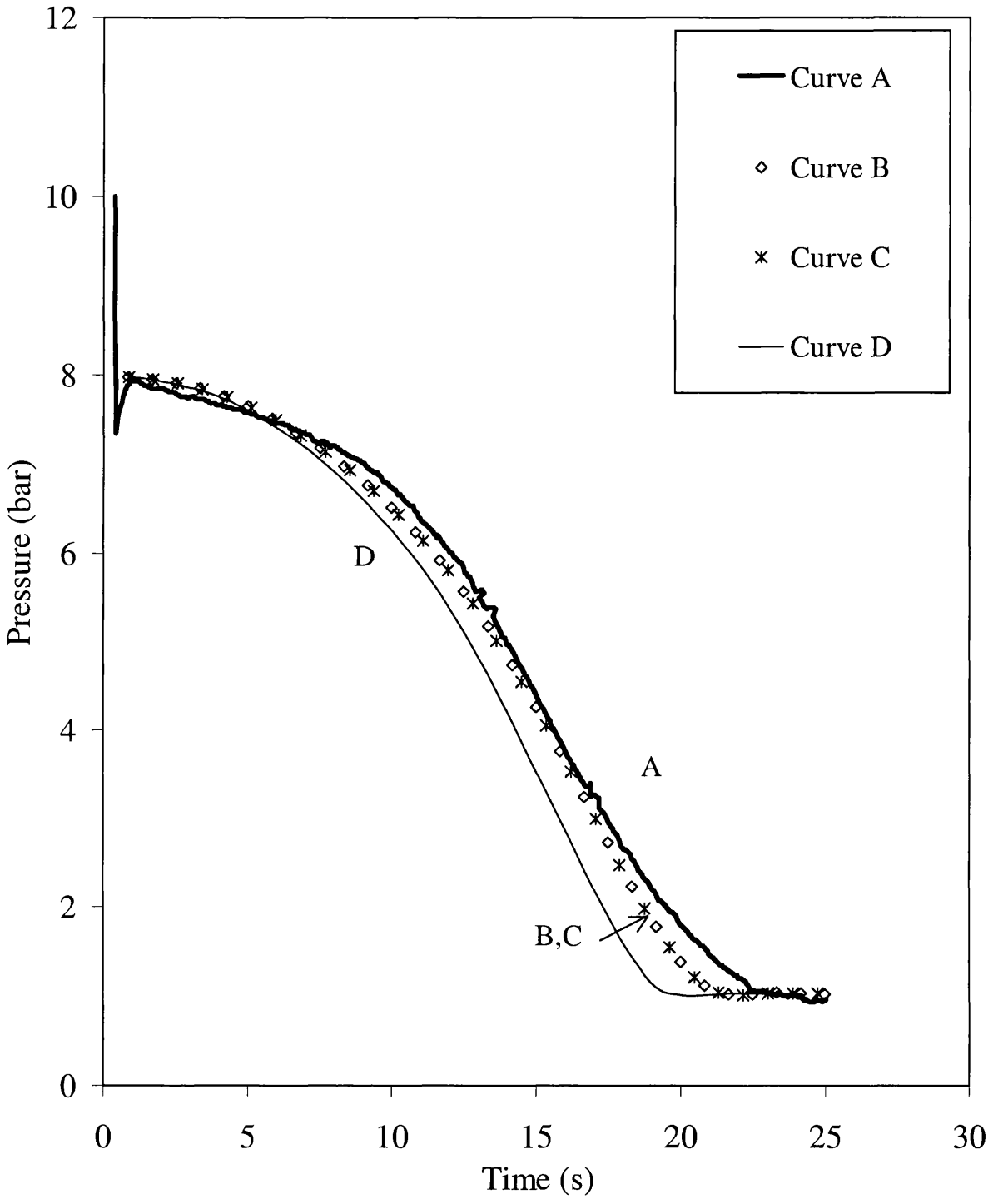

Figure 5.18 Intact end pressure variation with time for LPG40 following FBR based on different flow dependent friction factor correlations

Curve A: Experimental data

Curve B: Serghides (1984)

Curve C: Chen (1979)

Curve D: El-Emam et al. (1997)

In order to study the influence of the nature of fluid, the same tests were conducted using pure methane, which does not undergo phase transition during depressurisation.

Figure 5.19 shows the pressure variation with time at the rupture plane for pure methane (see table 5.2, however length of the pipeline is 10 km for this simulation and initial pressure is 40 bar, while the rest of the specifications remain the same.). Curves A, B, and C respectively show the results obtained by applying El-Emam et al., Serghides, and Chen friction factor correlations. Figures 5.20, 5.21 show the corresponding data for the intact end of the pipeline and variation of pipeline inventory.

Comparing the results of LPG 40 (two-phase) and pure methane (gas) simulations, it is clear that in both cases, the friction factor correlations proposed by Serghides and Chen produce almost identical predictions. Although El-Emam et al.'s correlation produces good agreement in the case of LPG. However in case of pure methane, it overestimates the pressure at the rupture plane and underestimates the pressure at the intact end when compared to the results based on Serghides and Chen correlations.

Since the pressure wave propagates from the rupture plane to the intact end, the rate of pressure drop at the rupture plane dictates the rate of pressure drop at the intact end. As such when comparing the two different case studies, if in one case the pressure variation with time at the rupture plane is faster than the others, it is expected that the pressure variation at the intact end must follow the same trend. As the perditions based on El-Emam et al.'s correlation are not consistent with the above argument, in the absence of experimental data this correlation is not employed in the present study.

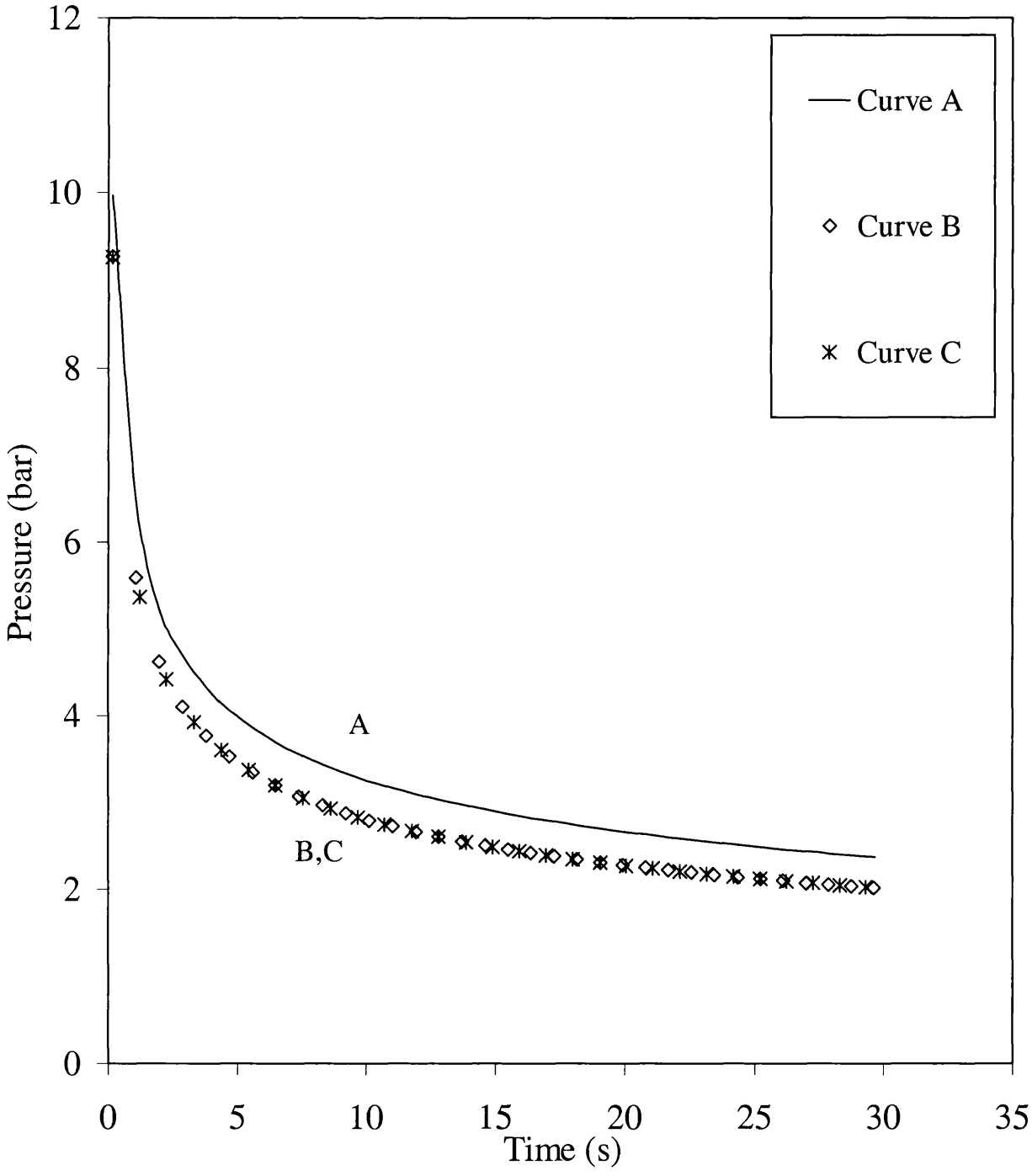

Figure 5.19 Rupture plane pressure variation with time for methane following FBR based on different flow dependent friction factor correlations

Curve A: El-Emam et al. (1997)

Curve B: Serghides (1984)

Curve C: Chen (1979)

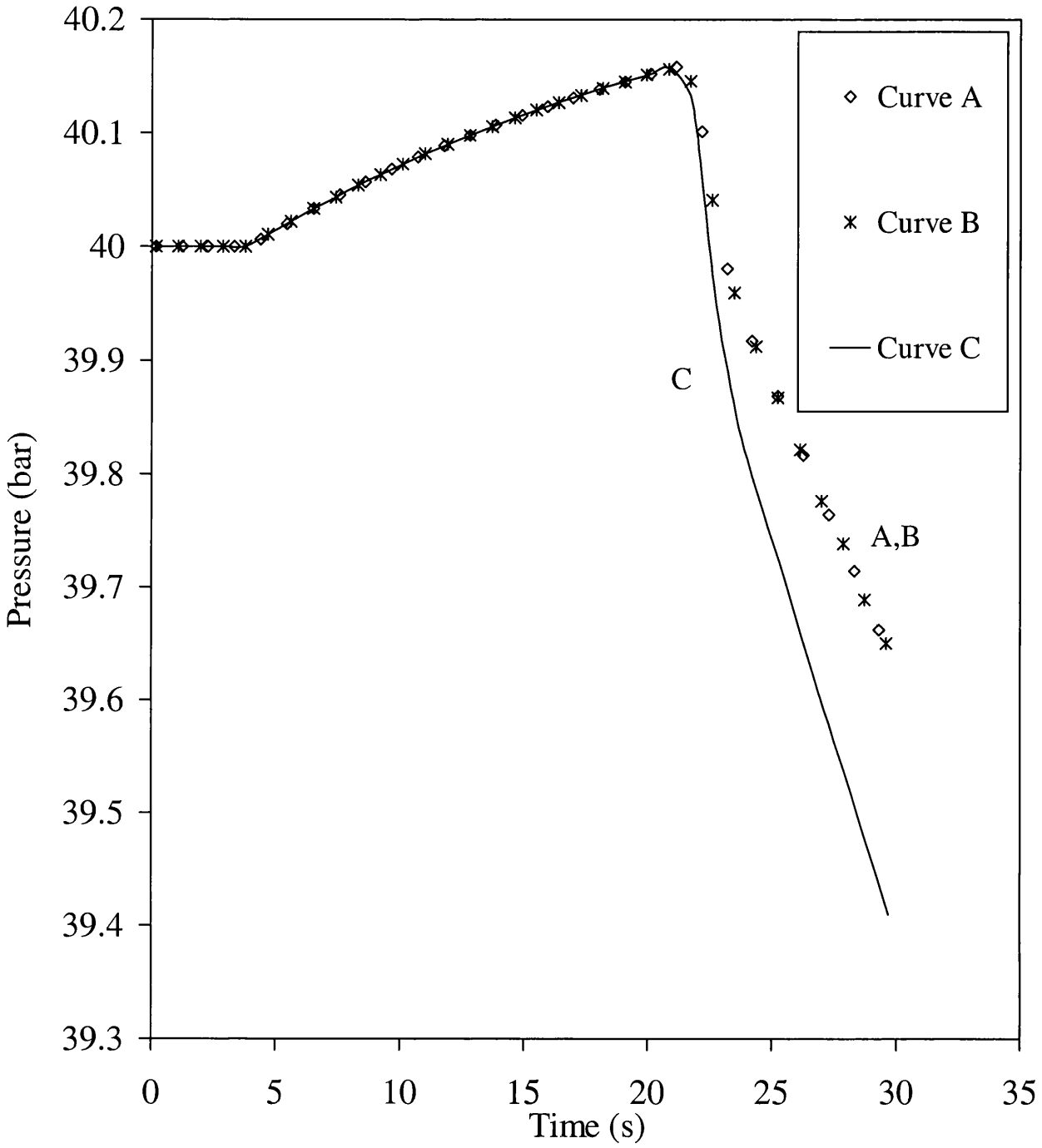

Figure 5.20 Intact end pressure variation with time at for methane following FBR based on different flow dependent friction factor correlations

Curve A: Chen (1979)

Curve B: Serghides (1984)

Curve C: El-Emam et al. (1997)

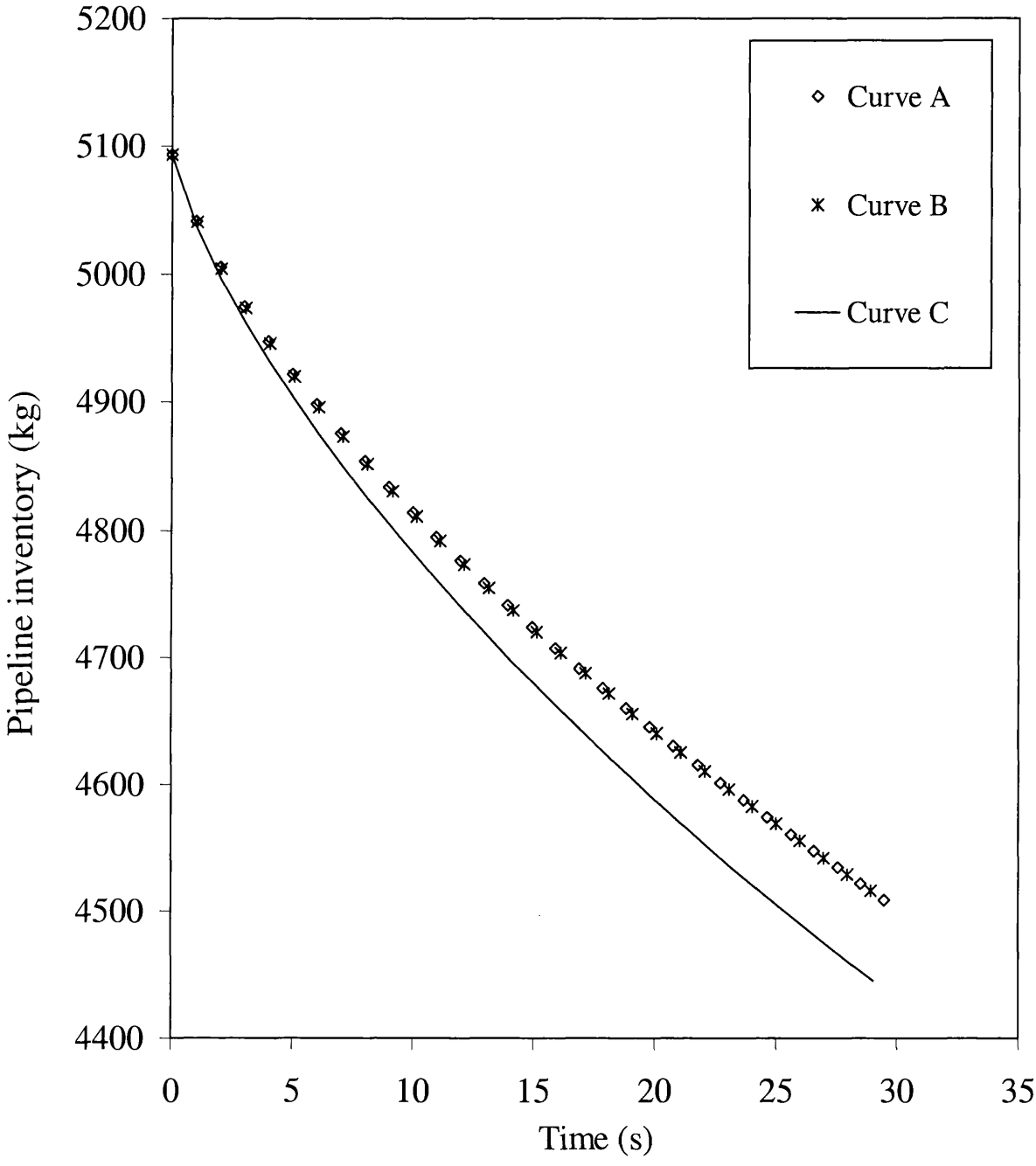

Figure 5.21 Pipeline inventory variation with time for methane following FBR based on different flow dependent friction factor correlations

Curve A: Chen (1979)

Curve B: Serghides (1984)

Curve C: El-Emam et al. (1997)

Figures 5.22, 5.23 respectively show the variation of open-end pressure, inventory with time following full bore rupture for the LPG 40 test. In both figures, curves A and B respectively show the results obtained by applying Nikuradse (flow independent) friction factor and Serghides friction factor (flow dependent) correlations. Curve C shows the experimental data. On the other hand figure 5.24 shows the intact end pressure variation with time for the same simulation. However in that figure curve A shows the experimental data and curves B and C respectively show the results obtained by applying Nikuradse (flow independent) friction factor and Serghides (flow dependent) friction factor correlations

Figure 5.25 shows the variation of open-end pressure with time based on Nikuradse (curve a) and Serghides (curve b) correlations in the case FBR of the methane pipeline. Figure 5.26 and 5.27 show the corresponding data for inventory and the intact end pressure variations with time.

Based on the data presented in figures 5.22 – 5.27, in the case of both condensable and non-condensable inventories, it is clear that Nikuradse's flow independent friction factor correlation produces very similar predictions to Serghides' flow dependent friction factor correlation.

In the case of highly transient flows such as FBR, the following conclusions may be made based on the above findings

- The friction factor is independent of Reynolds number.
- The Nikuradse's equation is recommended for calculating the flow independent (constant) friction factor.
- Chen, Serghides and Nikuradse friction factor correlations all perform identically. Also all three equations show very good agreement with experimental data.
- El-Emam et al.'s equation, which has been derived based on field data although applicable to two-phase mixtures, produces unrealistic results when simulating non-condensable gas flows.

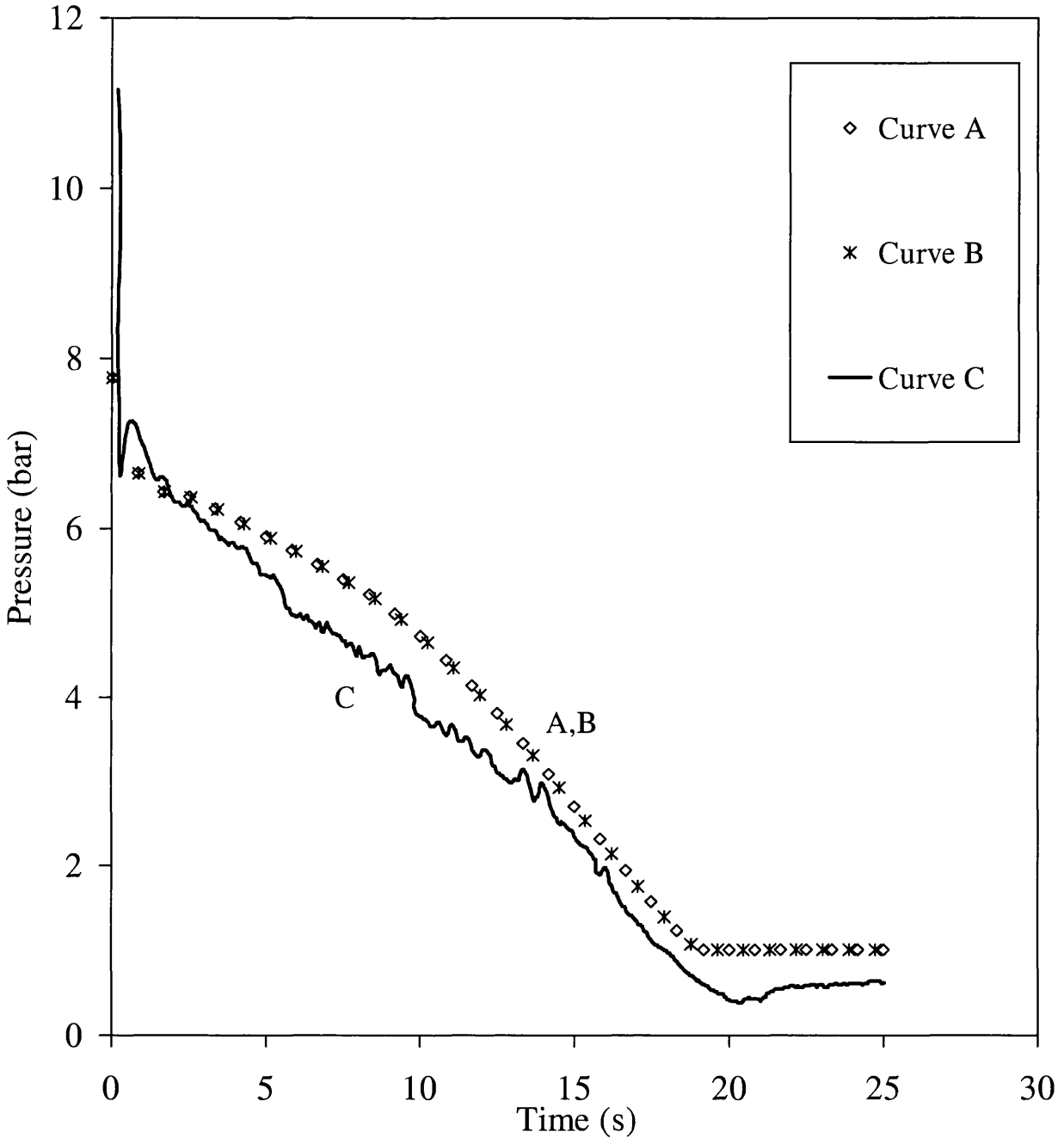

Figure 5.22 Rupture plane pressure variation with time for LPG40 following FBR based on flow dependent and flow independent friction factor correlations

Curve A: Nikuradse (1933)

Curve B: Serghides (1984)

Curve C: Experimental data

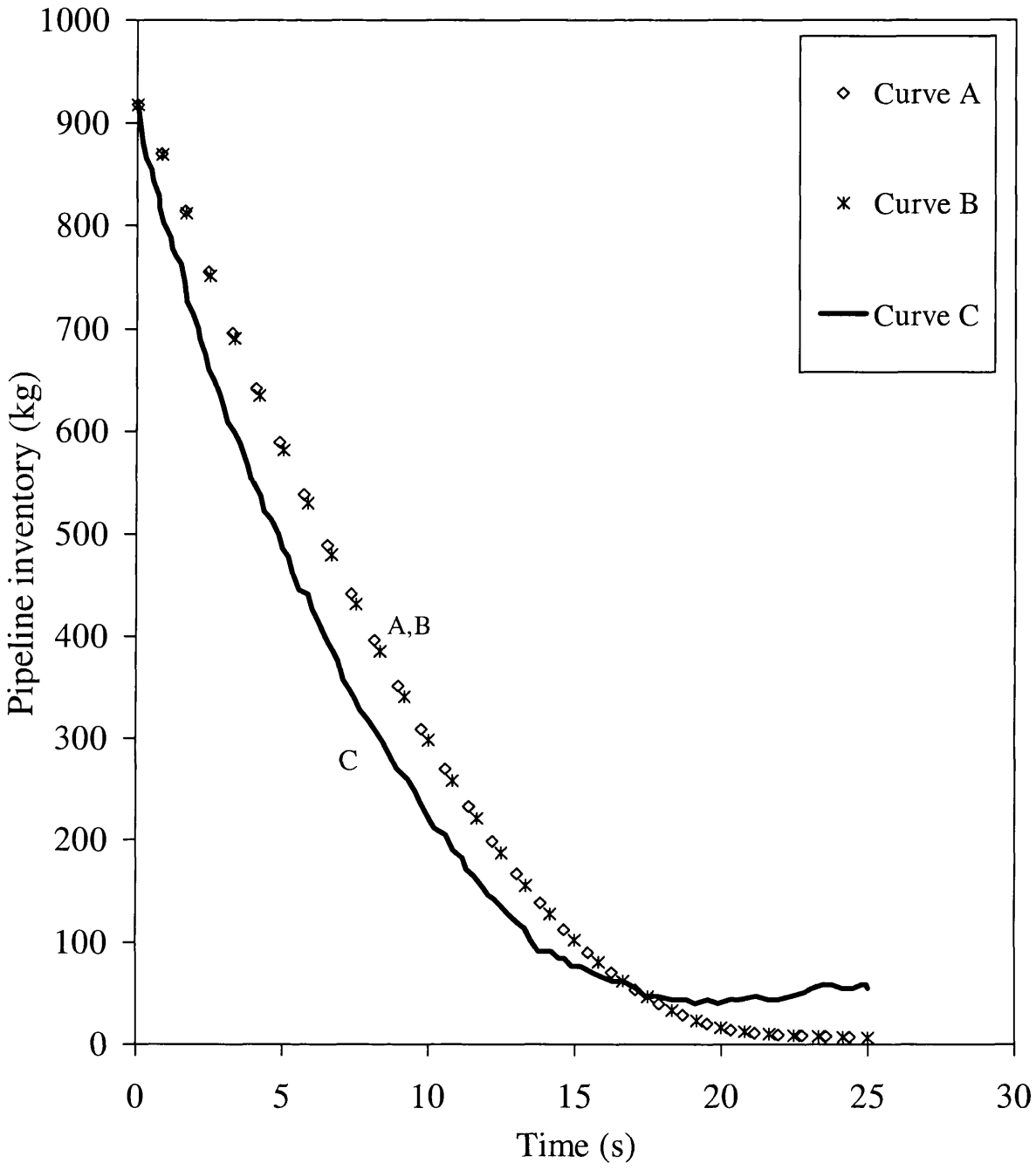

Figure 5.23 Pipeline inventory variation with time for LPG40 following FBR based on flow dependent and flow independent friction factor correlations

Curve A: Nikuradse (1933)

Curve B: Serighdes (1984)

Curve C: Experimental data

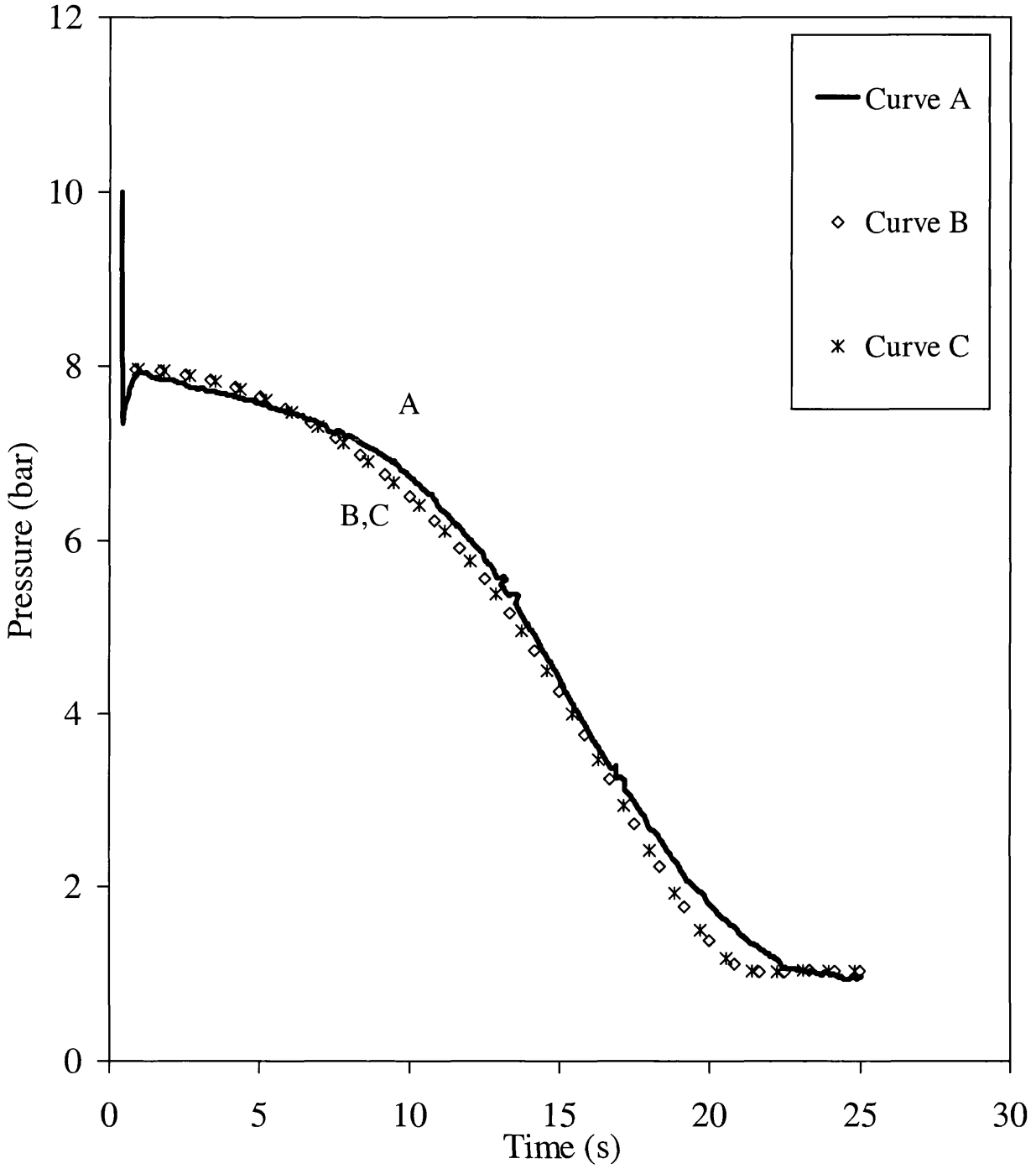

Figure 5.24 Intact end pressure variation with time for LPG40 following FBR based on flow dependent and flow independent friction factor correlations

Curve A: Experimental data

Curve B: Nikuradse (1933)

Curve C: Serghides (1984)

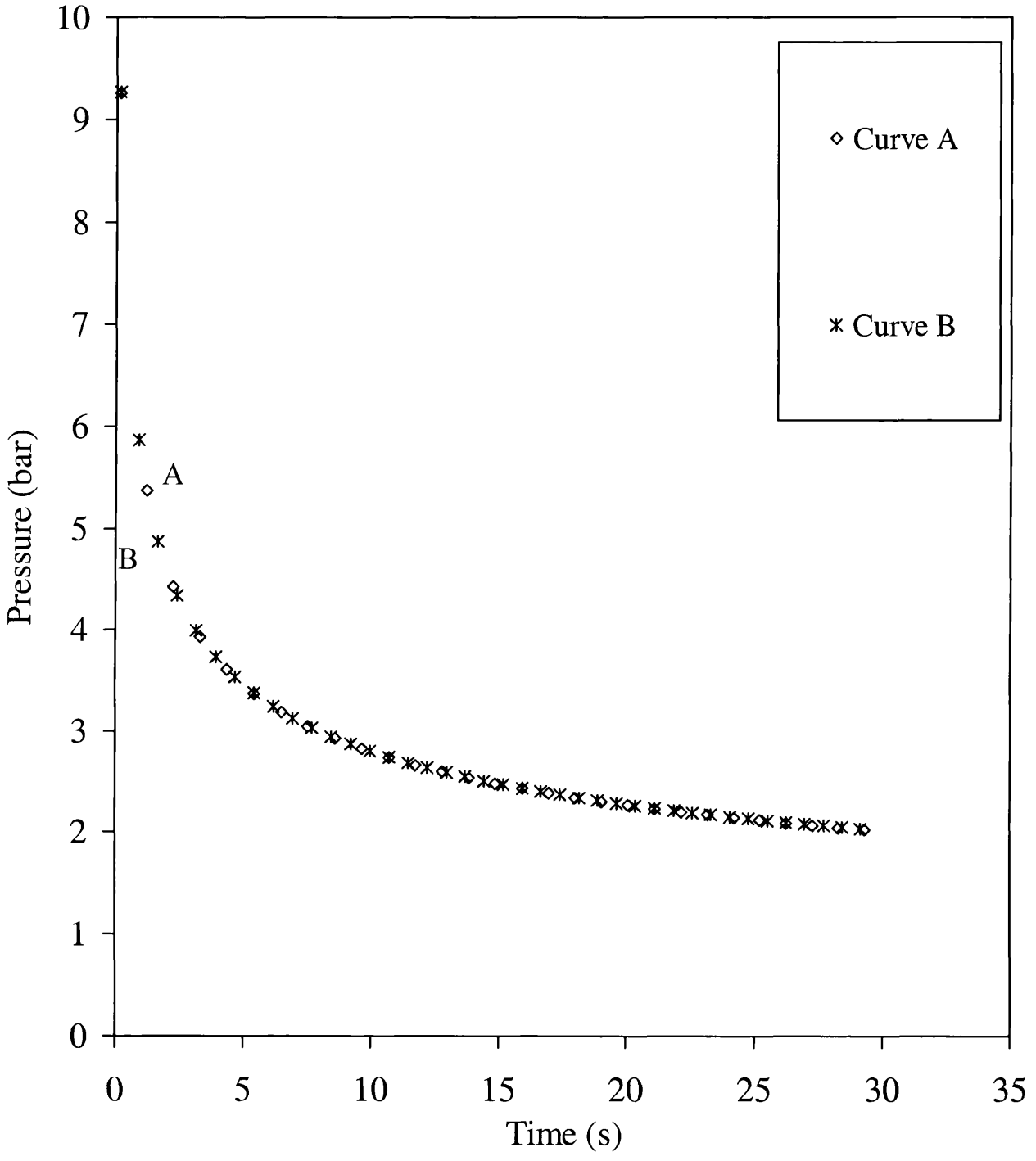

Figure 5.25 Rupture plane Pressure variation with time for methane following FBR based on different flow dependent friction factor correlations

Curve A: Nikuradse (1933).

Curve B: Serghides (1984).

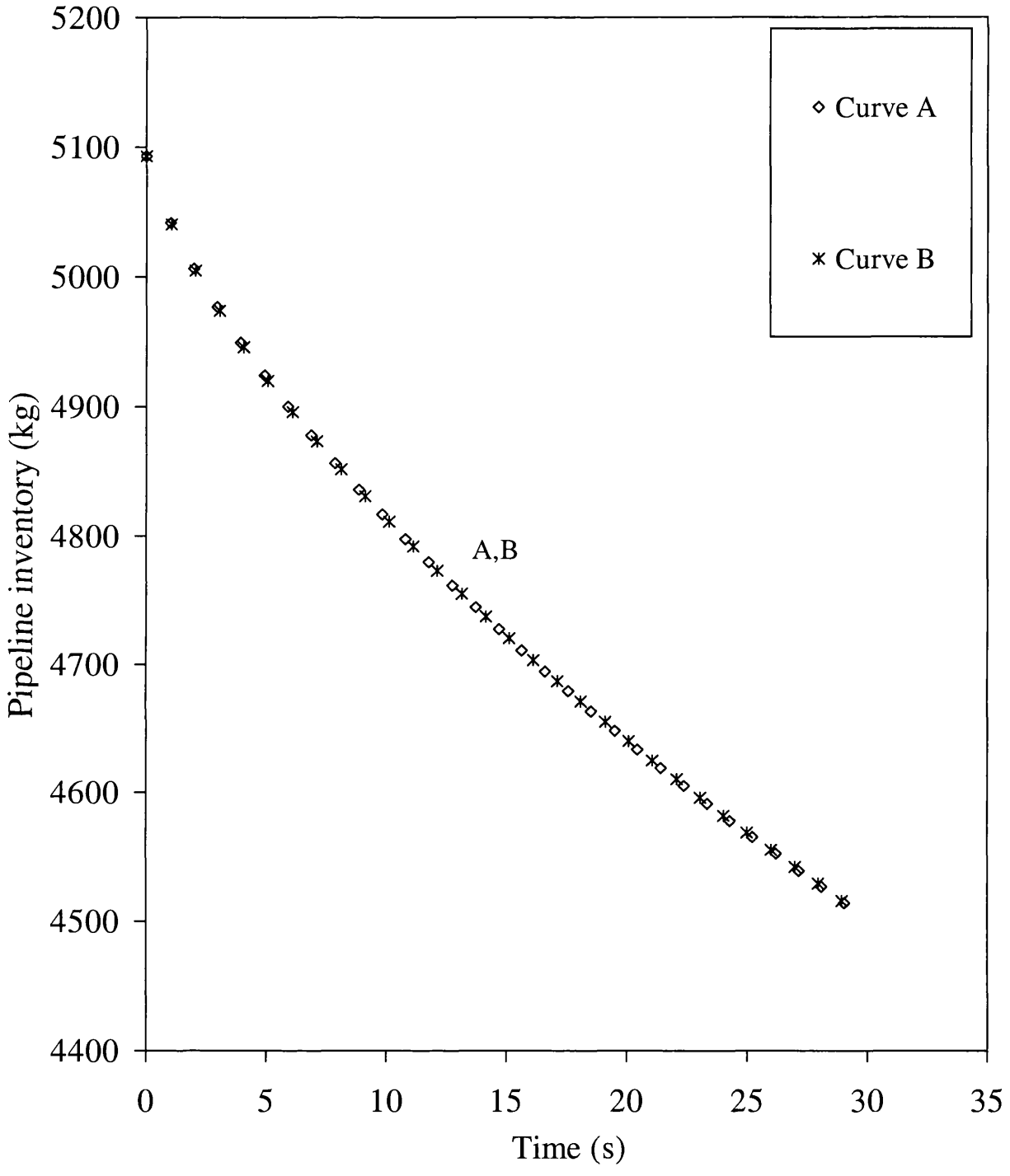

Figure 5.26 Pipeline inventory variation with time for methane following FBR based on flow dependent and flow independent friction factor correlations

Curve A: Nikuradse (1933).

Curve B: Serghides (1984)

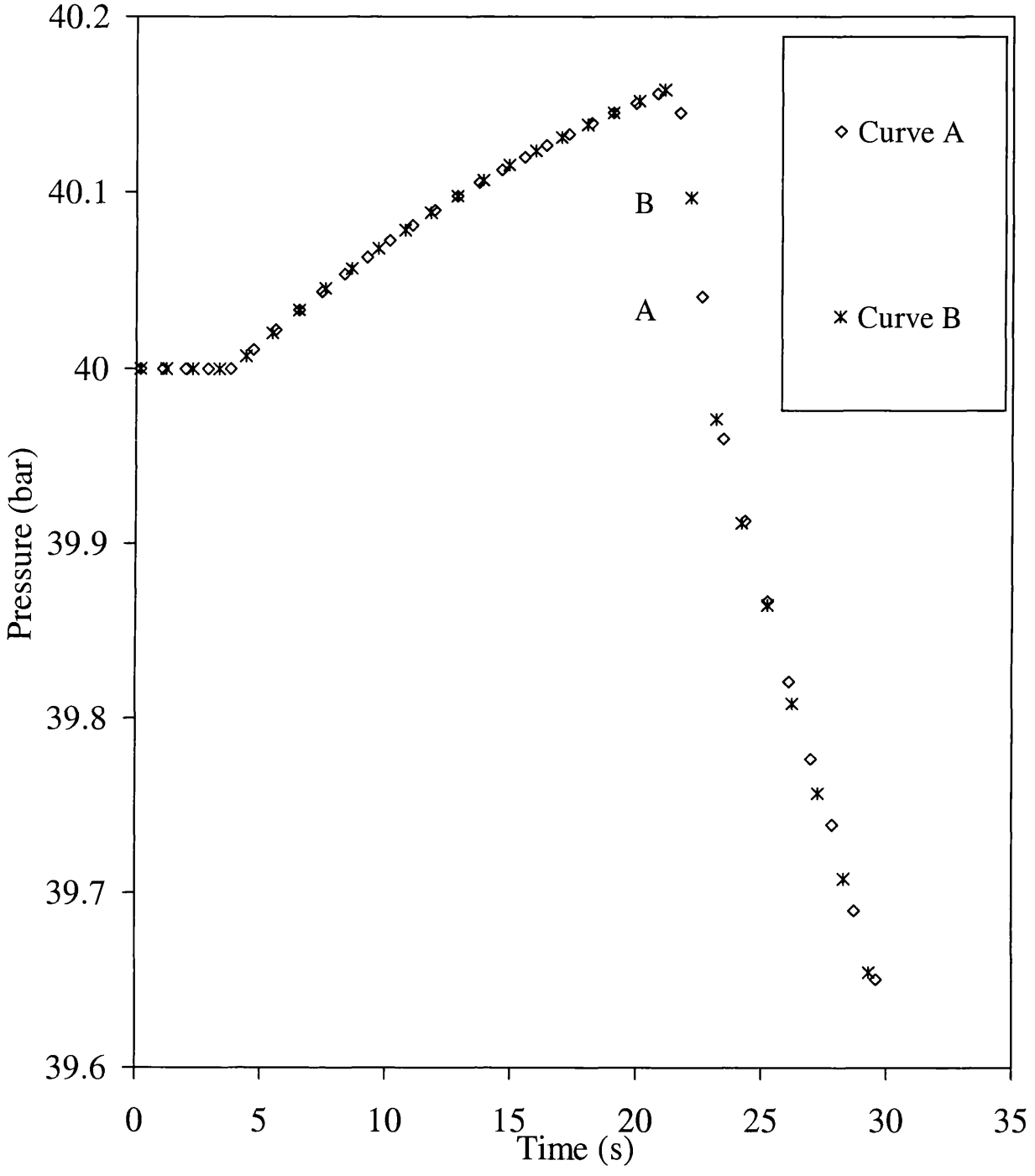

Figure 5.27 Intact end pressure variation with time for methane following FBR based on flow dependent and flow independent friction factor correlations

Curve A: Nikuradse (1933)

Curve B: Serghides (1984)

5.3 INCLINED PIPELINES

Inclined pipelines are generally used as links between different parts of transportation or exploration lines in the oil and gas industries. Therefore from the safety point of view, modelling fluid flow in an inclined pipeline following FBR is important. During the Piper Alpha tragedy for example (Cullen, 1990), the rupture of the main riser (the vertical section of the gas export line rising from the sea bed onto the platform) resulted in the collapse of the platform into the seabed.

Numerous experimental studies for fluid flow in inclined pipelines have been reported. However, the majority have been confined to steady state flow dealing with pipelines containing oil/water mixtures. Stanislav et al. (1986) for example performed a series of oil-water -gas flows in an inclined pipe, in order to determine the flow patterns, liquid hold up and pressure drop. The authors analysed the data obtained to test existing semi-theoretical models, and proposed a new and improved model. Oliemans (1987) investigated the accuracy of two-phase flow trunk line predictions by a one-dimensional steady model for stratified wavy flow in horizontal and inclined pipes. Lum et al. (2002) experimentally studied flow patterns of oil-water mixtures in a 5 ^{o} upwardly inclined pipeline and compared the results with similar studies in horizontal flow.

Outflow following FBR in an inclined pipeline was modelled in chapters 2 and 3. The following discusses the results based on the application of the model to various pipeline configurations. It is recalled that the model is based on the homogeneous equilibrium assumption where the constituent phases are at thermal and mechanical equilibrium with one another. Thus the model can only be applied to cases in which only single-phase flow exists, or in the case of two-phase flow, the pipeline length is sufficiently short so that phase slip may be ignored.

Outflow following FBR at both the high-pressure end (top end) and the low-pressure end (bottom end) of the inclined pipeline are simulated.

Figure 5.28 shows the variation of rupture plane pressure with time following top end FBR of the LPG40 pipeline (see table 5.1). Curves A and B respectively represent data for the 45° and 22° inclined pipeline. Curve C on the other hand represents the data for the horizontal pipeline. Based on the data, it is clear that at any given time following rupture, the open-end pressure decreases with the angle of elevation. Remarkably, the data for the 45 ° pipeline (curve A) exhibit a pressure recovery during the first 6 s following rupture. It is postulated that the above is a consequence of the flashing of LPG as a result of the significant reduction in the rate of its loss from the pipeline.

Figure 5.29 shows the corresponding data for the pipeline inventory variation with time. As it may be observed, the increase in the angle of elevation (increase in the gravitational field) results in a delay in the amount of inventory lost with time. However, this delay is a non-linear function of the angle of elevation, dramatically increasing at 45°.

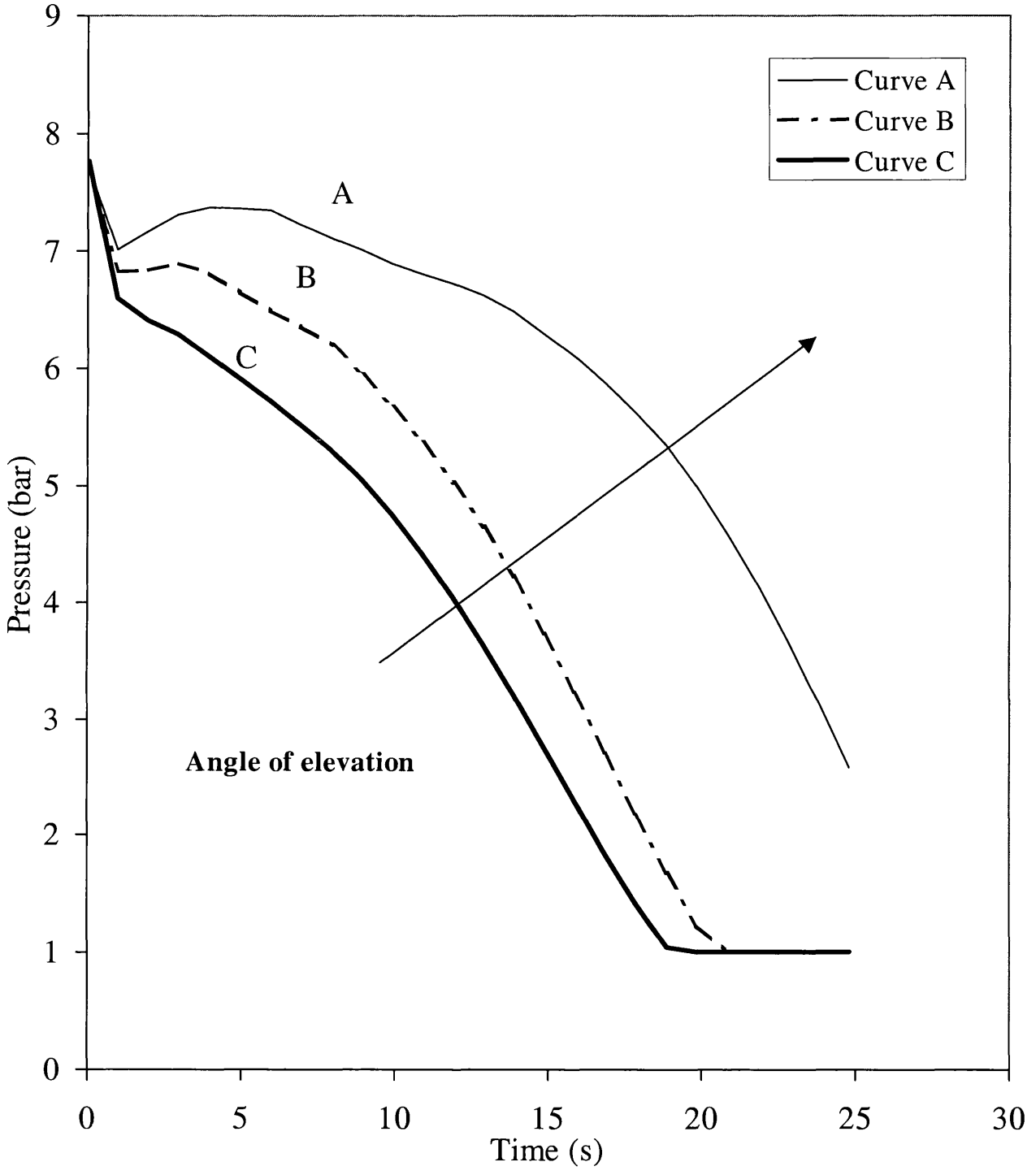

Figure 5.28 Rupture plane pressure variation with time for LPG40 at various angles of elevation following top end FBR

Curve A: 45° inclined pipeline

Curve B: 22° inclined pipeline

Curve C: Horizontal pipeline

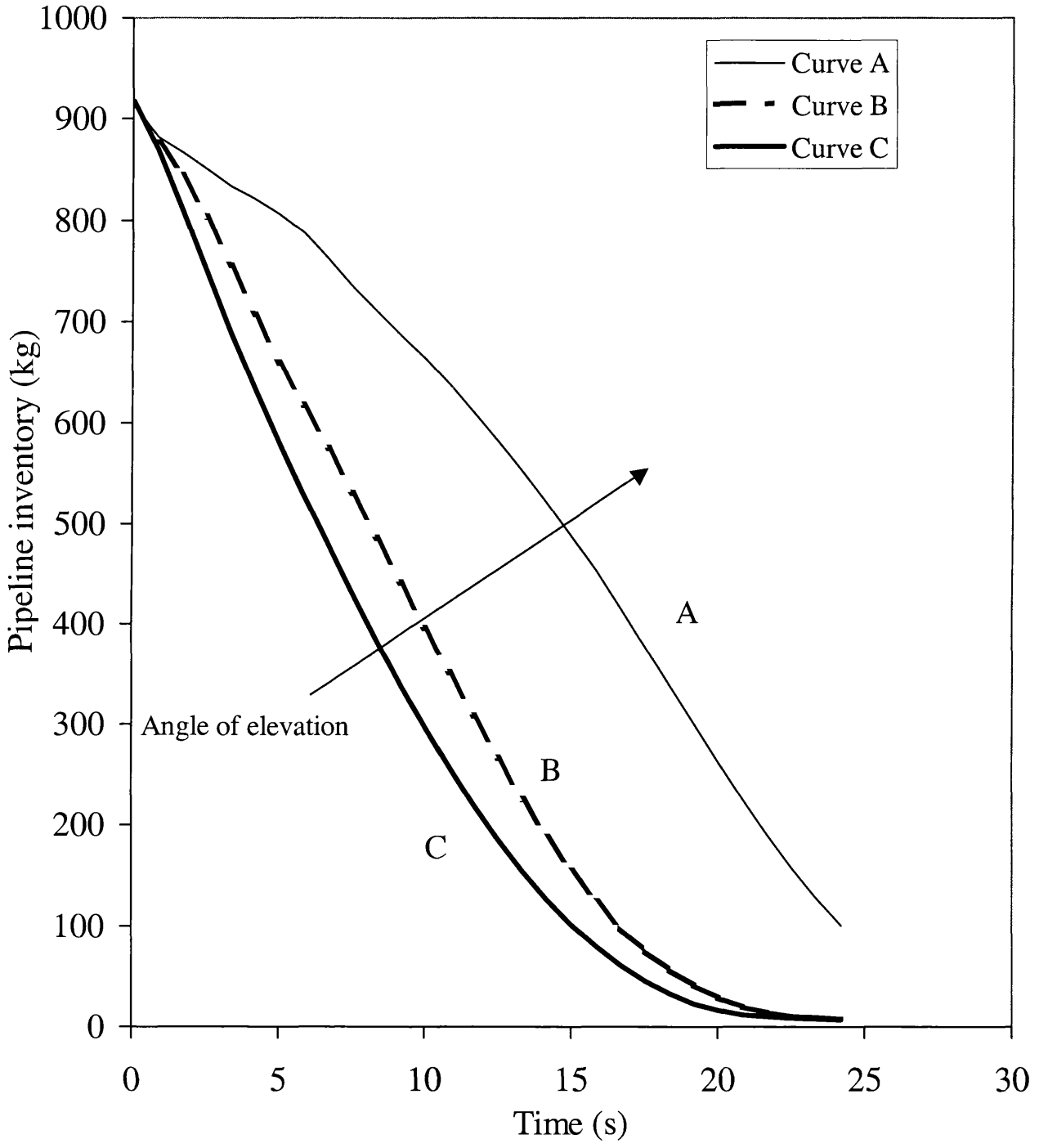

Figure 5.29 Pipeline inventory variation with time for LPG40 at various angles of elevation following top end FBR

Curve A: 45° inclined pipeline

Curve B: 22° inclined pipeline

Curve C: Horizontal pipeline

Figures 5.30 and 5.31 respectively represent the analogous data as in figures 5.28 and 5.29 but for the case of bottom end (high pressure end) FBR. The results follow an opposite trend as compared to those for top end rupture. Here, an increase in the angle of elevation results in a more rapid discharge of the inventory. Also, at any given time following FBR, the pressure at the rupture plane decreases with the increase in the angle of elevation. Interestingly, in contrast to top end rupture, the rates of variations of inventory and pressure with time are more linear functions of the angle of elevation.

The observed trends in the variations of inventory and rupture pressure with time are simply manifestations of the change in the expansion wave velocity. In the case of top end rupture, an increase in the angle of elevation slows down the propagation wave velocity. The opposite applies in the case of bottom end rupture.

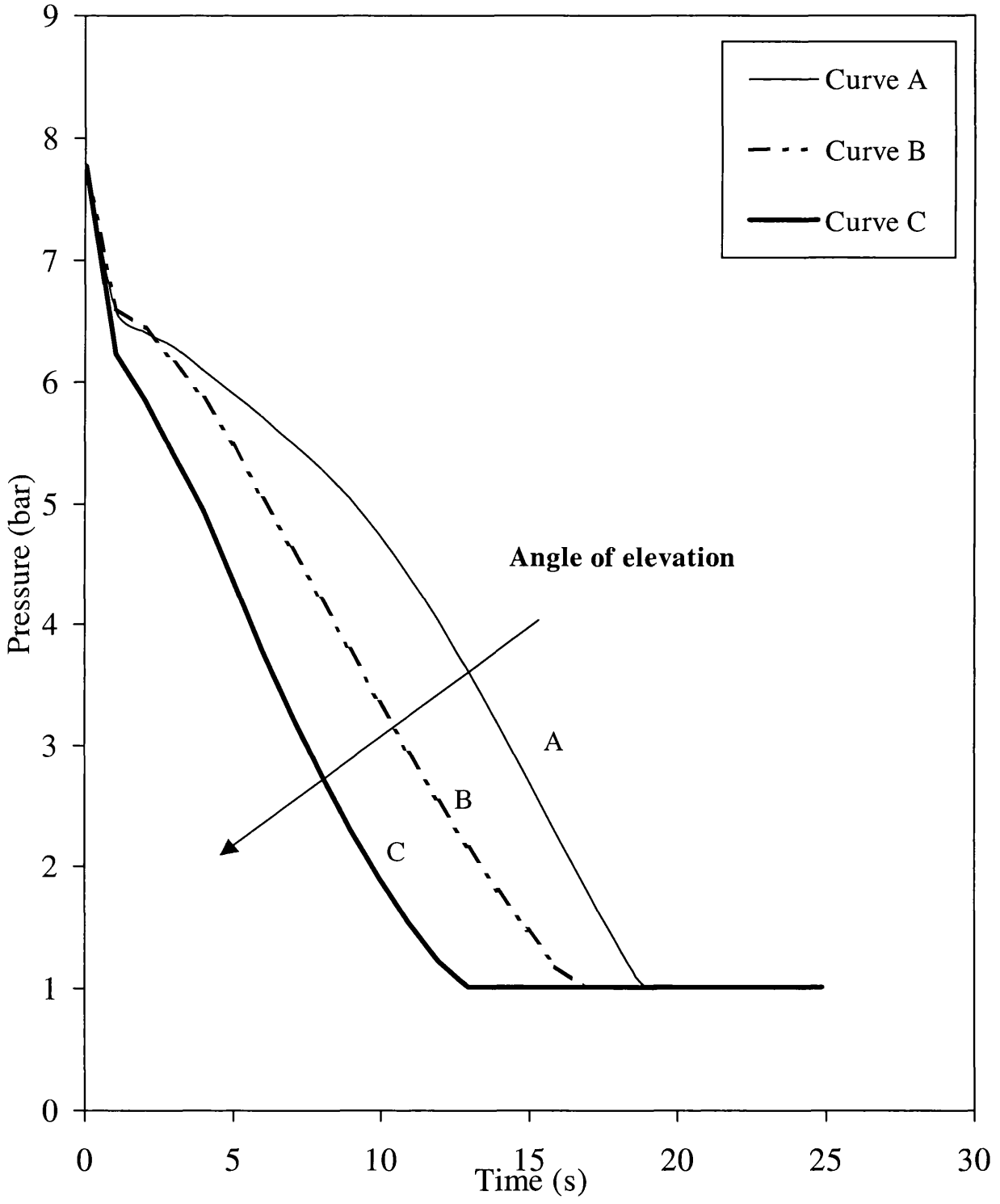

Figure 5. 30 Rupture plane pressure variation with time following bottom end FBR of LPG 40 pipeline at various angles of elevation

Curve A: Horizontal pipeline.

Curve B: 22° inclination angle.

Curve C: 45° inclination angle.

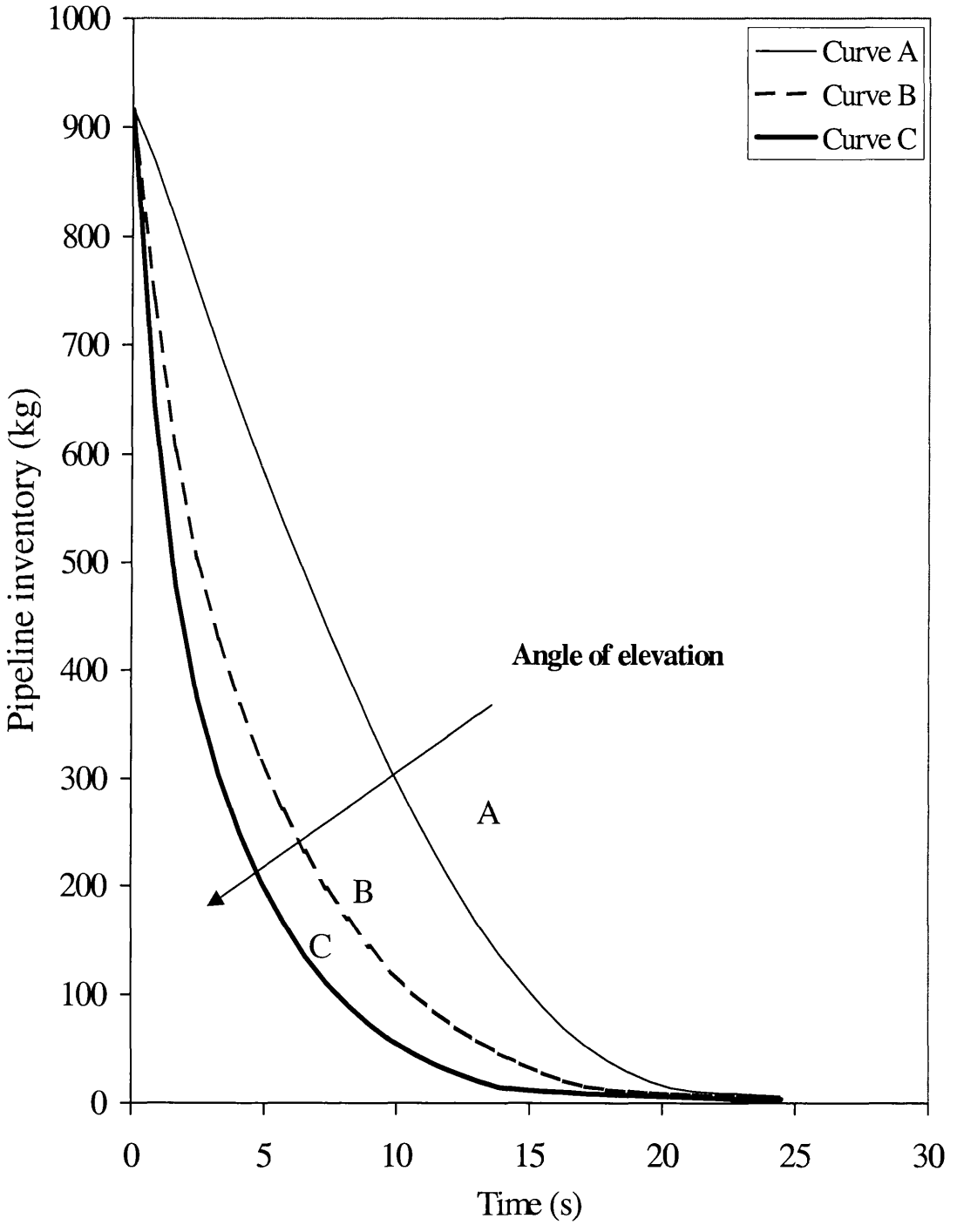

Figure 5.31 Pipeline inventory variation with time following bottom end FBR of LPG 40 pipeline at various angles of elevation

Curve A: Horizontal pipeline

Curve B: 22° inclined pipeline

Curve C: 45° inclined pipeline

The effects of the state of the inventory on the discharge process for inclined pipelines are discussed next. Figure 5.32 shows the pressure variation with time at the rupture plane following the top end rupture of the methane pipeline. Curve A represents data for the horizontal pipeline. Curves B and C on the other hand represent the inclined pipeline with 22^{o} and 45^{o} angle of inclination respectively. The pertaining conditions prior to the discharge process are given in table 5.2. However the length of the pipeline is 100m, since it is not realistic to consider 1km inclined pipeline. Exactly the same data were obtained in the case of bottom end rupture. Hence the results are not shown here.

For the conditions tested, in contrast LPG, the data in figure 5.33 indicate that the increase in the gravitational field as a result of the increase in the pipeline angle of elevation has negligible effect on the discharge process. This is purely a consequence of the much smaller density of methane as opposed to LPG. No discontinuities in the variation of open-end pressure with time are observed since methane, in contrast to the LPG mixture, remains in the gaseous state throughout the discharge process.

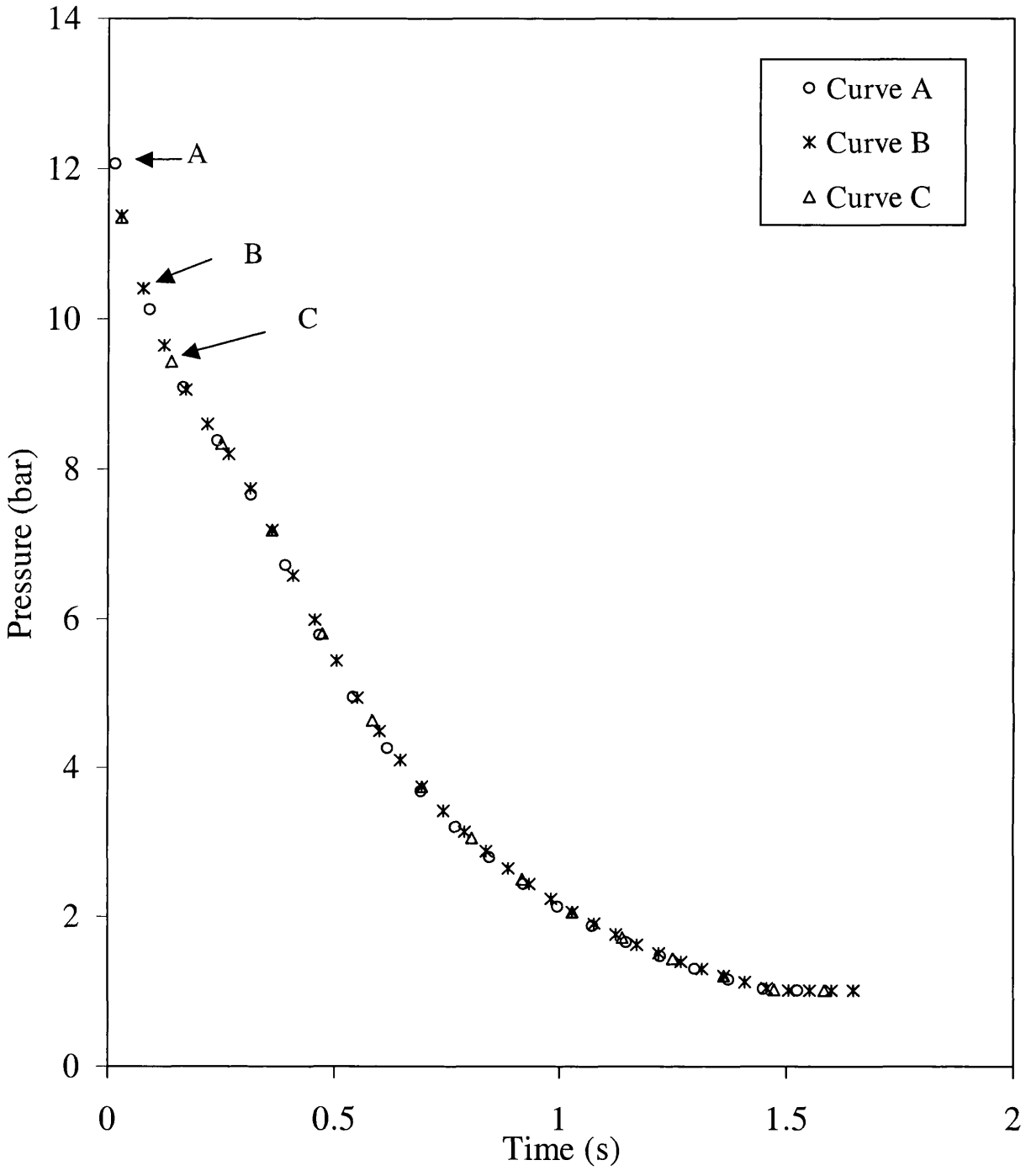

Figure 5.32 Rupture plane pressure variation with time following top end FBR of methane pipeline at various angles of elevation

Curve A: Horizontal pipeline

Curve B: 22° inclined pipeline

Curve C: 45° inclined pipeline

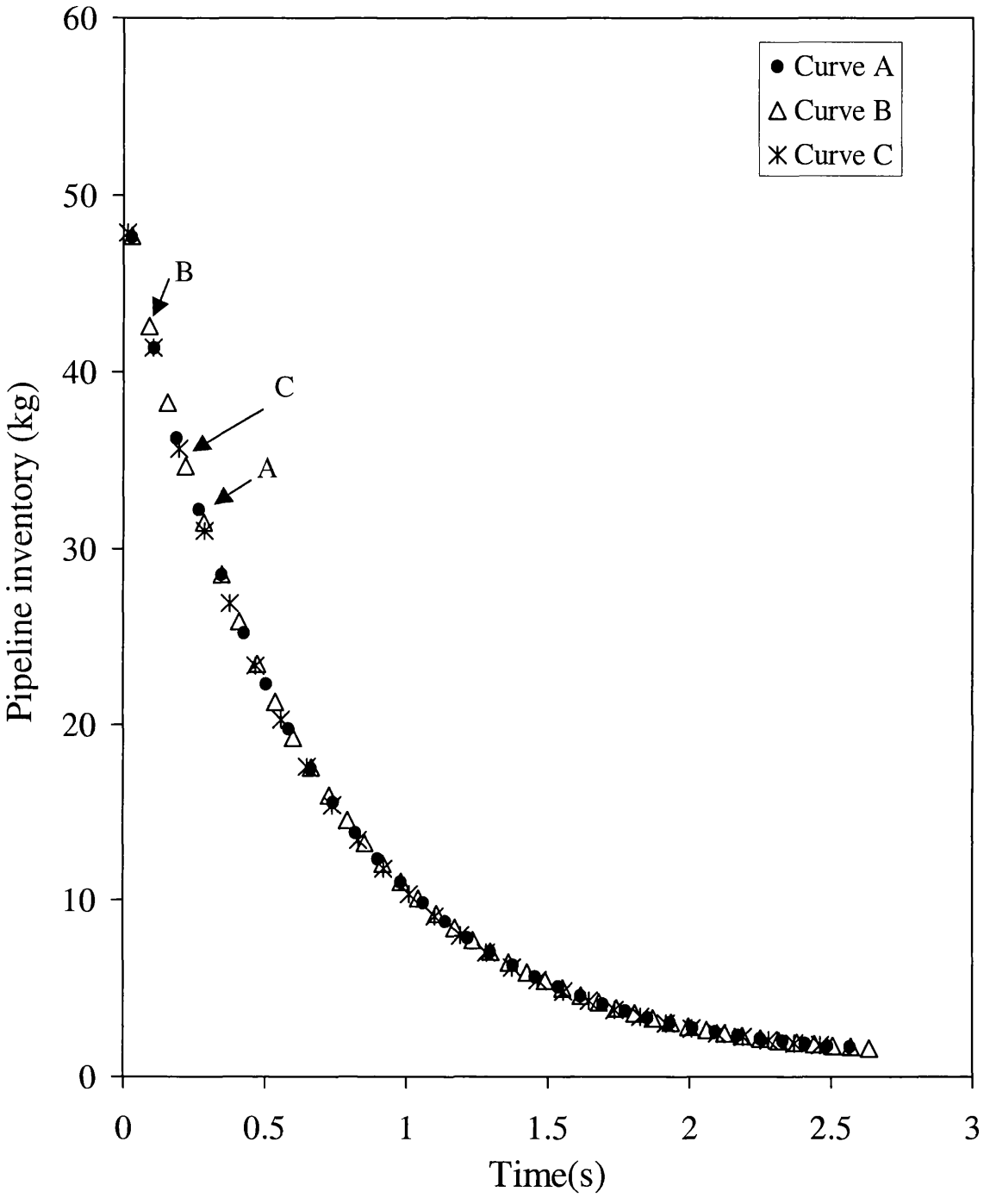

Figure 5.33 Pipeline inventory variation with time following top end FBR of pure methane at various angles of elevation

Curve A: Horizontal pipeline

Curve B: 22° inclined pipeline

Curve C: 45° inclined pipeline

5.4 ENLARGED PIPELINE

Generally long pipelines used in transporting systems are not of uniform cross section over their entire length. Moreover pipelines might be enlarged or reduced in size at some point along their entire length particularly at junctions where two lines of different diameter meet. Consequently, it is important to study the effect of pipeline enlargement on the discharge process following pipeline failure.

The results of the application of the model developed for rupture of an enlarged pipeline presented in chapter 4, are discussed in the following. In the absence of real data, the hypothetical scenario simulated relates to the rupture of a 1 km long pipeline containing Liquefied Natural Gas (LNG) at an inlet pressure of 50 bar. The initial flow rate is assumed to be 5 m/s with the pump ceasing to operate upon FBR. LNG is chosen as a case example as significant amounts are transported in long pipelines. Figure 5.34 shows a dimensioned schematic representation of the assumed pipeline configuration. The enlargement is assumed to start midway along the pipeline at an angle of 40° relative to the horizontal and extend over a distance of 0.412 m. The pipeline diameters at either end of the expansion zone are 0.15 m and 0.45 m. The pipe roughness is assumed to be 1 x 10^{-6} m. The respective ambient at fluid temperatures are 22°C and –162°C. The pump is assumed to be located at the inlet of the smaller diameter pipeline. Table 5.4 shows a summary of the pertinent data.

Fluid composition (% mol)	**Ambient temperature (°C)**	**Initial pressure (bar)**	**Pipe total length (m)**	**Pipe roughness (m)**	**Pipe diameter (m)**		**Initial temperature (°C)**
					D_1	**D_2**	
CH4: 90% C_2H6: 10%	22	50	1000	1 x 10^{-6}	0.15	0.45	-162

Table 5.4 LNG case study specification for pipeline enlargement simulation

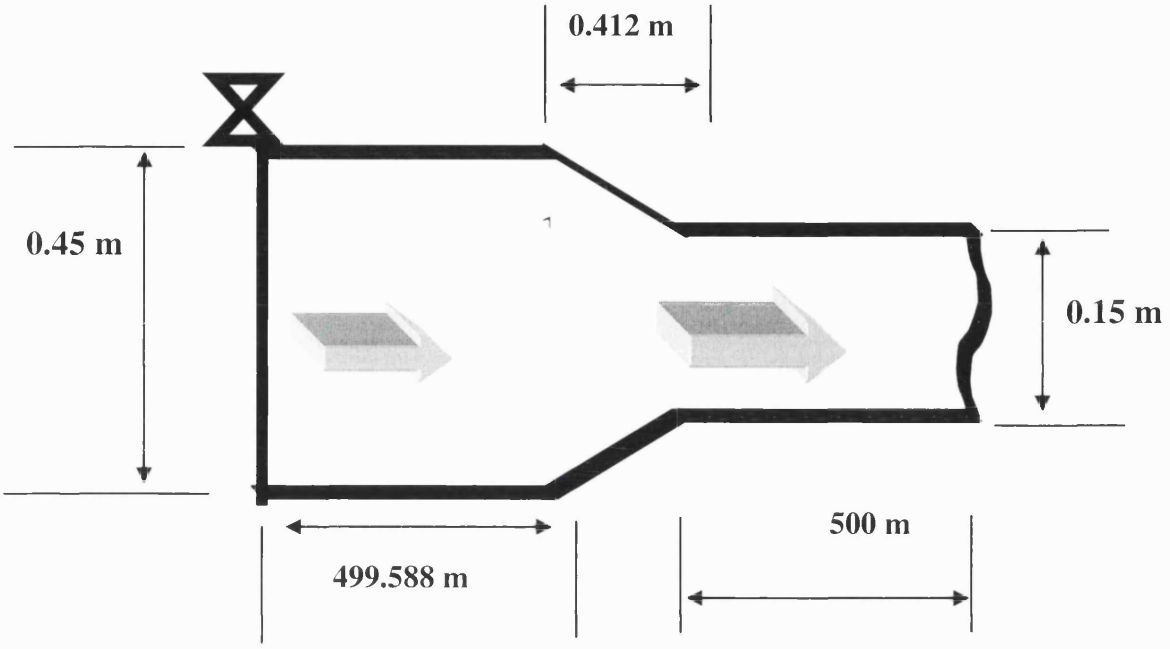

Figure 5.34 Schematic representation of enlarged pipeline simulation

Figure 5.35 curve A shows pressure variation with time at the intact end (low pressure end) following FBR of the LNG pipeline at its high pressure end (narrow end). In order to demonstrate the effect of enlargement, the analogous data for a 0.304 m diameter pipeline with the same length and containing the same amount of initial inventory (≈36900 kg) as the enlarged pipeline are also presented; curve B. It should be noted that FBR results in flow reversal involving fluid flow from the large diameter pipeline into the smaller diameter pipeline through a constriction.

The data for the uniform diameter pipeline show the expected trend indicating an almost instantaneous drop to atmospheric pressure following FBR. This is in contrast to the data for the enlarged pipeline where remarkably, a relatively slow drop in pressure is observed. This is expected to be a consequence of the drop in the pressure of the fast flowing fluid during its passage through the constriction.

The above observation may have important implications as according to the above finding pipeline enlargement or 'bottlenecking' may be used as an extremely effective

way of reducing the hazard following FBR by reducing the depressurisation and hence the discharge rate.

Figure 5.36, shows the corresponding variations of inventory within the pipeline versus time for the enlarged and the uniform pipelines. The inventory variation for the uniform pipeline (curve B) follows a very similar trend as the pressure data; a rapid drop in inventory to a constant value is observed during the first few seconds. The relatively slow drop in the intact end pressure with time for the enlarged pipeline (figure 5.35, curve A) on the other hand is manifested in significantly slower discharge behaviour as compared to the uniform pipeline (figure 5.36 curve B).

Both pipelines discharge relatively little amount of inventory following complete depressurisation as LNG stays in the liquid phase throughout.

Figures 5.37 and 5.38 show the analogous pressure and inventory versus time profiles for the enlarged and uniform pipelines containing pure methane chosen as a non-condensable gas example. The pertaining conditions are given in table 5.2. Both figures confirm the earlier observation that pipeline enlargement decelerates the pressure wave propagation and consequently delays the discharge process following FBR. However significantly larger proportions of inventory are lost as compared to the LNG since the inventory remains in the gaseous phase throughout the discharge process. This is of importance to the design engineer when making decisions or evaluating the implications of different inventories within a pipeline on the overall risk posed following its FBR.

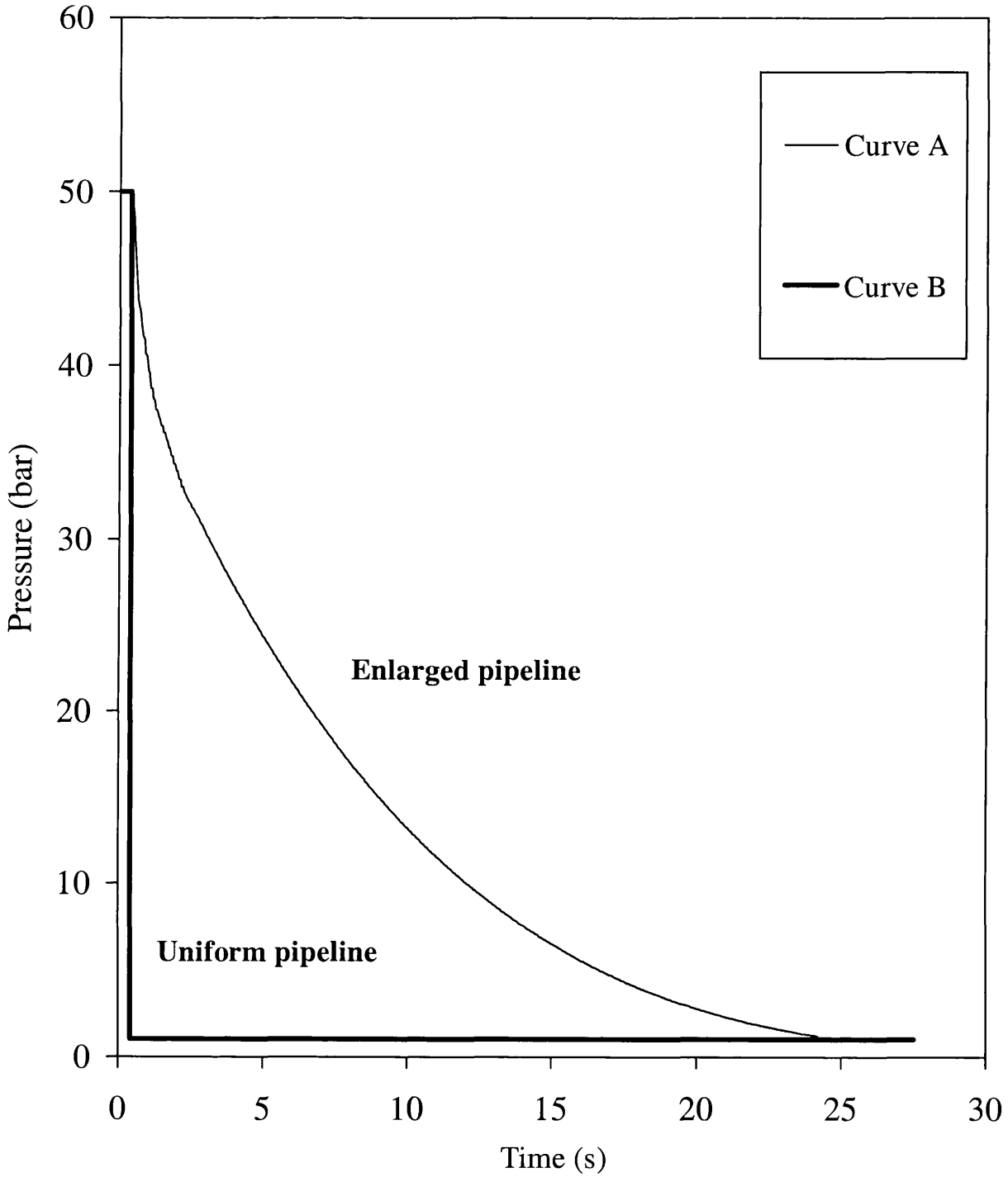

Figure 5.35 Intact end pressure variation with time for LNG following FBR

Curve A: Enlarged pipeline.

Curve B: Uniform pipeline.

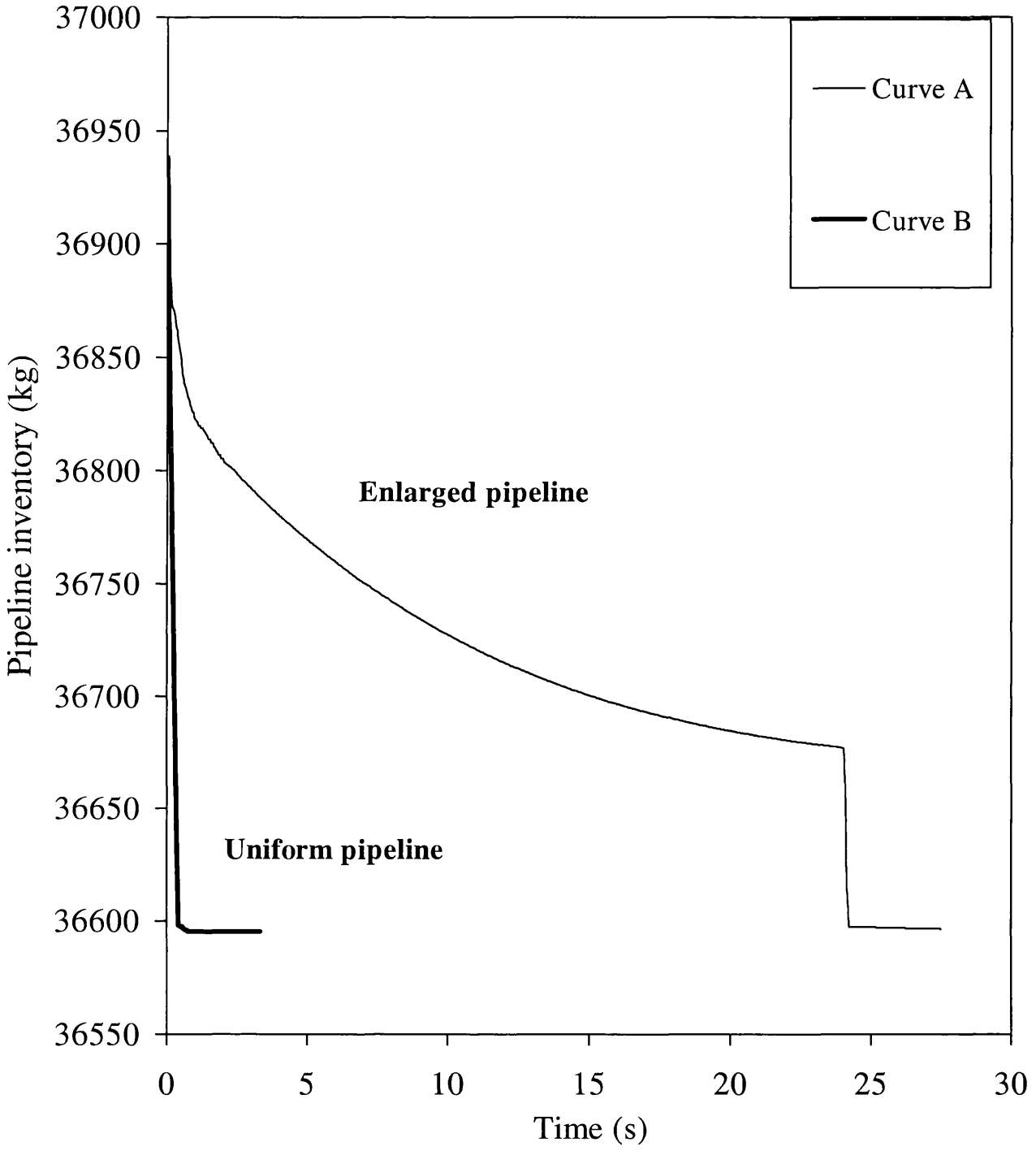

Figure 5.36 Pipeline inventory variation with time following FBR for LNG

Curve A: Enlarged pipeline

Curve B: Uniform pipeline

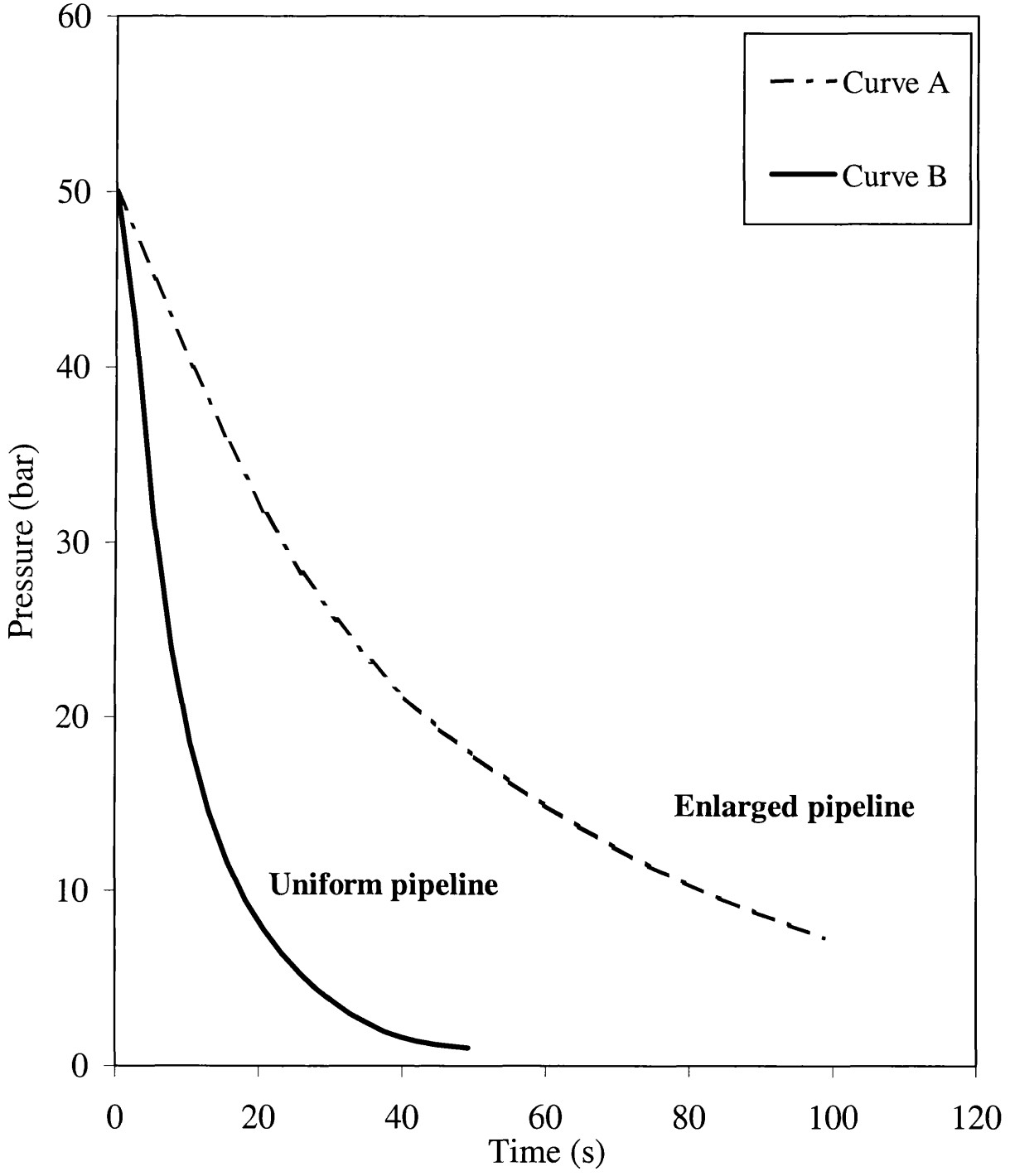

Figure 5.37 Intact end pressure variation with time for methane following FBR

Curve A: Enlarged pipeline

Curve B: Uniform pipeline

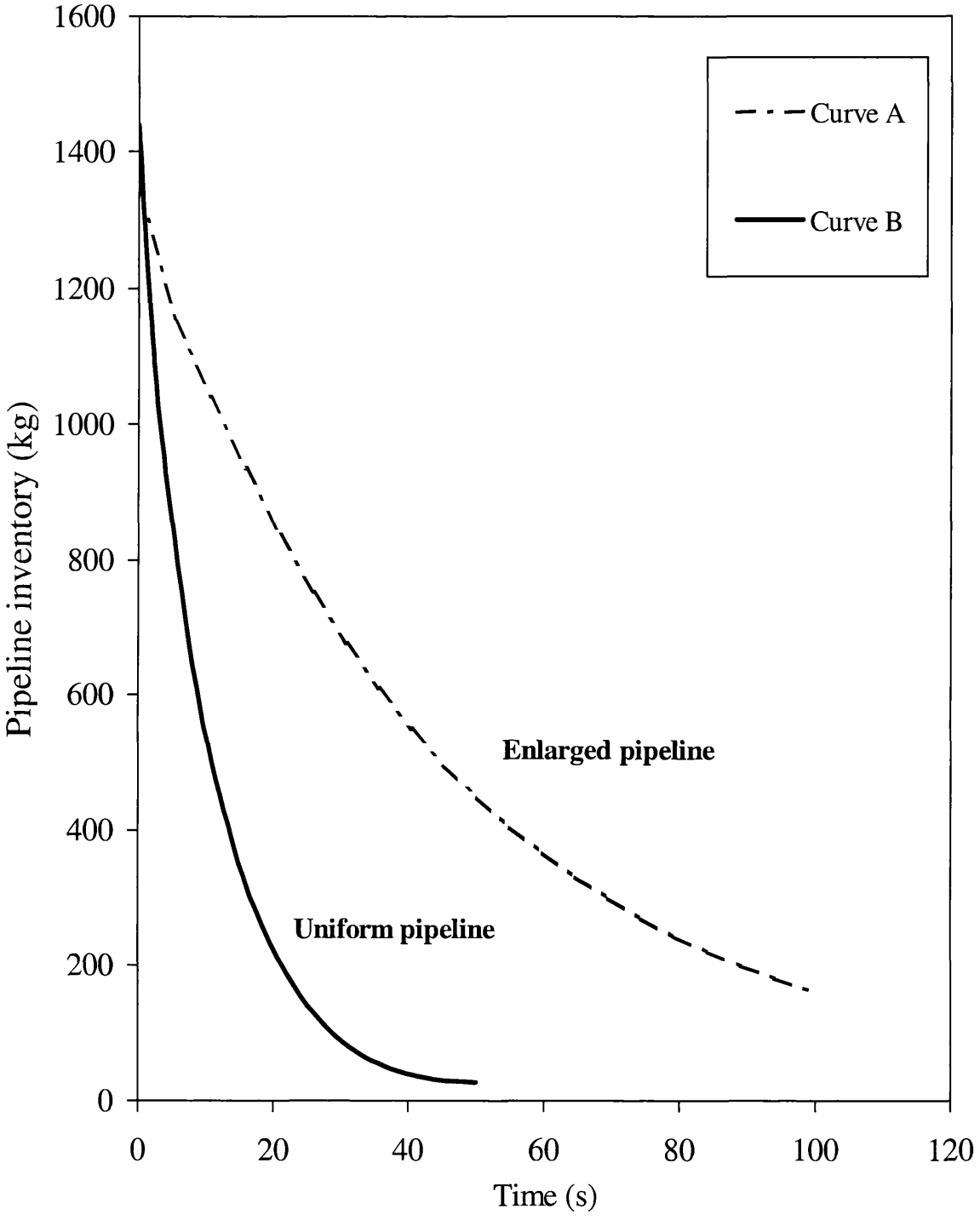

Figure 5.38 Pipeline inventory variation with time for methane following FBR

Curve A: Enlarged pipeline

Curve B: Uniform pipeline

Figures 5.39 and 5.40 respectively show the pressure and inventory versus time profiles following FBR of the enlarged and uniform pipelines containing LPG40 chosen as an example of a fluid undergoing two-phase transition during depressurisation. The fluid initial velocity is 1.5 m/s, the uniform pipe diameter is 0.217 m. The enlarged pipeline diameter is 0.15 m at the narrow end and 0.3 m at the wide end. The enlarged pipeline connector section is 0.28 m.

Both figures confirm the earlier observation that pipeline enlargement decelerates the pressure wave propagation and consequently delays the discharge process following FBR.

Figure 5.41 shows the velocity profiles along the pipeline at different time intervals for the enlarged pipeline containing LPG. The data indicate some intriguing trends. As expected the fluid velocity at the intact end (enlarged section) is zero throughout the discharge process. Negative sign for velocity indicates flow from the high-pressure end towards the intact end, as would be the case prior to rupture. FBR at the high-pressure end results in flow reversal at the rupture plane. The rest of the pipeline remains oblivious to FBR, with fluid flowing towards the intact end. With the passage of time, the entire fluid flow is towards the open end of the pipeline. Fluid passage through the constriction results in an initial significant increase in the fluid velocity followed by a reduction in the narrow section. As expected, the velocity profiles become more uniform as the pipeline depressurises.

Figure 5.42 shows a pictorial representation of the velocity profiles along the pipeline during the first second following FBR.

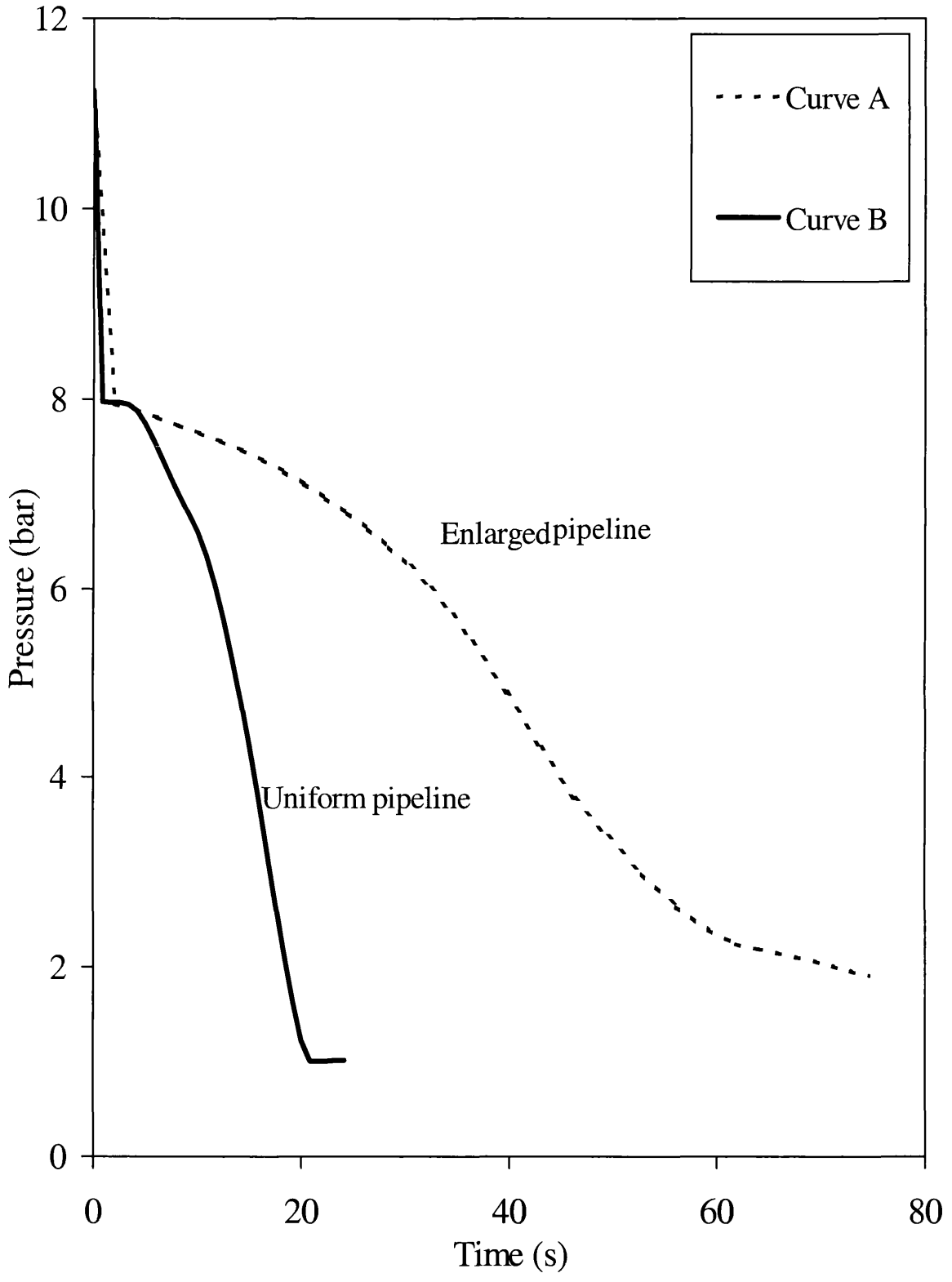

Figure 5.39 Intact end pressure variation with time for LPG following FBR

Curve A: Enlarged pipeline

Curve B: Uniform pipeline

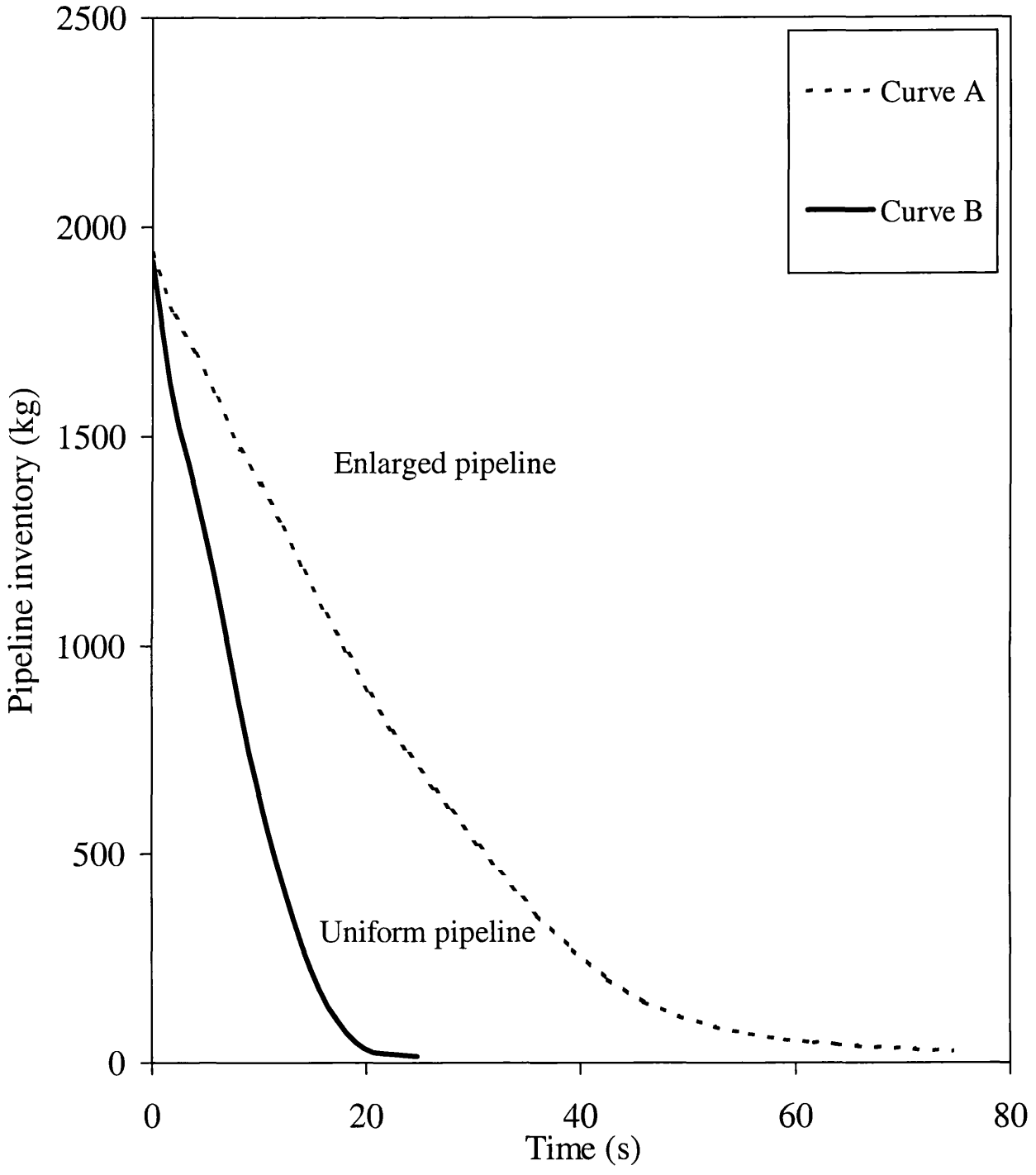

Figure 5.40 Pipeline inventory variation with time for LPG following FBR

Curve A: Enlarged pipeline

Curve B: Uniform pipeline

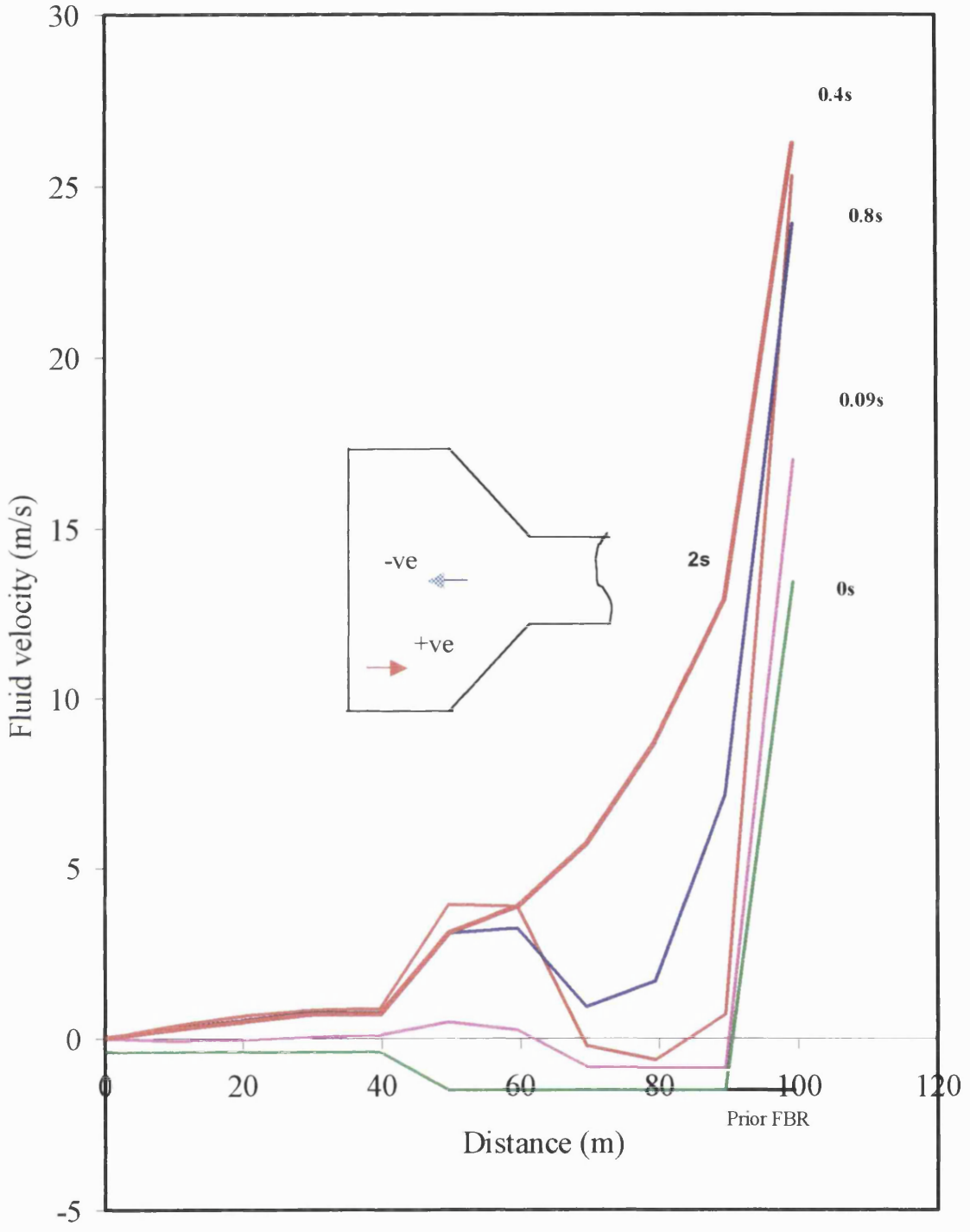

Figure 5.41 Velocity profiles along the pipeline at different time steps following FBR of an enlarged LPG pipeline

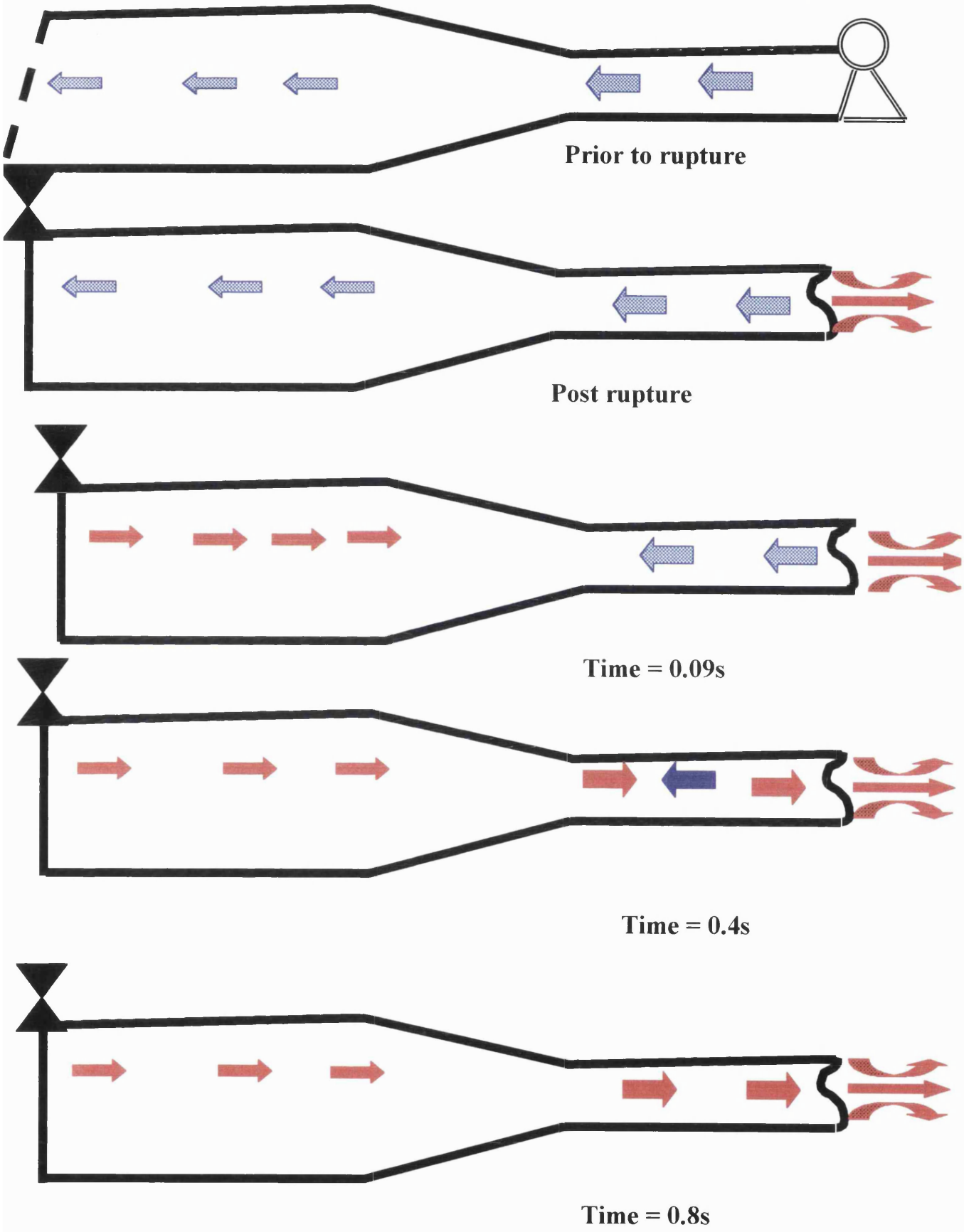

Figure 5.42 Schematic representation of velocity profile along an enlarged pipeline following FBR

CHAPTER 6
CONCLUSIONS AND SUGGESTIONS FOR FUTURE WORK

6.1 CONCLUSIONS

This thesis describes the development and application of a mathematical model based on the Method of Characteristics for simulating the fluid dynamic effects subsequent to full-bore rupture (FBR) of high pressure inclined or enlarged pipelines.

In chapter 2, the conservation equations governing the fluid flow through an inclined pipeline were derived. This was performed based on the assumptions of homogeneous equilibrium and viscid-inviscid fluid flow together with negligible heat conduction effects within the fluid. By making the assumption of homogeneous flow, a single momentum equation is sufficient for both liquid and gaseous phases. Likewise, the thermodynamic equilibrium assumption allows the application of a single energy equation for both phases.

The application of the thermodynamic relations derived above require a prior knowledge of the state of the mixture. This is provided by the Michelsen stability criterion, which also allows the accurate tracking of the phase boundary transition.

The procedure for modification of conservation equations for inclined pipelines to account for pipeline enlargement is extensively described in chapter 4.

The flow prior to rupture is assumed to be steady state, hence it is necessary to determine the fluid properties under such conditions. The corresponding equation for determining steady state pressure drop along an inclined pipeline was also derived in chapter 2.

The governing equations of flow, derived in chapter 2, must be solved numerically. The available numerical techniques were reviewed in chapter 3. Among the various

methods, the method of characteristics (MOC) owing to its capability in handling discontinuities encountered during fluid phase transitions and also its suitability for systems containing complex boundary conditions was chosen as the numerical technique adopted in the current study. A brief history of the development of MOC and its mathematical formulation were presented next. There are two main grid discretisation methods for MOC. The method of Specified Time Intervals (ST) was chosen in this work due to its vigour robustness.

In chapter 3, a critical review of the works relating to the modelling of outflow following pipeline rupture was presented. The review was carried out by focusing on the following parameters:

- The key attributes and limitations of the proposed models
- Taking into account real-fluid behaviour
- Validation by comparison against experimental data

Based on the above review, the following conclusions were made.

- No models relating to outflow simulation for an inclined or enlarged pipelines have been reported
- Among the models, which were reviewed, the homogenous equilibrium based models by Mahgerefteh et al. (1999, 2000), and Chen et al. (1995a, b) have been the most extensively validated against field data. Of these, Mahgerefteh et al.'s model performs better in terms of computational run time, simulates in-line dynamic effects following valve closure, and is based on a more robust numerical solution technique (MOC).
- The field experiments conducted by the Alberta Petroleum Industry to evaluate and improve H_2S isopleth prediction techniques are very useful in that they provide an important insight into the effects of various parameters affecting outflow following pipeline rupture.

The application of the method for pipeline rupture was presented in chapter 4. This involved two steps; transformation of the partial differential equations to ordinary differential equations followed by the solution of the latter equations. Following to the

description of the methods for pipeline's interior points calculation, the appropriate boundary and initial conditions for different pipeline rupture scenarios were described. The algorithms used to model inclined and enlarged pipeline were also presented. Finally the model presented in this study for calculation pressure drop along an inclined pipeline for steady state condition, was validated against experimental data. The mathematical algorithm presented in this chapter has been used to develop a computer program to simulate pipeline rupture. In the next chapter, the results of the simulation based on the mathematical model derived in this chapter were presented.

Chapter 5 dealt with the results of the application of the optimised outflow model to FBR of inclined and enlarged pipelines. The effects of changing a number of key parameters including the choice of curved as opposed to linear characteristics, the discretisation time step and friction factor on the model's performance were also investigated in the same chapter. The outflow model's performance was evaluated by comparison with the experimental data of Isle of Grain tests (Tam and Cowly, 1988). Some hypothetical simulations such as pure methane were also performed in order to show the effect of the fluid state on the model's performance.

The first series of simulation results presented in chapter 5 dealt with the comparison between the effects of using curved as opposed to linear characteristics in the outflow's model's formulation. It was observed that when the fluid is in two-phase region, the linear characteristics provides consistently better predictions than curved characteristics. Taking account of the CPU time, the simulations based on the linear characteristic also completed in much shorter times than those based on the curved characteristics. However when the fluid remains in gaseous phase, it was found that using either methodology does not affect the results obtained or the CPU time achieved.

The investigations revealed that the appropriate choice of the descretisation time step (Δt) is significantly influenced by the state of the fluid within the pipeline. As a result 1DDTS and 2DDTS discretisation schemes were developed in order to calculate the appropriate time step. It was concluded that in the presence of phase transition, it is

important to use very small time steps, updated both in time and in distance such as 2DDTS. However when no such phase transition occurs, larger time steps based on the 1DDTS scheme can be employed without any loss in accuracy and with significant reduction in computational run time.

It is well established that in all cases of depressurisation of a pipeline containing non-volatile liquid, volatile liquid or gas, the main contribution to the pressure drop in the pipeline can be attributed to frictional effects at the wall (Richardson and Saville, 1991). A number of correlations have been developed for this purpose. Some of the most widely used friction factor correlations were employed in order to identify the most suitable for the simulating outflow following FBR. These investigations revealed:

- The friction factor is independent of Reynolds number.
- The Nikuradse's equation is recommended for calculating the flow independent (constant) friction factor.
- Chen, Serghides and Nikuradse friction factor correlations all perform identically. Also all three equations show very good agreement with experimental data.
- El-Emam's equation, which has been derived based on field data although applicable to two-phase mixtures, produces unrealistic results when simulating non-condensable gas flows.

Inclined pipeline model simulations were performed based on the two scenarios involving rupture at either at the top end (low-pressure end) or the bottom end (high-pressure end). These investigations revealed that

- Gravitational effect on transient fluid flow very much depends on the state of the fluid.
- Pressure wave propagation during top end rupture for inclined pipeline is slower than that for horizontal pipeline. The converse applies in the case of bottom end rupture.

- In the case of top end rupture, increasing the angle of inclination results in a delay in the amount of inventory lost with time. However, this delay is a non-linear function of the angle of elevation, dramatically increasing with the angle of inclination. Remarkably, a pressure recovery during the first few seconds following the top end rupture of LPG simulation was observed. It was postulated that the above was a consequence of the fluid flashing as a result of the significant reduction in the rate of its loss from the pipeline.

The enlarged pipeline simulations lead to a potentially important observation in terms of reducing the hazard associated with pipeline rupture. These simulations indicate that pipeline enlargement or 'bottlenecking' may be used as an extremely effective way of reducing the hazard following FBR by reducing the depressurisation and hence the discharge rate. The simulations were performed for fluids in either gas, liquid or two-phase states. In all cases, a dramatic delay in depressurisation accompanied by a reduction in fluid discharge rate following FBR was observed.

6.2 SUGGESTIONS FOR FUTURE WORK

6.2.1 Use of an Implicit-Explicit Method of Characteristics Scheme

It is possible to model the characteristic curve refraction across the phase transition interface as a result of different fluid compressibility (Nakamura et al., 1995) using an implicit MOC. The drawback of this methodology is that it can only be applied when the acoustic effect is not important, i.e. for Mach numbers less than 0.5. However this method should be suitable for internal flows far from the rupture plane. The advantage is that it is implicit so that fluid parameter interpolations occur along the temporal axis instead of the spatial axis. An investigation of the use of this method in conjunction with the model developed in this thesis needs to be performed with the potential of further reductions in CPU time.

6.2.2 Use of Interpolation Techniques for the Calculation of Fluid Properties

A significant proportion of CPU time in FBR simulation is spent performing flash calculations. However during the relatively slow fluid flow away from the rupture plane, fluid thermodynamic properties vary much less rapidly than near the rupture plane. As such, the prediction of fluid properties based on various interpolation techniques should be tried as an alternative to solely performing flash calculations. Numerical tests need to be conducted to assess the impact on accuracy of using a variety of interpolation techniques that are available.

6.2.3 Use of Correction Factors to More Accurately Predict Liquid Density

It is well known that the use of cubic equations of state lead to under prediction of liquid mixture densities. The use of a volume correction factor such as that proposed by Peneloux et al. (1982) needs to be investigated to address this.

6.2.4 Pipeline Networks and Other Transient Flow Scenarios

Extension of the present model to study the effect of pipe networks on fluid transients should be attempted. There is also further scope for studying the effect of other equipment such as compressors in line.

6.2.5 The Development of Faster Iterative Techniques

The calculation of fluid properties at a solution point (intersection of characteristics lines) in the space and time domain involves extensive iteration. This is currently based on a combination of Newton Raphson as well as the Brent (Press et al., 1992) root techniques bracketing which are time consuming. Clearly development and utilisation of faster iteration techniques is a critical factor in reducing CPU.

6.2.6 Tracking of Single/Two Phase Interface

In the case of pipelines containing a gases or flashing liquids, rapid depressurisation as a result of pipeline rupture will, in most cases result in the formation of a two-phase mixture the front of which transverses from the rupture plane towards the intact end of the pipeline, eventually reverting to the gaseous state due to heat transfer from the pipeline walls. At present, the determination of the fluid state and hence the pertinent thermophysical and thermodynamic properties involve the use of a stability test based on minimisation of the Gibbs free energy (Michelsen, 1982a-b).

The development of an interface tracking algorithm in which the stability criteria is applied only from the rupture plane up to and including the liquid/gas interface is expected to result in a significant reduction in CPU time.

6.2.7 Hydrodynamic Constituent Equations

Clearly the correct estimation of hydrodynamic effects such as viscous drag forces at the fluid/wall interface has a direct bearing on the accurate estimations of the fluid flow transients following pipeline rupture. Studies have shown that such forces involve a linear combination of unsteady and steady wall drag or friction (Chen, 1993). From an earlier review (Saha, 1997), it seems that there is still some uncertainty in the accurate prediction of unsteady friction factor in rough pipes where highly turbulent flows prevail such as those encountered during FBR. The development of such empirical correlations should form part of the future study.

6.2.8 Thermodynamic Constituent Equations

At present, phase equilibrium data and the pertaining thermodynamic properties are generated using the SRK cubic equation of state. Despite its suitability for hydrocarbon mixtures, its main drawback is its inapplicability around the critical region. Future work should involve the use of more sophisticated equations of state which in addition to covering a broader range of conditions, are capable of handling water which is often present in practice as the third phase. Such capability will allow

an evaluation of the risk of the formation of solid hydrate, which may in turn lead to pipeline blockage during blowdown.

6.2.9 Flexible Pipelines and Fluid Structure Interaction

In the present study, the pipelines have been assumed to be rigid. Often the risers linking subsea wellhead clusters to semi-submersibles or sometimes floating production storage and off-loading systems (FPSO's) are flexible pipes and as a result are prone to the phenomenon of fluid structure interaction. In the case of non-rigidly clamped pipelines, fluid/structure interaction has to be taken into account (see for example Lavooij and Tijsselling (1990), Stittgen and Zielke (1990) and Rachid and Stuchenbruck (1990)) when modelling their failure behaviour. This is essentially a dynamic phenomenon, the interaction being caused by dynamic forces, which act conversely on the flowing fluid and pipe. These forces, which in essence are a consequence of rapid fluid pressure fluctuations, cause a pipe to expand or contract thereby creating axial stress waves in the pipe wall. The stress waves in return generate pressure fluctuations in the enclosed fluid, resulting in a phenomenon known as Poisson coupling. This problem can be especially dangerous in the case of compliant pipelines such as the flexible risers used in the offshore industry for exporting oil and gas offshore as their FBR rupture will be accompanied by sever gyration of the broken pipeline.

In addition, recent studies (see for example Zielke (1968), Hirose (1971) and Beauchemin and Marche (1992)) have shown apart from the obvious effect of fluid compressibility, sonic velocity in the fluid in a pipe is also influenced by the elasticity of the confining wall. As the elasticity of the wall material increases, the value of sonic velocity decreases. The net effect is an increase in valve activation time and hence a delay in its closure. This effect is commonly neglected for typical high-pressure gas pipelines. The variation of sound velocity with pipeline elasticity should be accounted for by modifying the continuity conservation equation.

6.2.10 Pipeline Rupture Risk Analysis During Blowdown

The term blowdown refers to rapid intentional depressurisation. In the offshore industry for example, blowdown of vessels or sections containing hydrocarbons is a common way of reducing the failure hazard in an emergency situation such as a fire. In recent years such operations have presented process and safety engineers with a dilemma.

The primary aim of blowdown is to reduce pressure and inventory in the least amount of time possible. However, rapid depressurisation results in a dramatic drop in the fluid temperature and hence a significant reduction in the pipeline wall temperature. If the wall temperature falls below the ductile-brittle transition temperature of the pipeline material, rupture is likely to occur.

The situation will be especially exasperated in a fire situation, as the resulting thermal loading from a fire builds up thermal stress in the vessel walls and this could in turn also lead to pipeline rupture.

As a useful extension of this work, the rapid transients in the fluid and wall temperatures should be modelled using MOC in conjunction with a heat transfer model. These data along with the pressure time profiles may be used to simulate the thermal stress profiles across the pipeline wall in contact with either fluid phase. The latter information forms the basis for assessing the risk of pipeline rupture during blowdown. The general engineering problem of extreme and varying thermal stresses on pipelines resulting from exposure of its different sections to different thermal environments should also be studied and modelled.

REFERENCES

Abbott, M.B., "An introduction to the method of characteristics", American Elsevier, New York, (1996).

APIGEC: Alberta Petroleum Industry Government Environmental Committee, "Hydrogen Sulphide Isopleth Prediction-Phase I: Model Sensitivity Study", (1978).

APIGEC: Alberta Petroleum Industry Government Environmental Committee, "Hydrogen Sulphide Isopleth Prediction-Phase II: Pipe Burst Study", (1979).

Allievi, L., "Notes I-IV", translated as "Theory of Waterhammer" by E. E. Holmes, Ricardo Garoni, Rome, 1925, (1903).

Assael, M. J., Martin Trusler, J. P. and Tsolakis, T., Thermophysical Properties of Fluids, Imperial College Press, London (1996).

Battara, V., Canuto, C., Quarteroni, A., "A Chebyshev spectral method for gas transients in pipelines", Computer Methods in Appl. Mech. Eng., **48**, 329 (1985).

Beauchemin, P. and Marche, C., "Transients in Complex Closed-Conduit Systems: Second-Order Explicit Finite Difference Schemes" in " Unsteady Flow and Fluid Transients", Bettes, R. and Watts, J. (Ed), Balkema, A. A., Roterdam, 31, (1992).

Bergeron, L., "Waterhammer in hydraulics and wave surges in electricity", J. Wiley, New York, (1961).

Bell, R.P., 'Isopleth Calculations for Ruptures in Sour Gas Pipelines', *Energy Processing/Canada*, 36, (1978).

Bisgaard, C., Sorensen, H. H., and Spangenberg, S., "A Finite Element Method for Transient Compressible Flow in Pipelines", *Int. J. Num. Meth. Fluids,* **7**, 291 (1987).

Boldy, A.P., "Analysis of Waterhammer in hydroelectric installation", *UKSC Conference on Computer simulation*, Bowwness-on-Windermere, (May 1975).

Botros, K. K., Jungowski, W. M. and Weiss, M. H., "Models and Methods of Simulating Gas Pipeline Blowdown", *Can. J. Chem. Eng.*, **67**, 529, (1989).

Chaudhry, H., Applied hydraulic transients, Van Nostrand Reinhold, (1987).

Chen, J.R., Richardson, S.M. and Saville, G., "Numerical Simulation of Full-bore Ruptures of Pipelines Containing Perfect Gases", *Trans. Inst. Chem. Eng. Part B*, **70**, 59 (1992).

Chen, J.R., Modelling of Transient Flow in Pipeline Blowdown Problems, PhD thesis, University of London, 81 (1993).

Chen, J.R., Richardson, S.M., and Saville, G., "A Simplified Numerical Method For Transient Two-Phase Pipe Flow", *Trans IChemE*, **71A**, 304 (1993).

Chen, J.R., Richardson, S.M., and Saville, G., "Modelling of Two-Phase Blowdown from Pipelines – I. A Hyperbolic Model Based on Variational Principles", *Chem. Eng. Sci.*, **50**, 695 (1995a).

Chen, J.R., Richardson, S.M., and Saville, G., "Modelling of Two-Phase Blowdown from Pipelines – II. A Simplified Numerical Method for Multi-Component Mixtures", *Chem. Eng. Sci.*, **50**, 2173 (1995b).

Chen, N.H., "An Explicit Equation for Friction Factor in Pipe", *Ind. Eng. Chem. Fundam.*, **18**, No. 3, 296 (1979).

Chin,Y. D., and Xu, Z., "Dynamic Processes of Multiphase Flow in Sub-sea Flowline / Riser Systems During ESD Valve Shut-down", *SPE Latin American and Caribbean Petroleum Engineering Conference*, Buenos Aires, Argentina, SPE 69418, (March 2001).

Churchill, S. W., "Friction Factor Equations Spans All Fluid Flow Regimes", Chem. Eng., 91, (1977).

Cullen, W. D., The public inquiry into the Piper Alpha disaster, Dept. of Energy, HMSO, (1990).

Colebrook, C. F., "Turbulent Flow in Pipes with Particular Reference to Transition Region Between the Smooth and Rough Pipes Laws", *J. Inst. Civil Eng.*, **11**,133, (1939).

Courant, R., Friedrichs, K.O., & Lewy H., "Uber die Partiellen Differenzengleichungen der mathematisches Physik", Math. Ann., **100**, 32, (1928), original in German translated by P. Fox. "On the partial difference equations of mathematical physics".

Courant, R., Isaacson, E., and Reeves, M., "On the Solution of Non-linear Hyperbolic Differential Equations by Finite Differences" *Comm. on Pure and Applied Mathematics*, **5**, 243 (1952).

Crane, Crane Technical Paper 410, Flow of Fluids through Valves, Fittings, and Pipe, 24th printing, Crane Company (1988).

Cronje, J. S., Bishnoi, P. B. and Svrcek, W. Y., "The Application of the Characteristic Method to Shock Tube Data That Simulate a Gas Pipeline Rupture", *Can. J. Chem. Eng.*, **58**, 289 (1980).

Crowl, D. A., Louvar, J. F., *Chemical Process Safety: Fundamentals with Application*, Prentice-Hall, New Jersey, (1990).

Darby, R., Meiller, P.R., Stockton, J.R., "Select the Best Model for Two-Phase Relief Sizing", *Chemical Engineering Progress*, **97 (5)**, 56 (May 2001).

de Reuck, K. M., Craven, R. J. B. and Elhassan, A. E., Transport Properties of Fluids: Their Correlation, Prediction and Estimation, Millat, J., Dymond, J. H. and Nieto de Castro, C. A., Eds., IUPAC, Cambridge Univ. Press, Cambridge (1996).

Douglas, J.F., Gasiorek, J.M. and Swaffield, J.A., Fluid Mechanics 3rd edition, (Longman Scientific & Technical),(1995).

Dukhovnaya, Y. and Adewumi, M.A., "Simulation of non-isothermal transients in gas/ condensate pipelines using TVD scheme", Powder Technology, **112**, 163 (2000).

Edwards, A.R., and O'Brien, T.P., "Studies of Phenomena Connected with the Depressurisation of Water Ractors", *J. Brit. Nucl. Energy Soc.*, **9**, 125 (Apr. 1970).

Eichinger, p., and Lein, G., "The influence of Friction on Unsteady Pipe flow", in Bettess, J., and Watts, J., " Unsteady Flow and Fluid Transients", Balchema, Rotterdam, 41, (1992).

El-Emam, N., Gad, F.K., Safwat Nafey, A., Zoghaib, N., "New friction factor derived from study of Egyptian gas-field pipeline", *Oil & gas Journal*, **95 (45)**, (1997).

Enver, K.J., "The Use of Computerised Graphical Method of Surge Analysis", The City University Pressure Transient Symposium, London, (Nov 1970).

Enver, K.J., "surge pressures in a Gas-liquid mixture with a low gas content", *Procs. 1st Int. Conf. Pressure Surges*, Canterbury, England, BHRA Fluid Eng., Paper C1, (Sept 1972).

Evangelisti, G., "Waterhammer analysis by the method of characteristics", L'Energia Ellectrica, **10**,10, (1969).

Ezekial, F. D. and Paynter, H. M., "Computer Representation of Engineering Systems Involving Fluid Transients", *Trans. ASME.*, **97**, (1957).

Fannelop, T. K., and Ryhming, I. L., "Massive Release of Gas from Long Pipelines", *J. Energy*, **6**, 132 (1982).

Finlayson, B. A., The Method of Weighted Residuals and Variational Principles, Academic Press, New York, (1972).

Flatt, R., "A Singly-Iterative Second Order Method of Characteristics for Unsteady Compressible One-Dimensional Flows", *Comm. in Applied Num. Meth.*, **1**, 269 (1985a).

Flatt, R., "On the Application of Numerical Methods of Fluid Mechanics to the Dynamics of Real Gases", *Forschung im Ingenieurwesen*, **51 (2)**, 41, in German (English translation: British Gas Translation No. T07823/BG/LRS/LRST817/86), (1985b).

Flatt, R., "Unsteady Compressible Flow in Long Pipelines Following a Rupture", *Int. J. Num. Meth. Fluids*, **6**, 83 (1986).

Flatt, R., "Unified Approach of Calculation of Mono-phase and Bi-phase/Homogeneous Flows of Condensable Pure Fluids", *Revue Entropie*, **149**, 48 (French), (1989).

Fox, J.A., "The use of the digital computer in the solution of waterhammer problems", Proc. I.C.E., **39**, (1968).

Fox, J.A., Hydraulic analysis of unsteady flow in pipe networks, Macmillan Press, London, (1977).

Fox, J.A., Transient flow in pipes, open channels and sewers, Ellis Horwood, Chichester, (1989).

Friedel, L., "Improved Friction Pressure Drop Correlations for Horizontal and Vertical Two-Phase Flow," *Proc. European Two-Phase Flow Group Meeting,* Ispra, Italy (1979).

Gray, C.A.M., " The analysis of the dissipation of energy in water hammer", Australian Journal of Applied Science, **5(2)**, 125 (1953).

Gray, C.A.M., " The analysis of the dissipation of energy in water hammer", *Procs. ASCE.*, **119** (1953).

Gray, C.A.M., "Analysis of water hammer by characteristics", *Procs. ASCE.* (1954).

Groves, T. K., Bishnoi, P. R. and Wallbridge, J. M. E., "Decompression Wave Velocities in Natural Gases in Pipelines", *Can. J. Chem. Eng.* **56**, 664, (1978).

Geurst, J. A. "Virtual mass in two-phase bubbly flow", *Physica*, **129A**, 233, (1985a).

Geurst, J. A. "Two-fluid hydrodynamics of bubbly liquid/vapour mixture including phase change", *Philips J. Res.* **40**, 352, (1985b).

Geurst, J. A. "Variational principles and two-fluid hydrodynamics of bubbly liquid/gas mixtures", *Physica*, **135A**, 455, (1986).

Guy, J. J., "Computation of unsteady gas flow in pipe networks" *Proceedings of Symposium of Efficient Methods for Practising Chemical Engineers*, Symposium Series **23**, London, Instn. Chem. Engrs. 139, (1967).

Haaland, S. E., "Simple and Explicit Formulas for the Friction Factor in Turbulent Pipe Flow", *J. Fluids Eng.*, **105** 89, (1983).

Harlow, F. H. and Amsden, A. A., "A Numerical Fluid Dynamics Calculation Method for All Flow Speeds", *J. Comput. Phys.* **8**, 197 (1971).

Hartree, D.R., Numerical Analysis, (Oxford University Press) (1958).

Hirose, M., "Frequency-Dependent Wall Shear in Transient Fluid Flow: Simulation of Unsteady Turbulent Flow", MSc. Dissertation, Massachusetts Institute of Technology, (1971).

WWW. hse.gov.uk/spd/spdpipe.htm

Issa, R. I., and Spalding, D. B., "Unsteady one-Dimensional compressible frictional flow with heat transfer", *J. Mech. Eng. Sci.*, **1496**, 365, (1972).

Jo, Y. D., and Ahn, B. J., "Analysis of Hazards Area Associated with High-Pressure Natural Gas Pipelines", *Journal of Loss Prevention in the process industries*, **15**, 179, (2002).

Jones, D. G. and Gough, D. W., "Rich Gas Decompression Behaviour in Pipelines", AGA-EPRG Pipeline Research Seminar IV, Duisburg, British Gas, Report No. ERSE 293, (1981).

Kameswara Rao. C.V., and Eswaran. K., "On the analysis of pressure transient in pipelines carrying compressible fluids", *Int. J. Pres. Ves. & Piping*, **56,** 107, (1993).

Ke, S.L. and Ti, H.C., "Transient analysis of isothermal gas flow in pipeline network", *Chemical Engineering Journal*, **76**,169, (2000).

Kimambo, C.Z., and A. Thorley, "Computer Modelling of Transients Ruptured High-pressure Natural Gas Pipelines: A Review of Experimental and Numerical Studies", *IMechE*, **C502/003**, 55 (1995).

Knox, H.W., Atwell, L.D., Angle, R., Willoughby, R., and Dielwart, .J., "Field Verification of Assumptions for Modelling Sour Gas Pipelines and Well Blowouts", Petroleum Society of CIM, *Paper No. 80,* 31, (1980).

Kunsch, J.P., Sjoen, K., and Fannelop, T.K., "Simulation of Unsteady Flow, Massive Release and Blowdown of Long High-pressure Pipelines", *Int. Gas Conf.*, Cannes, France, (1995).

Lamoen, J., "Le coup de belier d'Allieevi, compte tenu des pertes de charge continues", Bull. Centre de Etudes, de Recherches et d'Essaia Scientifiques des Constructions du Gerrie Civil et Hydraulique Fluviale, Tome II, Doseor, Liege, (1947).

Lang, E., "Gas Flow in Pipelines Following a Rupture Computed by a Spectral Method", *J. Appl. Math. and Physics (ZAMP)*, **42**, 183 (1991).

Lavooij, C. S. W., and Tijsseling, A. S., "Waterhammer with Fluid-Structure Interaction", *App. Scientific Research*, **5**, 573, (1991).

Lang, E., and T.K. Fannelop, "Efficient Computation of the Pipeline Break Problem", *3rd Symp. on Fluid-Transient in Fluid Structure Interaction*, **56**, 115 (1987).

Lax, P.D., "Weak Solutions of Non-linear Hyperbolic Equations and Their Numerical Computation", Comm. Pure Appl. Maths., **7**, 159 (1954).

Levenspiel, O., Engineering Flow and Heat Exchange, (Plenum Chemical Engineering Series, (1984).

Lister, M., "The numerical solution of hyperbolic partial differential equations by the method of characteristics", Numerical methods for digital computers, Ralston A. and Wilf H.S.(Eds), John Wiley and sons, New York,(1960).

Logan, J. D., "Invariant Variational Principles", Academic Press, New York, (1977).

Lum, Y. J., Lovick, J. and Angeli, P., "Two-phase liquid flows in inclined pipelines", *Proc. 3rd North American Conference on Multiphase technology*, Banff, Canada, 219, (2002).

Lyczkowski, R. W., Grimesey, R. A. and Solbrig, C. W., "Pipe Blowdown Analyses Using Explicit Numerical Schemes", *AIChE Symp. Ser.*, **74 (174),** 129 (1978).

Mahgerefteh, H., Saha, P., and Economou I. G., "A Study of the Dynamic Response of Emergency Shutdown Valves Following Full Bore Rupture of Gas Pipelines", *Trans. Inst. Chem. Eng., Part B*, **75**, 201 (1997).

Mahgerefteh, H., Saha, P., and I. G. Economou, "Fast Numerical Simulation for Full Bore Rupture of Pressurized Pipelines", *AIChE J.*, **45 (6)**, 1191 (1999).

Mahgerefteh, H., Saha, P. and Economou, I. G., "Modelling Fluid Phase Transition Effects on Dynamic Behaviour of ESDV", *AIChE J.*, **46(5)**, 997 (2000).

Massau, J., "Memoirs sur l'integration graphique des equations aux derivess partialles", Ann.Ass.Ingrs.Sortie de Ecoles Speciales de Gand., **23**, 95 (1900).Translated as Unsteady Flow, H.J.Putman,Rocky Mountain Hydrolic Lab., Colorado, (1948).

Maxey, W. A., Keifner, J. C., Eiber, R. J. and Duffy, A. R., "Ductile Fracture Initiation, Propagation and Arrest in Cylindrical Vessels", Fracture Toughness ASTM STP 514, American Society for Testing and Materials, 70, Philadelphia, (1972).

Michelsen, M. L., "The Isothermal Flash Problem. Part I. Stability", *Fluid Phase Equil.*, **9**, 1 (1982a).

Michelsen, M. L., "The Isothermal Flash Problem. Part II. Phase-split Calculation", *Fluid Phase Equil.*, **9**, 21 (1982b).

Michelsen, M. L., "Multi-phase Isenthalpic and Isentropic Flash Algorithms", *Fluid Phase Equil.*, **33**, 13 (1987).

Montiel, H., Vilchez, J. A., Casal, J., Arnaldos, J., "Mathematical Modelling of Accidental Gas Releases", *J. Hazard. Mater.*, **59**, 211 (1998).

Moody, L. F., "Friction Factors for Pipe Flow", *Trans. ASME*, **66**,671, (1944).

Morrow, T., Southwest Research Institute, San Antonio, Texas Private Communication, (1997).

Nakamura, S., Berger, M. A. and Spencer, A. C., "One Dimensional Implicit Characteristic Method for Compressible Two-Phase Coolant Flow", *Proc. Of the Conf. On Comp. Methods in Nuclear Eng.*, NYIS conf-750413, American Nuc. Soc., (April 1995).

Necmi, S and Hancox, W.T., "An Experimental and Theoretical Investigation of Blowdown from a Horizontal Pipe", *Proceedings of the 6th International Heat Transfer Conference*, Toronto, Canada (1978).

Nikuradse, J., Stromungsgesetze in Rauchen Roohren. Forschungsheft No. 361. Berlin: Verein Deutscher Ingenieure (1933).

Oliemans, R. V. A., " Modelling of Two-Phase Flow of Gas and Condensate in Horizontal and Inclined Pipes", Paper presented at the 6^{th} *ASME Annual Pipeline Engineering Symposium*, Dallas, (1987).

Olorunmaiye, J.A., and N.E. Imide, "Computation of Natural Gas Pipeline Rupture Problems Using the Method of Characteristics", *J. Hazard. Mater.*, **34**, 81 (1993).

Osiadacz, A., 'Optimal numerical methods for simulating dynamic flow of gas in pipelines', Int. J. Num. Methods in Fluids, **3**, 125, (1983).

Osiadacz, A., "Simulation of transient gas flow in network", *Int. J. Numer. Methods Fluids* , **4**, 13, 1984.

Parmakian, J., Water Hammer Analysis, Dover, New York, (1963).

Peneloux, A., Rauzy, E., and Freze, R., "A Consistent Correction for Redlich-Kwong-_Soave Volumes", *Fluid Phase Equi.*, **8**, 7, (1982).

Peng, D. Y., and D. B. Robinson, "A New Two-constant Equation of State", *Ind. Eng. Chem. Fund.*, **15**, 59 (1976).

Perkins, F.E., Tedrow, A.C., Eagleson, P.S. and Ippen, A.T., "Hydropower plant transients", Part II and III, Department of Civil Engineering, MIT, Report No.71, (Sept 1964).

Perry, R.H., and Chilton, C.H. (editors), Chemical Engineers' Handbook, McGraw-Hill, New York, 5th edition, (1973).

Picard, D. J., and Bishnoi, P. R., "Calculation of the Thermodynamic Sound Velocity in Two-Phase Multi-Component Fluids", *Int. J. Multiphase Flow*, **13(3)**, 295 (1987).

Picard, D.J., and Bishnoi, P.R., "The Importance of Real-Fluid Behaviour and Non-Isentropic Effects in Modelling Compression Characteristics of Pipeline Fluids for Application in Ductile Fracture Propagation Analysis", *Can. J. Chem. Eng.*, **66**, 3, (1988).

Picard, D. J., and Bishnoi P.R. "The Importance of Real-fluid Behaviour in Predicting Release Rates Resulting From High Pressure Sour-gas Pipeline Ruptures", *Can. J. Chem. Eng.*, **67**, 3 (1989).

Pickford, J.A., Analysis of surge, Macmillan, London, (1969).

Press, W.H., Teukolsky, S.A., Vetterling, W.T., and Flannery, B.P., Numerical Recipes in FORTRAN 77: The Art of Scientific Computing, Cambridge University Press, 2nd edition, (1992).

Rachid, F. B. F., and Stuckenbruck, S., "Transient in Liquid and Structure in Viscoelastic Pipes", in Thorley, A. R. D. (Ed.), *Proc. Of the 6th Int. Conf. On Pressure Surges*, BHRA, 69, (1990).

Rachford, H.H., and Dupont, T.A., "Fast highly accurate means of modelling transient flow in gas pipelines by variational methods", Soc. Pet. Eng. J., **14**,165, (1974).

Richardson, S.M., and Saville, G., "Analysis of flows in Piper Alpha gas import and export lines", Transcript of Days 90/91 of Piper Alpha Public Enquiry (1989).

Richardson, S.M., and Saville, G., "Blowdown of Pipelines", *Society of Petroleum Engineers Europe 91*, paper SPE 23070, Aberdeen, U.K., 369 (1991).

Richardson, S.M., and Saville, G., "Blowdown of LPG pipelines", *Trans. IChemE*, **74B**, 236 (1996).

Rich, G.R., Hydraulic transients, Dover, New York, (1963).

Richtmyer, R.D., and Morton, K.W., Difference Methods for Initial-value problems, Interscience, New York, (1967).

Rudinger, G., Nonsteady duct flow, Dover, NewYork, 186, (1969).

Saad, M. A., Compressible Fluid Flow, Prentice-Hall, (1985).

Saha, P., Modelling the Dynamic Response of Emergency Shutdown Valves Following Full Bore Rupture of Long Pipelines, PhD Thesis, University College London (1997).

Sand, I. O., Sjoen, K., and Bakke, J. R., " Modelling of Release of Gas from High-Pressure Pipelines", *International Journal for Numerical Methods in Fluids*, **23**, 953, (1996).

Sens, M., Jouve, P. and Pelletier, R., "Detection of a Break in a Gas Line", *11th International Gas Conference*, Moscow, Paper No. IGU/C37-70, in French, (English Translation: British Gas, Translation No. BG. TRANS 4910) (1970).

Serghides, T. K., "Estimate friction factor accurately", Chemical Engineering, (March 1984).

Shin, Y. W., "Two-Dimensional Fluid Transient Analysis By the Method of Characteristics", in "Fluid Transient and Acoustics in the Power Industry", Papadakis C. and Scarton H. (Ed.), ASME, New York, 179, (1978).

Simpson, L.L., "Estimate Two-Phase Flow in Safety Devices", *Engineering Practice, Chem. Eng.*, **98(8)**, 98, (August 1991).

Stanislav, J. F., Kokal, J. F., and Nicholson, M. K., "Gas Liquid Flow in Downward and Upward Inclined Pipes", *Canadian Journal of Chemical Engineering*, **64(6),** 881, (Dec 1986).

Stittgen, M. and Zielke, W., "Fluid Structure Interaction in Flexible Curved Pipes", in Thorley, A. R. D. (Ed.), *Proc. Of the 6th Int. Conf. On Pressure Surges*, BHRA, 101, (1990).

Stoner, M. A., "Analysis and Control of Natural Gas Piping Systems", *Trans. ASME j. Basic Eng.*, **91(3)**, (Sept 1969).

Streeter, V.L., and Lai, C., "Water hammer analysis including friction", *J.Hyd. Div., ASCE*, **88** (HY3), 79 (May 1962).

Streeter, V.L., "Valve stroking to control water hammer", *J.Hyd. Div., ASCE.*, **89** (HY2),3452,39(March 1963).

Streeter, V.L., "Computer solutions of surge problems", *Procs., I.Mech.E.*, 180 (1966).

Streeter, V.L., "Valve stroking for complex piping systems", J.*Hyd. Div., ASCE.*, **93** (HY3),81 (May 1967).

Streeter, V.L., and Wylie, E.B., Hydraulic Transients, (McGraw-Hill, New York), (1967).

Streeter, V.L., "Waterhammer analysis", *Procs., Jour. Hyd.Div., ASCE.*, **88** (HY3),79 (May 1969).

Streeter, V.L., "Unsteady flow calculations by numerical methods", *Jour. Basic Eng., ASME.*, **94**,457, (June 1972).

Stroud, K. A., Further Engineering Mathematics, Second Edition, Macmillan Education LTD, (1990).

Swaffield, J.A., "A study of column separation following valve closure in a pipeline carrying aviation |kerosene", Thermodynamics and Fluid Mechanics Convention, Steady and unsteady flows, *Procs. I.Mech.E.*, **57**, 184,(1970).

Swaffield, J.A., "Column separation in an aircraft fuel system", *Procs.1st Int. Conf. Pressure Surges*, Canterbury, England, Paper C2, BHRA Fluid Eng.,28, (Sept 1972).

Swaffield, J.A., and Boldy, A.P., Pressure Surge in Pipe and Duct Systems, (Ashgate Publishing Limited, Vermont, USA), (1993).

Swaffield, J.A., "A study of the influence of air release on column separation in an aviation kerosene pipeline", *procs. I.Mech.E., Thermodynamics and Fluid Mechanics Group*, **186(56/72)**, 693, (1972a).

Swamee, P. K., and Jain, A. K., "Explicit Equation for Pipe-Flow Problems", *J. Hydraulic Div. ASCE,* **(102)**: 657-664, (1976).

Tam, V.H.Y., and Cowley, L.T., Consequences of pressurised LPG releases: The Isle of Grain full Scale experiments, Proceedings of GASTECH88 Conference, Kuala Lumpur (1988)

Tao, W.Q., and Ti, H.C., "Transient analysis of gas pipeline network", *Chemical Engineering Journal*, **69**,47 (1998).

Thorley, A.R.D., and Tiley, C.H., "Unsteady and Transient Flow of Compressible Flows in Pipelines - A Review of Theoretical and Some Experimental Studies", *Int. J. of Heat and Fluid Flow*, **8(1)**, 3, (1987).

Tiley, C. H., "Pressure Transient in a Ruptured Gas Pipeline with Friction and Thermal Effects Included", PhD Thesis, City University, London, (1989).

Trikha, A. K., "An Efficient Method For Simulating Frequency Dependent Friction in Transient Liquid Flow", *ASME J. Fluid Eng.*, **97**, 97 (1975).

Uhl, A. E., Bischoff, K. B., Bukacek, R. F., Elllington, P. V., Kniebes, D. V., Staats, W. R., Worcester, D. A., and the NB-13 Committee, "Steady Flow in pipelines", American Gas Association incorporation, (July 1965).

Van Deen, J. K., and Reintsema, S.R., "Modelling of High Pressure Gas Transmission Lines", *App. Math. Modelling*, **7**, No. 4, 268, (1983).

Vardy, A.E., and Brown, J.M.B., "Transient, turbulent, smooth pipe friction", *J. Hydr. Res.*, **33**, 435, (1995).

Vardy, A.E., and Brown, J.M.B., "On turbulent, unsteady, smooth-pipe friction", *Proc. 7th Intl Conf on Pressure Surges and Fluid Transients*, Harrogate, 16-18 April, 289, BHRA Group, 1996.

Walas, S. M., Phase Equilibrium in Chemical Engineering, Butterworth Publishers. Boston, 15 (1985).

Wood, D.J., "An Explicit Friction Factor Relationship", Civ. Eng., **36**, 60, (1966).

Wood, D.J., and Funk, J.E., "A Boundary Layer Theory For Transient Viscous Losses in Turbulent Flow", *ASME J. Basic Eng.*, **92**, 865 (1970).

Wood, F.M., "Application of Heaviside's operational calculus to the solution of waterhammer problems", *Trans. ASME.*, **59**, 703, (Nov 1938).

Wylie, E.B., and Streeter, V.L., Fluid Transients, (McGraw-Hill Inc., USA) (1978).

Wylie E.B., and Streeter V.L., Fluid Transients, FEB Press, Ann Arbor, (1983).

Wylie E.B., and Streeter V.L., Fluid Transients in Systems, Prentice- Hall, New Jersey, (1993).

Zhou, J., and Adewumi, M.A., "The development and testing of a new flow equation", 27th Annual Meeting of Pipeline Simulation Interest Group (PSIG) (1995).

Zhou, X. X., Lea, C J., Bilo, M., and Maddison, T. E., "Three-Dimensional Computational Fluid Dynamic Modelling of Natural Gas Releases from High-Pressure Pipelines", *Pipes & Pipelines International*, 13 (1997).

Zhu, J., "Risk analysis of oil & gas pipeline", Proceedings of the 1998 International symposium SAF. SCI. TECHNOL, (1998).

Zielke, W., "Frequency-Dependent Friction in Transient Pipe Flow", ASME J. Fluid Eng., 90, 109, (1968).

Zigrang, D. J., and Sylvester, N. D., "Explicit Approximation to the Solution of Colebrook's Friction Factor Equation", *AIChE J.*, **28**, 514, (1982).

Zucrow, M. J., and J. D. Hoffman, Gas Dynamics, **I and II**, John Wiley and Sons, New York, 297 (1976).